Diploma Thesis | Experimental investigation & Development of a parametric predictive model for the appearance of Lüders Lines during copper tubes' bending tests

School of Mechanical Engineering NTUA
Machine Design Lab

Dimitrios I. Tsiakos mc17107
Mechanical Engineering Student

Supervisor: Dr. Vasileios Spitas, Associate Professor at NTUA
Section of Mechanical Design & Automatic Control

Athens, October 2022

Solemn declaration for plagiarism and copyright theft

I have read and understood the rules for plagiarism and how to properly cite the sources contained in the Diploma Thesis Writing Guide. I declare that, as far as I know, the content of this Thesis constitutes the product of my own work and there are references to all the sources that I have used.

The views and conclusions in this Dissertation belong to the author and should not be construed as representing the official positions of the School of Mechanical Engineering or the National Technical University of Athens.

Dimitrios I. Tsiakos

Acknowledgements

First of all, I would wish to thank my supervisor and Associate Professor Dr Vasileios Spitas for giving me the chance to work on a dissertation that covers the field of technical materials' technology, manufacturing processes and mechanical design. Also, he helped me a lot to understand deeply this industrial problem, he advised me for every issue that arose and encouraged me to go further and further by observing Lüders Lines' Project through multiple views.

I would like to thank very much my project coordinator PhD Candidate Christos Kalligeros for his continuous contribution to every stage of this work, for making me feel important, for his eternal technical knowledge that shared with me, for his passion, for his devotion, for his encouragement and for his exceptional handling of every aspect that we have discussed in this work.

Thank you to Panagiotis Christinakis, who is the Product Development Engineer of Halcor, with whom I collaborated three months while doing my full – time summer internship at the Technology Department of this company. He proposed me to Christos Kalligeros so as I undertook this innovative and creative work for my diploma thesis.

In addition, I would wish to thank my Professor Dr Dimitrios Manolakos for the whole support and the technical staff at Manufacturing Technology Lab at NTUA. They helped me to perform some additional experimental work in order to investigate more Lüders Lines' appearance. Their contribution was really significant for the completion of this project.

Finally, I thank my family and all my beloved persons for their continuous patience, care, and unwilling support during my studies at National Technical University of Athens.

Table of Contents

Abstract

The current dissertation constitutes the continuity of my full – time summer internship at Halcor's Department of Technology. It is about an industrial diploma thesis, which includes not only experimental part but also computational one. The aim of this work is to study extensively Lüders Lines, which appear on the surface of hard copper tubes during bending tests. The parameters that affect most the phenomenon have been found, the geometrical and the material ones, via qualitative and quantitative analysis.

By combining smartly the experimental data that we have at our disposal, we start to build semi – empirical formulas and functions, which enable us to create reliable criteria for the Lüders Lines' formation on copper tubes' specimens. Special importance has been given so as these formulas be easily perceivable, and they can be utilized without any particular technological background needed.

In this way, by making use of genetic algorithms as well, we managed to build a complete predictive model which includes specific formulas with respect to the available data for the tube and the bender. Significant effort has been made so as to find a critical strain upon which the danger of the appearance of this defect gets visible. At the same time, the micro – structure of Lüders Lines has been studied and this defect was faced as a failure in order to highlight maybe the potential cause and the material's wear.

All the useable results of this work are gathered and their utilitarian value as well. Consequently, guidelines can be given to Halcor's customers regarding the chance of Lüders Lines' appearance on its products and the way that this defect can be restricted or even avoided. Finally, some additional steps are proposed for the further investigation of this issue in experimental and computational level.

Περίληψη

Η παρούσα διπλωματική εργασία αποτελεί την συνέχεια της πρακτικής μου άσκησης στο Τμήμα Τεχνολογίας της Halcor. Πρόκειται για μια βιομηχανική διπλωματική εργασία, η οποία περιέχει τόσο πειραματικό μέρος όσο και αντίστοιχο υπολογιστικό. Στόχος της παρούσας δουλειάς είναι να μελετηθούν εκτενώς οι γραμμές Lüders, που εμφανίζονται στην επιφάνεια των σκληρών χαλκοσωλήνων κατά την διάρκεια των δοκιμών κάμψης. Έχουν βρεθεί οι παράμετροι που επηρεάζουν περισσότερο το συγκεκριμένο μη γραμμικό φαινόμενο, τόσο γεωμετρικές όσο και υλικού, μέσω ποιοτικής και ποσοτικής ανάλυσης.

Συνδυάζοντας έξυπνα όλα τα διαθέσιμα πειραματικά δεδομένα, ξεκινούμε να κτίζουμε ημι – εμπειρικούς τύπους και συναρτήσεις, που μας επιτρέπουν να δημιουργήσουμε αξιόπιστα κριτήρια για την εμφάνιση ή όχι γραμμών Lüders στα δοκίμια κάμψης χαλκοσωλήνων. Δόθηκε ιδιαίτερη σημασία ώστε αυτοί οι τύποι να είναι εύληπτοι και να μπορούν να αξιοποιηθούν άμεσα χωρίς να απαιτείται κάποιο πολύ υψηλό τεχνολογικό υπόβαθρο.

Με αυτόν τον τρόπο, αξιοποιώντας και γενετικούς αλγορίθμους, καταφέραμε να αναπτύξουμε ένα πλήρες προβλεπτικό μοντέλο το οποίο περιέχει συγκεκριμένους τύπους αναλόγως τα δεδομένα που έχουμε για το σωλήνα και τον κουρμπαδόρο στον οποίο έχει γίνει η κάμψη. Έγινε σημαντική προσπάθεια και στην εύρεση μιας τιμής της κρίσιμης παραμόρφωσης, πάνω από την οποία είναι ορατός ο κίνδυνος εμφάνισης αυτού του ελαττώματος. Συγχρόνως, μέσω μικροσκοπίου, μελετήθηκε η μικροδομή των γραμμών Lüders και αντιμετωπίστηκε ως αστοχία ενδεχομένως για την ανάδειξη των αιτιών εμφάνισης της και της φθοράς που δημιουργείται στο υλικό.

Συγκεντρώνονται όλα τα αξιοποιήσιμα αποτελέσματα της συγκεκριμένης εργασίας και η αντίστοιχη χρηστική τους αξία. Με αυτόν τον τρόπο μπορούν να δοθούν οδηγίες στους πελάτες της Halcor σχετικά με την πιθανότητα εμφάνισης γραμμών Lüders στα προϊόντα της και τον τρόπο περιορισμού ή αποφυγής αυτών. Τέλος, προτείνονται κάποια επιπλέον βήματα για την περαιτέρω διερεύνηση του συγκεκριμένου θέματος τόσο πειραματικά όσο και υπολογιστικά.

1. Introduction

1.1 Full – Time Summer Internship

I was given the chance to acquire practical experience regarding issues about the field of a Mechanical Engineer through the institution of the Summer Internship. I have worked for 2 + 1 months at Halcor – Copper & Alloys Extrusion Division of ElvalHalcor from the 12th of July until the 12th of September 2021.

I got employed at the Department of Technology of Halcor, which is the sector of this company that aims to improve continuously the products and develop them even more offering great residential and industrial solutions. So, my objective was to analyse all these parameters that affect the quality of the copper tubes and make an effort to assess if we can predict some phenomena (e.g. Defects during tube bending) or how to automate more some processes (Standards' automation).

The 4 distinct research fields that I had the opportunity to engage are listed below in the following bullet points:

- Copper Tubes' Bending Project
- Numerical investigation of the true stress σ – true strain ε curves for the copper material (given experimental flow curves)
- Simulation of the Forming Limit Curves – FLC as for copper
- Standards' and specifications' automation regarding copper and copper alloys tubes

For every single task I had the capability to study it not only theoretically but also practically. The theoretical approach has to do with the search of many scientific papers and handbooks as for the problem that we examined then. At the same time, I derived useful information thanks to the lessons learnt and the knowledge gained by attending the lectures at the Mechanical Engineering School – National Technical University of Athens (NTUA). In this way, I was able to recognize the basis of each emerging problem and I could proceed with further actions in order to solve it. Microsoft Excel and MATLAB were used to manage these tasks successfully ensuring the accuracy and the validity of my work.

At this point, I would like to thank you the professor at NTUA Mr. Dimitrios Manolakos, who proposed me for this role at Halcor. It was an honour to work with Panagiotis Christinakis, with whom I collaborate, and I had a useful training with him. He taught me many lessons regarding the job of a Mechanical Engineer and proposed me in for the current diploma thesis at the Machine Design Lab. In addition, I learnt many things from the supervisor George Hinopoulos, who possesses the demanding role of R&D, Technology and Marketing Director at Halcor.

Figure 1: Copper Tubes mix produced at Halcor

1.2 Technology & Research at Halcor

Halcor invests continuously in R&D of processes, products, and materials with the objective to introduce technology improvements in various metallurgical applications and thus offer cutting-edge products and integrated solutions. As an active member of the Hellenic Research Centre for Metals (ELKEME), Halcor also supports broader efforts to promote R&D in the copper sector and builds on the technical expertise of a network of research institutes, universities (such as National Technical University of Athens), and research companies. Through research, Halcor is able to accumulate significant knowledge in production process and product improvements to meet the most demanding and diversified customer requirements. Halcor's continuous advancements in technology enable the company to support clients as products and services evolve through time.

Figure 2: An effort at Halcor's Quality Control Lab

Proof of the company's ability to offer comprehensive services and product improvements is the establishment of the innovative Tube Heat Transfer Laboratory. The Tube Heat Transfer Laboratory allows Halcor to manufacture TALOS®Inner-Groove Tubes (IGT) and TALOS®ACR tubes based on different customer specifications, as well as introduce improvements in specific product applications.

Halcor is also a founding member of the Hellenic Copper Development Institute, actively involved in educational programs by providing materials, hosting, and financing specialised seminars across Greece. Through HCDI, a member of the European Copper Institute (ECI), Halcor is actively involved in major research projects concerning copper's impact on human health and the environment [1].

ΧΑΛΚΟΡ

ΤΟΜΕΑΣ ΣΩΛΗΝΩΝ ΧΑΛΚΟΥ της: ElvalHalcor

Figure 3: Halcor logo – Copper and Copper Alloys Extrusion Division of ElvalHalcor

1.3 Motivation for this dissertation

This diploma thesis constitutes the continuity of my summer internship and especially in the task of Copper Tubes' Bending Project. The entire work written in this book aims to produce a useful tool for the Lueders' Lines defect during copper tubes bending test. The appearance of these slotted diagonal lines can harm the mechanical strength of the product and generally its functionally in every possible application.

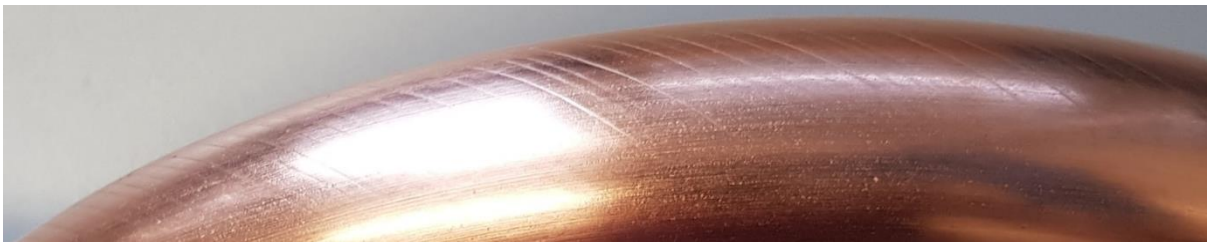

Image 1: Zoom on Lueders' Lines defect

These parallel diagonal lines that appear on the internal and the external hard copper tubes' surface present an extremely serious defect that degrades the degree of formability during bending tests. Lueders Lines decrease the wall thickness of the tube locally and in this way produce new material uniformity making it weaker and less useful. At the same times, even if we did not have any issues with the mechanical properties, this defect causes not negligible aesthetic problems on the hard copper tube. Consequently, this Halcor's product may not achieve the greatest possible commercial success.

As we had at our disposal may raw data regarding many bending tests, we would wish to creatively combine them to predict the phenomenon with an acceptable accuracy. For this reason, we created many empirical formulas that enable either the geometrical parameters or the mechanical/material properties of the tubes that had been bent. The goal was to develop a parametric predictive model for the appearance of Lueders Lines, so as everyone can use it and be aware of the frequency and the most affecting parameters of this defect. In this way, we will pave the way to implement more targeted experiments that may solve the problem in some needed cases.

On the other hand, no paper exists for the appearance of Lueders Lines during Copper Tubes' Bending. Some scientific work has to do with the appearance of Lueders Lines on aluminium or steel alloys during uniaxial tensile test. Therefore, we are going to give qualitative and quantitative answers for the appearance of this defect based on our experiments' investigation. In addition, this innovative diploma thesis has managed to develop some predictive criteria for the formation of this defect. Finally, we hope that we may enable other engineers to expand this research field with more experimental and computational work.

2. Literature Review

2.1 Plastic Strain Localization

Plastic strain localization in metals (e.g., copper $Cu - DHP$) occurs across a wide variety of materials, loading conditions and applications, and often has a determinative role in influencing the mechanical behaviour and consequently the suitability of a given material for an intended structural application [2].

Metals generally show a reduced strain hardening with increasing strain while the level of the stress continues to increase. At some point, the two values cross and the material is plastically unstable, and the smallest of defects is sufficient to promote localized deformation at that position [2].

However, most of the hardening mechanisms give rise to decreasing strain hardening (i.e., $\frac{d\sigma}{de} \downarrow$ as $e \uparrow$) and as a practical matter plastic instability usually does occur [2].

The greater the strain hardening exponent n ($\sigma = K\varepsilon^n$) the more plastic instability is delayed. Delaying plastic instability to higher strain levels is clearly desirable for forming operations (such as bending) and for increased toughness. With increasing strain rate or lower temperature, the point of tensile instability is shifted to larger plastic strains for FCC metals (such as copper) and alloys and to lower plastic strains for BCC materials. Thus, it has long been recognized that the deformation characteristics of a metal depend upon its crystal structure and chemical composition [2].

A fundamental tenant of strain localization is that there must be some degree of microstructural inhomogeneity (e.g., phases, dislocation substructure) for strain inhomogeneity to occur [2].

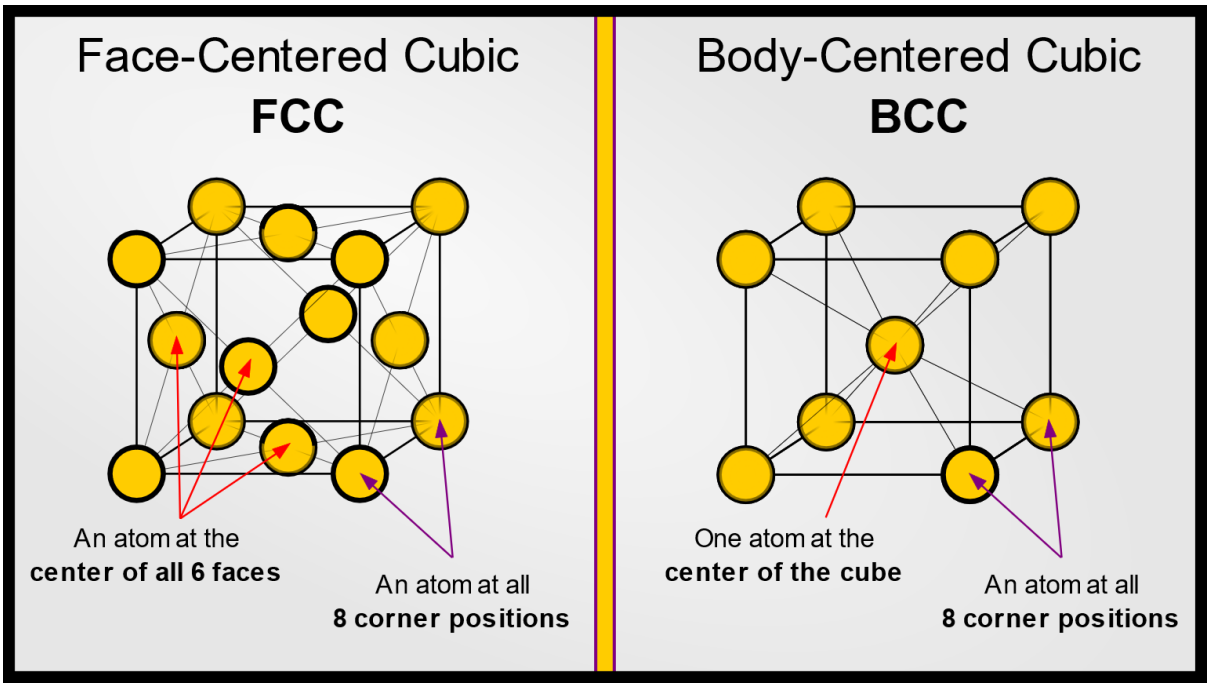

Figure 4: A comparison between different crystal lattices (FCC vs BCC)

2.2 Portevin – Le Chatelier (PLC) Theory

The Portevin Le Chatelier effect is a phenomenon in which serrated flow is observed (sometimes at a critical strain) for a given strain rate and temperature resulting in a kind of serrated stress strain curve. The PLC effect can lead to undesirable strain concentrations affecting fracture. This effect has been described by many authors to arise from a dynamic interaction between dislocations, solute atoms, and barriers such as forest dislocation, precipitates, and importantly grain boundaries including, of course grain size effects [2].

Substitutional solute atoms in aluminium usually diffuse too slowly to cause appreciable strain ageing at room temperature. However, if the concentration of vacancies is increased by plastic deformation or by quenching, the rate of diffusion may increase sufficiently to cause strain ageing during plastic deformation [3].

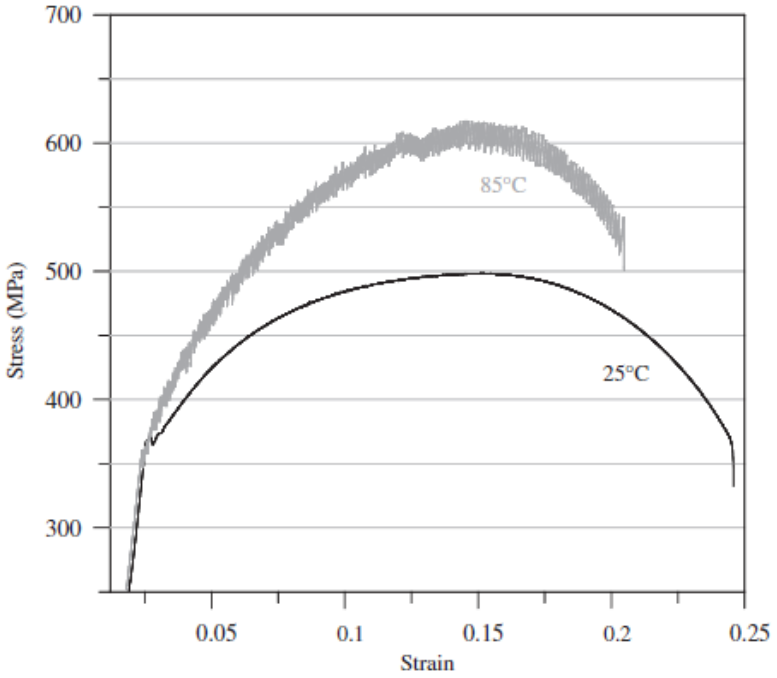

Figure 5: Regular and serrated flows of a low carbon steel strained at 25 and 85 ˚C at a strain rate of 1,6 x 10^{-6} s^{-1} [5]

It has been believed that the Portevin-Le Chatelier effects (serrated flow) in substitutional alloys are caused by interaction of solute atom with dislocation and that in various kinds of the interaction the most predominant one is due to the difference in atomic radii of component elements, that is, size effect [4].

The localized deformation associated with the PLC effect causes both cosmetic and structural problems. The PLC effect occurs in both substitutional and interstitial alloys such as alloys of aluminum, copper, zirconium, and austenitic, mild and low-carbon steels. The PLC effect affects most material properties. It increases flow stress, ultimate tensile strength and the work hardening rate. It decreases the ductility of metals with a corresponding decrease in elongation, the effective gauge cross-sectional area, the strain rate sensitivity coefficient and fracture toughness. Temperature and strain rate are the most significant external factors affecting the interactions between defects and the stability of plastic flow [5].

2.3 Types of PLC Bands

Various types of deformation bands induced by the PLC effect are known to exist; each type corresponds to a well-defined serration shape in the tensile test curve, as illustrated in the following figure. The band types are associated with the spatial-temporal organization of dislocations in the effective gauge of a specimen and are assigned as [5]:

- Type A
- Type B
- Type C

Type C bands are randomly nucleated, no propagating, or hopping bands throughout the specimen gauge and correspond to a tensile test curve with relatively consistent serrations around a certain amplitude and frequency [5].

Type B bands propagate in a gauge in an intermittent manner with roughly equal intervals. The amplitudes and frequencies in the corresponding tensile test curve appear somewhat irregular and are smaller than those of a type C curve [5].

Type A bands propagate continuously in a gauge resembling a longitudinal wave with arbitrarily located small stress drops embedded in the regular flow in the tensile test curve. Not all type A bands are alike.

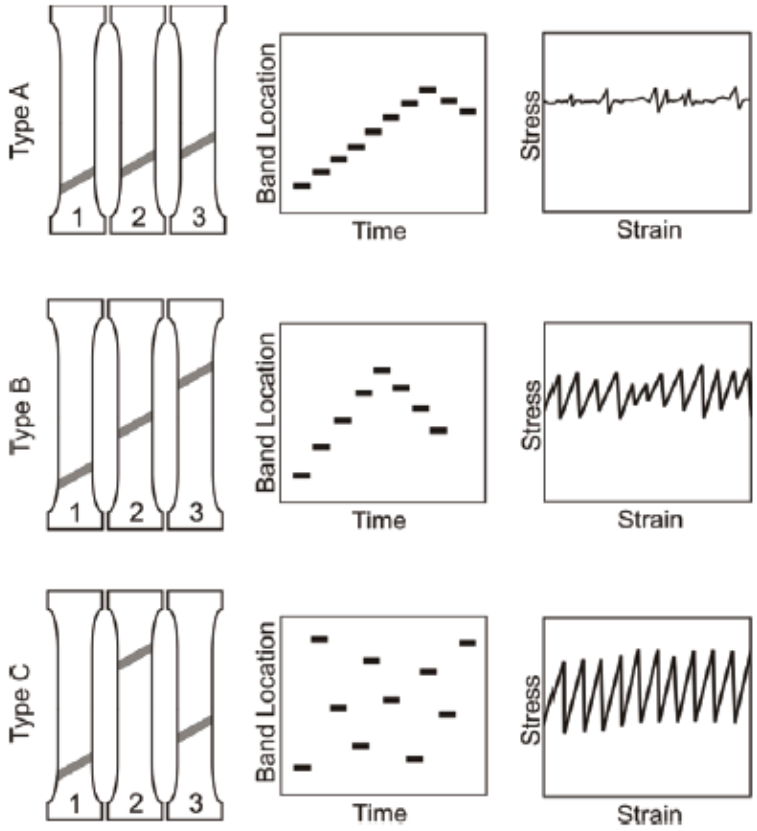

Figure 6: Schematics of motion, orientation, spatio – temporal appearances and strain – controlled tensile curve characteristics of the PLC bands [5]

Usually, higher strain rates are associated with type A bands, lower strain rates with type C bands and intermediate levels with type B bands [6]. The temperature has the opposite effect on the band type; with type C bands occurring at higher temperatures and type A bands occurring at lower ones [5].

Because the deformation bands of the PLC effect are transitional, different types of bands do not occur together except at the critical temperatures and strain rates [5].

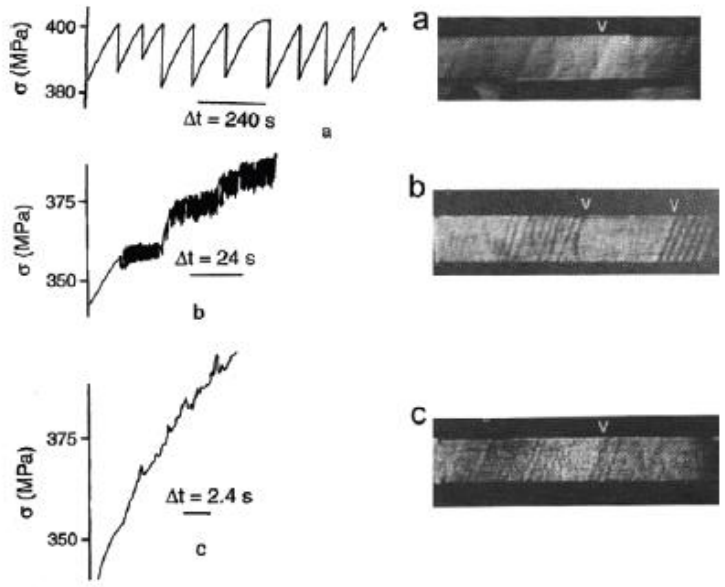

Figure 7: Stress – time curves for an Al -Mg alloy at T = 300 K showing the range from type C to type B and then to type A serrations with increasing strain rate [5]

It has also been shown by DIC that drops in the stress–strain curve are directly correlated with band nucleation and the subsequent strain buildup inside the band,. The bands remain unchanged during increases in stress, and cyclic strain accumulation occurs outside the bands shortly before a new band is generated [5].

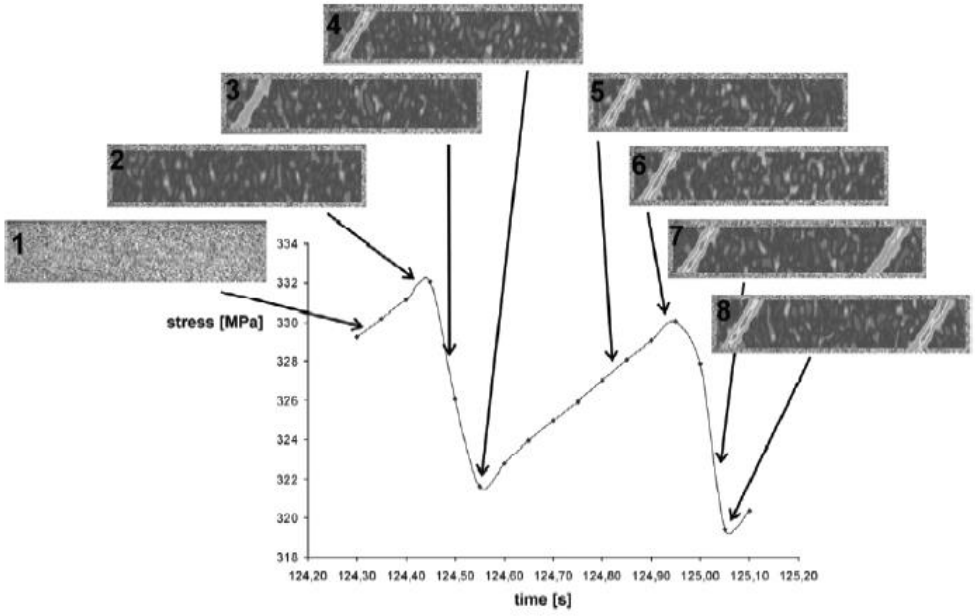

Figure 8: Band nucleation upon lowering of external stress. No significant change in strain occurs within the band when the stress is increased [5]

2.4 Lüders Lines – Yield Point Phenomenon

Lüders banding takes place during the initial part of the plastic regime of the material and results in macroscopic localized deformation. For example, in a uniaxial test on a strip it manifests as inclined bands of plasticized material that propagate from one end of the strip to the other while the stress remains nearly constant. Material behind such fronts is deformed to strains of 1–3% while ahead of them it is still elastic. When the whole specimen is consumed by Lüders deformation, the response starts to harden, and the deformation becomes homogeneous once more [7].

If the material contains zones with high structural and phase inhomogeneity, Lüders bands nucleate along the boundaries of these zones. The kinetics and morphology of the Lüders band fronts within these zones are considerably different from those observed in other areas of specimen [8].

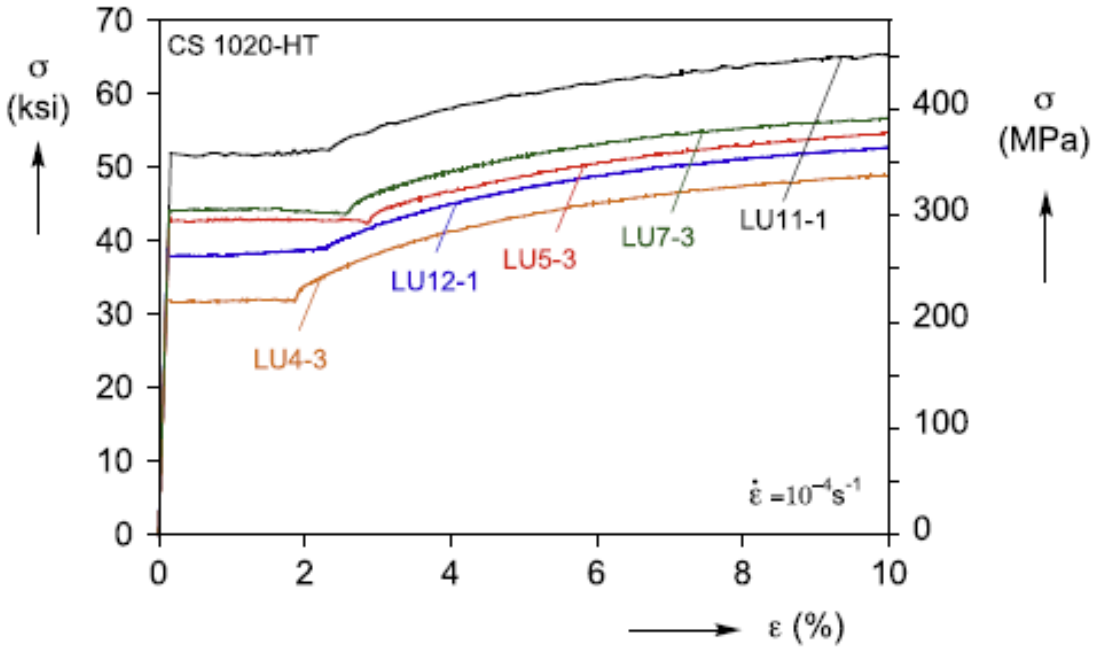

Figure 9: Stress – elongation responses from a set of tubes of various D/t and Lüders strains [8]

The elastic part of the stress-strain curve is followed by a perfectly plastic response, dubbed as the Lüders plateau, and only upon the termination of this plateau does the strain hardening portion begin [9].

Furthermore, strain rate has been shown to affect the plateau stress especially when the rate is properly measured locally in the propagating Lüders front [10].

The formation of Lüders bands, their distribution and the related features of the stress-strain curve (the sharp yield point and yield plateau) are associated with an increase in the number of mobile dislocations due to their unlocking or multiplication, as well as with the competing hardening process [8].

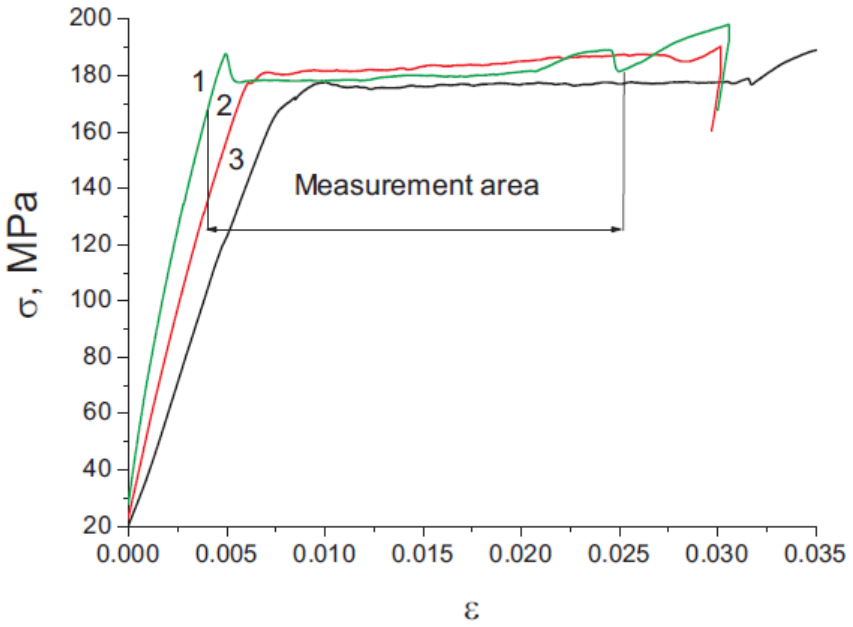

Figure 10: Stress – strain curves for homogeneous specimens [8]

It is seen that the sharp yield point may be very prominent ($\Delta\sigma \approx 10\ MPa$, curve 1), not prominent ($\Delta\sigma \approx 3\ MPa$, curve 3), or absent at all (curve 2). Irrespective of this, the Lüders band propagation is observed in all yield plateaus in all cases [8].

The Lüders strain is affected by the applied strain rate, solute concentration, test temperature, and the grain size. The conditions affecting the occurrence of an upper yield point have been most fully investigated in the case of iron and steel, and of these the most important are: rate of application of load, shape of test-piece, axial loading and heat treatment of the metal. The value of the upper yield point may, under favourable conditions, be raised momentarily above that of the breaking stress under a static test. The value of the lower yield is less affected by the conditions enumerated above and remains approximately constant for the material [11].

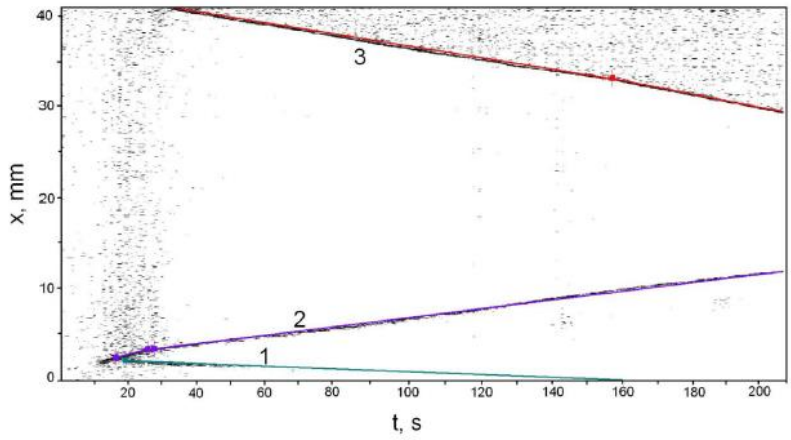

Figure 11: A chronograph of the propagation of fronts of Lüders band

All fronts of both bands move at interrelated velocities. When one front stops, the velocity of the other (or others) increases, as is seen in the chronograph [8].

2.5 Types of Lüders Lines

Two types of Lüders Lines exist, and these are classified as:

- Type A
- Type B

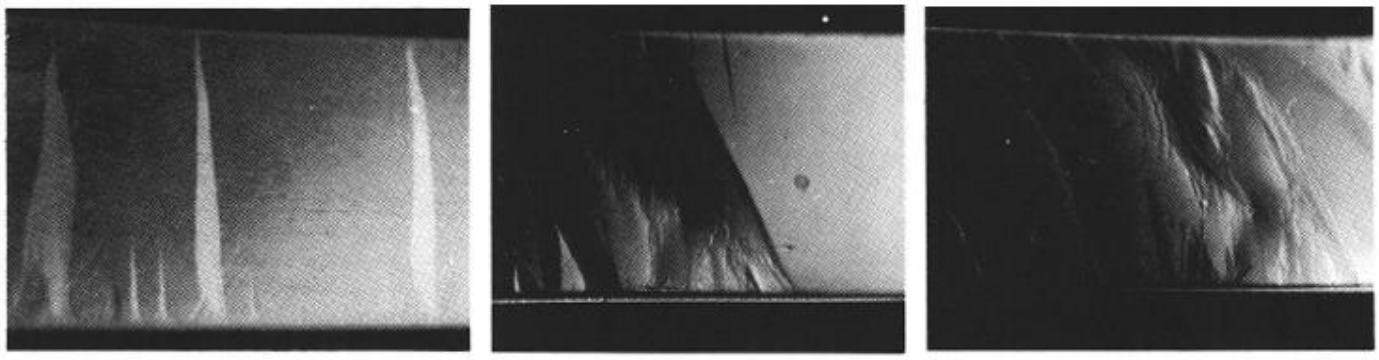

Image 2: Type A Lüders Lines

Type A lines result in the "flamboyant", "random" or "wedge"-shaped markings. Type B lines are symmetric when they appear in a plastically strained, uniaxially stressed strip or sheet. This latter type is the result of dynamic strain aging or the Portevin-le Chatelier effect, and these lines are dependent of microstructure. They are sensitive to the deformation conditions (temperature and strain rate) and to composition [12].

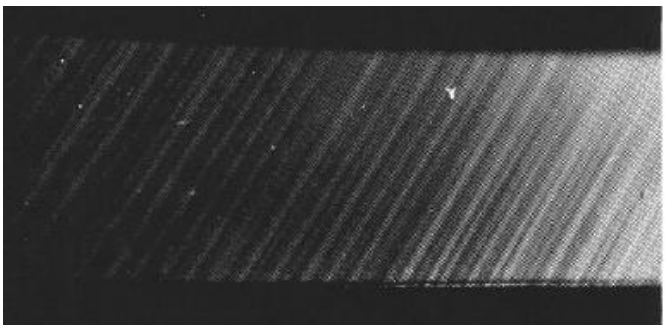

Image 3: Typical Type B Lüders Lines

The drop in load increases in size (as does the depth of the type B line on the surface of the specimen) as straining continues. Type B lines are always straight and at an angle of approximately 55° to the applied load. Often, dependent on machine stiffness, there is a plateau or reduced rate of hardening in the stress-strain curve until all the surface is covered by type B lines or further development is impeded by two oppositely inclined systems colliding [12].

Type B lines are due to the repeated pinning of dislocations by diffusion of magnesium atoms to the dislocation (strain aging or Portevin-le Chatelier effect) [12].

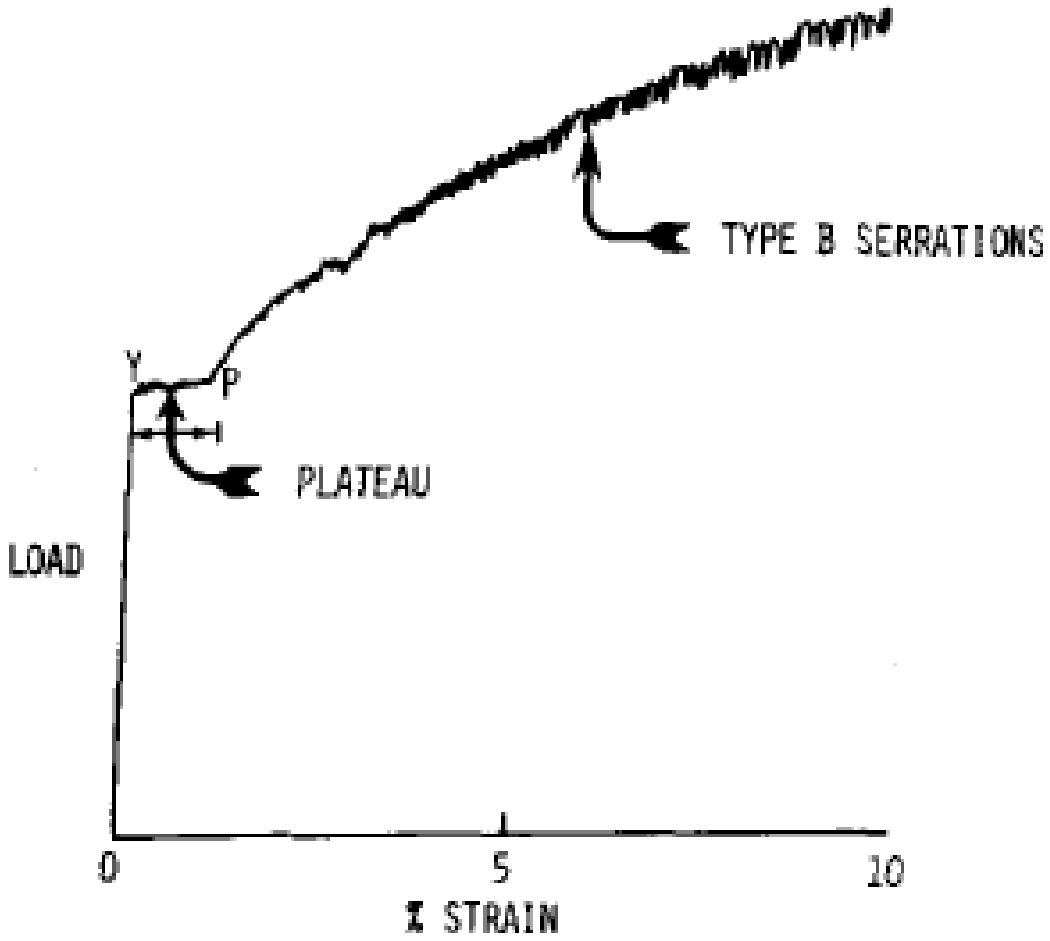

Figure 12: Tensile load – strain curve of a highly formable aluminium alloy. Type A Lüders Lines form during plateau region (YP)

Prominent type A or B lines cannot be successfully hidden with paint unless many coats and much careful sanding are employed. Grinding out Lüders lines is also extremely difficult, particularly if any ghosts of the lines are to be avoided [12].

The mechanisms of Lüders lines formation are not completely understood, though both type A and B lines are due to the interaction of magnesium atoms with dislocations as for an aluminium alloy, not for all materials. Magnesium atoms, which are larger than aluminum atoms, lower their energy by occupying lattice sites close to the missing half plane of atoms in the core of a dislocation. By occupying such a site they will increase the force necessary to move the dislocations and, hence, tend to "pin" the dislocation. If all or most available dislocations are so pinned, then on attempting to deform such a material no plastic deformation will occur until loads considerably higher than those necessary to move unpinned dislocations are applied.

As always happens in a tensile specimen (or in a pressing), somewhere the loads are slightly higher than at other places and dislocations will be pulled away from the pinning atoms at these points. Now such dislocations can keep moving at a reduced load since they are no longer pinned; thus, a burst of deformation occurs at one locality [12].

2.6 How to avoid Lüders Lines

Type A lines can be avoided by introducing unpinned dislocations (by cold working) after annealing, or by unpinning existing dislocations. Cold work, however, is not readily controlled at low levels of working and results in a considerable loss of formability with 5 or 10% cold rolling. Such processing will not eliminate the formation of type B lines [12].

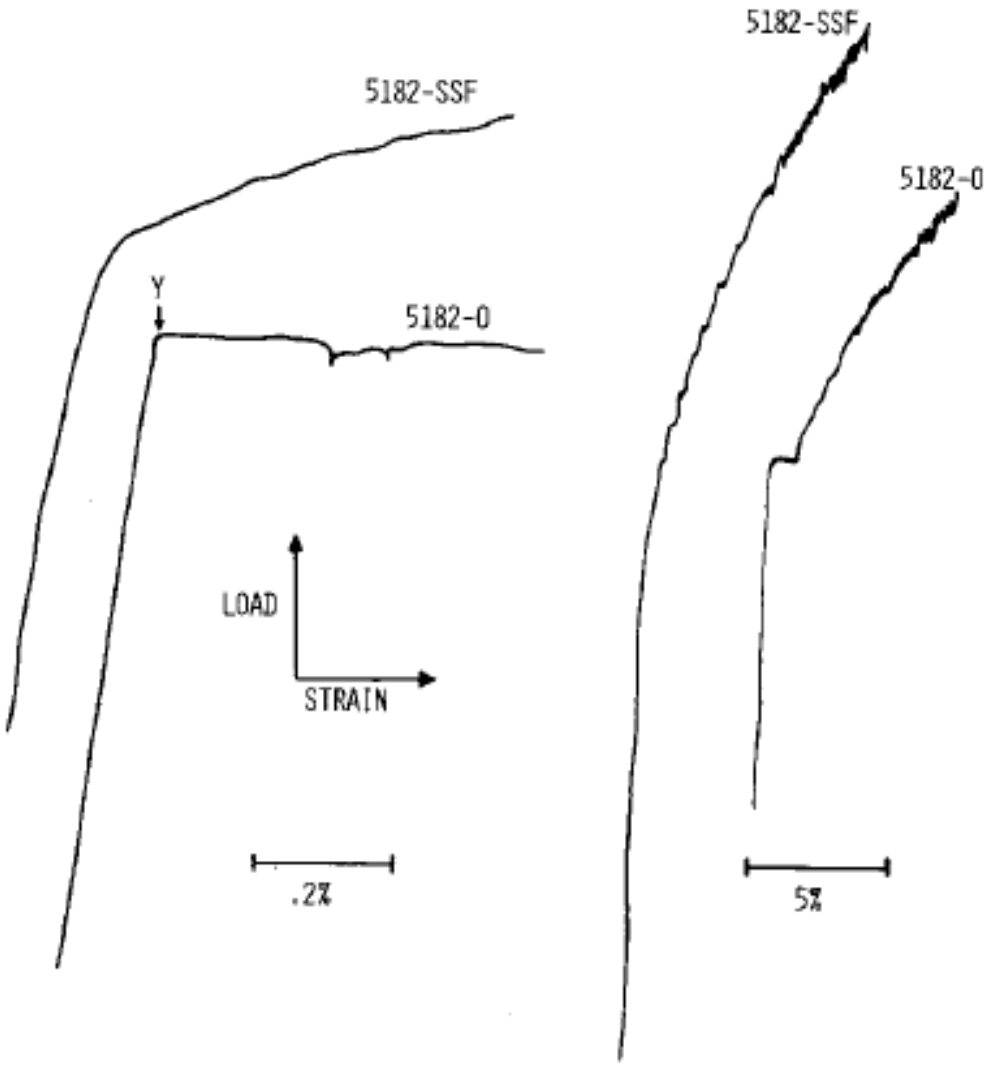

Figure 13: Load – strain curves of 5182 – SSF and 5182 – 0 (Aluminium Alloys) at two strain magnifications. Note that -SSF curve is smooth at the yield point – no indication of a plateau. Type B serrations are evident in both materials at higher strains.

At high strain rates (>1 s^{-1}) no type B Luder lines are formed in a tensile strip. At high temperatures and low strain rates magnesium atoms can migrate (diffuse) with the dislocations; thus, there is no sudden breaking away of dislocations and hence, type B lines do not form. At low temperatures and high strain rates diffusion of magnesium atoms to dislocations is so slow that repeated pinning is not possible; thus, again type B lines do not form [12].

2.7 PLC Theory vs Lüders Effect

The induced heterogeneous deformation can be classified into two general categories:

- Lüders Effect and
- Portevin -Le Chatelier (PLC) Effect.

These effects are governed by different microscopic mechanisms. The PLC effect is typically attributed to dynamic interactions between mobile dislocations and diffusing solutes (dynamic strain ageing - DSA).

On the other hand, the Lüders effect results from both the dislocation pinning/unpinning effect arising from Cottrell atmosphere constraints and the collective or self-organized dislocation multiplication and motion [13].

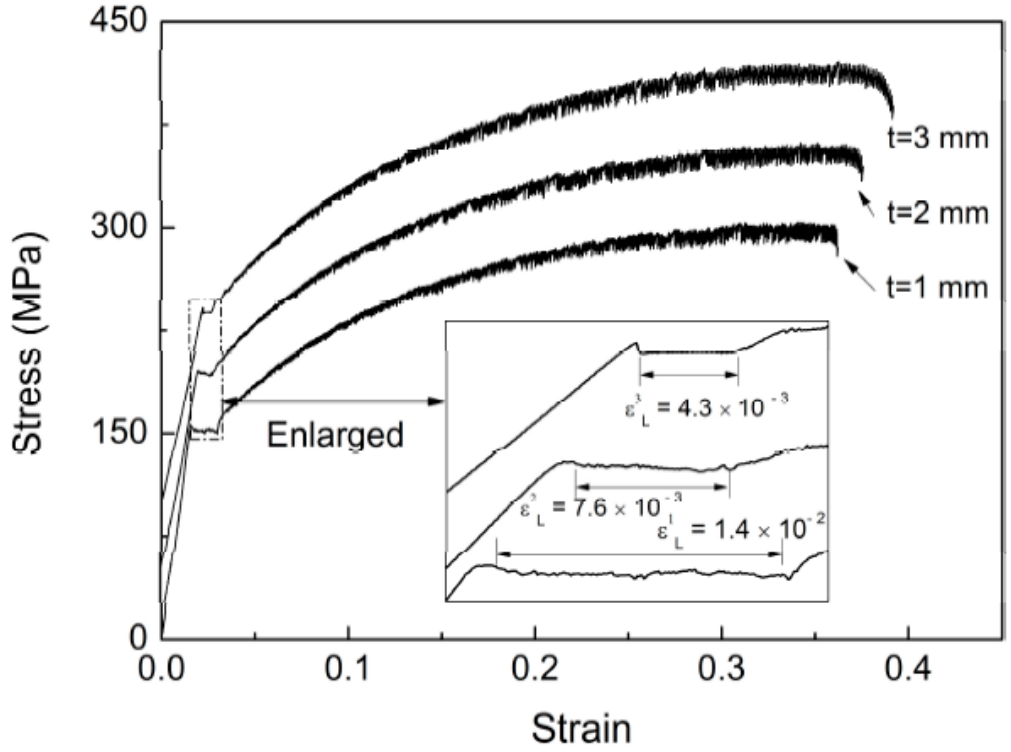

Figure 14: Engineering stress – strain curves for specimens with different thicknesses [13]

A PLC effect is visible almost immediately after the Lüders effect. It consists of a serrated flow with numerous stress drops. These serrations are of similar characteristics for the three tests. These results indicate that the specimen thickness influences the Lüders effect. In contrast, the PLC effect seems not to be influenced by the specimen thickness [13].

As a form of plastic instability, the Lüders effect differs compared to the PLC effect mainly on the serration morphology and the strain-localized band propagation. Generally, the continuous sweep corresponds to the smooth plateau of the Lüders effect; nevertheless, the propagation of PLC bands can be continuous, hopping, and even random along the sample with abrupt serrations [13].

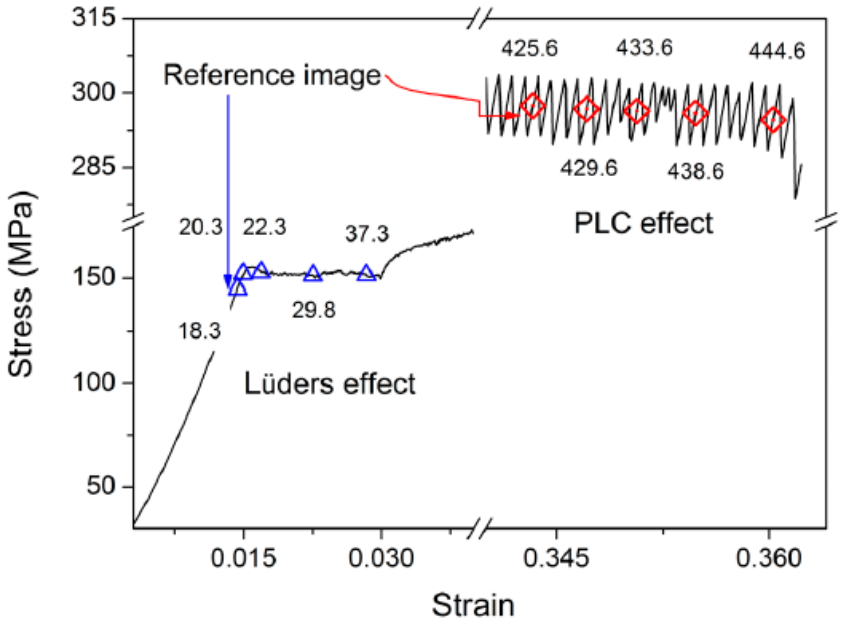

Figure 15: Stress – strain curve that shows the difference between Lüders & PLC Effect [13]

The DIC results revealed that the strain in the tensile direction of the PLC band is much higher than that of the Lüders. The Lüders band and the PLC band are similar in macroscopic deformation, which probably implies the same deformation mode [13].

Ludering, also known as yield-point elongation, occurs at both room temperature and 223 K, as can be seen in the stress–strain curves shown in the following figure. At room temperature, DSA takes over as soon as Ludering is complete, leading to the development of an inhomogeneous distribution of solute atoms and dislocations [14].

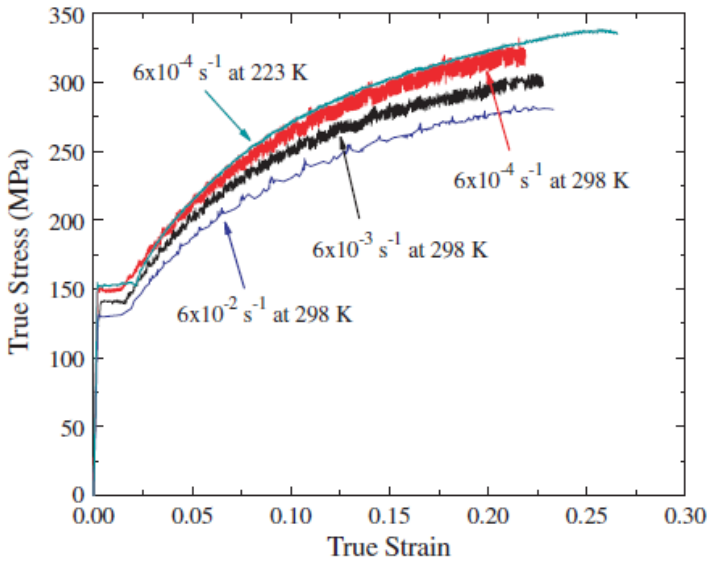

Figure 16: True stress – true strain curves of AA5754 alloy at various strain rates and temperature

At 223 K, however, Ludering is not followed by DSA. Instead, the PLC effect is suppressed and thus solute atoms do not segregate into temporarily arrested mobile dislocations [14].

2.8 What is the cause of Lüders Lines' appearance due to bending tests?

Most researchers are referred to heterogeneous localized deformation during a uniaxial tensile test by presenting the distinctive regions on the stress – strain $\sigma - \varepsilon$ graph. What we realize is that PLC effect means automatically serrated flow on such a figure, which is a phenomenon that does not exist in our case. And only that, serrated flow is required during strain – hardening at relatively high temperatures, not a cold process (e.g., tensile test at 298 K)

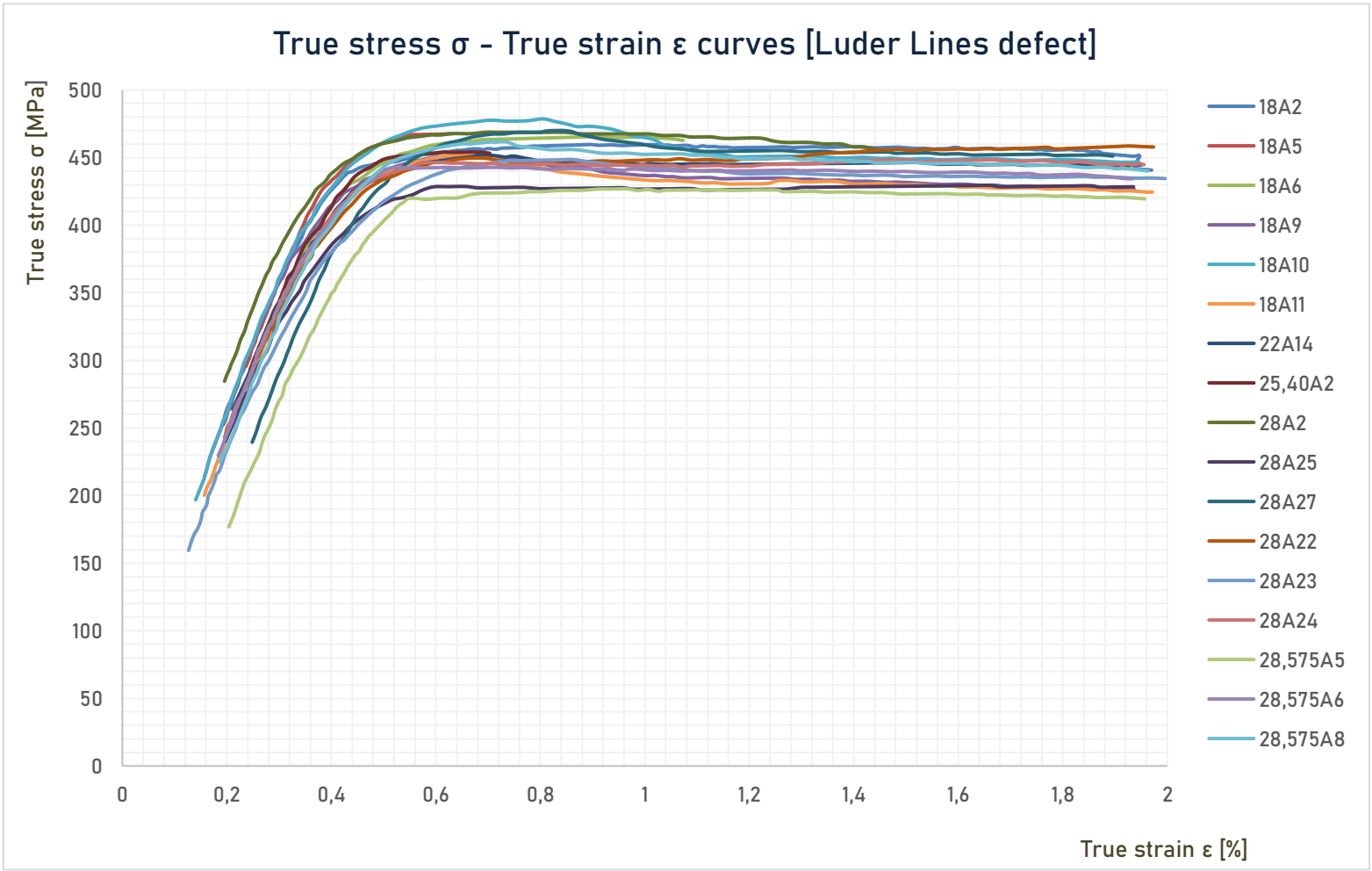

Figure 17: True stress – true strain curves of hard copper tube specimens [Lüders Lines defect]

According to the upper figure, almost all samples, that suffer from Lüders Lines defect, form together a strong stress plateau, starting from the true strain $\varepsilon = 1\,\%$. In this region stress remains almost constant although there seems to be that true stress σ is decreasing while true strain ε is increasing.

Finally, we conclude that the studied defect is manifested due to Lüders effect – Yield point elongation and this is the unique cause of the development of Lüders Lines due to a bending test. What can reinforce this argument is the fact that "Lüdering occurs at both room temperature".

There might be a little doubt of this interpretation because of the awareness that the Lüders bands and the PLC bands look alike in macroscopic scale!

3. Description of the experimental procedure

3.1 Why is the copper tubes' bending essential?

The use of copper tubes for the distribution of drinking water, for the conveyance of domestic and medical gases, and for heating, conditioning and refrigeration needs is widely spread and well established [15].

This is mainly due to the mechanical, technological, and chemical-physical properties of copper, in its $Cu-DHP$ composition (min. 99,90% pure copper). From a technological point of view, this material features good cold formability and high resistance to working pressures. A very low permeability makes copper tubes suited for the transportation of gases, both for civil and medical uses, and of liquid fuels [16].

For all these uses and applications, copper tubes shall not be straight, but we should give them another form such as an elbow – like shape, like the following picture:

Image 4: A copper tube shown after the bending test

We would wish to investigate experimentally the bending ability of the copper tubes because of their good formability and high elongation until fracture. That is why we perform many bending tests using 3 different kinds of pure copper with respect to the mechanical strength, retaining the same material properties such as chemical composition:

- Soft / Annealed Copper (R220)
- Semi – Hard (R250)
- Hard (R290)

Generally speaking, the softer (more ductile) the copper tubes' material is, the more easily the bending test can be executed. In this way, many defects are more likely to be prevented and as a result clear bending could be occurred.

3.2 Types of Bending

According to the literature and industrial experience, there are many different types of bending methods. Basic bending techniques are listed below:

- Rotary - Draw Bending
- Compression Bending
- Roll Bending; and
- Stretch Forming

Each type characteristically has certain applications and limitations with regard to the kinds of bends it produces and the maximum angle of bend it achieves as indicated in the following table. Selection of a bending process for tubing depends on [17]:

- Quality of bend and production rate required; and
- Diameter, Wall Thickness, and Minimum bend radius desired.

Capabilities of bending methods		
Bending Process	**Types of Bends usually accomplished**	**Maximum Angle of Bend**
Draw	Single, multiple, compound	Up to 180 °
Compression Ram and press Manual	Single Series of different bend angles Single, compound, spiral	Less than 180 ° Up to 165 ° 360 °
Roll	Circular, spiral, helical	360 °
Stretch Linear Radial	 Variable curvature Circles, ovals, rectangles, spirals	 180 ° 360 °

Table 1: Capabilities of bending techniques

The method of choice for bending our copper tubes is the rotary draw process due to its repeatability and productivity.

3.3 Rotary – Draw Bending & Tooling

Draw bending is the most common method used on rotary-type bending machines, which can be powered (hydraulic, pneumatic, electric/mechanical), manual, or numerically controlled. These machines handle about 95% of tube-bending operations [17]. The essential tooling for draw bending consists of the rotating bending form (or bend die), clamp(ing) die, and pressure die as shown in the following schematics.

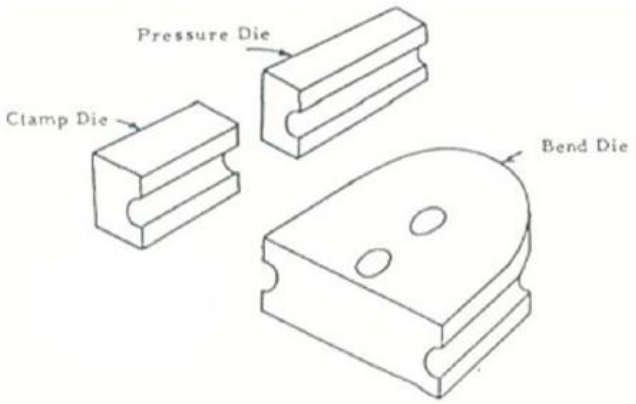

Image 5: Basic Tooling at Draw Bending (separately)

A bend die, clamp die, and pressure die are the minimum essentials to bend a tube properly. In draw bending, the bend die helps to prevent the tube from flattening and forms a given radius of bend [18]. The workpiece is secured to the bending form by the clamping die. As the bending die rotates, it draws the workpiece against the pressure die and, if necessary to prevent wall collapse, over an internal mandrel. The pressure die may remain fixed or move with the workpiece to eliminate the friction of sliding contact [17].

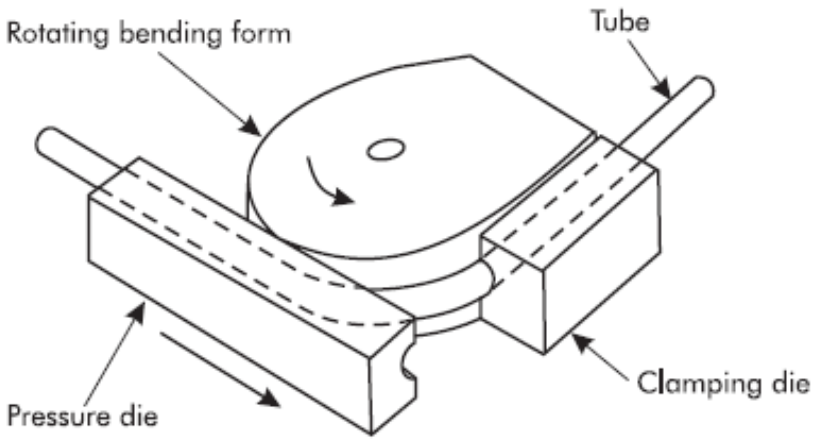

Image 6: Schematic of Rotary - Draw Bending Process at the end of the test

Draw bending is the most versatile and flexible bending method. It is used to make single bends up to 180° using standard tools and multiple or compound bends using special tools (for example, a mandrel). It also provides the close control of metal flow necessary for small-radius and thin-wall tube bending [17].

3.4 Benders used for the experimental procedure

To evaluate the bending capability of the copper tubes with respect to the outer diameter OD, the wall thickness WT and the bending radius CLR we ran through many different experiments that took place at Halcor's Quality Laboratory. Consequently, it was about an on – hands approach and we had the opportunity to realize the mechanical behaviour of the material and the way that gets deformed in real conditions.

We utilized two bender types that modify the parameters of the bending process such as the centre line radius or the amount of friction among the tube and the various dies. These benders are powered electrically, and they are called:

- REMS – CURVO (yellow one)
- Virax – Epernay (red one)

This design of experiment allows us to research the influence of a different machine on the bending outcome, while bending exactly the same tube as for the geometry (OD, WT) and material properties.

Image 7: Top view of Virax - Epernay bender

Image 8: Top view of REMS - Curvo bender

We present two distinctive screenshots from the place that labour work took place. The first one depicts the metallic case that REMS – Curvo bender is placed and contains all the essential accompanying and removable parts. The second one shows as the workbench before a soft tube's (R220) bending test is going to be executed.

Image 9: REMS – CURVO removable dies according to the outer diameter of the tube

Image 10: Picture shot from the workbench

Straight away after finishing the bending test of every single copper tube, we right down its geometrical characteristics, data regarding the material code, the order number, the defect which showed up and the bending machine. We can present a piece of paper on which we note all the aforementioned information.

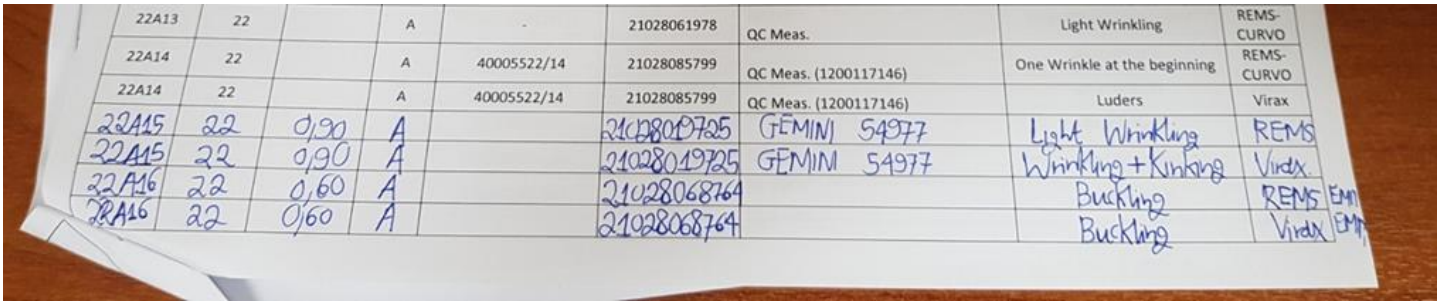

22A13	22		A	-	21028061978	QC Meas.	Light Wrinkling	REMS-CURVO
22A14	22		A	40005522/14	21028085799	QC Meas. (1200117146)	One Wrinkle at the beginning	REMS-CURVO
22A14	22		A	40005522/14	21028085799	QC Meas. (1200117146)	Luders	Virax
22A15	22	0,90	A		21028019725	GEMINI 54977	Light Wrinkling	REMS
22A15	22	0,90	A		21028019725	GEMINI 54977	Wrinkling + Kinking	Virax
22A16	22	0,60	A		21028068764		Buckling	REMS
22A16	22	0,60	A		21028068764		Buckling	Virax

Image 11: Taking notes after every single experiment

3.5 Possible Defects because of bending

Generally, the potential defects that can show up due to a rotary – draw bending test are shown in the following list. In terms of geometry, the bending force needed is rising according to the outer diameter OD and the bending difficulty becomes more and more apparent. On the other hand, in cases of very low values of the wall thickness WT, the tube may collapse during the bending test.

- Cracking: Fracture of the tube as the bending force has exceeded the ultimate tensile strength and the elongation at break.
- Flattening: Change of the cross – section's shape of the tube from circle to ellipse and levelling of the exterior collateral surface (Very rare defect)
- Wrinkling: A fold – like defect on the external surface of the tube
- Kinking: Localized dents on the exterior surface of the copper tube
- Buckling: When a cross – section of the tube is reduced significantly.
- Lueders Lines: Diagonal slotted lines on the internal and the external copper tube's surface, which are parallel along the length of it ---> This defect is very serious and can cause many aesthetic and functional problems as the wall thickness decreases locally, degrading the mechanical properties of the bent tube.

We present a photographic gallery which visualizes most of the defects explained before:

Image 12: Defects due to bending: (1) Buckling, (2) Kinking, (3) Lueders Lines, (4) Wrinkling, (5) Crack

3.6 Lueders Lines Photos

The current diploma thesis is focused on the Lueders Lines' investigation as it is the most interesting defect in terms of innovation and research. We would wish to assess deeply the aforementioned defect and that is why we present more distinctive and detailed photos right down:

Image 13: Detailed Lueders Lines photos (Front & Top View)

3.7 Data Gathering – Collection

Finally, the entire information is collected into a calculation sheet (Excel file .xlsx), that includes useful quantitative and qualitative data for all the specimens. We write down for each specimen the following properties:

- Sample's Code (e.g., $ODA\#$)
- Geometrical Parameters (OD_{av}, WT_{av})
- Material Characteristics (Yield Point $R_{p_{0,2}}, R_{p_1}$, Maximum stress at break R_m, Elongation at break $A50$ (%), Hardness HV)
- Bending Radius CLR
- Bending Outcome = Type of Defect or Clear Bending
- Bender Type (REMS – Curvo or Virax)

In this way, we manage to correlate the mechanical behaviour of the samples with their degree of formability and specially during a bending test. We give two screenshots from the Excel File, in which we keep the raw information as for the Lueders Lines Project [LLP]:

Sample's Code	ODmin	ODmax	ODav	Smin.	Smax.	Sav.	Rp0,2	Rp1	Rm	HV	Elongatio	Grain Size	CLR	Outcomes	Bender Types
15A6	14,97	15,02	14,995	0,61	0,63	0,620	421,2		443	129	4,8	-	55	No Wrinkling	REMS-CURVO
15A10	14,98	15,02	15,000	0,52	0,54	0,530	436,3		451	131	6,6		55	Light Kinking	REMS-CURVO
15A11	14,96	15,04	15,000	0,64	0,66	0,650	461,4	463,3	465	128	6,8		55	Light Wrinkling	REMS-CURVO
15A11	14,96	15,04	15	0,64	0,66	0,65	461,397	463,3	465	127,5	6,8		45	Buckling	Virax
15A12	14,95	15,05	15,000	0,72	0,78	0,750	438,6		445	129	4,3		55	OK	REMS-CURVO
15A12	14,95	15,05	15	0,72	0,78	0,75	438,624	-	445	129,4	4,3		45	Wrinkling	Virax
15A13	14,99	15,03	15,010	0,51	0,56	0,535	441,6	475,3	476	139	12,3		55	Buckling	REMS-CURVO
15A13	14,99	15,03	15,01	0,51	0,56	0,535	441,584	475,3	476	139,1	12,3		45	Buckling	Virax
15A15	15,01	15,06	15,035	0,45	0,46	0,455	444,5	455,1	465	139	7,7		55	Buckling	REMS-CURVO
15A15	15,01	15,06	15,035	0,45	0,46	0,455	444,494	455,1	465	139,4	7,7		45	Crack	Virax
15A16	14,98	15,00	14,990	0,68	0,71	0,695	464,3	463,1	473	140	9,0		55	OK	REMS-CURVO
15A16	14,98	15	14,99	0,68	0,71	0,695	464,25	463,1	473	140,4	9		45	Buckling + Cracking	Virax
15A17	14,96	15,02	14,990	0,68	0,70	0,690	443,1	453,0	456	132	10,0		55	OK	REMS-CURVO
15A17	14,96	15,02	14,99	0,68	0,7	0,69	443,112	453	456	131,7	10		45	Buckling	Virax
15,875A2	15,84	15,88	15,86	0,73	0,75	0,74	455,09	450,9	460	137	7,7		63	OK	REMS-CURVO
15,875A2	15,84	15,88	15,86	0,73	0,75	0,74	455,09	450,9	460	137	7,7		48	OK	Virax

Table 2: 1st Screenshot from the Excel file retaining part of the raw data

28A25	27,96	28,03	27,995	0,87	0,92	0,895	425,150	435,300	436	120,7	7,2		102	OK	REMS-CURVO
28A25	27,96	28,03	27,995	0,87	0,92	0,895	425,150	435,300	436	120,7	7,2		84	Luders and Kinking	Virax
28A27	27,95	28,05	28	0,75	0,81	0,780	464,064	461,700	467	138,1	9,7		102	Light Kinking + Luder Lines	REMS-CURVO
28A27	27,95	28,05	28	0,75	0,81	0,780	464,064	461,700	467	138,1	9,7		84	Kinking + Luder Lines	Virax
28,575B1	28,54	28,59	28,565	0,78	0,89	0,835	448,000		456	133	4,6	-	132	Wrinkling 33% + Luder Lines	?
28,575A5	28,52	28,56	28,54	0,87	0,92	0,875	423,704	435,300	437	129	8,4		115	Luder Lines	REMS-CURVO
28,575A6	28,52	28,57	28,545	0,86	0,9	0,880	441,004	443,300	445	138,1	6,4		115	Luder Lines	REMS-CURVO
28,575A8	28,54	28,61	28,575	0,92	0,96	0,940	458,411	457,700	464	130,9	7,2		115	Luder Lines	REMS-CURVO
35A5	34,96	35,06	35,01	0,99	1,03	1,01	403,7		450	125,6	8,5	-	140	Light Wrinkling	REMS-CURVO
35A7	34,97	35,07	35,02	1,07	1,1	1,085	407,66	438,8	439	140,4	5,5		140	OK	REMS-CURVO
35A8	34,99	35,09	35,04	1,07	1,11	1,09	404,101	434,9	436	135,3	7,65		140	OK	REMS-CURVO
35A10	34,97	35,07	35,02	0,97	1,05	1,01	379,735	403,9	404	136,4	5,8		140	OK	REMS-CURVO
35A11	34,95	35,06	35,005	0,88	0,92	0,9	414,123	440,4	441	139,4	5,6		140	Flattening	REMS-CURVO
35A12	35,03	35,07	35,05	1	1,07	1,035	404,471	454,4	455	136,2	13		140	OK	REMS-CURVO

Table 3: 2nd Screenshot from the Excel file including part of the raw data

4. Creative utilization of raw experimental data

4.1 Qualitative Observations

4.1.1 Outer Diameter's (OD) Influence

OD = 15 mm | OD = 15,875 mm | OD = 16 mm | OD = 25,40 mm

All tubes with nominal OD (Outer Diameter) equal to either $OD = 15\ mm$ or $OD = 15{,}875\ mm$ ($\frac{5}{8}$") or $OD = 16\ mm$ or $OD = 25{,}40\ mm$ do **not** suffer from Luder Lines regardless of the bender type. The principal defects are Buckling and Kinking. Only 1 sample has appeared Light Wrinkling. The referenced specimens are:

Sample's Code	ODav	Sav.	Rp0,2	Rp1	Rm	HV	Elongatio	Grain Si	CLR	Outcomes	Bender Type
15A17	14,990	0,690	443,1	453,0	456	132	10,0		55	OK	REMS-CURVO
15A17	14,99	0,69	443,112	453	456	131,7	10		45	Buckling	Virax
15A16	14,990	0,695	464,3	463,1	473	140	9,0		55	OK	REMS-CURVO
15A16	14,99	0,695	464,25	463,1	473	140,4	9		45	Buckling + Cracking	Virax
15A6	14,995	0,620	421,2		443	129	4,8	-	55	No Wrinkling	REMS-CURVO
15A10	15,000	0,530	436,3		451	131	6,6		55	Light Kinking	REMS-CURVO
15A11	15,000	0,650	461,4	463,3	465	128	6,8		55	Light Wrinkling	REMS-CURVO
15A11	15	0,65	461,3969	463,3	465	127,5	6,8		45	Buckling	Virax
15A12	15,000	0,750	438,6		445	129	4,3		55	OK	REMS-CURVO
15A12	15	0,75	438,6238	-	445	129,4	4,3		45	Wrinkling	Virax
15A13	15,010	0,535	441,6	475,3	476	139	12,3		55	Buckling	REMS-CURVO
15A13	15,01	0,535	441,5836	475,3	476	139,1	12,3		45	Buckling	Virax
15A15	15,035	0,455	444,5	455,1	465	139	7,7		55	Buckling	REMS-CURVO
15A15	15,035	0,455	444,4939	455,1	465	139,4	7,7		45	Crack	Virax
15,875A7	15,855	0,56	474,656	-	480	139,1	0,2		63	Kinking	REMS-CURVO
15,875A7	15,855	0,56	474,656		480	139,1	0,2		48	Kinking	Virax
15,875A2	15,86	0,74	455,09	450,9	460	137	7,7		63	OK	REMS-CURVO
15,875A2	15,86	0,74	455,09	450,9	460	137	7,7		48	OK	Virax
15,875A4	15,865	0,71	456,008	-	461	137,6	8,8		63	OK	REMS-CURVO
15,875A4	15,865	0,71	456,008		461	137,6	8,8		48	OK	Virax
16A4	16	0,47	453,8825	461,8	463	117,2	9,7		60	Buckling	REMS-CURVO
16A4	16	0,47	453,8825	461,8	463	117,2	9,7		48	Buckling	Virax

Table 4: Raw experimental data for OD = 15 mm - 25,40 mm

We can see the respective samples on the picture above:

- $\boldsymbol{OD = 15\ mm}$: 8 distinct samples (15A6, 15A10, 15A11, 15A12, 15A13, 15A15, 15A16, 15A17). 2 of them (more specifically 15A6 & 15A10) have been subjected to bending test only once with the aid of REMS – CURVO bender. So, we have 14 samples overall of nominal outer diameter $OD = 15\ mm$.
- $\boldsymbol{OD = 15{,}875\ mm}$ ($\frac{5}{8}$"): 3 distinct samples (15,875A2, 15,875A4, 15,875A7) bent with both REMS and Virax. Overall 6 samples
- $\boldsymbol{OD = 16\ mm}$: Only 1 sample (16A4), which has been bent twice -> 2 samples
- $\boldsymbol{OD = 25{,}4\ mm}$: Only 2 samples (25,40A1, 25,40A2), which have been bent only once (REMS - CURVO)

So, we have to focus on the tubes' bending with nominal $OD = 16\ mm$ & $OD = 25{,}4\ mm$ in order to investigate their behaviour. Additional experiments regarding the tubes of $OD = 15\ mm$ and $OD = 15{,}875\ mm$ ($\frac{5}{8}$") may be needed to confirm the trend of the Luder Lines' absence.

Luder Lines' appearance: **0/13 (or 0/23)**
NO Luder Lines: **13/13 (or 23/23)**

OD = 18 mm

It is observed that bent copper tubes of nominal outer diameter $OD = 18\ mm$ do **not** manifest any Luder Lines, if they are bent with the aid of REMS – CURVO bender. For some reason, REMS – CURVO bender does **not** cause any defect according to our samples. We do not know if this trend is incidental or not, because it should be examined furtherly with more experiments. All problems (Kinking, Buckling, Luder Lines) appear because of the Virax bending machine in this case. We have to investigate the different behaviour of the material due to other type of bender.

$OD = 18\ mm$: 8 distinct samples (18A2, 18A4, 18A5, 18A6, 18A8, 18A9, 18A10, 18A11) bent with 2 bender types -> 16 samples

Luder Lines' appearance: **7/8 (or 7/16)**
NO Luder Lines: **1/8 (9/16)**

Consequently, $OD = 18\ mm$ seems to be pretty prone to Luder Lines defect because of the bending test, especially when it is executed with Virax machine.

18A9	17,990	0,650	446,5	445,2	454	136	7,8		70	OK	REMS-CURVO
18A9	17,99	0,65	446,498	445,2	454	135,6	7,8		54	Kinking + Slight Luder Lines	Virax
18A11	17,990	0,700	447,0	439,6	453	126	9,7		70	OK	REMS-CURVO
18A11	17,99	0,7	446,986	439,6	453	126,2	9,7		54	Kinking + Slight Luder Lines	Virax
18A10	18,000	0,605	467,8	459,8	477	143	9,6		70	OK	REMS-CURVO
18A10	18	0,605	467,776	459,8	477	142,6	9,6		54	Kinking + Luder Lines	Virax
18A6	18,000	0,700	458,7	-	463	119	8,2		70	OK	REMS-CURVO
18A6	18	0,7	458,6607	-	463	118,7	8,2		54	Slight Luders, Light Wrinkling, Kinking	Virax
18A8	18,005	0,610	447,9	462,9	464	126	8,3		70	OK	REMS-CURVO
18A8	18,005	0,61	447,9253	462,9	464	126,2	8,3		54	Buckling	Virax
18A5	18,005	0,735	472,6	-	473	120	7,2		70	OK	REMS-CURVO
18A5	18,005	0,735	472,5625	-	473	120,2	7,2		54	Slight Luders	Virax
18A2	18,010	0,735			459	120	12,0	-	70	No Wrinkling	REMS-CURVO
18A2	18,01	0,735			459	120,2	12	-	54	Luder Lines (with some crack)	Virax
18A4	18,015	0,610	448,3		459	131	6,0		70	No Wrinkling	REMS-CURVO
18A4	18,015	0,61	448,29		459	131,4	6		54	Kinking with Luder Crack	Virax

Table 5: Raw experimental data for OD = 18 mm

OD = 22 mm

Luder Lines' defect is manifested again only due to **Virax** bender for two samples. All copper tubes appear problems because of bending test. It might be different foe each bender for the same tube.

$OD = 22\ mm$: 4 distinct samples (22A7, 22A11, 22A14, 22A16). The specimen named 22A7 was bent with Virax machine only -> 7 samples

Luder Lines' appearance: **2/4 (or 2/7)**
NO Luder Lines: **2/4 (5/7)**

22A16	21,980	0,560	450,2	446,0	456	137	9,7		77	Buckling	REMS-CURVO
22A16	21,98	0,560	450,242	446,000	456	137,1	9,7		66	Buckling	Virax
22A7	21,990	0,655				136			77	No Wrinkling	REMS-CURVO
22A11	22,020	0,605	454,5		458	137	3,8	-	77	Light Waved Wrinkling	REMS-CURVO
22A11	22,02	0,605	454,500		458	137,3	3,8	-	66	Luder Crack	Virax
22A14	22,025	0,700	448,3	457,0	457	128	6,2		77	One Wrinkle at the beginning	REMS-CURVO
22A14	22,025	0,700	448,281	457,000	457	127,6	6,2		66	Luders	Virax

Table 6: Raw experimental data for OD = 22 mm

OD = 28 mm

For this outer diameter, it is the first time that **Luder Lines** appeared due to **REMS – CURVO** bender type. It is apparent that most copper tubes suffer from Luder Lines' defect, as it seen with light red lines. It can be observed that the bending result is **not the same** for every bender. This means that the process differentiates a lot if tooling parameters are not the same. We have at our disposal the most samples compared to other nominal outer diameters.

All samples processed by **Virax** bender have manifested **Luder Lines** defect!

$OD = 28\ mm$: 15 distinct samples (28A2, 28A11, 28A14, 2815, 28A16, 28A17, 28A18, 28A19, 28A20, 28A21, 28A22, 28A23, 28A24, 28A25, 28A27). The samples with No. ID: 28A2, 28A22, 28A23, 28A24, 28A25, 28A27 have been bent twice -> 21 samples

28A19	27,995	0,880	262,050		288	99	23	?	102	Wrinkles	REMS-CURVO
28A2	27,995	0,89	463,15		476	130,2	6,2	-	102	Light Wrinkling	REMS-CURVO
28A2	27,995	0,89	463,15		476	130,2	6,2	-	84	Luder Lines & LL Fracture	Virax
28A25	27,995	0,895	425,150	435,300	436	120,7	7,2		102	OK	REMS-CURVO
28A25	27,995	0,895	425,150	435,300	436	120,7	7,2		84	Luders and Kinking	Virax
28A11	28	0,710			463	130,7	6,3	-	102	Buckling	REMS-CURVO
28A27	28	0,780	464,064	461,700	467	138,1	9,7		102	Light Kinking + Luder Lines	REMS-CURVO
28A27	28	0,780	464,064	461,700	467	138,1	9,7		84	Kinking + Luder Lines	Virax
28A22	28	0,890	445,203	453,100	454	131,3	8,4		102	One Wrinkle at the beginning	REMS-CURVO
28A22	28	0,890	445,203	453,100	454	131,3	8,4		84	Luders	Virax
28A23	28	0,900	432,219	449,000	453	134,5	4,4		102	No Wrinkling (Tendency to Light Wrinkling)	REMS-CURVO
28A23	28	0,900	432,219	449,000	453	134,5	4,4		84	Luders	Virax
28A21	28,005	0,900	284,000	325,000	325	103,2	17,8		102	OK	REMS-CURVO
28A24	28,01	0,970	448,247	450,600	452	128,9	7,6		102	OK	REMS-CURVO
28A24	28,01	0,970	448,247	450,600	452	128,9	7,6		84	Luders	Virax
28A16	28,02	0,875	327,000		378	111,7	5,2	?	102	OK	REMS-CURVO
28A15	28,02	0,885	283,400		309	102,7	12,2	?	102	Wrinkles	REMS-CURVO
28A18	28,03	0,870	397,400		425	116	4,4	?	102	Slight Luders	REMS-CURVO
28A17	28,035	0,870	416,310		440	111,6	3,6	?	102	Luders	REMS-CURVO
28A14	28,035	0,885	382,000		398	120	6,9	?	102	Slight Luders	REMS-CURVO
28A20	28,035	0,895	304,270	314,100	315	105,4	18,8		102	OK	REMS-CURVO

Table 7: Raw experimental data for OD = 28 mm (including some half - hard tubes)

According to mechanical measurements, the samples named **28A15, 28A16, 28A19, 28A20, 28A21** may be **Half – Hard (M)** tubes and NOT Hard (H) copper tubes. If we eliminate these samples, we have the following situation:

28A2	27,995	0,89	463,15		476	130,2	6,2	-	102	Light Wrinkling	REMS-CURVO
28A2	27,995	0,89	463,15		476	130,2	6,2	-	84	Luder Lines & LL Fracture	Virax
28A25	27,995	0,895	425,150	435,300	436	120,7	7,2		102	OK	REMS-CURVO
28A25	27,995	0,895	425,150	435,300	436	120,7	7,2		84	Luders and Kinking	Virax
28A11	28	0,710			463	130,7	6,3	-	102	Buckling	REMS-CURVO
28A27	28	0,780	464,064	461,700	467	138,1	9,7		102	Light Kinking + Luder Lines	REMS-CURVO
28A27	28	0,780	464,064	461,700	467	138,1	9,7		84	Kinking + Luder Lines	Virax
28A22	28	0,890	445,203	453,100	454	131,3	8,4		102	One Wrinkle at the beginning	REMS-CURVO
28A22	28	0,890	445,203	453,100	454	131,3	8,4		84	Luders	Virax
28A23	28	0,900	432,219	449,000	453	134,5	4,4		102	No Wrinkling (Tendency to Light Wrinkling)	REMS-CURVO
28A23	28	0,900	432,219	449,000	453	134,5	4,4		84	Luders	Virax
28A24	28,01	0,970	448,247	450,600	452	128,9	7,6		102	OK	REMS-CURVO
28A24	28,01	0,970	448,247	450,600	452	128,9	7,6		84	Luders	Virax
28A18	28,03	0,870	397,400		425	116	4,4	?	102	Slight Luders	REMS-CURVO
28A17	28,035	0,870	416,310		440	111,6	3,6	?	102	Luders	REMS-CURVO
28A14	28,035	0,885	382,000		398	120	6,9	?	102	Slight Luders	REMS-CURVO

Table 8: Raw experimental data for OD = 28 mm

$OD = 28\ mm$: 10 distinct samples (28A2, 28A11, 28A14, 28A17, 28A18, 28A22, 28A23, 28A24, 28A25, 28A27) and some of them bent with both REMS and Virax -> 16 samples

Luder Lines' appearance: **9/10 (10/16)**
NO Luder Lines: **1/10 (6/16)**

OD = 28,575 mm

In this case, **all specimens** have suffered from **Luder Lines** defect. The sample size is too small to extract reliable conclusions, but copper tubes of this outer diameter seem to be extremely **sensitive** to this kind of defect, if subjected to a bending test. Virax bender cannot support copper tubes' bending in this dimension.

28,575B1 sample has been processed by a competitive company and the tube has been bent with a higher CLR (Centre Line Radius).

28,575A5	28,54	0,875	423,704	435,300	437	129	8,4		115	Luder Lines	REMS-CURVO
28,575A6	28,545	0,880	441,004	443,300	445	138,1	6,4		115	Luder Lines	REMS-CURVO
28,575B1	28,565	0,835	448,000		456	133	4,6	-	132	Wrinkling 33% + Luder Lines	?
28,575A8	28,575	0,940	458,411	457,700	464	130,9	7,2		115	Luder Lines	REMS-CURVO

Table 9: Raw experimental data for OD = 28.575 mm

$OD = 28{,}575\ mm$: 4 distinct samples (28,575A5, 28,575A6, 28,575B1, 28,575A8) bent once.

Luder Lines' appearance: **4/4 (4/4)**
NO Luder Lines: **0/4 (0//4)**

OD = 35 mm

As in the first case of copper tubes with Nominal Outer Diameter (either $OD = 15\ mm$ or $OD = 15{,}875\ mm$ or $OD = 16\ mm$ or $OD = 25{,}40\ mm$), all the samples do **not** appear Luder Lines. We have to zero in on this dimension in order to verify experimentally if this fact happened apparently or it is something deeper that has to be researched.

35A11	35,005	0,9	414,1227	440,4	441	139,4	5,6		140	Flattening	REMS-CURVO
35A5	35,01	1,01	403,7		450	125,6	8,5	-	140	Light Wrinkling	REMS-CURVO
35A10	35,02	1,01	379,7346	403,9	404	136,4	5,8		140	OK	REMS-CURVO
35A7	35,02	1,085	407,6599	438,8	439	140,4	5,5		140	OK	REMS-CURVO
35A8	35,04	1,09	404,1009	434,9	436	135,3	7,65		140	OK	REMS-CURVO
35A12	35,05	1,035	404,471	454,4	455	136,2	13		140	OK	REMS-CURVO

Table 10: Raw experimental data for OD = 35 mm

$OD = 35\ mm$: 6 distinct samples (35A5, 35A7, 35A8, 35A10, 35A11, 35A12) bent once.

Luder Lines' appearance: **0/6 (0/6)**
NO Luder Lines: **6/6 (6/6)**

Comparative and analytical evaluation of the nominal outer diameter's influence on Luder Lines defect due to bending test

As we have collected the whole information from the previous pages, we can present some useful tables and graphs that visualize the results and make them more perceivable.

Result	Ratio	Percentage
Luder Lines' appearance	22/45 (23/71)	**48,89% (32,39%)**
NO Luder Lines	23/45 (48/71)	51,11% (67,61%)

Table 11: General stats as for the frequency of Luder Lines' occurrence

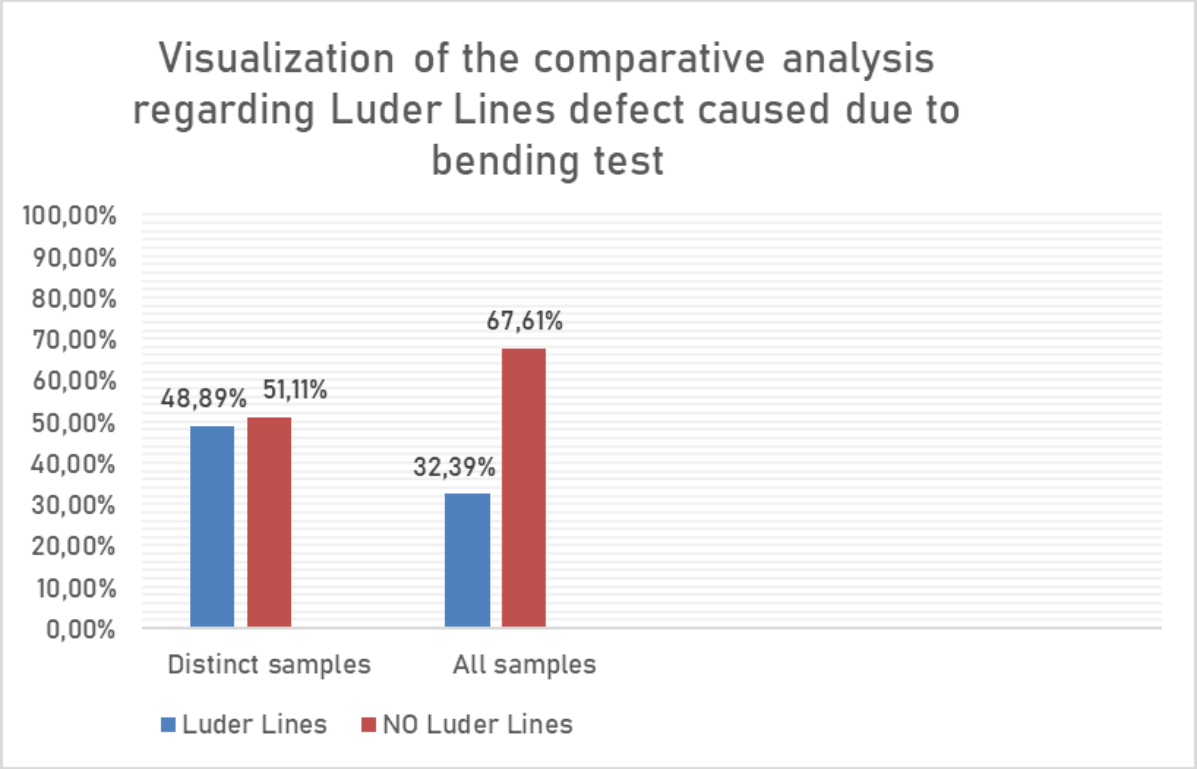

Figure 18: Visualization of the comparative analysis regarding Luder Lines defect caused due to bending test

Distinct samples have the meaning of the unique samples. For instance, if a copper tube has been bent twice (REMS & Virax) then we count it as 1 **physical** sample, although it has been bent twice (e.g. There are two rows of 28A22 sample, but we have 1 distinct sample)

All samples reflect to **all executed** bending **tests**. If we have processed the same copper tube with the aid of 2 different benders, then we count 2 samples not one.

In the table down below, we will use the term **"all samples"** to extract the respective values.

Result	$OD = 15\ mm$ $OD = 15{,}875\ mm$ $OD = 16\ mm$ $OD = 25{,}4\ mm$	$OD = 18\ mm$	$OD = 22\ mm$	$OD = 28\ mm$	$OD = 28{,}575\ mm$	$OD = 35\ mm$
Luder Lines (Ratio)	0/23	7/16	2/7	10/16	4/4	0/6
NO Luder Lines (Ratio)	23/23	9/16	5/7	6/16	0/4	6/6
Luder Lines (Percent)	0%	43,75%	28,57%	62,50%	100%	0%
NO Luder Lines (Ratio)	100%	56,25%	71,43%	37,50%	0%	100%

Table 12: Detailed stats regarding Luder Lines' appearance with respect to Outer Diameter (OD)

According to our previous analysis, there is no sufficient correlation between the values of the nominal outer diameter (OD) and the probability of Luder Lines' appearance. However, we have arrived at some interesting conclusions that need experimental verification and further research.

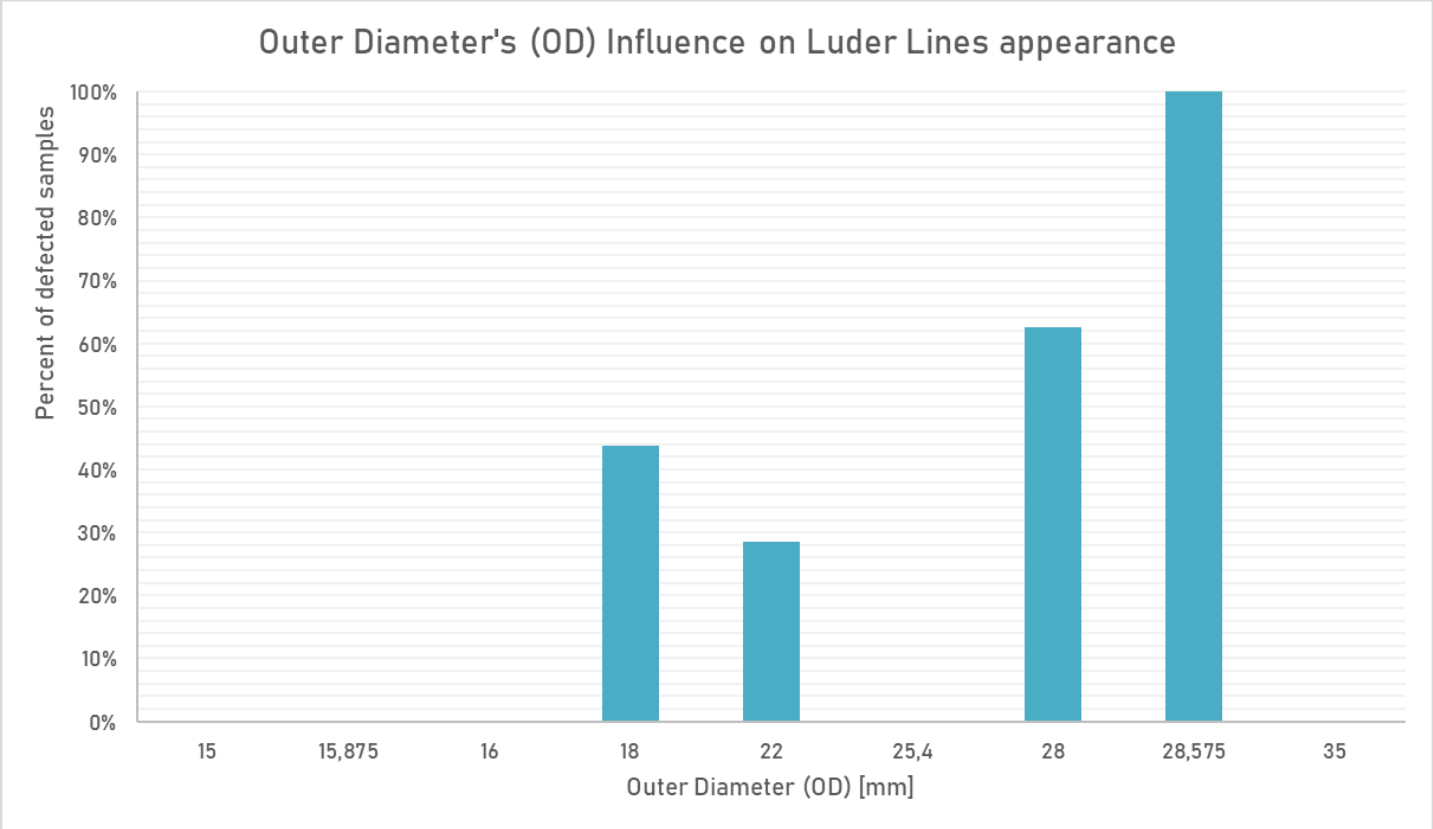

Figure 19: Outer Diameter's Effect on Luder Lines' appearance

4.1.2 Wall Thickness' (WT) Influence

$\mathbf{0,455 \leq WT_{av} \leq 0,56\ [mm]}$

Regardless of the bender type (REMS or Virax), it is observed that **none** of the following specimens have appeared **Luder Lines** plus the fact that none of them had **clear bending** (without defect). Most of them suffer from Buckling and Kinking (No Wrinkling) which seems quite reasonable.

15A15	15,035	0,455	444,5	455,1	465	139	7,7		55	Buckling	REMS-CURVO
15A15	15,035	0,455	444,4939	455,1	465	139,4	7,7		45	Crack	Virax
16A4	16	0,47	453,8825	461,8	463	117,2	9,7		60	Buckling	REMS-CURVO
16A4	16	0,47	453,8825	461,8	463	117,2	9,7		48	Buckling	Virax
15A10	15,000	0,530	436,3		451	131	6,6		55	Light Kinking	REMS-CURVO
15A13	15,010	0,535	441,6	475,3	476	139	12,3		55	Buckling	REMS-CURVO
15A13	15,01	0,535	441,5836	475,3	476	139,1	12,3		45	Buckling	Virax
15,875A7	15,855	0,56	474,656	-	480	139,1	0,2		63	Kinking	REMS-CURVO
15,875A7	15,855	0,56	474,656		480	139,1	0,2		48	Kinking	Virax
22A16	21,980	0,560	450,2	446,0	456	137	9,7		77	Buckling	REMS-CURVO
22A16	21,98	0,560	450,242	446,000	456	137,1	9,7		66	Buckling	Virax

Table 13: Raw experimental data for 0,455 ≤ WTav ≤ 0,56 [mm]

$0{,}455 \leq WT_{av} < 0{,}605$: 11 samples (15A15-1, 15A15-2, 16A4-1, 16A4-2, 15A10, 15A13-1, 15A13-2, 15,875A7-1, 15,875A7-2, 22A16-1, 22A16-2)

Luder Lines' appearance: **0/11 -> 0%**
NO Luder Lines: 11/11 -> 100%

$\mathbf{0,56 < WT_{av} < 0,605\ [mm]}$

None of the bent tubes have wall thickness in this region and that is why we do not possess any data. This wall thickness interval must be investigated to ascertain if the trend of Luder Lines' absence is about to be continued or not.

$\mathbf{0,605 \leq\ WT_{av} \leq 0,75\ [mm]}$

This wide region contains useful information about wall thickness' influence on Luder Lines' manifestation, because it contains more samples than all other regions. Observing carefully, **none of the tubes**, which have been processed with **REMS** – CURVO, appeared **Luder Lines.** Some copper tubes (e.g. 18A5, 18A6, 18A9, 18A10, 18A11) give even clear bending (no defect) with REMS but Luder Lines with Virax. So, the ratio $\frac{CLR}{WT}$ is important to distinguish the samples' behaviour during bending test. CLR factor expresses the influence of the bender's type.

$0{,}605 \leq WT_{av} < 0{,}75$: 36 samples (in terms of "all samples")

Luder Lines' appearance: **9/36 -> 25%**
NO Luder Lines: 27/36 -> 75%

18A10	18,000	0,605	467,8	459,8	477	143	9,6		70	OK	REMS-CURVO
18A10	18	0,605	467,776	459,8	477	142,6	9,6		54	Kinking + Luder Lines	Virax
22A11	22,020	0,605	454,5		458	137	3,8	-	77	Light Waved Wrinkling	REMS-CURVO
22A11	22,02	0,605	454,500		458	137,3	3,8	-	66	Luder Crack	Virax
18A8	18,005	0,610	447,9	462,9	464	126	8,3		70	OK	REMS-CURVO
18A8	18,005	0,61	447,925	462,9	464	126,2	8,3		54	Buckling	Virax
18A4	18,015	0,610	448,3		459	131	6,0		70	No Wrinkling	REMS-CURVO
18A4	18,015	0,61	448,29		459	131,4	6		54	Kinking with Luder Crack	Virax
15A6	14,995	0,620	421,2		443	129	4,8	-	55	No Wrinkling	REMS-CURVO
15A11	15,000	0,650	461,4	463,3	465	128	6,8		55	Light Wrinkling	REMS-CURVO
15A11	15	0,65	461,397	463,3	465	127,5	6,8		45	Buckling	Virax
18A9	17,990	0,650	446,5	445,2	454	136	7,8		70	OK	REMS-CURVO
18A9	17,99	0,65	446,498	445,2	454	135,6	7,8		54	Kinking + Slight Luder Lines	Virax
22A7	21,990	0,655				136			77	No Wrinkling	REMS-CURVO
15A17	14,990	0,690	443,1	453,0	456	132	10,0		55	OK	REMS-CURVO
15A17	14,99	0,69	443,112	453	456	131,7	10		45	Buckling	Virax
15A16	14,990	0,695	464,3	463,1	473	140	9,0		55	OK	REMS-CURVO
15A16	14,99	0,695	464,25	463,1	473	140,4	9		45	Buckling + Cracking	Virax
18A11	17,990	0,700	447,0	439,6	453	126	9,7		70	OK	REMS-CURVO
18A11	17,99	0,7	446,986	439,6	453	126,2	9,7		54	Kinking + Slight Luder Lines	Virax
18A6	18,000	0,700	458,7	-	463	119	8,2		70	OK	REMS-CURVO
18A6	18	0,7	458,661	-	463	118,7	8,2		54	Slight Luders, Light Wrinkling, Kinking	Virax
22A14	22,025	0,700	448,3	457,0	457	128	6,2		77	One Wrinkle at the beginning	REMS-CURVO
22A14	22,025	0,700	448,281	457,000	457	127,6	6,2		66	Luders	Virax
15,875A4	15,865	0,71	456,008	-	461	137,6	8,8		63	OK	REMS-CURVO
15,875A4	15,865	0,71	456,008		461	137,6	8,8		48	OK	Virax
28A11	28	0,710			463	130,7	6,3	-	102	Buckling	REMS-CURVO
18A5	18,005	0,735	472,6	-	473	120	7,2		70	OK	REMS-CURVO
18A5	18,005	0,735	472,563	-	473	120,2	7,2		54	Slight Luders	Virax
18A2	18,010	0,735			459	120	12,0	-	70	No Wrinkling	REMS-CURVO
18A2	18,01	0,735			459	120,2	12	-	54	Luder Lines (with some crack)	Virax
15,875A2	15,86	0,74	455,09	450,9	460	137	7,7		63	OK	REMS-CURVO
15,875A2	15,86	0,74	455,09	450,9	460	137	7,7		48	OK	Virax
15A12	15,000	0,750	438,6		445	129	4,3		55	OK	REMS-CURVO
15A12	15	0,75	438,624	-	445	129,4	4,3		45	Wrinkling	Virax

Table 14: Raw experimental data for 0,605 ≤ WTav ≤ 0,75 [mm]

If this mathematical expression $\mathbf{0,455 \leq WT_{av} \leq 0,75}$ is valid & copper tubes are processed with the aid of **REMS – CURVO only,** then there is **no** appearance of **Luder Lines.** Actually, **Virax** machine creates a broad range of problems for the same tube.

$\mathbf{0,75 < WT_{av} < 0,78}$ $[\boldsymbol{mm}]$

There is shortage of data -> To be researched

$\mathbf{0,78 \leq WT_{av} \leq 0,885}$ $[\boldsymbol{mm}]$

For this wall thickness' interval, all specimens suffer from Luder Lines' defect regardless of the bender type. More specifically, for $WT_{av} = 0{,}78$ there is a combination of Kinking + Luder Lines. Most samples have been processed with Virax machine.

28A27	28	0,780	464,064	461,700	467	138,1	9,7		102	Light Kinking + Luder Lines	REMS-CURVO
28A27	28	0,780	464,064	461,700	467	138,1	9,7		84	Kinking + Luder Lines	Virax
28,575B1	28,565	0,835	448,000		456	133	4,6	-	132	Wrinkling 33% + Luder Lines	?
28A18	28,03	0,870	397,400		425	116	4,4	?	102	Slight Luders	REMS-CURVO
28A17	28,035	0,870	416,310		440	111,6	3,6	?	102	Luders	REMS-CURVO
28,575A5	28,54	0,875	423,704	435,300	437	129	8,4		115	Luder Lines	REMS-CURVO
28,575A6	28,545	0,880	441,004	443,300	445	138,1	6,4		115	Luder Lines	REMS-CURVO
28A14	28,035	0,885	382,000		398	120	6,9	?	102	Slight Luders	REMS-CURVO

Table 15: Raw experimental data for 0,78 ≤ WTav ≤ 0,885 [mm]

$0{,}78 \leq WT_{av} \leq 0{,}885$: 8 samples

Luder Lines' appearance: **8/8 -> 100%**
NO Luder Lines: 0/0 -> 100%

$\mathbf{0,89 \leq WT_{av} \leq 1,09\ [mm]}$

Virax bender, once again, causes Luder Lines' defect for some tubes although they will present other problems (such as Wrinkling) if they are bent with REMS – Curvo. Only 1 sample manifests Luder Lines, while is it processed with REMS, maybe because of the fact that $R_{p_{0,2}} > R_{p_1}$ but it is not clear yet.

28A2	27,995	0,89	463,15		476	130,2	6,2	-	102	Light Wrinkling	REMS-CURVO
28A2	27,995	0,89	463,15		476	130,2	6,2	-	84	Luder Lines & LL Fracture	Virax
28A22	28	0,890	445,203	453,100	454	131,3	8,4		102	One Wrinkle at the beginning	REMS-CURVO
28A22	28	0,890	445,203	453,100	454	131,3	8,4		84	Luders	Virax
28A25	27,995	0,895	425,150	435,300	436	120,7	7,2		102	OK	REMS-CURVO
28A25	27,995	0,895	425,150	435,300	436	120,7	7,2		84	Luders and Kinking	Virax
28A23	28	0,900	432,219	449,000	453	134,5	4,4		102	No Wrinkling (Tendency to Light Wrinkling)	REMS-CURVO
28A23	28	0,900	432,219	449,000	453	134,5	4,4		84	Luders	Virax
35A11	35,005	0,9	414,123	440,4	441	139,4	5,6		140	Flattening	REMS-CURVO
28,575A8	28,575	0,940	458,411	457,700	464	130,9	7,2		115	Luder Lines	REMS-CURVO
28A24	28,01	0,970	448,247	450,600	452	128,9	7,6		102	OK	REMS-CURVO
28A24	28,01	0,970	448,247	450,600	452	128,9	7,6		84	Luders	Virax
35A5	35,01	1,01	403,7		450	125,6	8,5	-	140	Light Wrinkling	REMS-CURVO
35A10	35,02	1,01	379,735	403,9	404	136,4	5,8		140	OK	REMS-CURVO
35A12	35,05	1,035	404,471	454,4	455	136,2	13		140	OK	REMS-CURVO
35A7	35,02	1,085	407,66	438,8	439	140,4	5,5		140	OK	REMS-CURVO
35A8	35,04	1,09	404,101	434,9	436	135,3	7,65		140	OK	REMS-CURVO

Table 16: Raw experimental data for 0,89 ≤ WTav ≤ 1,09 [mm]

$0,89 \leq WT_{av} \leq 1,09$: 17 samples

Luder Lines' appearance: **6/17 -> 35,29 %**
NO Luder Lines: 11/17 -> 64,71 %

$\mathbf{WT_{av} > 1,09\ [mm]}$

There is a lack of specimens. So, we wish to have some bent coper tubes for this region to observe what happens in this case.

Comparative and analytical evaluation of the nominal wall thickness' influence on Luder Lines defect due to bending test

We can collect there our observations in order to see if any possible trend exist for Luder Lines' appearance. In order to gather our notes, we compress this valuable information into the following table, which is shown down below:

Wall thickness' interval	Luder Lines (REMS)	Luder Lines (Virax)	Luder Lines (overall)
$WT_{av} < 0{,}455$		No data	
$0{,}455 \leq WT_{av} \leq 0{,}56$	NO	NO	NO
$0{,}56 < WT_{av} < 0{,}605$		No data	
$0{,}605 \leq WT_{av} < 0{,}75$	NO	YES	YES (25%)
$0{,}75 < WT_{av} < 0{,}78$		No data	
$0{,}78 \leq WT_{av} \leq 0{,}885$	YES	YES	YES (100%)
$0{,}89 \leq WT_{av} \leq 1{,}09$	NO (except for 1 sample)	YES	YES (35,29%)
$WT_{av} > 1{,}09$		No data	

Table 17: Detailed stats regarding Luder Lines' appearance with respect to Wall Thickness (WT)

Consequently, we can extract the **mathematical rule:**

$(0{,}455 \leq WT_{av} \leq 0{,}56$ **OR** $0{,}605 \leq WT_{av} < 0{,}75$ **OR** $0{,}89 \leq WT_{av} \leq 1{,}09)$ **AND**
(REMS – CURVO Bender) => **NO Luder Lines**

$(0{,}78 \leq WT_{av} \leq 0{,}885)$ **AND** (REMS – CURVO **OR** Virax) => **Luder Lines**

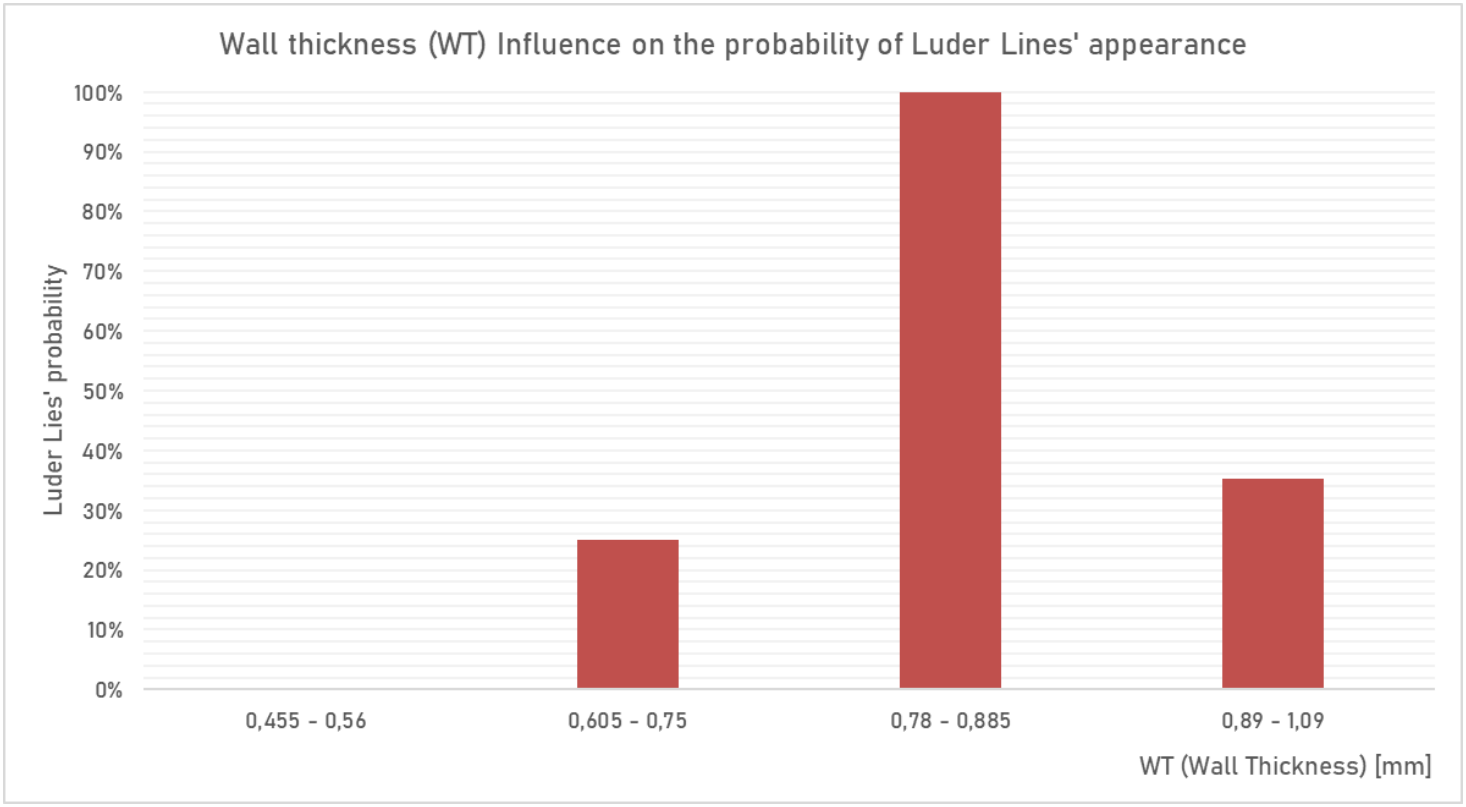

Figure 20: Wall Thickness' Effect on Luder Lines' appearance

4.1.3 Stress $R_{p_{0,2}}{}'s$ Influence

At first glance, the values of $R_{p_{0,2}}$ seem not to correlate with the bending test result (e.g. Luder Lines that we investigate). For the sake of completeness, we will check in which degree this parameter influences the Luder Lines' appearance

$$\mathbf{379 \leq R_{p_{0,2}} \leq 444,5\ [MPa]}$$

Our samples do not have bad results if this material property exists into that range. This factor does not separate the results properly, but we will see what happens in advance:

$379 \leq R_{p_{0,2}} \leq 444$: 25 samples

Luder Lines' appearance: **7/25 -> 28 %**
NO Luder Lines: 18/25 -> 72 %

35A10	35,02	1,01	379,735	403,9	404	136,4	5,8		140	OK	REMS-CURVO
28A14	28,035	0,885	382,000		398	120	6,9	?	102	Slight Luders	REMS-CURVO
28A18	28,03	0,870	397,400		425	116	4,4	?	102	Slight Luders	REMS-CURVO
35A5	35,01	1,01	403,7		450	125,6	8,5	-	140	Light Wrinkling	REMS-CURVO
35A8	35,04	1,09	404,101	434,9	436	135,3	7,65		140	OK	REMS-CURVO
35A12	35,05	1,035	404,471	454,4	455	136,2	13		140	OK	REMS-CURVO
35A7	35,02	1,085	407,66	438,8	439	140,4	5,5		140	OK	REMS-CURVO
35A11	35,005	0,9	414,123	440,4	441	139,4	5,6		140	Flattening	REMS-CURVO
28A17	28,035	0,870	416,310		440	111,6	3,6	?	102	Luders	REMS-CURVO
15A6	14,995	0,620	421,2		443	129	4,8	-	55	No Wrinkling	REMS-CURVO
28,575A5	28,54	0,875	423,704	435,300	437	129	8,4		115	Luder Lines	REMS-CURVO
28A25	27,995	0,895	425,150	435,300	436	120,7	7,2		102	OK	REMS-CURVO
28A25	27,995	0,895	425,150	435,300	436	120,7	7,2		84	Luders and Kinking	Virax
28A23	28	0,900	432,219	449,000	453	134,5	4,4		102	No Wrinkling (Tendency to Light Wrinkling)	REMS-CURVO
28A23	28	0,900	432,219	449,000	453	134,5	4,4		84	Luders	Virax
15A10	15,000	0,530	436,3		451	131	6,6		55	Light Kinking	REMS-CURVO
15A12	15,000	0,750	438,6		445	129	4,3		55	OK	REMS-CURVO
15A12	15	0,75	438,624	-	445	129,4	4,3		45	Wrinkling	Virax
28,575A6	28,545	0,880	441,004	443,300	445	138,1	6,4		115	Luder Lines	REMS-CURVO
15A13	15,010	0,535	441,6	475,3	476	139	12,3		55	Buckling	REMS-CURVO
15A13	15,01	0,535	441,584	475,3	476	139,1	12,3		45	Buckling	Virax
15A17	14,990	0,690	443,1	453,0	456	132	10,0		55	OK	REMS-CURVO
15A17	14,99	0,69	443,112	453	456	131,7	10		45	Buckling	Virax
15A15	15,035	0,455	444,5	455,1	465	139	7,7		55	Buckling	REMS-CURVO
15A15	15,035	0,455	444,494	455,1	465	139,4	7,7		45	Crack	Virax

Table 18: Raw experimental data for 379 ≤ Rp0,2 ≤ 444,5

$$\mathbf{445 \leq R_{p_{0,2}} \leq 459\ [MPa]}$$

For this stress interval, only 1 sample suffered from Luder Lines and bent with REMS – Curvo. The other specimens, in which this local failure is noted, have been processed with Virax machine.

$445 \leq R_{p_{0,2}} \leq 459$: 28 samples

Luder Lines' appearance: **10/28 -> 35,7 %**
NO Luder Lines: 18/28 -> 64,3 %

28A22	28	0,890	445,203	453,100	454	131,3	8,4		102	One Wrinkle at the beginning	REMS-CURVO
28A22	28	0,890	445,203	453,100	454	131,3	8,4		84	Luders	Virax
18A9	17,990	0,650	446,5	445,2	454	136	7,8		70	OK	REMS-CURVO
18A9	17,99	0,65	446,498	445,2	454	135,6	7,8		54	Kinking + Slight Luder Lines	Virax
18A11	17,990	0,700	447,0	439,6	453	126	9,7		70	OK	REMS-CURVO
18A11	17,99	0,7	446,986	439,6	453	126,2	9,7		54	Kinking + Slight Luder Lines	Virax
18A8	18,005	0,610	447,9	462,9	464	126	8,3		70	OK	REMS-CURVO
18A8	18,005	0,61	447,9253	462,9	464	126,2	8,3		54	Buckling	Virax
28,575B1	28,565	0,835	448,000		456	133	4,6	-	132	Wrinkling 33% + Luder Lines	?
28A24	28,01	0,970	448,247	450,600	452	128,9	7,6		102	OK	REMS-CURVO
28A24	28,01	0,970	448,247	450,600	452	128,9	7,6		84	Luders	Virax
22A14	22,025	0,700	448,3	457,0	457	128	6,2		77	One Wrinkle at the beginning	REMS-CURVO
22A14	22,025	0,700	448,281	457,000	457	127,6	6,2		66	Luders	Virax
18A4	18,015	0,610	448,3		459	131	6,0		70	No Wrinkling	REMS-CURVO
18A4	18,015	0,61	448,29		459	131,4	6		54	Kinking with Luder Crack	Virax
22A16	21,980	0,560	450,2	446,0	456	137	9,7		77	Buckling	REMS-CURVO
22A16	21,98	0,560	450,242	446,000	456	137,1	9,7		66	Buckling	Virax
16A4	16	0,47	453,8825	461,8	463	117,2	9,7		60	Buckling	REMS-CURVO
16A4	16	0,47	453,8825	461,8	463	117,2	9,7		48	Buckling	Virax
22A11	22,020	0,605	454,5		458	137	3,8	-	77	Light Waved Wrinkling	REMS-CURVO
22A11	22,02	0,605	454,500		458	137,3	3,8	-	66	Luder Crack	Virax
15,875A2	15,86	0,74	455,09	450,9	460	137	7,7		63	OK	REMS-CURVO
15,875A2	15,86	0,74	455,09	450,9	460	137	7,7		48	OK	Virax
15,875A4	15,865	0,71	456,008	-	461	137,6	8,8		63	OK	REMS-CURVO
15,875A4	15,865	0,71	456,008		461	137,6	8,8		48	OK	Virax
28,575A8	28,575	0,940	458,411	457,700	464	130,9	7,2		115	Luder Lines	REMS-CURVO
18A6	18,000	0,700	458,7	-	463	119	8,2		70	OK	REMS-CURVO
18A6	18	0,7	458,6607	-	463	118,7	8,2		54	Slight Luders, Light Wrinkling, Kinking	Virax

Table 19: Raw experimental data for 445 ≤ $Rp_{0,2}$ ≤ 459

So, there is a greater probability for the bent copper tube to appear Luder Lines if the conventional yield point $R_{p_{0,2}}$ satisfies the following mathematical relation: $444 \leq R_{p_{0,2}} \leq 459$ compared to the previous situation.

$$\mathbf{461 \leq R_{p_{0,2}} \leq 475\ [MPa]}$$

Few tubes appear clear bending in this region. Tubes bent with REMS machine appeared Luder Lines once, in contrast with Virax bender.

$461 \leq R_{p_{0,2}} \leq 475$: 18 samples

Luder Lines' appearance: **6/18 -> 33,33 %**
NO Luder Lines: 12/18 -> 66,67 %

15A11	15,000	0,650	461,4	463,3	465	128	6,8		55	Light Wrinkling	REMS-CURVO
15A11	15	0,65	461,3969	463,3	465	127,5	6,8		45	Buckling	Virax
28A2	27,995	0,89	463,15		476	130,2	6,2	-	102	Light Wrinkling	REMS-CURVO
28A2	27,995	0,89	463,15		476	130,2	6,2	-	84	Luder Lines & LL Fracture	Virax
28A27	28	0,780	464,064	461,700	467	138,1	9,7		102	Light Kinking + Luder Lines	REMS-CURVO
28A27	28	0,780	464,064	461,700	467	138,1	9,7		84	Kinking + Luder Lines	Virax
15A16	14,990	0,695	464,3	463,1	473	140	9,0		55	OK	REMS-CURVO
15A16	14,99	0,695	464,25	463,1	473	140,4	9		45	Buckling + Cracking	Virax
18A10	18,000	0,605	467,8	459,8	477	143	9,6		70	OK	REMS-CURVO
18A10	18	0,605	467,776	459,8	477	142,6	9,6		54	Kinking + Luder Lines	Virax
18A5	18,005	0,735	472,6	-	473	120	7,2		70	OK	REMS-CURVO
18A5	18,005	0,735	472,5625	-	473	120,2	7,2		54	Slight Luders	Virax
15,875A7	15,855	0,56	474,656	-	480	139,1	0,2		63	Kinking	REMS-CURVO
15,875A7	15,855	0,56	474,656		480	139,1	0,2		48	Kinking	Virax
22A7	21,990	0,655	-			136			77	No Wrinkling	REMS-CURVO
28A11	28	0,710	-		463	130,7	6,3	-	102	Buckling	REMS-CURVO
18A2	18,010	0,735	-		459	120	12,0	-	70	No Wrinkling	REMS-CURVO
18A2	18,01	0,735	-		459	120,2	12	-	54	Luder Lines (with some crack)	Virax

Table 20: Raw experimental data for 461 ≤ $Rp_{0,2}$ ≤ 475

Comparative and analytical evaluation of the conventional yield point's ($R_{p_{0,2}}$) influence on Luder Lines result because of bending test

For comparative reasons, we create the following table in order to collect the probability of Luder Lines' appearance in the tree upper cases of conventional yield point's $R_{p_{0,2}}$ value:

Conventional yield point $R_{p_{0,2}}$ interval	Luder Lines' appearance (probability)
$379 \leq R_{p_{0,2}} \leq 444$	28%
$445 \leq R_{p_{0,2}} \leq 459$	35,7%
$461 \leq R_{p_{0,2}} \leq 475$	33,33%

Table 21: General stats regarding Luder Lines' appearance with respect to conventional yield point

Concluding, after this analysis regarding this material characteristic, the factor $R_{p_{0,2}}$ cannot stand for the Luder Lines' manifestation or not. And that is why the values of probability, on the table, do not have any statically important difference.

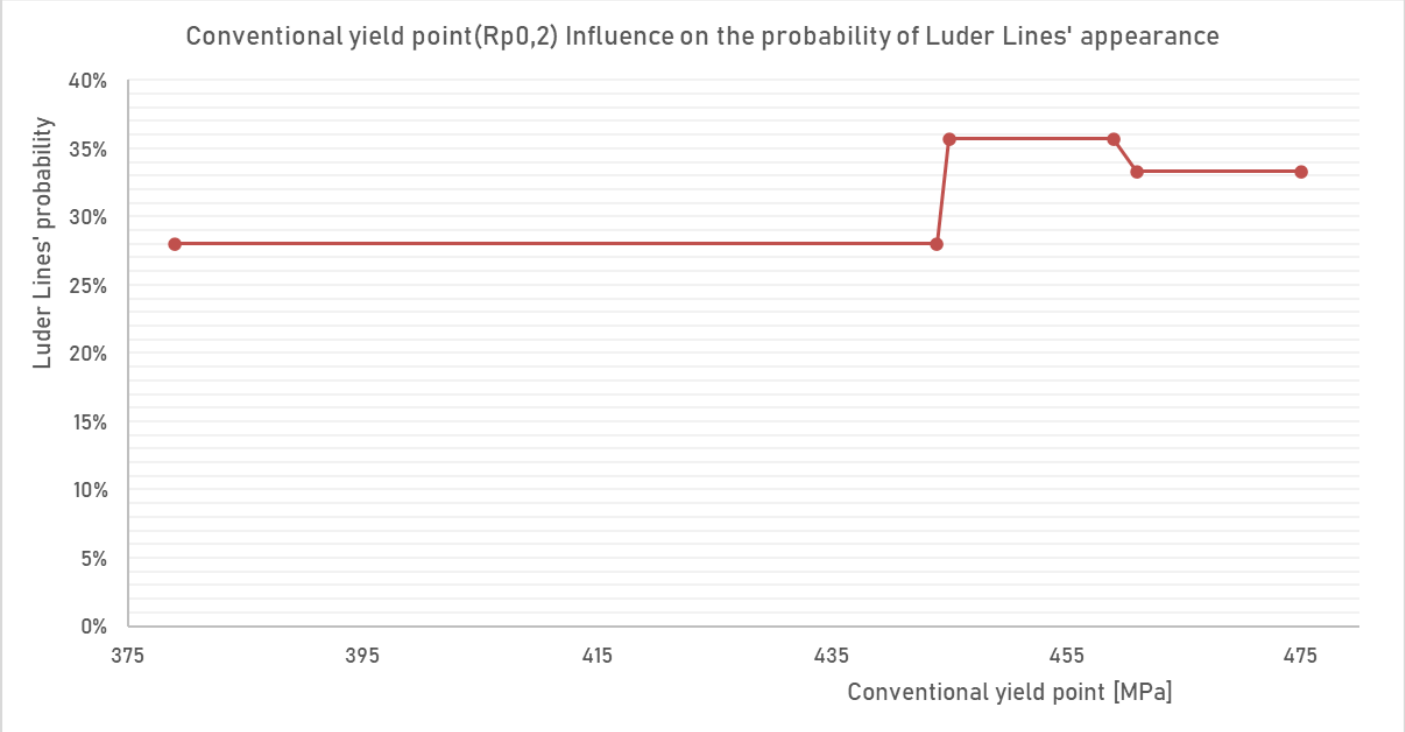

Figure 21: Conventional yield point's effect on Luder Lines' appearance

** Important note: The influence of factors R_{p_1} and **Grain Size** cannot be studied, as we do not have sufficient data for all samples at our disposal. Moreover, the **elongation** parameter does not separate the samples well (along the 2 conditions: Luder Lines or not) and seems to be that there is no correlation.

4.1.4 Stress at Maximum Load R_m Influence

We expect that this factor cannot account for the Luder Lines' appearance on its own, but it is worth giving a try to observe the results.

$398 \leq R_m \leq 445$ $[MPa]$

It seems that many tubes appear Luder Lines on their bent surface in this stress region. The **principal** defect is **Luder Lines**, while only two tubes note different behaviour (e.g. Flattening, Wrinkling) after the plastic deformation occurred, except for these who perform clear bending.

$398 \leq R_m \leq 445$

Luder Lines' appearance: **6/14 -> 42,86 %**
NO Luder Lines: 8/14 -> 57,14 %

28A14	28,035	0,885	382,000		398	120	6,9	?	102	Slight Luders	REMS-CURVO
35A10	35,02	1,01	379,7346	403,9	404	136,4	5,8		140	OK	REMS-CURVO
28A18	28,03	0,870	397,400		425	116	4,4	?	102	Slight Luders	REMS-CURVO
28A25	27,995	0,895	425,150	435,300	436	120,7	7,2		84	Luders and Kinking	Virax
28A25	27,995	0,895	425,150	435,300	436	120,7	7,2		102	OK	REMS-CURVO
35A8	35,04	1,09	404,1009	434,9	436	135,3	7,65		140	OK	REMS-CURVO
28,575A5	28,54	0,875	423,704	435,300	437	129	8,4		115	Luder Lines	REMS-CURVO
35A7	35,02	1,085	407,6599	438,8	439	140,4	5,5		140	OK	REMS-CURVO
28A17	28,035	0,870	416,310		440	111,6	3,6	?	102	Luders	REMS-CURVO
35A11	35,005	0,9	414,1227	440,4	441	139,4	5,6		140	Flattening	REMS-CURVO
15A6	14,995	0,620	421,2		443	129	4,8	-	55	No Wrinkling	REMS-CURVO
15A12	15	0,75	438,6238	-	445	129,4	4,3		45	Wrinkling	Virax
15A12	15,000	0,750	438,6		445	129	4,3		55	OK	REMS-CURVO
28,575A6	28,545	0,880	441,004	443,300	445	138,1	6,4		115	Luder Lines	REMS-CURVO

Table 22: Raw experimental data for 398 ≤ Rm ≤ 445

$450 \leq R_m \leq 467$ $[MPa]$

As there was not any discontinuity of the stress at maximum load (in this dataset), we have to focus on all these samples, shown in the next page. Most cases of Luder Lines' appearance are due to bending test with Virax bender.

$450 \leq R_m \leq 467$

Luder Lines' appearance: **14/43-> 32,56 %**
NO Luder Lines: 29/43 -> 67,44 %

35A5	35,01	1,01	403,7		450	125,6	8,5	-	140	Light Wrinkling	REMS-CURVO
15A10	15,000	0,530	436,3		451	131	6,6		55	Light Kinking	REMS-CURVO
28A24	28,01	0,970	448,247	450,600	452	128,9	7,6		84	Luders	Virax
28A24	28,01	0,970	448,247	450,600	452	128,9	7,6		102	OK	REMS-CURVO
18A11	17,99	0,7	446,986	439,6	453	126,2	9,7		54	Kinking + Slight Luder Lines	Virax
18A11	17,990	0,700	447,0	439,6	453	126	9,7		70	OK	REMS-CURVO
28A23	28	0,900	432,219	449,000	453	134,5	4,4		84	Luders	Virax
28A23	28	0,900	432,219	449,000	453	134,5	4,4		102	No Wrinkling (Tendency to Light Wrinkling)	REMS-CURVO
18A9	17,99	0,65	446,498	445,2	454	135,6	7,8		54	Kinking + Slight Luder Lines	Virax
18A9	17,990	0,650	446,5	445,2	454	136	7,8		70	OK	REMS-CURVO
28A22	28	0,890	445,203	453,100	454	131,3	8,4		84	Luders	Virax
28A22	28	0,890	445,203	453,100	454	131,3	8,4		102	One Wrinkle at the beginning	REMS-CURVO
35A12	35,05	1,035	404,471	454,4	455	136,2	13		140	OK	REMS-CURVO
15A17	14,99	0,69	443,112	453	456	131,7	10		45	Buckling	Virax
15A17	14,990	0,690	443,1	453,0	456	132	10,0		55	OK	REMS-CURVO
22A16	21,98	0,560	450,242	446,000	456	137,1	9,7		66	Buckling	Virax
22A16	21,980	0,560	450,2	446,0	456	137	9,7		77	Buckling	REMS-CURVO
28,57581	28,565	0,835	448,000		456	133	4,6	-	132	Wrinkling 33% + Luder Lines	?
22A14	22,025	0,700	448,281	457,000	457	127,6	6,2		66	Luders	Virax
22A14	22,025	0,700	448,3	457,0	457	128	6,2		77	One Wrinkle at the beginning	REMS-CURVO
22A11	22,02	0,605	454,500		458	137,3	3,8	-	66	Luder Crack	Virax
22A11	22,020	0,605	454,5		458	137	3,8	-	77	Light Waved Wrinkling	REMS-CURVO
18A4	18,015	0,61	448,29		459	131,4	6		54	Kinking with Luder Crack	Virax
18A2	18,01	0,735	-		459	120,2	12	-	54	Luder Lines (with some crack)	Virax
18A4	18,015	0,610	448,3		459	131	6,0		70	No Wrinkling	REMS-CURVO
18A2	18,010	0,735	-		459	120	12,0	-	70	No Wrinkling	REMS-CURVO
15,875A2	15,86	0,74	455,09	450,9	460	137	7,7		48	OK	Virax
15,875A2	15,86	0,74	455,09	450,9	460	137	7,7		63	OK	REMS-CURVO
15,875A4	15,865	0,71	456,008		461	137,6	8,8		48	OK	Virax
15,875A4	15,865	0,71	456,008	-	461	137,6	8,8		63	OK	REMS-CURVO
16A4	16	0,47	453,8825	461,8	463	117,2	9,7		48	Buckling	Virax
18A6	18	0,7	458,6607	-	463	118,7	8,2		54	Slight Luders, Light Wrinkling, Kinking	Virax
16A4	16	0,47	453,8825	461,8	463	117,2	9,7		60	Buckling	REMS-CURVO
18A6	18,000	0,700	458,7	-	463	119	8,2		70	OK	REMS-CURVO
28A11	28	0,710	-		463	130,7	6,3	-	102	Buckling	REMS-CURVO
18A8	18,005	0,61	447,9253	462,9	464	126,2	8,3		54	Buckling	Virax
18A8	18,005	0,610	447,9	462,9	464	126	8,3		70	OK	REMS-CURVO
28,57SA8	28,575	0,940	458,411	457,700	464	130,9	7,2		115	Luder Lines	REMS-CURVO
15A11	15	0,65	461,3969	463,3	465	127,5	6,8		45	Buckling	Virax
15A15	15,035	0,455	444,4939	455,1	465	139,4	7,7		45	Crack	Virax
15A11	15,000	0,650	461,4	463,3	465	128	6,8		55	Light Wrinkling	REMS-CURVO
15A15	15,035	0,455	444,5	455,1	465	139	7,7		55	Buckling	REMS-CURVO
28A27	28	0,780	464,064	461,700	467	138,1	9,7		84	Kinking + Luder Lines	Virax
28A27	28	0,780	464,064	461,700	467	138,1	9,7		102	Light Kinking + Luder Lines	REMS-CURVO

Table 23: Raw experimental data for 450 ≤ Rm ≤ 467

$473 \leq R_m \leq 480$ $[MPa]$

We have both Kinking and Buckling apart from Luder Lines' Defect there. Unfortunately, the value matching to 22A7 sample is missing.

$473 \leq R_m \leq 480$

Luder Lines' appearance: **3/13 -> 23,1 %**
NO Luder Lines: 10/13 -> 76,9 %

15A16	14,99	0,695	464,25	463,1	473	140,4	9		45	Buckling + Cracking	Virax
18A5	18,005	0,735	472,563	-	473	120,2	7,2		54	Slight Luders	Virax
15A16	14,990	0,695	464,3	463,1	473	140	9,0		55	OK	REMS-CURVO
18A5	18,005	0,735	472,6	-	473	120	7,2		70	OK	REMS-CURVO
15A13	15,01	0,535	441,584	475,3	476	139,1	12,3		45	Buckling	Virax
15A13	15,010	0,535	441,6	475,3	476	139	12,3		55	Buckling	REMS-CURVO
28A2	27,995	0,89	463,15		476	130,2	6,2	-	84	Luder Lines & LL Fracture	Virax
28A2	27,995	0,89	463,15		476	130,2	6,2	-	102	Light Wrinkling	REMS-CURVO
18A10	18	0,605	467,776	459,8	477	142,6	9,6		54	Kinking + Luder Lines	Virax
18A10	18,000	0,605	467,8	459,8	477	143	9,6		70	OK	REMS-CURVO
15,875A7	15,855	0,56	474,656		480	139,1	0,2		48	Kinking	Virax
15,875A7	15,855	0,56	474,656	-	480	139,1	0,2		63	Kinking	REMS-CURVO
22A7	21,990	0,655	-			136			77	No Wrinkling	REMS-CURVO

Table 24: Raw experimental data for 473 ≤ Rm ≤ 480

Comparative and analytical evaluation of the stress at maximum load (R_m) influence on Luder Lines defect because of bending test

We follow the same comparative format as in the case of conventional yield point $R_{p_{0,2}}$ in order to visualize our conclusions.

Stress at maximum load (R_m) interval	Luder Lines' appearance (probability)
$398 \leq R_m \leq 445$	42,86%
$450 \leq R_m \leq 467$	32,56%
$473 \leq R_m \leq 480$	23,10%

Table 25: General stats regarding Luder Lines' appearance with respect to stress at maximum load

It seems to be that the probability of Luder Lines' appearance is decreasing (reducing) while the stress at maximum load R_m is increasing. This **trend** should be investigated experimentally so as to verify if this noun is valid.

$\boldsymbol{R_m}$ ↑=> **Luder Lines'** appearance ↓

We present the respective graph to possess a more perceivable approach:

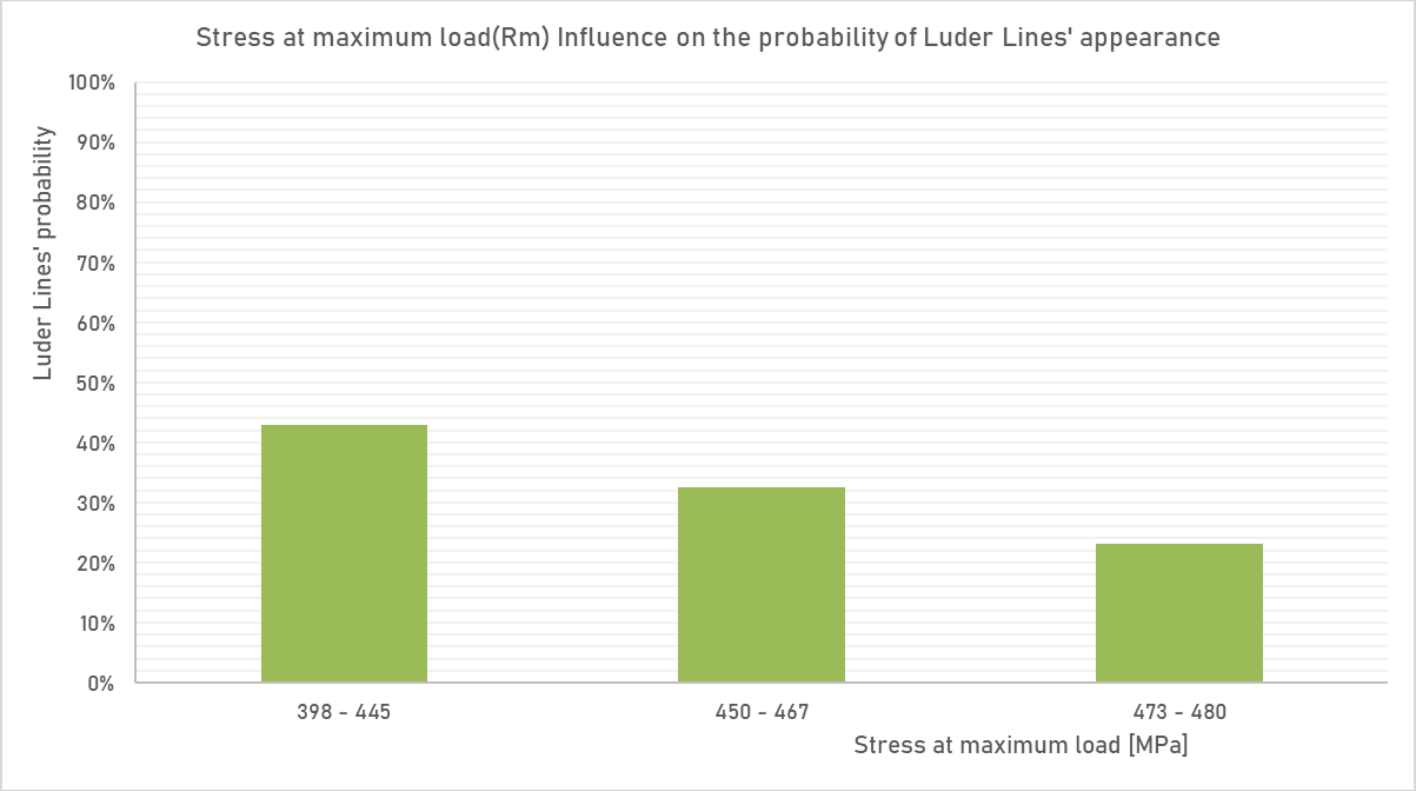

Figure 22: Stress' at maximum load effect on Luder Lines' appearance

4.1.5 Hardness HV Influence

This is a great parameter that expresses a material property as for the resistance to localized plastic deformation induced by either mechanical indentation or abrasion. We expect that it will give us some important results.

$$\mathbf{111 \leq HV \leq 121}$$

It is obvious that almost half of the samples have appeared Luder Lines after their bending defect. So, we have to zero in on this hardness region.

$111 \leq HV \leq 121$

Luder Lines' appearance: **7/13 -> 53,85%**
NO Luder Lines: 6/13 -> 46,15 %

Sample's Code	ODa	Sav.	Rp0,	Rp1	Rm	HV	Elongati	Grain Si	CLR	Outcomes
28A17	28,035	0,870	416,310		440	111,6	3,6	?	102	Luders
28A18	28,03	0,870	397,400		425	116	4,4	?	102	Slight Luders
16A4	16	0,47	453,882	461,8	463	117,2	9,7		48	Buckling
16A4	16	0,47	453,882	461,8	463	117,2	9,7		60	Buckling
18A6	18	0,7	458,661	-	463	118,7	8,2		54	Slight Luders, Light Wrinkling, Kinking
18A6	18,000	0,700	458,7	-	463	119	8,2		70	OK
28A14	28,035	0,885	382,000		398	120	6,9	?	102	Slight Luders
18A2	18,01	0,735	-		459	120,2	12	-	54	Luder Lines (with some crack)
18A2	18,010	0,735	-		459	120	12,0	-	70	No Wrinkling
18A5	18,005	0,735	472,563	-	473	120,2	7,2		54	Slight Luders
18A5	18,005	0,735	472,6	-	473	120	7,2		70	OK
28A25	27,995	0,895	425,150	435,300	436	120,7	7,2		84	Luders and Kinking
28A25	27,995	0,895	425,150	435,300	436	120,7	7,2		102	OK

Table 26: Raw experimental data for 111 ≤ HV ≤ 121

$$\mathbf{126 \leq HV \leq 138}$$

We observe also many bent hard copper tubes that suffer from Luder Lines. Also, some others appear Wrinkles or Buckling effect. Special attention should be given to the following hardness region: $136 \leq HV \leq 137$

$126 \leq HV \leq 138$

Luder Lines' appearance: **15/46 -> 32,61%**
NO Luder Lines: 31/46 -> 67,39 %

35A5	35,01	1,01	403,7		450	125,6	8,5	-	140	Light Wrinkling	REMS-CURVO
18A11	17,99	0,7	446,986	439,6	453	126,2	9,7		54	Kinking + Slight Luder Lines	Virax
18A11	17,990	0,700	447,0	439,6	453	126	9,7		70	OK	REMS-CURVO
18A8	18,005	0,61	447,925	462,9	464	126,2	8,3		54	Buckling	Virax
18A8	18,005	0,610	447,9	462,9	464	126	8,3		70	OK	REMS-CURVO
15A11	15	0,65	461,397	463,3	465	127,5	6,8		45	Buckling	Virax
15A11	15,000	0,650	461,4	463,3	465	128	6,8		55	Light Wrinkling	REMS-CURVO
22A14	22,025	0,700	448,281	457,000	457	127,6	6,2		66	Luders	Virax
22A14	22,025	0,700	448,3	457,0	457	128	6,2		77	One Wrinkle at the beginning	REMS-CURVO
15A6	14,995	0,620	421,2		443	129	4,8	-	55	No Wrinkling	REMS-CURVO
28A24	28,01	0,970	448,247	450,600	452	128,9	7,6		84	Luders	Virax
28A24	28,01	0,970	448,247	450,600	452	128,9	7,6		102	OK	REMS-CURVO
28,575A5	28,54	0,875	423,704	435,300	437	129	8,4		115	Luder Lines	REMS-CURVO
15A12	15	0,75	438,624	-	445	129,4	4,3		45	Wrinkling	Virax
15A12	15,000	0,750	438,6		445	129	4,3		55	OK	REMS-CURVO
28A2	27,995	0,89	463,15		476	130,2	6,2	-	84	Luder Lines & LL Fracture	Virax
28A2	27,995	0,89	463,15		476	130,2	6,2	-	102	Light Wrinkling	REMS-CURVO
15A10	15,000	0,530	436,3		451	131	6,6		55	Light Kinking	REMS-CURVO
28A11	28	0,710	-		463	130,7	6,3	-	102	Buckling	REMS-CURVO
28,575A8	28,575	0,940	458,411	457,700	464	130,9	7,2		115	Luder Lines	REMS-CURVO
28A22	28	0,890	445,203	453,100	454	131,3	8,4		84	Luders	Virax
28A22	28	0,890	445,203	453,100	454	131,3	8,4		102	One Wrinkle at the beginning	REMS-CURVO
18A4	18,015	0,61	448,29		459	131,4	6		54	Kinking with Luder Crack	Virax
18A4	18,015	0,610	448,3		459	131	6,0		70	No Wrinkling	REMS-CURVO
15A17	14,99	0,69	443,112	453	456	131,7	10		45	Buckling	Virax
15A17	14,990	0,690	443,1	453,0	456	132	10,0		55	OK	REMS-CURVO
28,575B1	28,565	0,835	448,000		456	133	4,6	-	132	Wrinkling 33% + Luder Lines	?
28A23	28	0,900	432,219	449,000	453	134,5	4,4		84	Luders	Virax
28A23	28	0,900	432,219	449,000	453	134,5	4,4		102	No Wrinkling (Tendency to Light Wrinkling)	REMS-CURVO
35A8	35,04	1,09	404,101	434,9	436	135,3	7,65		140	OK	REMS-CURVO
18A9	17,99	0,65	446,498	445,2	454	135,6	7,8		54	Kinking + Slight Luder Lines	Virax
18A9	17,990	0,650	446,5	445,2	454	136	7,8		70	OK	REMS-CURVO
35A12	35,05	1,035	404,471	454,4	455	136,2	13		140	OK	REMS-CURVO
22A7	21,990	0,655	-			136			77	No Wrinkling	REMS-CURVO
35A10	35,02	1,01	379,735	403,9	404	136,4	5,8		140	OK	REMS-CURVO
15,875A2	15,86	0,74	455,09	450,9	460	137	7,7		48	OK	Virax
15,875A2	15,86	0,74	455,09	450,9	460	137	7,7		63	OK	REMS-CURVO
22A16	21,98	0,560	450,242	446,000	456	137,1	9,7		66	Buckling	Virax
22A16	21,980	0,560	450,2	446,0	456	137	9,7		77	Buckling	REMS-CURVO
22A11	22,02	0,605	454,500		458	137,3	3,8	-	66	Luder Crack	Virax
22A11	22,020	0,605	454,5		458	137	3,8	-	77	Light Waved Wrinkling	REMS-CURVO
15,875A4	15,865	0,71	456,008		461	137,6	8,8		48	OK	Virax
15,875A4	15,865	0,71	456,008	-	461	137,6	8,8		63	OK	REMS-CURVO
28,575A6	28,545	0,880	441,004	443,300	445	138,1	6,4		115	Luder Lines	REMS-CURVO
28A27	28	0,780	464,064	461,700	467	138,1	9,7		84	Kinking + Luder Lines	Virax
28A27	28	0,780	464,064	461,700	467	138,1	9,7		102	Light Kinking + Luder Lines	REMS-CURVO

Table 27: Raw experimental data for 126 ≤ HV ≤ 138

The probability of Luder Lines' appearance in this case ($126 \leq HV \leq 138$) is significantly lower than in the previous one ($111 \leq HV \leq 121$). Let us research if this trend is going to be true.

$139 \leq HV \leq 143$

Almost all samples do **not** appear Luder Lines. So, it is valid that increasing the hardness HV factor means decreasing the probability of Luder Lines' manifestation. In this way, we correlate this material parameter with the Luder Lines defect.

$139 \leq HV \leq 143$
Luder Lines' appearance: **1/12 -> 8,33%**
NO Luder Lines: 11/12 -> 91,67 %

15A13	15,01	0,535	441,5836	475,3	476	139,1	12,3		45	Buckling	Virax
15A13	15,010	0,535	441,6	475,3	476	139	12,3		55	Buckling	REMS-CURVO
15,875A7	15,855	0,56	474,656		480	139,1	0,2		48	Kinking	Virax
15,875A7	15,855	0,56	474,656	-	480	139,1	0,2		63	Kinking	REMS-CURVO
35A11	35,005	0,9	414,1227	440,4	441	139,4	5,6		140	Flattening	REMS-CURVO
15A15	15,035	0,455	444,4939	455,1	465	139,4	7,7		45	Crack	Virax
15A15	15,035	0,455	444,5	455,1	465	139	7,7		55	Buckling	REMS-CURVO
35A7	35,02	1,085	407,6599	438,8	439	140,4	5,5		140	OK	REMS-CURVO
15A16	14,99	0,695	464,25	463,1	473	140,4	9		45	Buckling + Cracking	Virax
15A16	14,990	0,695	464,3	463,1	473	140	9,0		55	OK	REMS-CURVO
18A10	18	0,605	467,776	459,8	477	142,6	9,6		54	Kinking + Luder Lines	Virax
18A10	18,000	0,605	467,8	459,8	477	143	9,6		70	OK	REMS-CURVO

Table 28: Raw experimental data for 139 ≤ HV ≤ 143

Comparative and analytical evaluation of the hardness (HV) influence on Luder Lines defect because of bending test

We can assess the hardness' HV influence on the probability of Luder Lines' manifestation more easily if we create the table down below. In this way, we gather all our results together so as to find a specific trend in order to predict this defect as precisely as it is possible.

Hardness (HV) interval	Luder Lines' appearance (probability)
$111 \leq HV \leq 121$	53,85%
$126 \leq HV \leq 138$	32,61%
$139 \leq HV \leq 143$	8,33%

Table 29: General stats regarding Luder Lines' appearance with respect to hardness

Visualizing the Hardness interval – Luder Lines' appearance graph, we understand that if the factor of hardness rises, the probability of Luder Lines' appearance is even lower. So, these two characteristics are inversely proportional!

$\boldsymbol{HV}$ ↑=> **Luder Lines'** appearance ↓

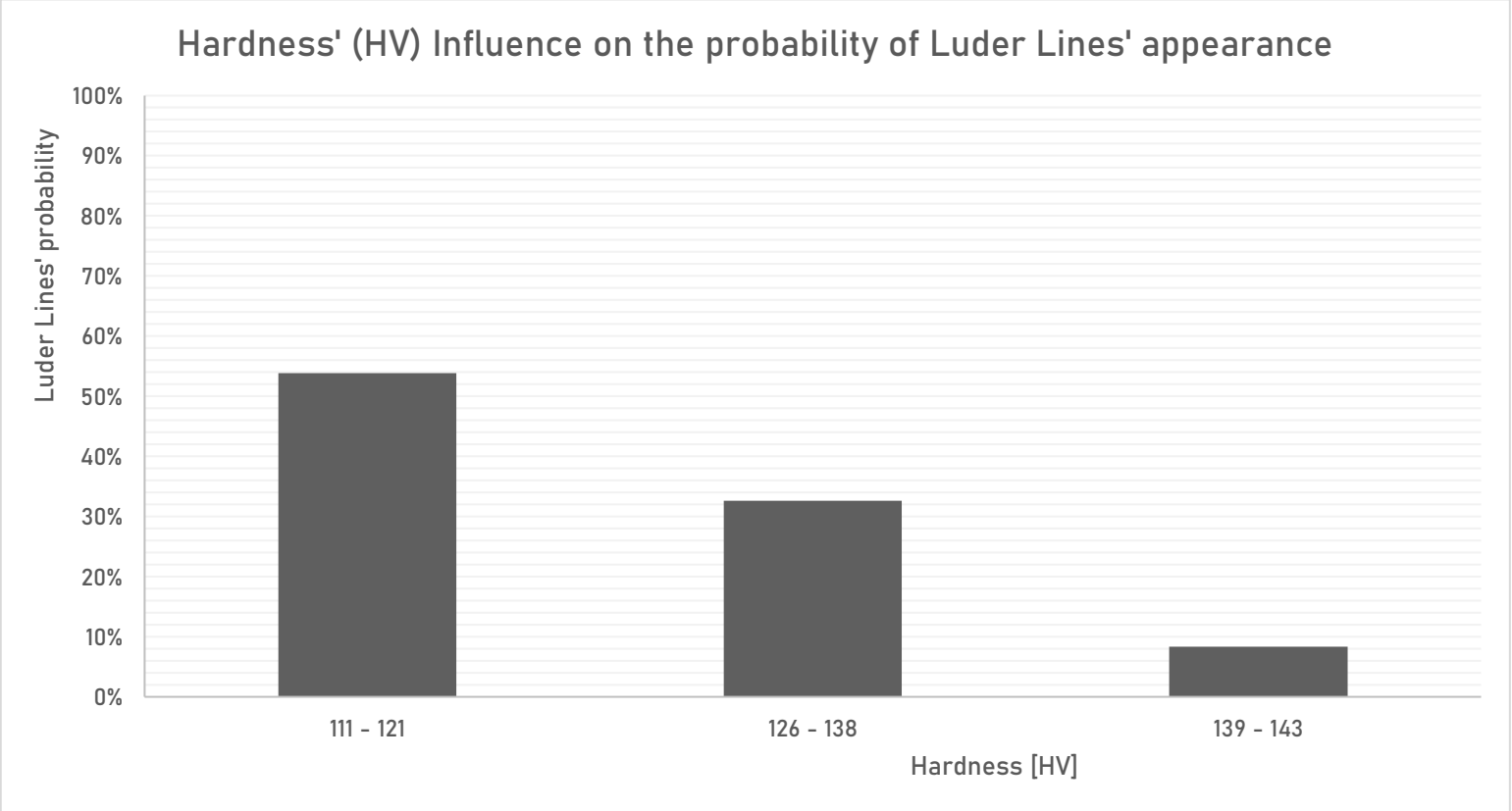

Figure 23: Hardness' effect on Luder Lines' occurrence

** This finding is extremely significant because we are able to perform hardness test for a small part of copper tube and we do not need the whole tube. So, at any time we can measure the value of this material characteristic.

4.1.6 Bending Radius' CLR Influence

Bending tests are affected by the value of bending radius CLR. Sorting the numbers of this parameter we can extract really useful findings. It should be pointed out that this parameter (CLR) depends on the nominal outer diameter (OD) and the bender type (Virax or REMS) according to the table down below:

OD	VIRAX	REMS
	BENDING RADIUS - CLR (mm)	
3/8"	30	43
10	30	40
12	36	45
1/2"	36	52
14	42	50
15	45	55
5/8"	48	63
16	48	60
18	54	70
3/4"	54	75
22	66	77
7/8"		98
1"		101
28	84	102
1 1/8"		115
1 1/4"		133
1 3/8"		140
35		140

Table 30: CLR values according to the bender type and the outer diameter

We possess hard copper tubes' samples, which have been bent, for these nominal outer diameters: $OD = 15\,mm$, $OD = 15{,}875\ \left(\frac{5''}{8}\right)mm$, $OD = 16\,mm$ (only 1 sample), $OD = 16\,mm$, $OD = 18\,mm$, $OD = 22\,mm$, $OD = 25{,}40\ (1'')\,mm$ (only 2 samples), $OD = 28\,mm$, $OD = 28{,}575\ (1\frac{1}{8}'')mm$, $OD = 35\,mm$.

$CLR = 45$ or $CLR = 48$

We perceive easily that no bent tube of this class has appeared Luder Lines, even when tested with Virax bender. Virax enhances Luder Lines generally, as it has been proved in the previous pages of this work.

15A12	15	0,75	438,6238	-	445	129,4	4,3		45	Wrinkling	Virax
15A11	15	0,65	461,3969	463,3	465	127,5	6,8		45	Buckling	Virax
15A15	15,035	0,455	444,4939	455,1	465	139,4	7,7		45	Crack	Virax
15A16	14,99	0,695	464,25	463,1	473	140,4	9		45	Buckling + Cracking	Virax
15A17	14,99	0,69	443,112	453	456	131,7	10		45	Buckling	Virax
15A13	15,01	0,535	441,5836	475,3	476	139,1	12,3		45	Buckling	Virax
15,875A7	15,855	0,56	474,656		480	139,1	0,2		48	Kinking	Virax
15,875A2	15,86	0,74	455,09	450,9	460	137	7,7		48	OK	Virax
15,875A4	15,865	0,71	456,008		461	137,6	8,8		48	OK	Virax
16A4	16	0,47	453,8825	461,8	463	117,2	9,7		48	Buckling	Virax

Table 31: Raw experimental data for CLR = 45 or CLR = 48

$CLR = 45$
Luder Lines' appearance: **0/6 -> 0%**
NO Luder Lines: 6/6 -> 100 %

$CLR = 48$
Luder Lines' appearance: **0/4 -> 0%**
NO Luder Lines: 4/4 -> 100 %

$CLR = 54$

Here, we have the exact opposite situation regarding the hard copper tube's behaviour during bending test. It can be observed that almost all specimens suffer from Luder Lines' defect. So, this bending radius is hazardous for bending test and should be avoided if possible, because there is a great risk of Luder Lines' appearance.

18A4	18,015	0,61	448,29		459	131,4	6		54	Kinking with Luder Crack	Virax
18A5	18,005	0,735	472,5625	-	473	120,2	7,2		54	Slight Luders	Virax
18A9	17,99	0,65	446,498	445,2	454	135,6	7,8		54	Kinking + Slight Luder Lines	Virax
18A6	18	0,7	458,6607	-	463	118,7	8,2		54	Slight Luders, Light Wrinkling, Kinking	Virax
18A8	18,005	0,61	447,9253	462,9	464	126,2	8,3		54	Buckling	Virax
18A10	18	0,605	467,776	459,8	477	142,6	9,6		54	Kinking + Luder Lines	Virax
18A11	17,99	0,7	446,986	439,6	453	126,2	9,7		54	Kinking + Slight Luder Lines	Virax
18A2	18,01	0,735	-		459	120,2	12	-	54	Luder Lines (with some crack)	Virax

Table 32: Raw experimental data for CLR = 54

$CLR = 54$
Luder Lines' appearance: **7/8 -> 87,5 %**
NO Luder Lines: 1/8 -> 12,5 %

$CLR = 55$ *or* $CLR = 60$ *or* $CLR = 63$

We can note there that none of the specimens has appeared Luder Lines, which is the desired condition. However, we cannot be sure about the tubes' bending behaviour if $CLR = 60$, since we possess only 1 sample.

15A12	15,000	0,750	438,6		445	129	4,3		55	OK	REMS-CURVO
15A6	14,995	0,620	421,2		443	129	4,8	-	55	No Wrinkling	REMS-CURVO
15A10	15,000	0,530	436,3		451	131	6,6		55	Light Kinking	REMS-CURVO
15A11	15,000	0,650	461,4	463,3	465	128	6,8		55	Light Wrinkling	REMS-CURVO
15A15	15,035	0,455	444,5	455,1	465	139	7,7		55	Buckling	REMS-CURVO
15A16	14,990	0,695	464,3	463,1	473	140	9,0		55	OK	REMS-CURVO
15A17	14,990	0,690	443,1	453,0	456	132	10,0		55	OK	REMS-CURVO
15A13	15,010	0,535	441,6	475,3	476	139	12,3		55	Buckling	REMS-CURVO
16A4	16	0,47	453,8825	461,8	463	117,2	9,7		60	Buckling	REMS-CURVO
15,875A7	15,855	0,56	474,656	-	480	139,1	0,2		63	Kinking	REMS-CURVO
15,875A2	15,86	0,74	455,09	450,9	460	137	7,7		63	OK	REMS-CURVO
15,875A4	15,865	0,71	456,008	-	461	137,6	8,8		63	OK	REMS-CURVO

Table 33: Raw experimental data for CLR = 55 or CLR = 60 or CLR = 63

$CLR = 55$
Luder Lines' appearance: **0/8 -> 0 %**
NO Luder Lines: 8/8 -> 100 %

$CLR = 60$ (Only 1 specimen)
Luder Lines' appearance: **0/1 -> 0 %**
NO Luder Lines: 1/1 -> 100 %

$CLR = 63$
Luder Lines' appearance: **0/3 -> 0 %**
NO Luder Lines: 3/3 -> 100 %

$CLR = 66$

Unfortunately, we have few samples (3 samples) for this category and that is why it is difficult to extract a safe deduction for the probability of Luder Lines' manifestation.

22A11	22,02	0,605	454,500		458	137,3	3,8	-	66	Luder Crack	Virax
22A14	22,025	0,700	448,281	457,000	457	127,6	6,2		66	Luders	Virax
22A16	21,98	0,560	450,242	446,000	456	137,1	9,7		66	Buckling	Virax

Table 34: Raw experimental data for CLR = 66

$CLR = 66$
Luder Lines' appearance: **2/3 -> 66,67 %**
NO Luder Lines: 1/3 -> 33,33 %

$CLR = 70$ *or* $CLR = 77$

Hopefully, no hard copper tube has shown Luder Lines defect during bending test. For the bending radius equal to $CLR = 70$, our result is more reliable since the samples' size is bigger than the category of $CLR = 77$.

18A4	18,015	0,610	448,3		459	131	6,0		70	No Wrinkling	REMS-CURVO
18A5	18,005	0,735	472,6	-	473	120	7,2		70	OK	REMS-CURVO
18A9	17,990	0,650	446,5	445,2	454	136	7,8		70	OK	REMS-CURVO
18A6	18,000	0,700	458,7	-	463	119	8,2		70	OK	REMS-CURVO
18A8	18,005	0,610	447,9	462,9	464	126	8,3		70	OK	REMS-CURVO
18A10	18,000	0,605	467,8	459,8	477	143	9,6		70	OK	REMS-CURVO
18A11	17,990	0,700	447,0	439,6	453	126	9,7		70	OK	REMS-CURVO
18A2	18,010	0,735	-		459	120	12,0	-	70	No Wrinkling	REMS-CURVO
22A11	22,020	0,605	454,5		458	137	3,8	-	77	Light Waved Wrinkling	REMS-CURVO
22A14	22,025	0,700	448,3	457,0	457	128	6,2		77	One Wrinkle at the beginning	REMS-CURVO
22A16	21,980	0,560	450,2	446,0	456	137	9,7		77	Buckling	REMS-CURVO
22A7	21,990	0,655	-			136			77	No Wrinkling	REMS-CURVO

Table 35: Raw experimental data for CLR = 70 or CLR = 77

$CLR = 70$
Luder Lines' appearance: **0/8 -> 0 %**
NO Luder Lines: 8/8 -> 100 %

$CLR = 77$
Luder Lines' appearance: **0/4 -> 0 %**
NO Luder Lines: 4/4 -> 100 %

$CLR = 84$

Unfortunately, all bent tubes have appeared Luder Lines or combination of Luder Lines and Kinking, even crack / fracture after Luder Lines formation. Apart from $CLR = 54$ this bending radius seems to be risky for Luder Lines free bending tests.

$CLR = 84$
Luder Lines' appearance: **6/6 -> 100 %**
NO Luder Lines: 0/6 -> 0 %

28A23	28	0,900	432,219	449,000	453	134,5	4,4		84	Luders	Virax
28A2	27,995	0,89	463,15		476	130,2	6,2	-	84	Luder Lines & LL Fracture	Virax
28A25	27,995	0,895	425,150	435,300	436	120,7	7,2		84	Luders and Kinking	Virax
28A24	28,01	0,970	448,247	450,600	452	128,9	7,6		84	Luders	Virax
28A22	28	0,890	445,203	453,100	454	131,3	8,4		84	Luders	Virax
28A27	28	0,780	464,064	461,700	467	138,1	9,7		84	Kinking + Luder Lines	Virax

Table 36: Raw experimental data for CLR = 84

$CLR = 102$

It is the first case of bending radius CLR, in which the condition of Luder Lines' appearance is not so clear compared to the lower values of CLR. It seems that it is more probable to observe some other defects or clear bending rather than Luder Lines.

28A17	28,035	0,870	416,310		440	111,6	3,6	?	102	Luders	REMS-CURVO
28A18	28,03	0,870	397,400		425	116	4,4	?	102	Slight Luders	REMS-CURVO
28A23	28	0,900	432,219	449,000	453	134,5	4,4		102	No Wrinkling (Tendency to Light Wrinkling)	REMS-CURVO
28A2	27,995	0,89	463,15		476	130,2	6,2	-	102	Light Wrinkling	REMS-CURVO
28A11	28	0,710	-		463	130,7	6,3	-	102	Buckling	REMS-CURVO
28A14	28,035	0,885	382,000		398	120	6,9	?	102	Slight Luders	REMS-CURVO
28A25	27,995	0,895	425,150	435,300	436	120,7	7,2		102	OK	REMS-CURVO
28A24	28,01	0,970	448,247	450,600	452	128,9	7,6		102	OK	REMS-CURVO
28A22	28	0,890	445,203	453,100	454	131,3	8,4		102	One Wrinkle at the beginning	REMS-CURVO
28A27	28	0,780	464,064	461,700	467	138,1	9,7		102	Light Kinking + Luder Lines	REMS-CURVO

Table 37: Raw experimental data for CLR = 102

$CLR = 102$
Luder Lines' appearance: **4/10 -> 40 %**
NO Luder Lines: 6/10 -> 60 %

$CLR = 115$

It can be observed there that all samples suffer from Luder Lines defect. However, we need more samples to verify our conclusion. 28,575B1 stands for a bent sample (hard copper tube) bent by a competitor company with another bender type of higher bending radius

28,575A6	28,545	0,880	441,004	443,300	445	138,1	6,4		115	Luder Lines	REMS-CURVO
28,575A8	28,575	0,940	458,411	457,700	464	130,9	7,2		115	Luder Lines	REMS-CURVO
28,575A5	28,54	0,875	423,704	435,300	437	129	8,4		115	Luder Lines	REMS-CURVO
28,575B1	28,565	0,835	448,000		456	133	4,6	-	132	Wrinkling 33% + Luder Lines	?

Table 38: Raw experimental data for CLR = 115

$CLR = 115$
Luder Lines' appearance: **4/4 -> 100 %**
NO Luder Lines: 0/4 -> 0 %

$CLR = 140$

Our 6 bent copper tubes of the highest bending radius and nominal outer diameter do not form Luder Lines on their surface. In addition, 4 of them had clear bending, which is the best-case scenario (the desired one).

35A7	35,02	1,085	407,6599	438,8	439	140,4	5,5		140	OK	REMS-CURVO
35A11	35,005	0,9	414,1227	440,4	441	139,4	5,6		140	Flattening	REMS-CURVO
35A10	35,02	1,01	379,7346	403,9	404	136,4	5,8		140	OK	REMS-CURVO
35A8	35,04	1,09	404,1009	434,9	436	135,3	7,65		140	OK	REMS-CURVO
35A5	35,01	1,01	403,7		450	125,6	8,5	-	140	Light Wrinkling	REMS-CURVO
35A12	35,05	1,035	404,471	454,4	455	136,2	13		140	OK	REMS-CURVO

Table 39: Raw experimental data for CLR = 140

$CLR = 140$
Luder Lines' appearance: **0/6 -> 0 %**
NO Luder Lines: 6/6 -> 100 %

Comparative and analytical evaluation of the bending radius (CLR) influence on Luder Lines defect because of bending test

This analysis has many similarities with the nominal outer diameter's (OD) effect on Luder Lines formation. In the same way, we create the table which relates the available CLR values with the bending result.

Bending Radius (CLR) value	Luder Lines' appearance (probability)
$CLR = 45$	0%
$CLR = 48$	0%
$CLR = 54$	87,5%
$CLR = 55$	0%
$CLR = 60$	0%
$CLR = 63$	0%
$CLR = 66$	66,67%
$CLR = 70$	0%
$CLR = 77$	0%
$CLR = 84$	100%
$CLR = 102$	40%
$CLR = 115$	100%
$CLR = 140$	0%

Table 40: General stats regarding Luder Lines' appearance with respect to bending radius

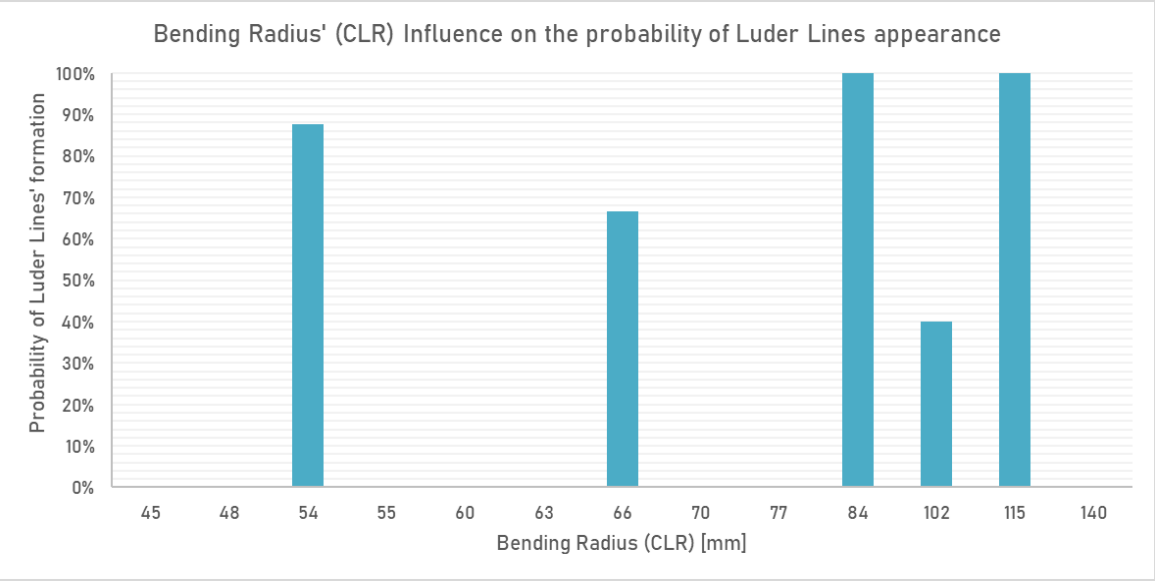

Figure 24: Bending radius effect on Luder Lines' formation

4.2 Key Findings & Respective Trends

The practical purpose of this qualitative analysis lies in the trends' finding for Luder Lines' appearance or not. According to the previous pages, we can summarize the most momentous findings in the following bullet points:

- **No** sufficient correlation among the values of the **nominal outer diameter** ($\boldsymbol{OD}$) and the probability of **Luder Lines'** appearance.

Result	$OD = 15\ mm$ $OD = 15{,}875\ mm$ $OD = 16\ mm$ $OD = 25{,}4\ mm$	$\boldsymbol{OD = 18\ mm}$	$\boldsymbol{OD = 22\ mm}$	$\boldsymbol{OD = 28\ mm}$	$\boldsymbol{OD = 28{,}575\ mm}$	$OD = 35\ mm$
Luder Lines (Percent)	0%	**43,75%**	**28,57%**	**62,50%**	**100%**	0%

Table 41: Probability of Luder Lines' formation with respect to the outer diameter

- **Considerable** influence of the nominal **wall thickness** ($\boldsymbol{WT}$) on the probability of **Luder Lines'** occurrence => Semi – empirical rule extracted:

  $(0{,}455 \leq WT_{av} \leq 0{,}56$ **OR** $0{,}605 \leq WT_{av} < 0{,}75$ **OR** $0{,}89 \leq WT_{av} \leq 1{,}09)$ **AND**
  (REMS – CURVO Bender) => **NO Luder Lines**

  $(0{,}78 \leq WT_{av} \leq 0{,}885)$ **AND** (REMS – CURVO **OR** Virax) => **Luder Lines**

- The probability of **Luder Lines'** appearance is decreasing while the **stress at maximum load** $\boldsymbol{R_m}$ is rising.

  $\boldsymbol{R_m}$ ↑=> Probability of **Luder Lines'** appearance ↓

- The **hardness** factor is inversely related to the probability of Luder Lines' occurrence.

  $\boldsymbol{HV}$ ↑=> Probability of **Luder Lines'** appearance ↓

- The **bender type** (tool of plastic deformation) plays a major role in the upcoming result of bending test (e.g. OK [Clear Bending], Wrinkling, Kinking, Crack, Buckling, **Luder Lines**]. For instance, the same physical sample gives different defects after the bending tests, if bent with REMS and Virax. This parameter is modelled through the physical quantity of bending radius $\boldsymbol{CLR}$. And it has been proved that 5 critical $\boldsymbol{CLR}$ values exist.

  IF $(\boldsymbol{CLR = 54\ OR\ CLR = 66\ OR\ CLR = 88\ OR\ CLR = 102\ OR\ CLR = 115})$ => Great probability of **Luder Lines'** occurrence
  ELSEIF => **NO** Luder Lines

- The factors named conventional yield point $\boldsymbol{R_{p_{0,2}}}$ and **elongation** cannot account for the variation of the results. At the same time, we do not have sufficient data for the parameters of $\boldsymbol{R_{p_1}}$ and **Grain Size.**

The most **influencing factors** for the Luder Lines' occurrence seem to be the following ones:

- OD, WT, CLR (Geometry)
- HV, R_m (Material)

4.3 Quantitative Analysis

4.3.1 Created Indices and Metrics

On this page all metrics, indices and formulas are included to have a total representation of the work done in the Excel files. The following mathematical approach is written down below:

1. $\frac{WT_{av}\, CLR}{OD_{av}}$ (Index used by Panagiotis Christinakis during my summer internship)
2. $\frac{CLR-(\frac{OD_{av}}{2})}{WT_{av}}$ (Index recommended in a paper)
3. $\frac{(\,OD_{av}-WT_{av})^2}{WT_{av}\, CLR}$ (Index recommended in a paper)
4. $BF = \frac{{OD_{av}}^2}{WT_{av}\, CLR}$ (Bending difficulty factor)
5. $BF_{new} = \sqrt{\frac{OD/t}{(CLR/OD)^3}} = \frac{OD^2}{CLR^{1,5}\, {WT_{av}}^{0,5}}$

   The indices 2 – 6 correlate the geometrical properties of the tube (Outer Diameter OD and Wall Thickness WT) with the bender type (CLR: Centre Line Radius) solely. They cannot explain differences regarding material properties.
6. $\frac{\sigma_{UTS}-\sigma_{0.2}}{\sigma_{UTS}} = \frac{R_m-R_{p_{0,2}}}{R_m}$ (Call Spitas 20-01-21.mp4)
7. $\frac{\sigma_{UTS}-\sigma_{1.0}}{\sigma_{UTS}} = \frac{R_m-R_{p_1}}{R_m}$

   The metrics 1, 7 & 8 focus on the tailored material characteristics extracted from a typical true stress σ – true stress ε curve such as the yield point $\sigma_{0.2}$, the stress point for 1% elongation $\sigma_{1.0}$ and the ultimate tensile strength σ_{UTS}. Special reference has been given for the index No. 1
8. $\frac{BF_{new}}{Elongation}$
9. $BF_{new} HV^{1,5}$
10. $BF_{new} HV^{1,1} CLR^{0,7} {R_{p_{0,2}}}^{-1,5}$

    As the **formula 6 ($\boldsymbol{BF_{new}}$)** is the **most effective way** to **discrete Luder Lines'** appearance among other results (OK, Wrinkling, Buckling, Kinking, Crack), we have decided to correlate this index with some other characteristics used before to achieve much higher accuracy for our predictive empirical model. Consequently, we have created the above metrices 9, 10 & 11.
11. $\frac{(\frac{OD_{av}}{WT_{av}})^3}{HV} - 15\frac{CLR}{OD_{av}}$ (C -Factor)
12. $R_{p_{0,2}} - R_m$
13. CLR/WT_{av}
14. CLR/OD_{av}
15. $\boldsymbol{BF_{adj} = \frac{OD^{2,2}}{CLR^{1,3}\, {WT_{av}}^{-0,7}}}$

4.3.2 Reliable Geometrical Index BF_{adj}

As it has been mentioned before, the metric No. 6 BF_{new} can **separate** somewhat effectively the dataset between the 2 conditions: **Luder Lines** or **Any Result** we decide to focus on the parameters (exponents) of this equation. This index can be written in general form in this way:

$$BF_{general} = \frac{OD^{\boldsymbol{n}}}{CLR^{\boldsymbol{m}}\, WT_{av}{}^{\boldsymbol{p}}}$$

Through the method of trial and error (although it is not a systematic way) altering the exponents $(\boldsymbol{n}, \boldsymbol{m}, \boldsymbol{p})$ we end up to this adjusted formula:

$$BF_{adj} = \frac{OD^{\mathbf{2,2}}}{CLR^{\mathbf{1,3}}\, WT_{av}{}^{\mathbf{-0,7}}}$$

It should be pointed out that we split our dataset into 2 distinct categories (sub - datasets:

- Copper tubes bent with **REMS – CURVO**
- Copper tubes bent with **Virax**

In this way, we can have more reliable results as for our formulas and metrics. Each type of bender has different tooling parameters (CLR, friction between various dies, bending speed, plastic deformation mechanism). So, it is not fair to compare our metrics without dividing our samples.

We will begin our quantitative analysis of the dataset by investigating the influence of the BF_{adj} metric on the probability of Luder Lines' occurrence on the hard copper tubes' surface.

Metric 16 BF_{adj} | REMS – CURVO Samples

We wish to know the exact BF_{adj} region in which Luder Lines are formed. In this way, we manage to have a predictive tool to determine the behaviour of the hard copper tube after bending test. The sample size of our data set for **REMS – CURVO** bending is 48. Only 7 out of 48 samples **(14,58%)** appeared **Luder Lines.**

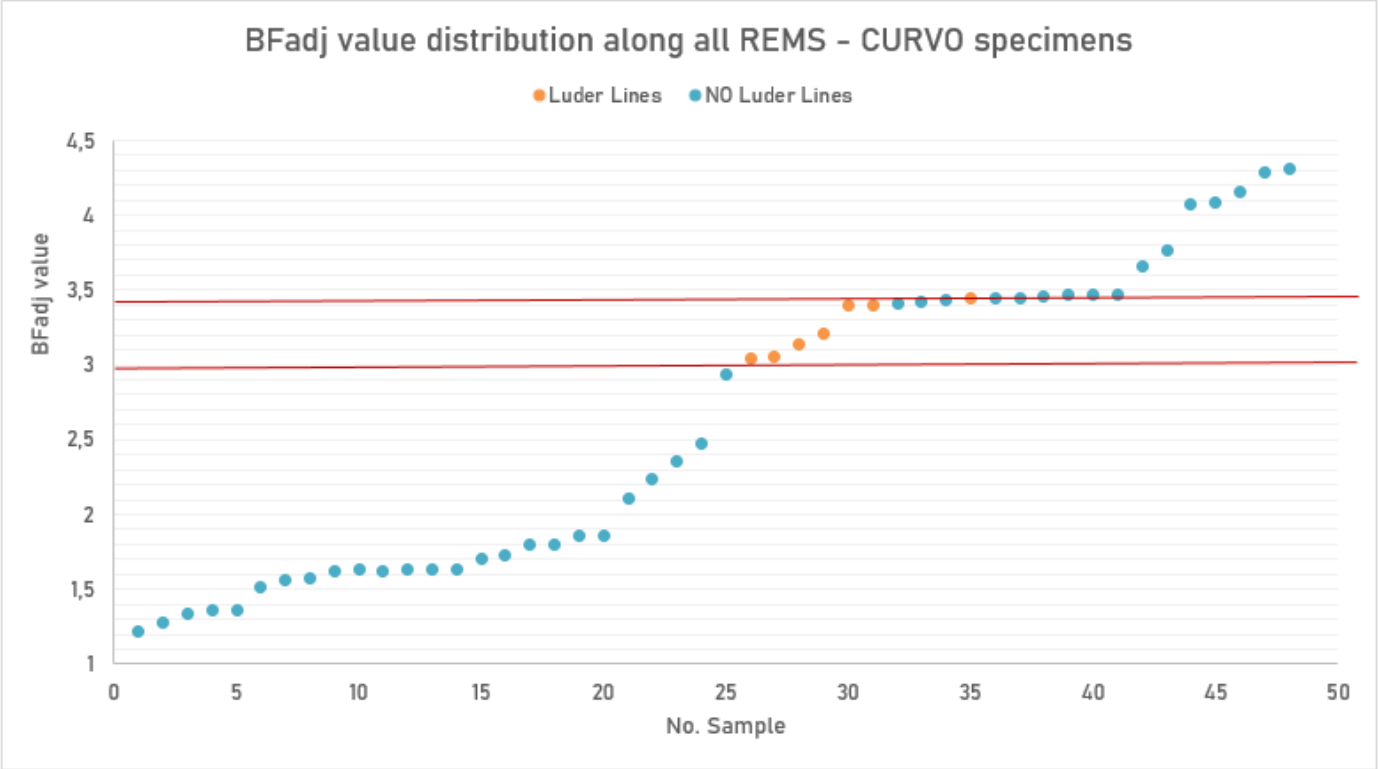

Figure 25: Scatter chart which shows the critical zone of Luder Lines' appearance [REMS - CURVO]

It can be pinpointed that a specific BF_{adj} interval exists where the probability of Luder Lines' occurrence is very high. According to our samples we can split the BF_{adj} interval into 3 sub – intervals:

- $0 \leq BF_{adj} \leq 3$: **NO** Luder Lines (25/25 -> **100%)**
- $3 < BF_{adj} \leq 3{,}45$: **Luder Lines** appearance (7/12 -> **58,33%)**
- $BF_{adj} > 3{,}45$: **NO** Luder Lines (11/11 -> **100%**)

Metric 16 BF_{adj} | Virax Samples

The remaining 27 specimens have been bent with the aid of Virax bender, as it does not support so many outer diameters (OD) as the REMS – CURVO machine. We keep in mind that Virax accounts for many samples that have appeared Luder Lines, while REMS -Curvo did not cause any defect for the same hard copper tube.

We present the distinctive figure visualizing the BF_{adj} value along these 27 samples.

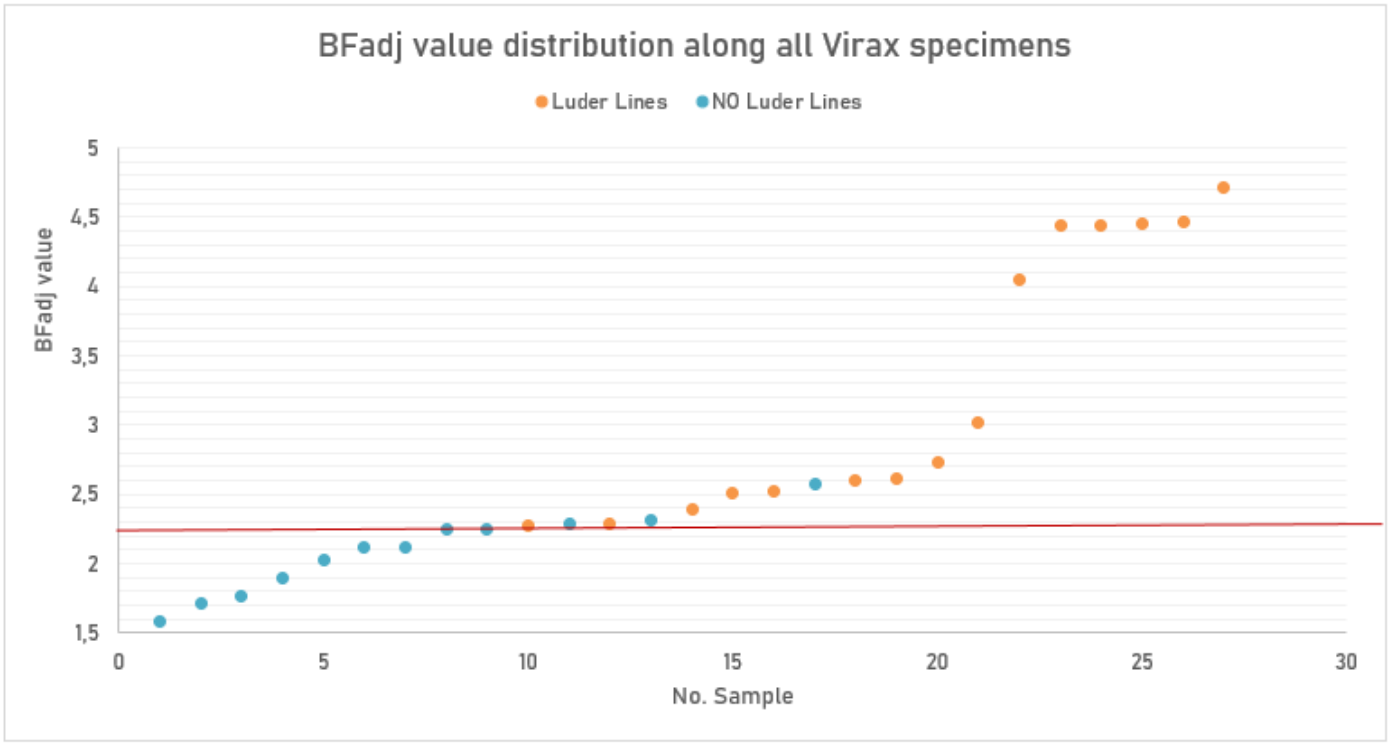

Figure 26: Scatter chart which shows the critical zone of Luder Lines' appearance [Virax]

There is a certain threshold, which seems to determine the copper tubes' behaviour during bending. Therefore, we write down a semi – empirical rule to predict the Luder Lines' appearance for tubes bent with Virax.

- $0 \leq BF_{adj} \leq 2{,}25$: **NO** Luder Lines (9/9 -> **100%)**
- $BF_{adj} > 2{,}25$: **Luder Lines** appearance (15/18 -> **83,33%**)

4.4 Material Characterization

4.4.1 How to model the material's behaviour?

We wish to obtain a quite different approach to predict the Luder Lines' manifestation ignoring the geometry coefficients. Actually, what we would desire is to make creative use of the materials' behaviour. The material is common for all specimens: Cu – DHP – Hard Temper (99,9% Cu) and is modelled through the available data:

- Hardness HV
- Stress at maximum load R_m
- Engineering stress s – engineering strain e graph

Despite the fact that the material is exactly the same for all samples, each tube has not achieved the same production quality. Therefore, there are some important variations along the above parameters.

The scope of this analysis is to extract a semi – empirical rule to predict the non – linear phenomenon (Luder Lines) relied on the material properties solely. That is why we have to extract more detailed information from stress – strain diagrams.

We will zero in on the insightful stress – strain diagrams in order to extract some interesting trends. We will set our criteria in order to realize what is going on.

4.4.2 Focus on the flow curves

We have at our disposal 35 different engineering stress s – engineering strain e diagrams for each sample. These graphs come from a uniaxial tension test performed in Halcor's Quality Control Laboratory. Every single hard copper tube presents a different deformation behaviour.

Let us visualize a typical s – e curve (Hard Temper always):

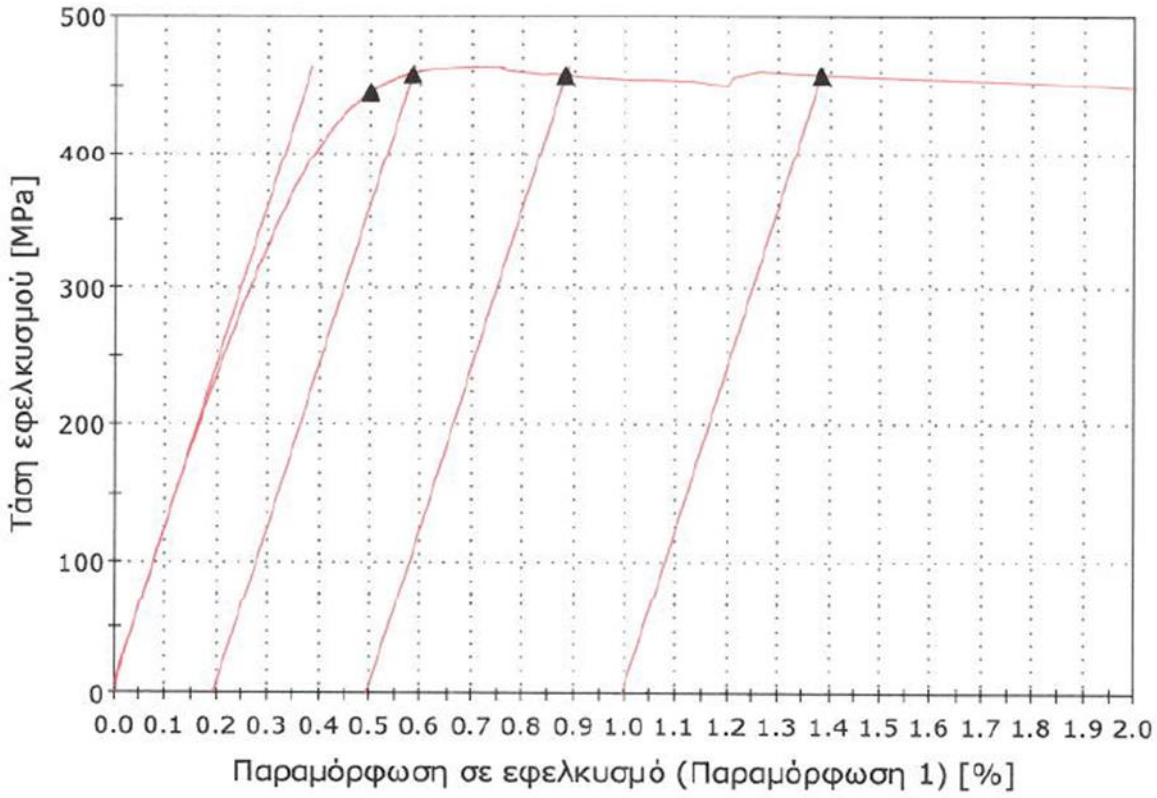

Figure 27: Typical engineering stress - strain graph for hard copper Cu - DHP

We are going to perform many quantitative manipulations in order to achieve as detailed information as possible. The range of our interest starts from the yield point σ_Y and ends up to ultimate tensile strength (UTS) σ_{UTS}. We ignore the linear part that describes the elastic region of the material. We focus on the plastic region of the curves, where deformation /strain is permanent and cannot avoided after unloading.

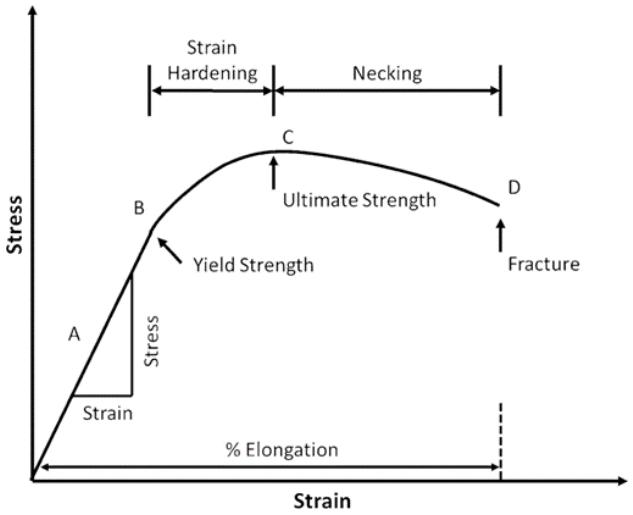

Figure 28: Typical stress - strain curve of a metallic material

** We have decided that $\sigma_Y \cong \sigma_{0,3\%}$ (the same) for each hard copper tube and σ_{UTS} will be the stress point at which strain hardening ends.

Our experimental data points (which come from digitization of the s – e curves) have to be transformed to the desired ones following the algorithm down below:

1. True (total) strain's dependency from engineering strain

$\varepsilon_{\mathrm{T}} = ln(e+1)$, where: $e = \frac{\Delta \mathrm{L}}{L}$

2. True plastic strain (True Elastic strain ε_{T} substructure from true (total) strain)

$\varepsilon_P = \varepsilon_{\mathrm{T}} - \varepsilon_E \Rightarrow \varepsilon_P = \varepsilon_{\mathrm{T}} - \frac{s}{E}$

3. True stress relation to engineering stress

$\sigma = s(\varepsilon_P + 1)$

Assumption: Copper unloads following a line whose slope equals to the initial modulus of elasticity E.

In addition, a schematic illustration of the transformation is attached in order to present shortly the idea.

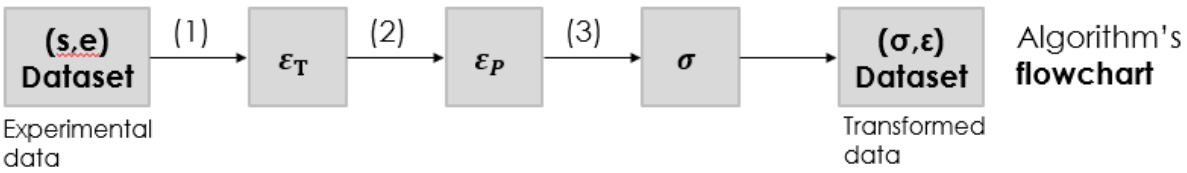

Figure 29: Engineering stress - strain values to true ones through a transformation

The whole quantitative information is enclosed into the Excel file "Stress – Strain Data Points (All Curves).xlsx" that contains the analytical computations and the modulus of elasticity E for each sample.

18A11		22A16		25,40A2		28A2	
εp	σ(εp)	εp	σ(εp)	εp	σ(εp)	εp	σ(εp)
0,157003	200,314	0,248343	270,6705	0,244983	293,4254	0,195453	284,5001
0,16244	206,4572	0,256166	276,707	0,253288	301,8042	0,200603	289,7614
0,170572	212,6069	0,263771	284,7491	0,261691	310,1846	0,205661	293,968
0,178676	221,8242	0,2689	290,7798	0,270013	316,4772	0,208232	297,1266
0,186788	230,0207	0,276722	296,8191	0,278425	323,8158	0,215868	303,4379
0,195009	237,1964	0,281742	303,8537	0,286736	331,1551	0,220917	308,701
0,200335	244,3662	0,289562	309,8947	0,292373	336,3974	0,225957	315,0197
0,208555	251,5439	0,297274	316,9394	0,300682	343,7388	0,233592	321,3335
0,216665	259,7453	0,304984	323,9851	0,306309	350,0272	0,238632	327,6535
0,224792	265,9025	0,312803	330,0291	0,311845	355,2712	0,24378	332,9193
0,230216	273,0762	0,320621	336,0741	0,317372	361,5606	0,251405	340,291
0,238334	280,2582	0,328439	342,12	0,328589	366,8264	0,256452	345,5577
0,243757	287,4336	0,336256	348,1668	0,336886	375,2181	0,261499	350,825
0,251882	293,5948	0,346644	356,2306	0,348064	384,6675	0,266654	355,0376
0,257314	299,7489	0,357141	363,2928	0,362048	392,0393	0,274277	362,4125
0,265438	305,9119	0,367527	371,3599	0,37882	399,4241	0,281916	367,6772
0,273553	313,0991	0,375223	379,4183	0,390002	407,8344	0,287062	372,9473
0,278992	318,2323	0,391204	385,5022	0,401102	414,1545	0,297284	379,2652
0,287114	324,3981	0,404385	392,5811	0,409511	420,4648	0,305013	385,5886

Image 14: Screenshot from the excel file containing the stress - strain curves

4.4.3 Visualizing the flow curves

We divide the hard copper tubes' specimens into two distinct categories:

- Samples appeared Luder Lines due to bending test
- Samples manifested Another Defect or Clear Bending / OK because of the bending test

If we deem that Luder Lines appear then it should be manifested at least one time either with Virax or REMS – CURVO bender.

We present the diagram that depicts the plastic region from the true strain of the yield point σ_Y to 2 % true strain ε for the samples that suffer from Luder Lines defect.

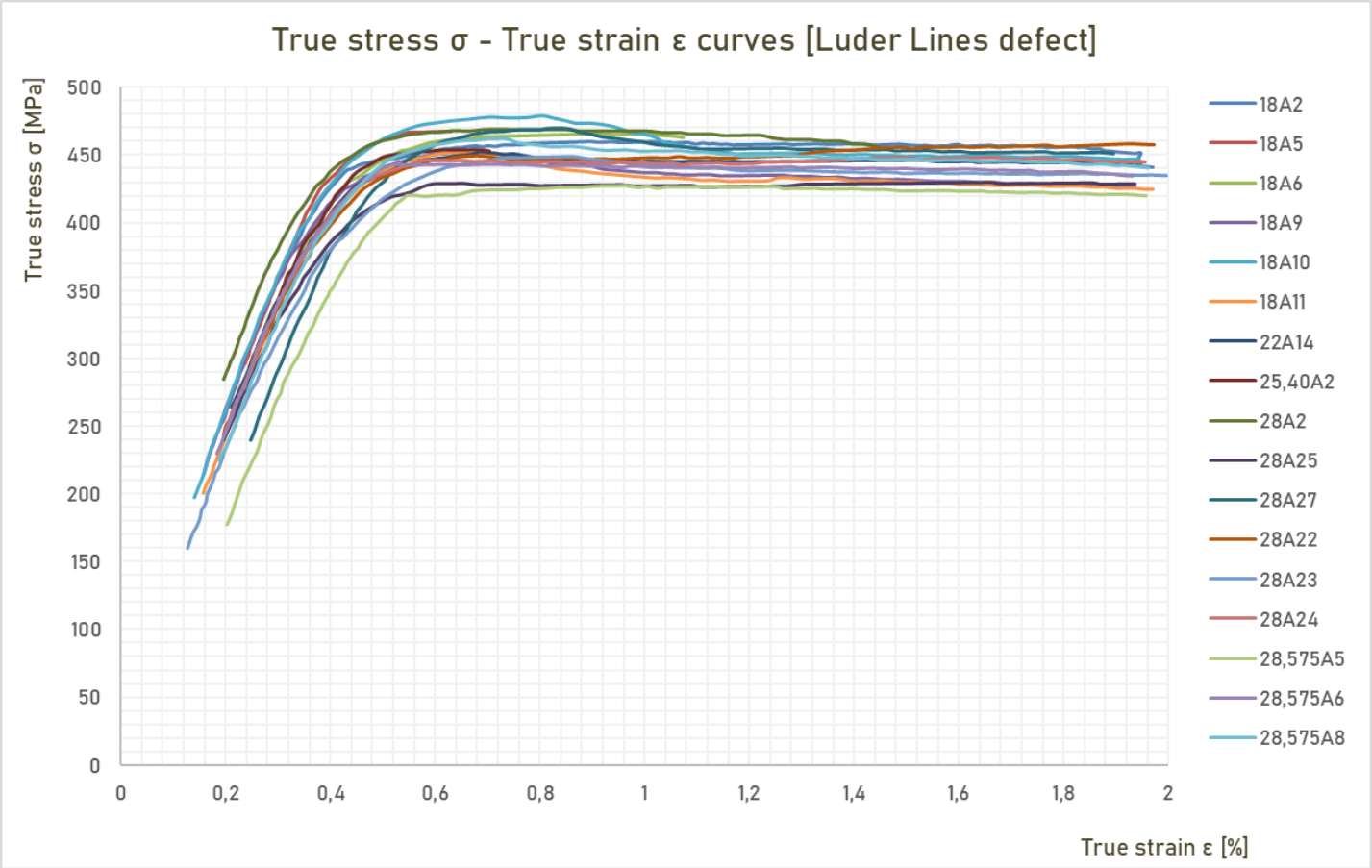

Figure 30: True stress - strain curves [Luder Lines]

At first glance, we can write down many qualitative observations.

- The true strain ε point at which plastic region begins is not the same for each sample. The same occurs for the true stress σ at this point.
- By plotting these flow curves, almost all samples form together a strong stress plateau, starting from the true strain ε = 1 % having a width of $\Delta\sigma \cong 35\ MPa$. In this region stress remains almost constant although there seems to be that true stress σ is decreasing while true strain ε is increasing → This is called "**strain – softening**" phenomenon after reaching the ultimate tensile strength.
- Despite that, it does not mean that all samples which suffer from Luder Lines have this distinctive stress plateau. For instance, samples ID 18A5, 28A2 and 25,40A2 either crack or appear an unusual kind of strain – softening.

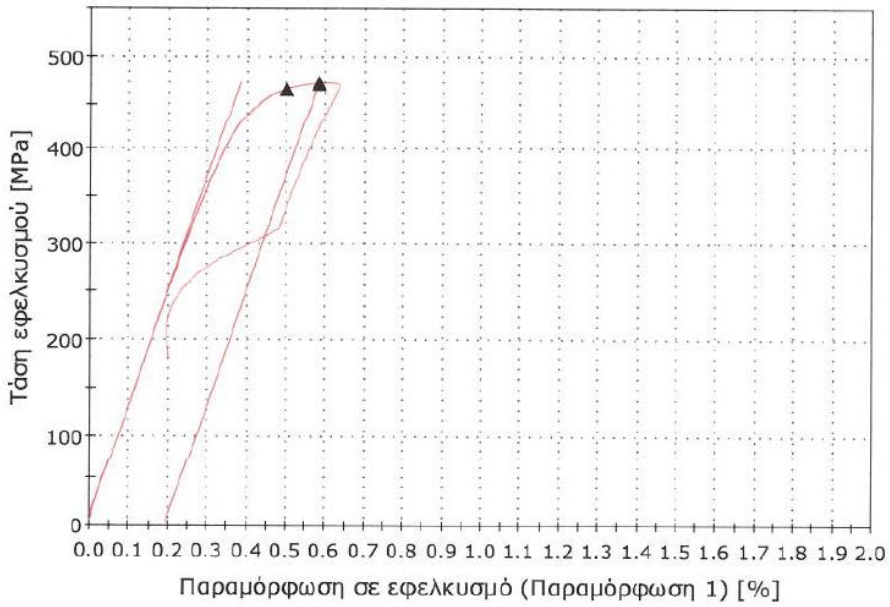

Figure 31: 18A5 stress - strain curve

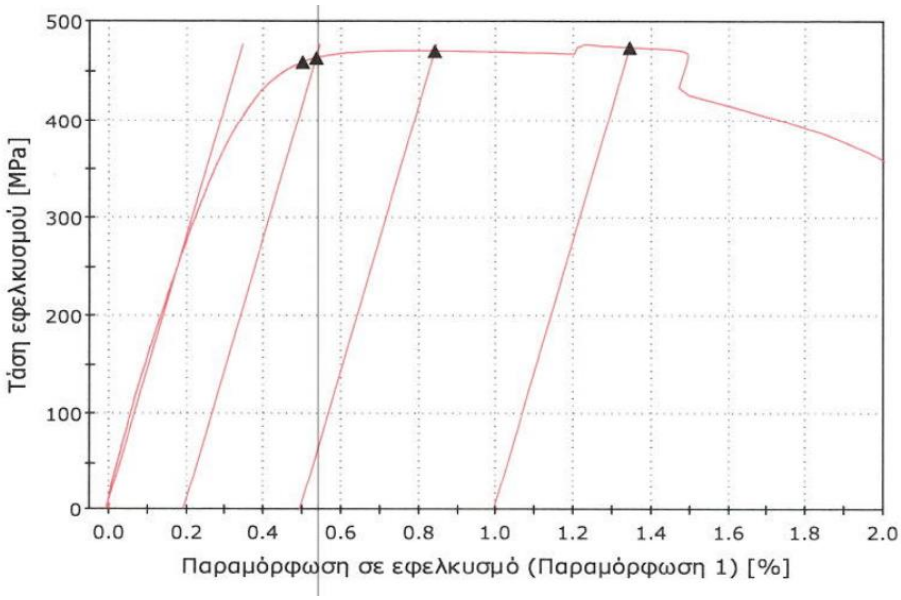

Figure 32: 28A2 stress - strain curve

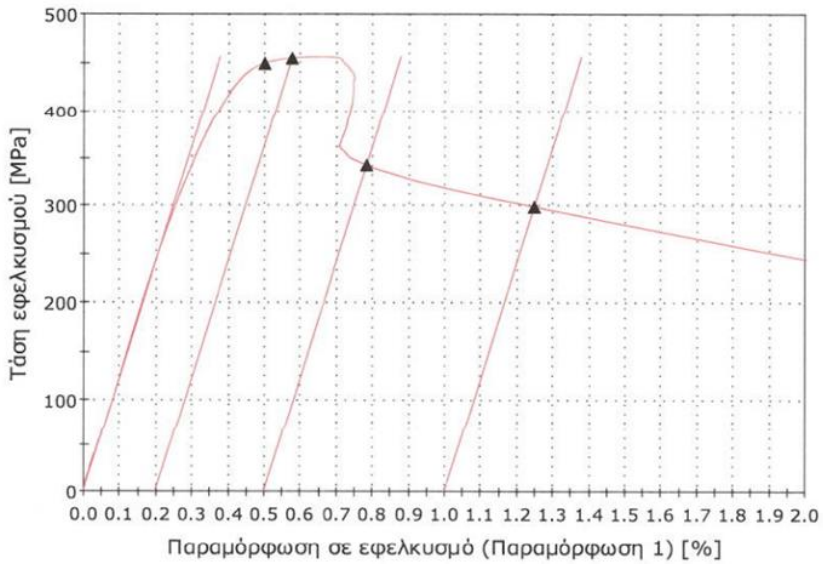

Figure 33: 25,40A2 stress -strain curve

We present the chart that depicts the plastic region from the true strain of the yield point σ_Y to 2% true strain ε for the samples that had appeared another defect (such as Wrinkling, Buckling, Kinking) or had clear bending (OK).

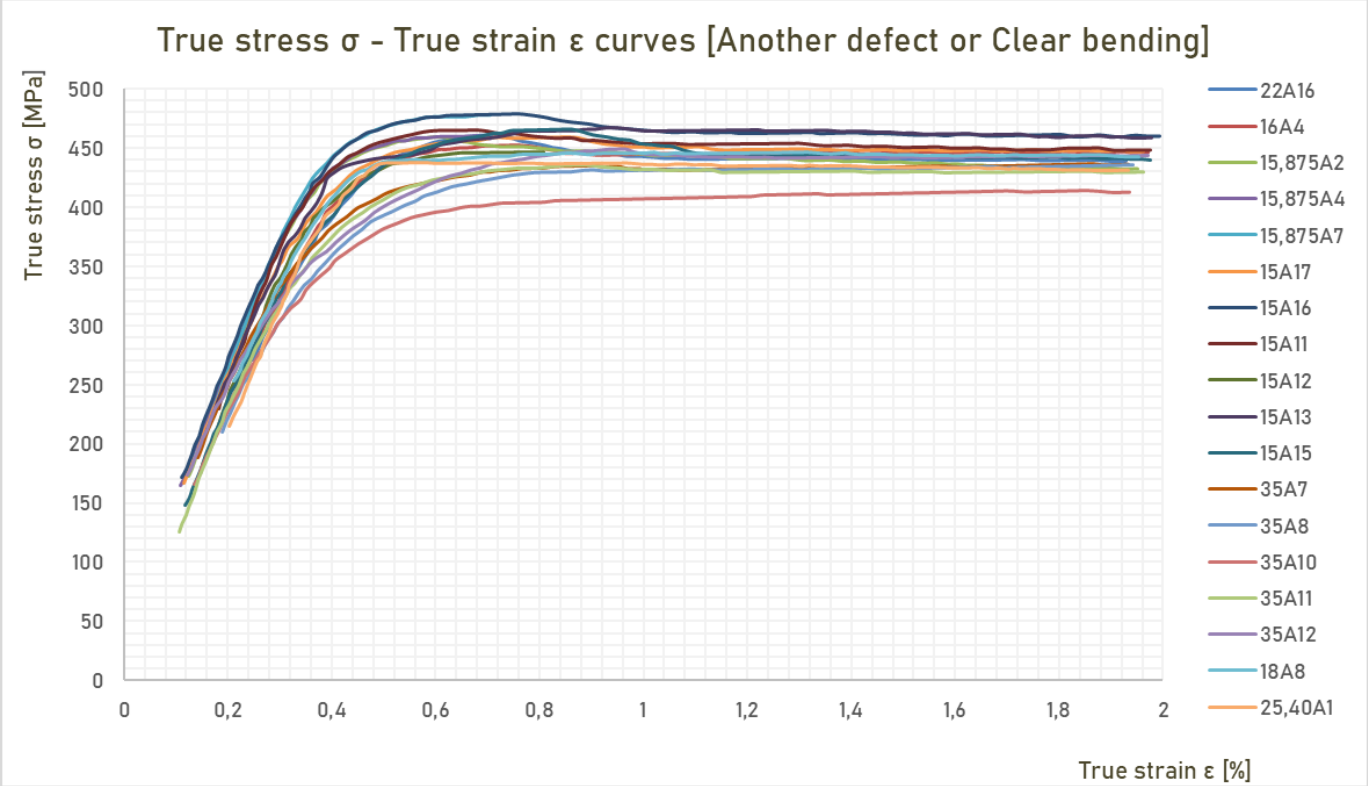

Figure 34: True stress - strain curves [Another Defect or Clear Bending]

We can note the following observations for these flow curves:

- It can be seen that the slope of the stress plateaus is smoother than the case of Luder Lines' appearance. But all the referred slopes can be computed analytically in order to realize if this could be a specific trend.
- 35A10 sample seems to appear **strain hardening** after reaching the ultimate tensile strength and gets lower true stress σ values.

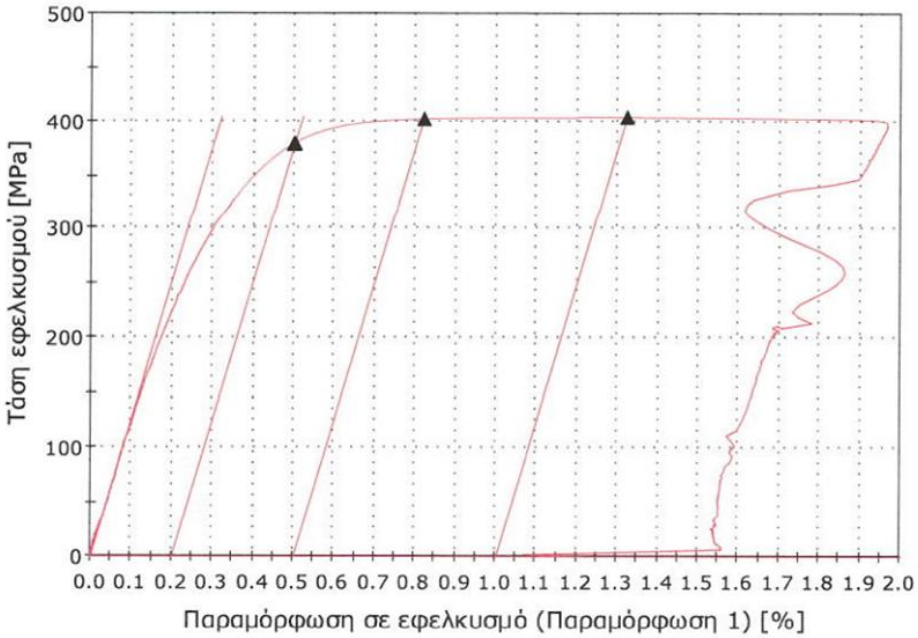

Figure 35:35A10 stress - strain curve

For the sake of completeness, we attach the respective true stress σ – true strain ε graphs for the hard copper tubes that had clear bending / OK. In this way, we investigate optically these flow curves in order to find similarities or trends.

Figure 36: True stress - strain curves [Clear Bending / OK]

All these curves do not dispose sharp edges, but smooth form. Except for this, they seem to get lower values of true stress σ at stress plateau. The slope of this line may be almost zero for almost all samples.

Consequently, after these optical observations, we are able to perform some computational work. We will adopt some easily perceivable mathematical tools in order to manipulate quantitively our data.

4.4.4 Indices regarding the true stress σ – true strain ε diagram

We would wish to investigate more the hidden information included in the stress – strain graphs. That is why we introduce the following 7 easily perceivable indices:

- E: Modulus of elasticity describing the linear behaviour of the copper
- ε_{start}: The value of the true strain where the plastic deformation begins
- σ_{start}: The true stress σ value at true strain equal to ε_{start}
- σ_Y: The yield point according to the assumption referred before: $\sigma_Y \cong \sigma_{0,3\%}$
- σ_{UTS}: The ultimate tensile strength after which a stress plateau appears
- ε_{UTS}: The respective strain at the ultimate tensile strength
- Δs: The stress drop that appears at engineering strain $e = 1{,}2\%$ because of the abrupt change of the strain rate $\dot{\varepsilon}$ (velocity of the tensile test machine)
- $Slope\ of\ the\ linear\ part$: It corresponds to the slope of the linear region (stress plateau) in the graph after the ultimate tensile strength

We provide the following schematic in order to visualize these 6 parameters and realize their physical meaning:

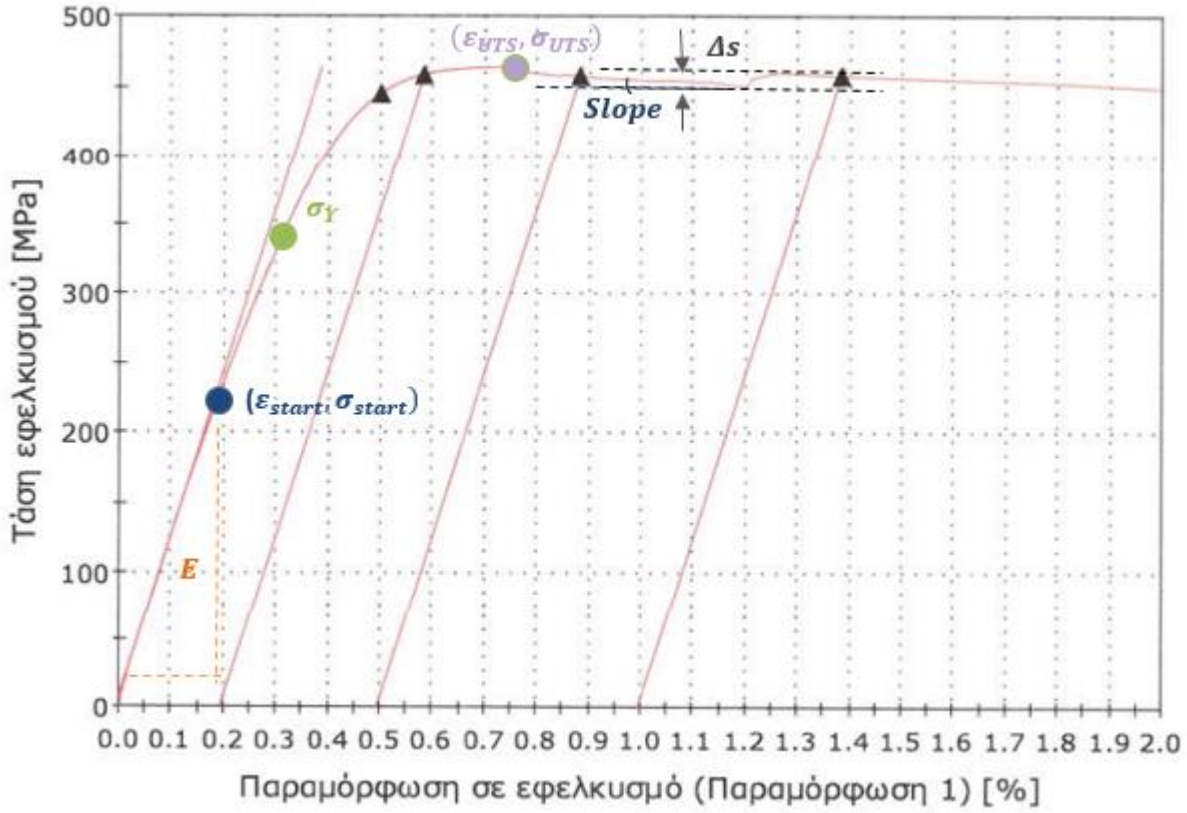

Figure 37: Distinctive graph that includes needed material parameters

The scope of this analysis is to determine the influence of the most affecting factors as for the Luder Lines' occurrence. Relied on these results, we will make an effort to create a more robust formula to predict the non – linear phenomenon through the most suitable combination of these 7 parameters.

We present the whole information regarding these 7 indices to the following table:

Sample ID	$E\ [GPa]$	ε_{start}	σ_{start}	$\sigma_Y \cong \sigma_{0,3\%}$	σ_{UTS}	ε_{UTS}	Δs	$Slope$
15,875A2	126,269	0,125057544	172,2581528	367,7682973	458,708229	0,612885097	10,7527	-32,25931873
15,875A4	130,454	0,108775436	165,0729637	367,0484707	459,5048088	0,684032658	N/A	N/A
15,875A7	123,646	0,124493997	176,624113	371,9012317	477,5045676	0,705940329	N/A	N/A
15A11	104,267	0,183334159	229,1427281	365,9946083	464,8500399	0,681811903	15,9575	-23,62326429
15A12	110,577	0,146709769	174,993156	341,0256455	446,7381173	0,807887507	N/A	N/A
15A13	107,647	0,154482951	204,275484	349,5524607	466,7712323	0,950531684	14,8515	-9,219595236
15A15	113,721	0,118027132	148,1988086	330,4145672	466,1815082	0,861578154	13,803	-69,09758459
15A16	136,779	0,111284413	171,4708082	372,3482181	478,4322134	0,759014176	11,3792	-38,10924603
15A17	127,455	0,116723302	166,7800442	350,5183018	459,3097114	0,723671312	11,047	-32,97815881
16A4	106,949	0,203200214	234,5568535	317,9579323	452,6367095	0,75679658	14,7588	-15,63759877
18A10	126,531	0,140346004	196,8128318	359,497226	477,6019707	0,703842459	14,2029	-53,82351171
18A11	112,916	0,157002659	200,3140053	337,73805	451,9777176	0,667762548	9,1837	-42,02923921
18A2	128,788	0,193452769	252,5290813	358,0081286	459,6661109	0,897213107	12,8665	-8,23255786
18A5	123,301	0,237009123	295,7627272	358,6905847	467,5452451	0,6305308	N/A	N/A
18A6	109,591	0,215342452	265,8176941	345,4550247	465,5078517	0,908116344	N/A	N/A
18A8	117,67	0,212204163	253,0538537	335,5439067	444,6467055	0,825271219	12,9496	-0,127201918
18A9	124,758	0,157060767	214,0611789	357,9360649	452,0928182	0,684428527	10,7843	-36,32624183
22A14	123,413	0,211040808	263,7908339	342,1935936	452,3477696	0,686247908	10,2941	-15,51882042
22A16	106,208	0,248342839	270,6705257	316,9393843	461,3424226	0,729786596	12	-48,82568012
25,40A1	104,231	0,203147494	214,5289266	312,3413637	437,4361689	0,5833233	10,0671	-4,866831943
25,40A2	112,149	0,24498324	293,4253863	343,7387636	454,112965	0,680927053	N/A	N/A
28,575A5	85,893	0,203622486	176,8695143	269,2585764	426,9023417	0,965790014	10,7382	-5,131542048
28,575A6	123,605	0,183382186	229,4602189	340,5911198	442,719878	0,533797088	10,3758	-4,175830209
28,575A8	111,137	0,186755775	224,9090477	331,6060185	461,5338336	0,735662074	9,1836	-27,70624405
28A2	131,971	0,195453061	284,5000794	379,2651518	467,7279096	0,629669112	10,1814	-9,995923719
28A22	122,53	0,196855027	244,0725251	337,8830251	449,7124822	0,68065177	7,4461	-1,728348256
28A23	124,309	0,126764001	159,4437614	315,6628194	448,5107379	0,862933803	10,6946	-29,32061205
28A24	122,856	0,195195526	242,6228664	342,138215	446,360891	0,611473597	6,5289	-4,245175798
28A25	102,169	0,19665941	239,7964567	330,2097317	428,6372775	0,656246433	6,7416	-4,890620569
28A27	88,001	0,248370516	239,4281957	292,1406189	469,9580915	0,845177587	12,6213	-57,05669044
35A10	116,14	0,135059834	166,214286	302,4728478	413,8727765	1,702061539	0	11,75404588
35A11	107,263	0,106469477	125,9071101	312,254473	435,8202058	0,893929178	9,2783	-21,94603245
35A12	114,471	0,121906212	173,9317755	318,9995013	448,6092086	0,964910495	14,3383	-28,93365436
35A7	124,832	0,143285338	188,7393489	331,9144156	434,8907375	0,905602999	9,2526	-11,93053125
35A8	102,908	0,18918121	209,9019452	301,5775349	431,7352508	0,906483386	9,667	0,814291226

Table 42: Material indices' values for all samples

4.4.5 Young's modulus E $[GPa]$ influence on the Luder Lines' appearance [1st index]

Young's modulus E is defined as the gradient of the linear part of the stress – strain curve. This quantity is a measure of the ability of the hard copper to withstand changes in length, when under uniaxial tension test. We will examine the variation along the 35 samples.

$85,893 \leq E \leq 117,67$ $[GPa]$

Sample	a	b	c	E [GPa]
28,575A5	-7,846	-2,633	443,1	85,893
28A27	-21,42	-1,956	509,1	88,001
28A25	-12,65	-1,985	463,2	102,169
35A8	-8,997	-2,293	438,7	102,908
25,40A1	-5,406	-2,817	469,9	104,231
15A11	-2,658	-3,118	476,8	104,267
22A16	-19,09	-1,902	502,9	106,208
16A4	-5,916	-2,697	469,8	106,949
35A11	-11,25	-2,091	453,2	107,263
15A13	-3,319	-2,959	468,8	107,647
18A6	-4,696	-2,801	475,7	109,591
15A12	-2,605	-3,178	455	110,577
28,575A8	-10,24	-2,302	488,4	111,137
25,40A2	-3,114	-3,102	469,5	112,149
18A11	-10	-2,224	481,6	112,916
15A15	-15,47	-1,986	492,2	113,721
35A12	-41,6	-1,205	496,1	114,471
35A10	-6,727	-2,376	415,1	116,14
18A8	-1,641	-3,586	451,5	117,67

Table 43: Raw experimental data for 85,893 ≤ E ≤ 117,67 [GPa]

It should be noted that most samples, in this region, do not suffer from Luder Lines defect as they get relatively low values of modulus of elasticity.

$85,893 \leq E \leq 117,67$
Luder Lines' appearance: **7/19 -> 36,84 %**
NO Luder Lines: 12/19 -> 63,16 %

$122,53 \leq E \leq 136,779$ $[GPa]$

28A22	-13,28	-2,006	483,1	122,53
28A24	-9,209	-2,267	479,2	122,856
18A5	-2,627	-3,233	483,5	123,301
22A14	-6,639	-2,488	471,6	123,413
28,575A6	-29,84	-1,51	523,5	123,605
15,875A7	-2,093	-3,348	486,7	123,646
28A23	-14,33	-2,031	474	124,309
18A9	-6,776	-2,379	473,8	124,758
35A7	-9,162	-2,137	448,3	124,832
15,875A2	-2,558	-3,117	472,9	126,269
18A10	-5,416	-2,676	492,3	126,531
15A17	-7,144	-2,403	477,3	127,455
18A2	-1,198	-3,745	461,6	128,788
15,875A4	-1,64	-3,444	468,8	130,454
28A2	-2,402	-3,093	478,5	131,971
15A16	-2,72	-3,174	488,7	136,779

Table 44: Raw experimental data for 122,53 ≤ E ≤ 136,779 [GPa]

In comparison with the previous case, many samples appear Luder Lines on their surface. The more robust the material (copper – hard temper) is, the higher probability of Luder Lines' appearance exists. So, if we get relatively high values of Young's modulus, there is a great risk/hazard of Luder Lines' formation

$122,53 \leq E \leq 136,779$
Luder Lines' appearance: **10/16 -> 62,50 %**
NO Luder Lines: 6/16 -> 37,5 %

4.4.6 True strain ε_{start} influence on the Luder Lines appearance [2nd index]

We are going to investigate the degree of influence of the 2nd factor on the Luder Lines' occurrence.

$0,1065\ \% \leq \varepsilon_{start} \leq 0,1545\ \%$

Sample	a	b	c	εstart
35A11	-11,25	-2,091	453,2	0,10646948
15,875A4	-1,64	-3,444	468,8	0,10877544
15A16	-2,72	-3,174	488,7	0,11128441
15A17	-7,144	-2,403	477,3	0,1167233
15A15	-15,47	-1,986	492,2	0,11802713
35A12	-41,6	-1,205	496,1	0,12190621
15,875A7	-2,093	-3,348	486,7	0,124494
15,875A2	-2,558	-3,117	472,9	0,12505754
28A23	-14,33	-2,031	474	0,126764
35A10	-6,727	-2,376	415,1	0,13505983
18A10	-5,416	-2,676	492,3	0,140346
35A7	-9,162	-2,137	448,3	0,14328534
15A12	-2,605	-3,178	455	0,14670977
15A13	-3,319	-2,959	468,8	0,15448295

Table 45: Raw experimental data for $0,1065 \leq \varepsilon_{start} \leq 0,1545$ [%]

Almost all samples had clear bending result or suffered from another defect (e.g. Buckling) and not Luder Lines formation. This means that relatively low ε_{start} values do not enhance this defect.

So, if a hard copper tube delays being inserted in the plastic deformation region, then it is more likely to have Luder Lines on its surface after bending test.

$0,1065\ \% \leq \varepsilon_{start} \leq 0,1545\ \%$
Luder Lines' appearance: **2/14 -> 14,29 %**
NO Luder Lines: 12/14 -> 85,71 %

$0,1570\ \% \leq \varepsilon_{start} \leq 0,2484\ \%$

18A11	-10	-2,224	481,6	0,15700266
18A9	-6,776	-2,379	473,8	0,15706077
15A11	-2,658	-3,118	476,8	0,18333416
28,575A6	-29,84	-1,51	523,5	0,18338219
28,575A8	-10,24	-2,302	488,4	0,18675577
35A8	-8,997	-2,293	438,7	0,18918121
18A2	-1,198	-3,745	461,6	0,19345277
28A24	-9,209	-2,267	479,2	0,19519553
28A2	-2,402	-3,093	478,5	0,19545306
28A25	-12,65	-1,985	463,2	0,19665941
28A22	-13,28	-2,006	483,1	0,19685503
25,40A1	-5,406	-2,817	469,9	0,20314749
16A4	-5,916	-2,697	469,8	0,20320021
28,575A5	-7,846	-2,633	443,1	0,20362249
22A14	-6,639	-2,488	471,6	0,21104081
18A8	-1,641	-3,586	451,5	0,21220416
18A6	-4,696	-2,801	475,7	0,21534245
18A5	-2,627	-3,233	483,5	0,23700912
25,40A2	-3,114	-3,102	469,5	0,24498324
22A16	-19,09	-1,902	502,9	0,24834284
28A27	-21,42	-1,956	509,1	0,24837052

Table 46: Raw experimental data for $0,1570 \leq \varepsilon_{start} \leq 0,2484$ [%]

In comparison with the previous true strain ε_{start} interval, most specimens appear Luder Lines because of bending tests. Few hard copper tubes avoid this specific defect.

$0{,}1570\ \% \leq \varepsilon_{start} \leq 0{,}2484\ \%$
Luder Lines' appearance: **15/21 -> 71,43 %**
NO Luder Lines: 6/21 -> 28,57 %

It can be noted that there is a clear correlation between the true strain ε_{start} and the probability of the Luder Lines' appearance. More specifically, when ε_{start} rises, so does the respective probability.

True strain ε_{start} interval [MPa]	Luder Lines' appearance (probability)
$0{,}1065\ \% \leq \varepsilon_{start} \leq 0{,}1545\ \%$	14,29 %
$0{,}1570\ \% \leq \varepsilon_{start} \leq 0{,}2484\ \%$	**71,43 %**

Table 47: Probability of Luder Lines' formation with respect to ε_{start}

Consequently, the true strain ε_{start} is proportional to the probability of Luder Lines' formation. Adopting a mathematical representation, the following relation is valid:

$\boldsymbol{\varepsilon_{start}}$ ↑ => Probability of **Luder Lines'** appearance ↑

4.4.7 True stress σ_{start} influence on the Luder Lines appearance [3rd index]

There are three distinct intervals as for this index. In this way, we can find some interesting trends regarding the true stress σ_{start} [MPa].

$\boldsymbol{125{,}91\ MPa \leq \sigma_{start} \leq 174{,}99\ MPa}$

Sample	a	b	c	εstart	σstart
35A11	-11,25	-2,091	453,2	0,10646948	125,9071101
15A15	-15,47	-1,986	492,2	0,11802713	148,1988086
28A23	-14,33	-2,031	474	0,126764	159,4437614
15,875A4	-1,64	-3,444	468,8	0,10877544	165,0729637
35A10	-6,727	-2,376	415,1	0,13505983	166,214286
15A17	-7,144	-2,403	477,3	0,1167233	166,7800442
15A16	-2,72	-3,174	488,7	0,11128441	171,4708082
15,875A2	-2,558	-3,117	472,9	0,12505754	172,2581528
35A12	-41,6	-1,205	496,1	0,12190621	173,9317755
15A12	-2,605	-3,178	455	0,14670977	174,993156

Table 48: Raw experimental data for $125{,}91 \leq \sigma_{start} \leq 174{,}99$ [MPa]

In this sub – dataset, only 1 sample forms Luder Lines on its surface as its bending result. All the other specimens either had clear bending or suffered from another defect.

$125{,}91\ MPa \leq \sigma_{start} \leq 174{,}99\ MPa$
Luder Lines' appearance: 1/10 -> **10 %**
NO Luder Lines: 9/10 -> 90 %

$176,62\ MPa \leq \sigma_{start} \leq 234,56\ MPa$

15,875A7	-2,093	-3,348	486,7	0,124494	176,624113
28,575A5	-7,846	-2,633	443,1	0,20362249	176,8695143
35A7	-9,162	-2,137	448,3	0,14328534	188,7393489
18A10	-5,416	-2,676	492,3	0,140346	196,8128318
18A11	-10	-2,224	481,6	0,15700266	200,3140053
15A13	-3,319	-2,959	468,8	0,15448295	204,275484
35A8	-8,997	-2,293	438,7	0,18918121	209,9019452
18A9	-6,776	-2,379	473,8	0,15706077	214,0611789
25,40A1	-5,406	-2,817	469,9	0,20314749	214,5289266
28,575A8	-10,24	-2,302	488,4	0,18675577	224,9090477
15A11	-2,658	-3,118	476,8	0,18333416	229,1427281
28,575A6	-29,84	-1,51	523,5	0,18338219	229,4602189
16A4	-5,916	-2,697	469,8	0,20320021	234,5568535

Table 49: Raw experimental data for 176,62 ≤ σstart ≤ 234,56 [MPa]

A balanced situation is observed, in which there is no separation regarding the bending result along the bent hard copper tubes.

$176,62\ MPa \leq \sigma_{start} \leq 234,56\ MPa$
Luder Lines' appearance: **6/13** -> **46,15 %**
NO Luder Lines: 7/13 -> 53,85 %

$239,43\ MPa \leq \sigma_{start} \leq 295,76\ MPa$

28A27	-21,42	-1,956	509,1	0,24837052	239,4281957
28A25	-12,65	-1,985	463,2	0,19665941	239,7964567
28A24	-9,209	-2,267	479,2	0,19519553	242,6228664
28A22	-13,28	-2,006	483,1	0,19685503	244,0725251
18A2	-1,198	-3,745	461,6	0,19345277	252,5290813
18A8	-1,641	-3,586	451,5	0,21220416	253,0538537
22A14	-6,639	-2,488	471,6	0,21104081	263,7908339
18A6	-4,696	-2,801	475,7	0,21534245	265,8176941
22A16	-19,09	-1,902	502,9	0,24834284	270,6705257
28A2	-2,402	-3,093	478,5	0,19545306	284,5000794
25,40A2	-3,114	-3,102	469,5	0,24498324	293,4253863
18A5	-2,627	-3,233	483,5	0,23700912	295,7627272

Table 50: Raw experimental data for 239,43 ≤ σstart ≤ 295,76 [MPa]

This defect is more frequently observed when higher values of true stress σ_{start} exist.

$239,43\ MPa \leq \sigma_{start} \leq 295,76\ MPa$
Luder Lines' appearance: **10/12** -> **83,33 %**
NO Luder Lines: 2/12 -> 16,67 %

These results could be expectable as true strain ε_{start} and true stress σ_{start} are proportional (1st and 2nd index). According to the previous analysis, we have found that there is a really high chance of Luder Lines occurrence if true stress σ_{start} rises accordingly.

True stress σ_{start} interval [MPa]	Luder Lines' appearance (probability)
$125,91 \leq \sigma_{start} \leq 174,99$	10 %
$176,62 \leq \sigma_{start} \leq 234,56$	46,15 %
$\mathbf{239,43 \leq \sigma_{start} \leq 295,76}$	**83,33 %**

Table 51: Probability of Luder Lines' formation with respect to σstart

The higher the true stress σ_{start} is, the higher the chance Luder Lines to be manifested.

$\boldsymbol{\sigma_{start}}$ ↑ => Probability of **Luder Lines'** appearance ↑

4.4.7 True stress $\sigma_Y \cong \sigma_{0,3\%}$ influence on the Luder Lines appearance [4th index]

It is clear that there are 2 separate categories according to the values of the 4th index in the ascending order. We can sort the assumed yield point's values as it is noted below:

$269,26\ MPa \leq \sigma_Y \leq 335,54\ MPa$

Sample	a	b	c	εstart	σstart	σY
28,575A5	-7,846	-2,633	443,1	0,20362249	176,8695143	269,259
28A27	-21,42	-1,956	509,1	0,24837052	239,4281957	292,141
35A8	-8,997	-2,293	438,7	0,18918121	209,9019452	301,578
35A10	-6,727	-2,376	415,1	0,13505983	166,214286	302,473
35A11	-11,25	-2,091	453,2	0,10646948	125,9071101	312,254
25,40A1	-5,406	-2,817	469,9	0,20314749	214,5289266	312,341
28A23	-14,33	-2,031	474	0,126764	159,4437614	315,663
22A16	-19,09	-1,902	502,9	0,24834284	270,6705257	316,939
16A4	-5,916	-2,697	469,8	0,20320021	234,5568535	317,958
35A12	-41,6	-1,205	496,1	0,12190621	173,9317755	319
28A25	-12,65	-1,985	463,2	0,19665941	239,7964567	330,21
15A15	-15,47	-1,986	492,2	0,11802713	148,1988086	330,415
28,575A8	-10,24	-2,302	488,4	0,18675577	224,9090477	331,606
35A7	-9,162	-2,137	448,3	0,14328534	188,7393489	331,914
18A8	-1,641	-3,586	451,5	0,21220416	253,0538537	335,544

Table 52: Raw experimental data for 296,26 ≤ σY ≤ 335,54 [MPa]

Most samples do not form Luder Lines on their surface as it happens in the case of low values of σ_{start} & ε_{start}.

$269,26\ MPa \leq \sigma_Y \leq 335,54\ MPa$
Luder Lines' appearance: **5/15** -> **33,33 %**
NO Luder Lines: 10/15 -> 66,67 %

$337,74\ MPa \leq \sigma_Y \leq 379,27\ MPa$

18A11	-10	-2,224	481,6	0,15700266	200,3140053	337,738
28A22	-13,28	-2,006	483,1	0,19685503	244,0725251	337,883
28,575A6	-29,84	-1,51	523,5	0,18338219	229,4602189	340,591
15A12	-2,605	-3,178	455	0,14670977	174,993156	341,026
28A24	-9,209	-2,267	479,2	0,19519553	242,6228664	342,138
22A14	-6,639	-2,488	471,6	0,21104081	263,7908339	342,194
25,40A2	-3,114	-3,102	469,5	0,24498324	293,4253863	343,739
18A6	-4,696	-2,801	475,7	0,21534245	265,8176941	345,455
15A13	-3,319	-2,959	468,8	0,15448295	204,275484	349,552
15A17	-7,144	-2,403	477,3	0,1167233	166,7800442	350,518
18A9	-6,776	-2,379	473,8	0,15706077	214,0611789	357,936
18A2	-1,198	-3,745	461,6	0,19345277	252,5290813	358,008
18A5	-2,627	-3,233	483,5	0,23700912	295,7627272	358,691
18A10	-5,416	-2,676	492,3	0,140346	196,8128318	359,497
15A11	-2,658	-3,118	476,8	0,18333416	229,1427281	365,995
15,875A4	-1,64	-3,444	468,8	0,10877544	165,0729637	367,048
15,875A2	-2,558	-3,117	472,9	0,12505754	172,2581528	367,768
15,875A7	-2,093	-3,348	486,7	0,124494	176,624113	371,901
15A16	-2,72	-3,174	488,7	0,11128441	171,4708082	372,348
28A2	-2,402	-3,093	478,5	0,19545306	284,5000794	379,265

Table 53: Raw experimental data for 337,74 ≤ σY ≤ 379,27 [MPa]

In this interval, many samples suffer from Luder Lines defect while others either appear Wrinkling, Buckling or have Clear Bending.

$337{,}74\ MPa \leq \sigma_Y \leq 379{,}27\ MPa$
Luder Lines' appearance: **12/20** -> **60 %**
NO Luder Lines: 8/20 -> 40 %

To assess the assumed yield point σ_Y effect on the Luder Lines defect, we construct the table right down:

True stress $\sigma_Y \cong \sigma_{0,3\%}$ interval [MPa]	Luder Lines' appearance (probability)
$269{,}26 \leq \sigma_Y \leq 335{,}54$	33,33 %
$337{,}74 \leq \sigma_Y \leq 379{,}27$	60 %

Table 54: Probability of Luder Lines' formation with respect to σ_Y

Increasing the true stress σ_Y means higher probability of Luder Lines' occurrence. For this reason, we perceive that the 4th index is one of the most determined ones.

$\boldsymbol{\sigma_Y \cong \sigma_{0,3\%}}$ ↑ => Probability of **Luder Lines'** appearance ↑

4.4.8 True strain ε_{UTS} influence on the Luder Lines appearance [6th index]

In this case, we divide the dataset into 2 categories according to the specimens' bending result (Luder Lines or Another defect / Clear Bending).

$\mathbf{0{,}5338\ \% \leq \varepsilon_{UTS} \leq 0{,}7038\ \%}$

Sample	a	b	c	εstart	σstart	σY	σUTS	εUTS
28,575A6	-29,84	-1,51	523,5	0,18338219	229,4602189	340,591	442,7199	0,5337971
25,40A1	-5,406	-2,817	469,9	0,20314749	214,5289266	312,341	437,4362	0,5833233
28A24	-9,209	-2,267	479,2	0,19519553	242,6228664	342,138	446,3609	0,6114736
15,875A2	-2,558	-3,117	472,9	0,12505754	172,2581528	367,768	458,7082	0,6128851
28A2	-2,402	-3,093	478,5	0,19545306	284,5000794	379,265	467,7279	0,6296691
18A5	-2,627	-3,233	483,5	0,23700912	295,7627272	358,691	467,5452	0,6305308
28A25	-12,65	-1,985	463,2	0,19665941	239,7964567	330,21	428,6373	0,6562464
18A11	-10	-2,224	481,6	0,15700266	200,3140053	337,738	451,9777	0,6677625
28A22	-13,28	-2,006	483,1	0,19685503	244,0725251	337,883	449,7125	0,6806518
25,40A2	-3,114	-3,102	469,5	0,24498324	293,4253863	343,739	454,113	0,6809271
15A11	-2,658	-3,118	476,8	0,18333416	229,1427281	365,995	464,85	0,6818119
15,875A4	-1,64	-3,444	468,8	0,10877544	165,0729637	367,048	459,5048	0,6840327
18A9	-6,776	-2,379	473,8	0,15706077	214,0611789	357,936	452,0928	0,6844285
22A14	-6,639	-2,488	471,6	0,21104081	263,7908339	342,194	452,3478	0,6862479
18A10	-5,416	-2,676	492,3	0,140346	196,8128318	359,497	477,602	0,7038425

Table 55: Raw experimental data for 0,5338 ≤ εUTS ≤ 0,7038 [%]

Here, we have the opposite observation compared to the true strain ε_{start}. The low values of ε_{UTS} reinforce the Luder Lines defect! If we quantify the above table, we get the following information:

$0{,}5338\ \% \leq \varepsilon_{UTS} \leq 0{,}7038\ \%$
Luder Lines' appearance: **11/15** -> **73,33 %**
NO Luder Lines: 4/15 -> 26,67 %

$0,7059\ \% \leq \varepsilon_{UTS} \leq 1,7021\ \%$

15,875A7	-2,093	-3,348	486,7	0,124494	176,624113	371,901	477,5046	0,7059403
15A17	-7,144	-2,403	477,3	0,1167233	166,7800442	350,518	459,3097	0,7236713
22A16	-19,09	-1,902	502,9	0,24834284	270,6705257	316,939	461,3424	0,7297866
28,575A8	-10,24	-2,302	488,4	0,18675577	224,9090477	331,606	461,5338	0,7356621
16A4	-5,916	-2,697	469,8	0,20320021	234,5568535	317,958	452,6367	0,7567966
15A16	-2,72	-3,174	488,7	0,11128441	171,4708082	372,348	478,4322	0,7590142
15A12	-2,605	-3,178	455	0,14670977	174,993156	341,026	446,7381	0,8078875
18A8	-1,641	-3,586	451,5	0,21220416	253,0538537	335,544	444,6467	0,8252712
28A27	-21,42	-1,956	509,1	0,24837052	239,4281957	292,141	469,9581	0,8451776
15A15	-15,47	-1,986	492,2	0,11802713	148,1988086	330,415	466,1815	0,8615782
28A23	-14,33	-2,031	474	0,126764	159,4437614	315,663	448,5107	0,8629338
35A11	-11,25	-2,091	453,2	0,10646948	125,9071101	312,254	435,8202	0,8939292
18A2	-1,198	-3,745	461,6	0,19345277	252,5290813	358,008	459,6661	0,8972131
35A7	-9,162	-2,137	448,3	0,14328534	188,7393489	331,914	434,8907	0,905603
35A8	-8,997	-2,293	438,7	0,18918121	209,9019452	301,578	431,7353	0,9064834
18A6	-4,696	-2,801	475,7	0,21534245	265,8176941	345,455	465,5079	0,9081163
15A13	-3,319	-2,959	468,8	0,15448295	204,275484	349,552	466,7712	0,9505317
35A12	-41,6	-1,205	496,1	0,12190621	173,9317755	319	448,6092	0,9649105
28,575A5	-7,846	-2,633	443,1	0,20362249	176,8695143	269,259	426,9023	0,96579
35A10	-6,727	-2,376	415,1	0,13505983	166,214286	302,473	413,8728	1,7020615

Table 56: Raw experimental data for 0,7059 ≤ ε_{UTS} ≤ 1,7021 [%]

$0,7059\ \% \leq \varepsilon_{UTS} \leq 1,7021\ \%$
Luder Lines' appearance: **6/20** -> **30 %**
NO Luder Lines: 14/20 -> 70 %

Rising the true strain ε_{UTS} at ultimate tensile strength point means lowering the chance to form Luder Lines during bending test. So, these characteristics are inversely proportional one another.

True strain ε_{UTS} interval [%]	Luder Lines' appearance (probability)
$0,5338 \leq \varepsilon_{UTS} \leq 0,7038$	**73,33 %**
$0,7059\ \% \leq \varepsilon_{UTS} \leq 1,7021\ \%$	30 %

Table 57: Probability of Luder Lines' formation with respect to ε_{UTS}

$\boldsymbol{\varepsilon_{UTS}}$ ↓ => Probability of **Luder Lines'** appearance ↑

**** Important note:** The 1st 4th, 6th and 7th index ($E, \sigma_{UTS}, \Delta s, Slope\ of\ the\ linear\ part$) do **not** separate the samples well (along the 2 conditions: Luder Lines or not) and it seems to be that there is no correlation between them and the bending result

4.5 Main findings from stress – strain graphs' manipulation

This kind of analysis, focused on the material properties, aims to extract useful hidden information regarding the deformation behaviour of the copper Cu – DHP (Hard Temper). In this way, we will manage to predict accurately the chance of Luder Lines' occurrence. Our findings are based on the defined metrics referred in the previous page of the technical report

- The most influencing factors are these 4 following parameters:
  - True stress $\sigma_Y \cong \sigma_{0,3\%}$
  - True stress σ_{start}
  - True strain ε_{start}
  - True strain ε_{UTS}

- The probability of Luder Lines' appearance is rising while the true stress σ_{start} is increasing.
  $\boldsymbol{\sigma_{start}}$ ↑ => Probability of **Luder Lines'** appearance ↑

- The assumed yield point $\sigma_Y \cong \sigma_{0,3\%}$ is accordingly related to the chance of Luder Lines' occurrence
  $\boldsymbol{\sigma_Y \cong \sigma_{0,3\%}}$ ↑ => Probability of **Luder Lines'** appearance ↑

- The probability of Luder Lines' formation on the interior and exterior copper tube surface is increasing while the true strain ε_{start} gets higher values
  $\boldsymbol{\varepsilon_{start}}$ ↑ => Probability of **Luder Lines'** appearance ↑

- The true strain ε_{UTS} is inversely related to the chance of Luder Lines' appearance
  $\boldsymbol{\varepsilon_{UTS}}$ ↓ => Probability of **Luder Lines'** appearance ↑

Index	σ_{start} ↑	$\sigma_Y \cong \sigma_{0,3\%}$ ↑	ε_{start} ↑	ε_{UTS} ↓
Probability of Luder Lines' appearance	↑	↑	↑	↑

Table 58: Probability of Luder Lines' formation with respect to material indices

4.6 Metrics including only the 4 material indices plus hardness HV and stress at maximum load R_m - Quantitative Operations

On this page, we try to creatively link the material properties σ_{start}, ε_{start}, ε_{UTS}, $\sigma_Y \cong \sigma_{0,3\%}$, HV & R_m so as to produce some empirical rules to predict the Luder Lines appearance. In the following list, we give the tested functions:

1. $f_1 = 50 \frac{\varepsilon_{start}^{1,5} \cdot \sigma_{start}}{\sigma_Y}$
2. $f_2 = 0{,}3 \frac{\varepsilon_{start}^{1,5} \cdot \sigma_{start}}{\varepsilon_{UTS}}$
3. $\boldsymbol{f_3 = 100 \frac{\varepsilon_{start}^{1,5}}{\varepsilon_{UTS}}}$

The first three formulas have the capability to separate the two conditions (Luder Lines or not) sufficiently in the dataset. However, we continue this procedure as none of these formulas can incorporate all the available material characteristics. They exploit 2 or 3 of them (6 overall)!

4. $f_4 = 10 \frac{\varepsilon_{start}^{0,8} \cdot \sigma_{start}^{0,8}}{\varepsilon_{UTS} \cdot \sigma_Y}$
5. $\boldsymbol{f_5 = 20 \frac{\varepsilon_{start}^{0,8} \cdot \sigma_{start}^{1,2}}{\varepsilon_{UTS}^{0,8} \cdot \sigma_Y^{1,2}}}$

The functions f_4, f_5 include the 4 indices from the true stress – strain graph only and their only difference lies on the coefficients' weights and the powers' values. Both the formulas can separate equally satisfyingly the dataset. We prefer the formula f_5 as it is dimensionless.

6. $f_6 = 120 \varepsilon_{start}^{(\frac{\sigma_{start}}{100})} \varepsilon_{UTS}$
7. $f_7 = \varepsilon_{start}^{(\frac{\sigma_{start}}{100})} \varepsilon_{UTS} \sigma_Y$
8. $\boldsymbol{f_8 = \varepsilon_{start}^{(\frac{\sigma_{start}}{100})} \varepsilon_{UTS}^{1,2} \sigma_Y}$

Among the functions f_6, f_7, f_8 the last one is the most efficient and gives interesting results. To incorporate all the material parameters, we introduce the factors HV & R_m in order to achieve a more robust and reliable formula.

9. $f_9 = \frac{100\ \varepsilon_{start}^{(\frac{\sigma_{start}}{100})} \varepsilon_{UTS}\ \sigma_Y}{0{,}7\ R_m}$
10. $\boldsymbol{f_{10} = \frac{100\ \varepsilon_{start}^{(\frac{\sigma_{start}}{100})} \varepsilon_{UTS}\ \sigma_Y}{0{,}7\ R_m \cdot 0{,}01\ HV}}$

We opt for the formula 10 as the most efficient as it combines in an optimized way all the available material properties.

4.6.1 Formula f_3 plot along samples

This predictive tool has the distinctive advantage that uses only two inputs ε_{start}, ε_{UTS} that can be measured easily through the true stress – strain σ – ε graph. To get an idea about its effectiveness, we present the following scatter diagram:

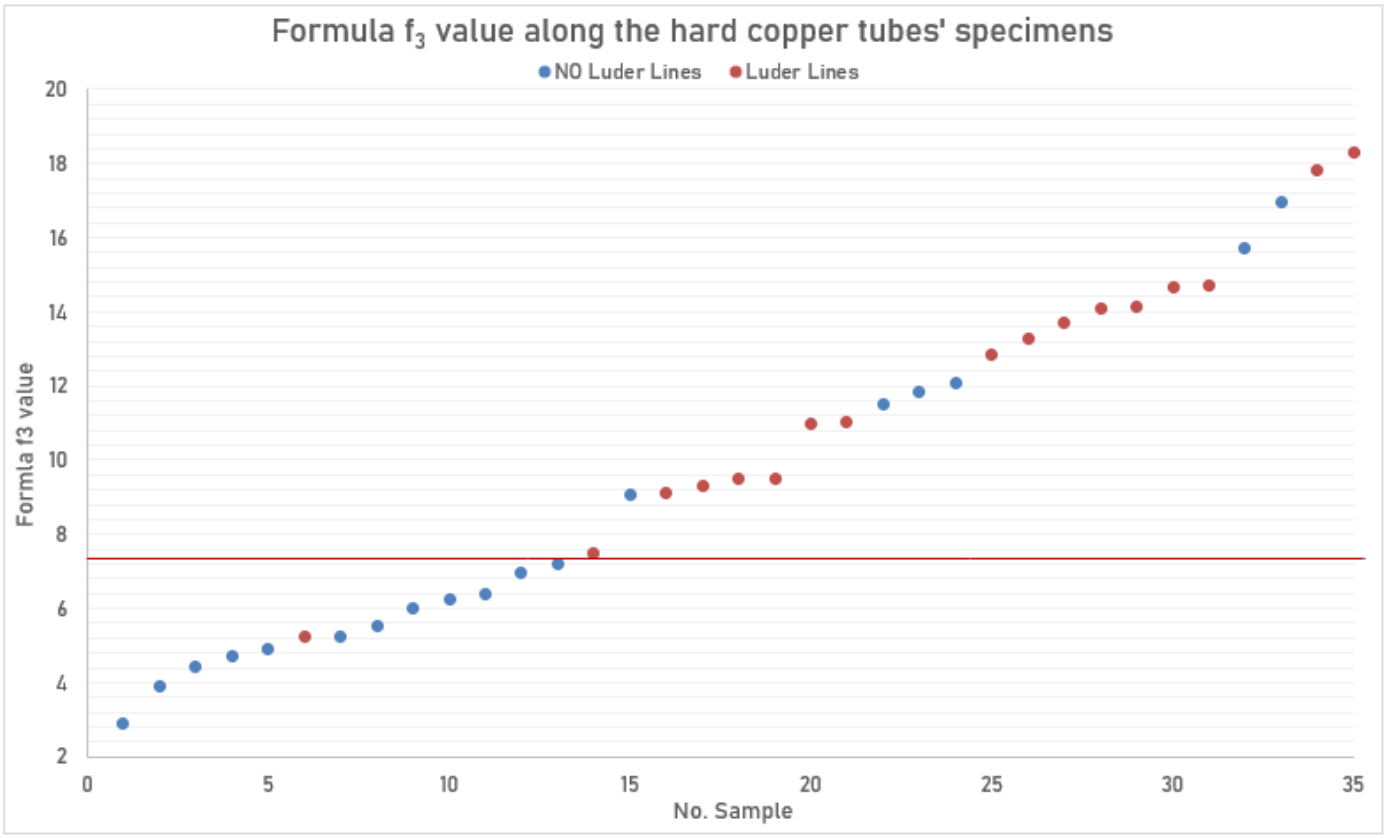

Figure 38: Scatter graph that visualizes formula f_3 with respect to the samples

There is a certain threshold, which seems to determine the copper tubes' behaviour during bending. Therefore, we write down a semi – empirical rule to predict the Luder Lines' appearance for hard copper tubes:

- $0 \leq f_3 < 7{,}47$: **NO** Luder Lines (12/13 -> **92,31 %)**
- $f_3 \geq 7{,}47$: **Luder Lines** appearance (16/22 -> **72,73%**)

4.6.2 Formula f_5 plot along samples

This formula should be examined further as it does not have any dimensions. So, the values are standardized. We provide the following schematic in order to represent the appeared trend with the aid of this function:

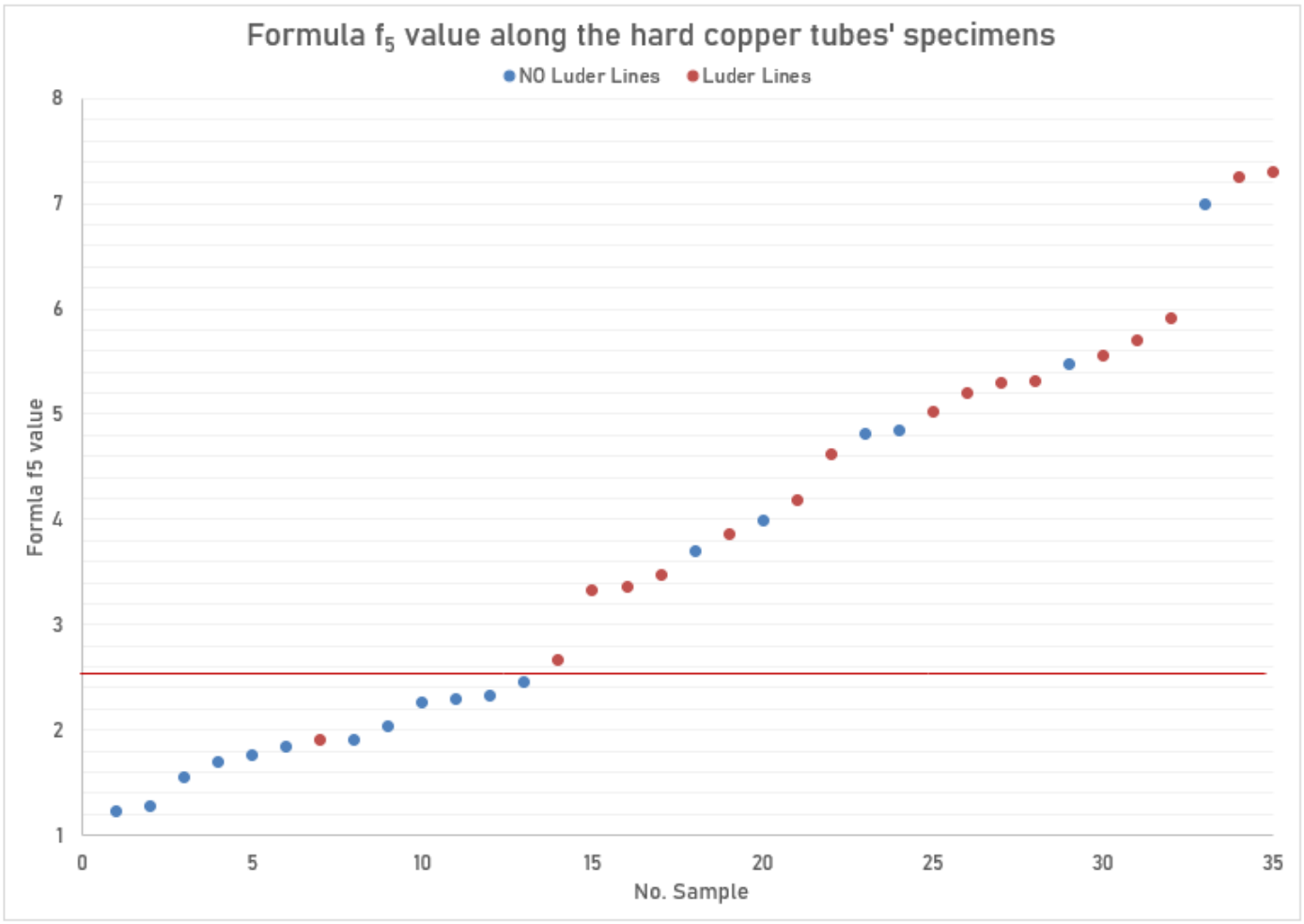

Figure 39: Scatter graph that visualizes formula f_5 with respect to the samples

The dark red line accounts for the limit upon this there is a great risk of Luder Lines' appearance. According to the previous page, we are interested in the formula region in which there is a really high chance of Luder Lines' occurrence:

- $0 \leq f_5 < 2{,}67$: **NO** Luder Lines (12/13 -> **92,31 %)**
- $f_5 \geq 2{,}67$: **Luder Lines** appearance (16/22 -> **72,73 %**)

4.6.3 Formula f_{10} plot along specimens

This function contains 6 material characteristics that can be extracted through uniaxial tensile tests and hardness' measurements. So, we need additional time and effort to get the HV values.

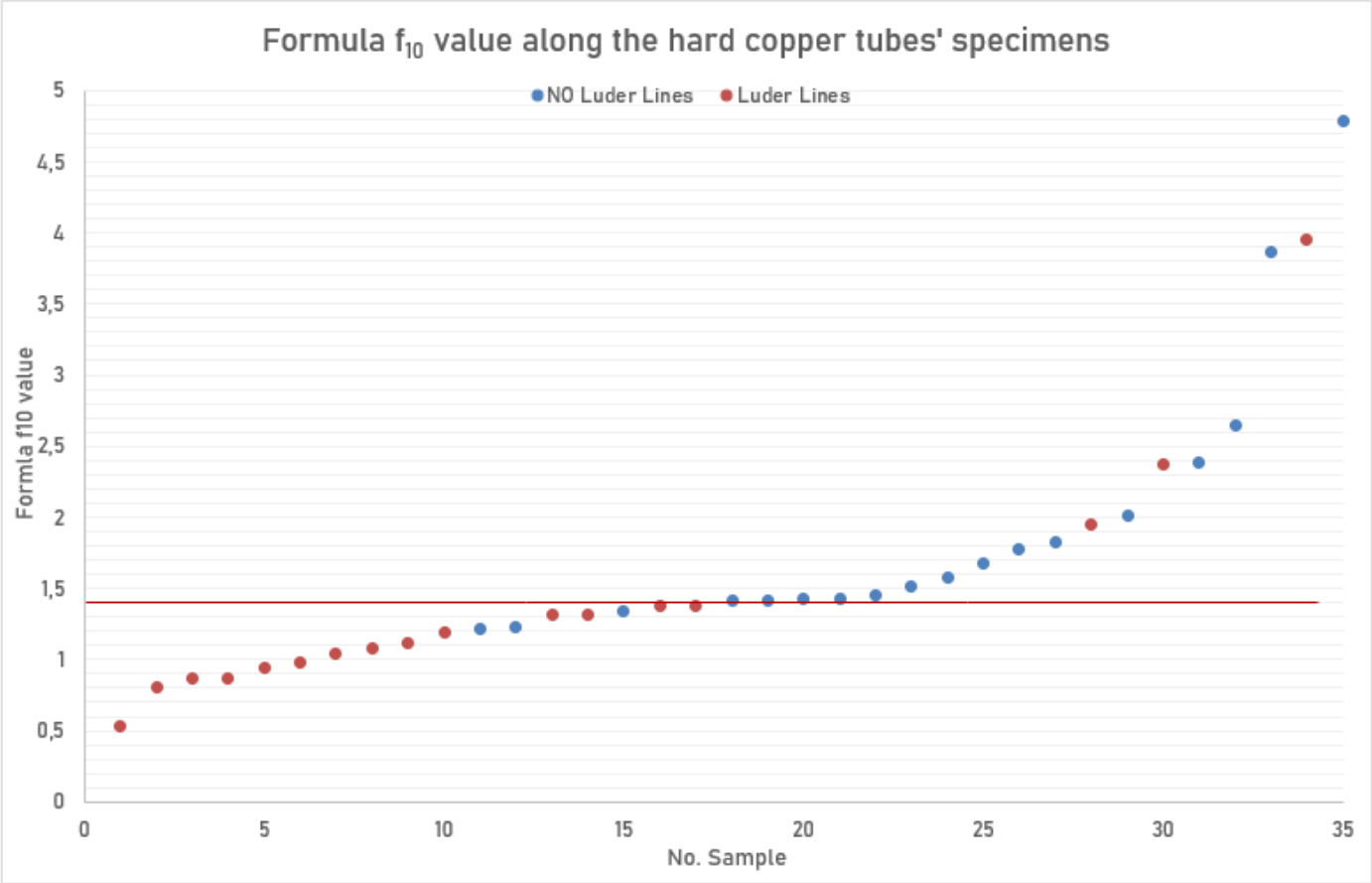

Figure 40: Scatter graph that visualizes formula f_{10} with respect to the samples

If this formula gets relatively low values, then there is a pretty high probability of Luder Lines' formation on the surfaces of the hard copper tube. So, we note the following predictive rule:

- $0 \leq f_{10} \leq 1{,}38$: **Luder Lines** appearance (14/17 -> **82,35 %**)
- $f_{10} > 1{,}38$: **NO** Luder Lines (15/18 -> **83,33 %**)

5. Analytical determination of the critical strain ε_{crit}

5.1 Theoretical background regarding plastic deformation

A bending test constitutes a process in which plastic deformation occurs. This means that the hard copper tube is subjected to stress higher than yield point σ_{start} and is under permanent changes as for geometrical and dimensional parameters (wall thickness WT_{av} and outer diameter OD_{av}).

We would wish to describe mathematically the plastic behaviour of the hard copper tube through an analytical mathematical model, that involves both geometrical and material properties. This can be achieved thanks to plastic – deformation theory.

From the deformation theory of plastic flow, strains and stresses can be expressed as [19]:

$$\begin{cases} \delta_x = \frac{1}{D}\left(\sigma_x - \mu(\sigma_c + \sigma_r)\right) \\ \delta_c = \frac{1}{D}\left(\sigma_c - \mu(\sigma_x + \sigma_r)\right) \\ \delta_r = \frac{1}{D}\left(\sigma_r - \mu(\sigma_c + \sigma_x)\right) \end{cases}$$

where: $\delta = \Delta l/l$: Deformation of unit length
D: Plastic flow modulus of the hard tube (copper)
μ: Poisson ratio (for plastic deformation (e.g., bending test) μ=0,5)

We are interested in the plastic flow modulus D parameter, which will be computed from experimental data for each sample. This parameter may give us useful information about the critical strain above which Luder Lines' formation risk exists.

The stresses σ_x, σ_c and σ_r will be specified with the aid of mathematical relations with respect to angular position a and geometrical parameter k, as it is shown right down [19]:

$$\begin{cases} \sigma_x = \frac{\sigma_{start}\,(2k+1)}{2k+2-cosa} & (Longitudinal) \\ \sigma_c = \frac{-\sigma_{start}(1-cosa)}{2k+2-cosa} & (Circumferential) \\ \sigma_r = 0 & (Radial) \end{cases}$$

Since the wall thickness is much smaller than the radius of the tube, the radial stress σr can be neglected.

We will zero in on the longitudinal strain δ_x, which depends on the plastic flow modulus D, poisson ratio μ and the stresses at longitudinal and circumferential direction, σ_x and σ_c respectively.

5.2 Calculation of longitudinal deformation δ_x

The initial mathematical relation, which give us the longitudinal strain, can be written as:

$$\delta_x = \frac{1}{D}\left(\sigma_x - \mu(\sigma_c + \sigma_r)\right)$$

However, the radial stress constitutes a negligible quantity and can be eliminated ($\sigma_r = 0$). In addition, poisson ratio gets a constant value equal to $\mu = 0{,}5$. Applying these observations to the initial formula, we take:

$$\delta_x = \frac{1}{D}(\sigma_x - 0{,}5\sigma_c)$$

The stresses in the two directions have been given analytically in the previous page and for sake of completeness, we rewrite them right down:

$$\sigma_x = \frac{\sigma_{start}\ (2k+1)}{2k+2-cosa}$$

$$\sigma_c = \frac{-\sigma_{start}(1-cosa)}{2k+2-cosa}$$

Utilizing the above formulas to the longitudinal deformation δx equation, we can present the final result:

$$\delta_x\ (a, D, \sigma_{start}, k) = \frac{\sigma_{start}\ (2k+1{,}5-0{,}5cosa)}{D\ (2k+2-cosa)}$$

If we substitute $a = 0\ rad => cosa = 1$, we eliminate the geometrical factor:

$$\delta_x\ (a = 0\ rad) = \frac{\sigma_{start}}{D}$$

On the other hand, if we substitute $a = \frac{\pi}{2}\ rad => cosa = 0$, we possess a metric which combines both geometrical and material properties:

$$\delta_x\left(a = \frac{\pi}{2}\ rad\right) = \frac{\sigma_{start}\ (2k+1{,}5)}{D\ (2k+2)}$$

Therefore, we compute the deformation δ_x for two angular positions for every single sample, so as to proceed to a comparative evaluation.

5.3 Focus on the plastic flow modulus D

This material property is the analogous of the young modulus of elasticity E, but it refers to the plastic region of the stress – strain $\sigma-\varepsilon$ curve. Plastic flow modulus D is also called tangent modulus of elasticity and can be denoted by E_t. It is mostly used to describe the stiffness of a material in the plastic range.

It is defined as the instantaneous rate of change of stress as a function of strain. In other words, it can be computed as the slope at any point on a stress-strain diagram. This means that D does not take a constant value, but it gets different value while strain ε is increasing.

$$D = E_t = \frac{d\sigma}{d\varepsilon}, \varepsilon\acute{\alpha}\nu\ \sigma > \sigma_Y$$

The following schematic visualizes the theoretical information given above and indicates a computational way to specify plastic flow modulus.

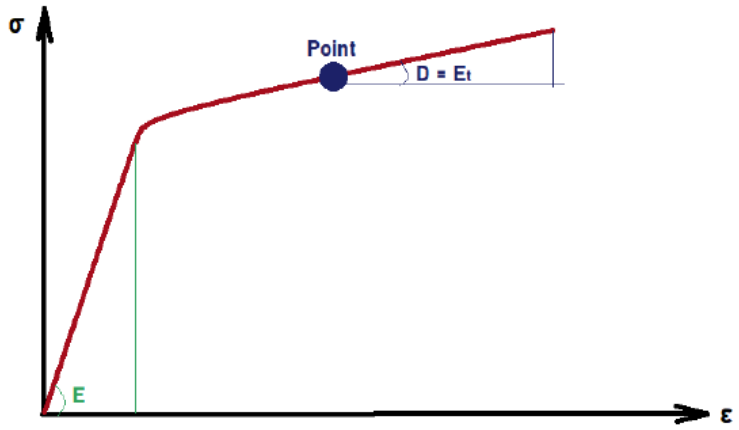

Figure 41: Simplified schematic to define plastic flow modulus

We will smartly compute this material property, so as to possess a powerful metric to compute longitudinal deformation δ_x. We are going to compute the values of plastic flow modulus per 5 discrete data points (σ,ε) according to the following indicative stress – strain curve:

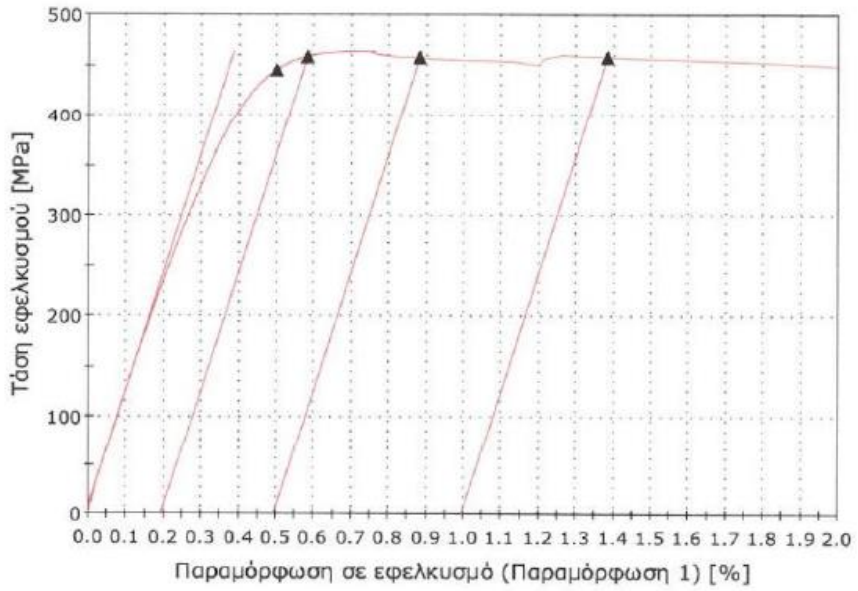

Figure 42: Indicative stress - strain graph for a hard copper tube

Now that we have computed the plastic flow modulus distribution for the 35 samples that we dispose their true stress – strain curves, we can plot these values versus the number of intervals. This number responds to the intervals that we need so as to cover the plastic region starting from the point ($\varepsilon_{start}, \sigma_{start}$) and ending to the strain equal to $\varepsilon = 2\%$ for each specimen. The respective graph for the samples that form Luder Lines during bending tests is shown right down:

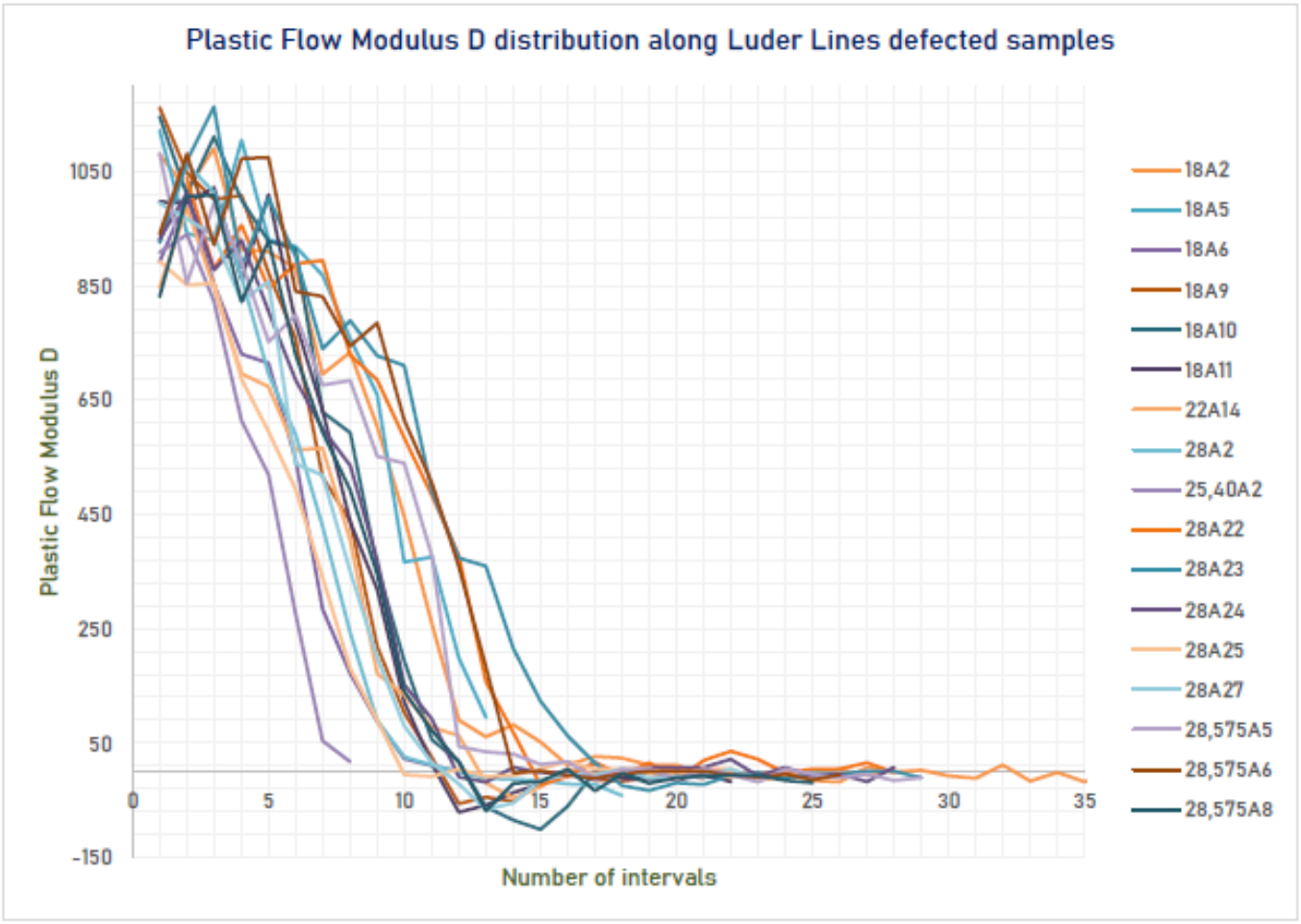

Figure 43: Plastic Flow Modulus' visualization with respect to Luder Lines defected specimens

According to the above graph, there is no clear correlation between the form of the plastic flow modulus distribution and the Luder Lines formation. What it can be observed is that shortly after the elastic region, plastic flow modulus takes relatively high values. Also, it seems to appear a gradual reduction, while strain ε is increasing. Finally, an asymptotic behavior is noted, as there is a distinctive region in which true stress σ remains almost constant, although true strain ε rises. Almost all specimens have negative value of plastic flow modulus (mild strain softening phenomenon) for an extended plastic deformation region (more intense in 18A10, 28,575A8, 28A23). But this is not a rule that should be obeyed. For instance, only 2 samples (25,40A2 & 18A5) do not appear this asymptotic horizontal line, but the stress is rising while strain is increasing (strain hardening phenomenon). This is why plastic flow modulus gets only positive values in these cases.

The plastic flow modulus D distribution is presented for the specimens that had another defect (expect for Luder Lines) or had clear bending.

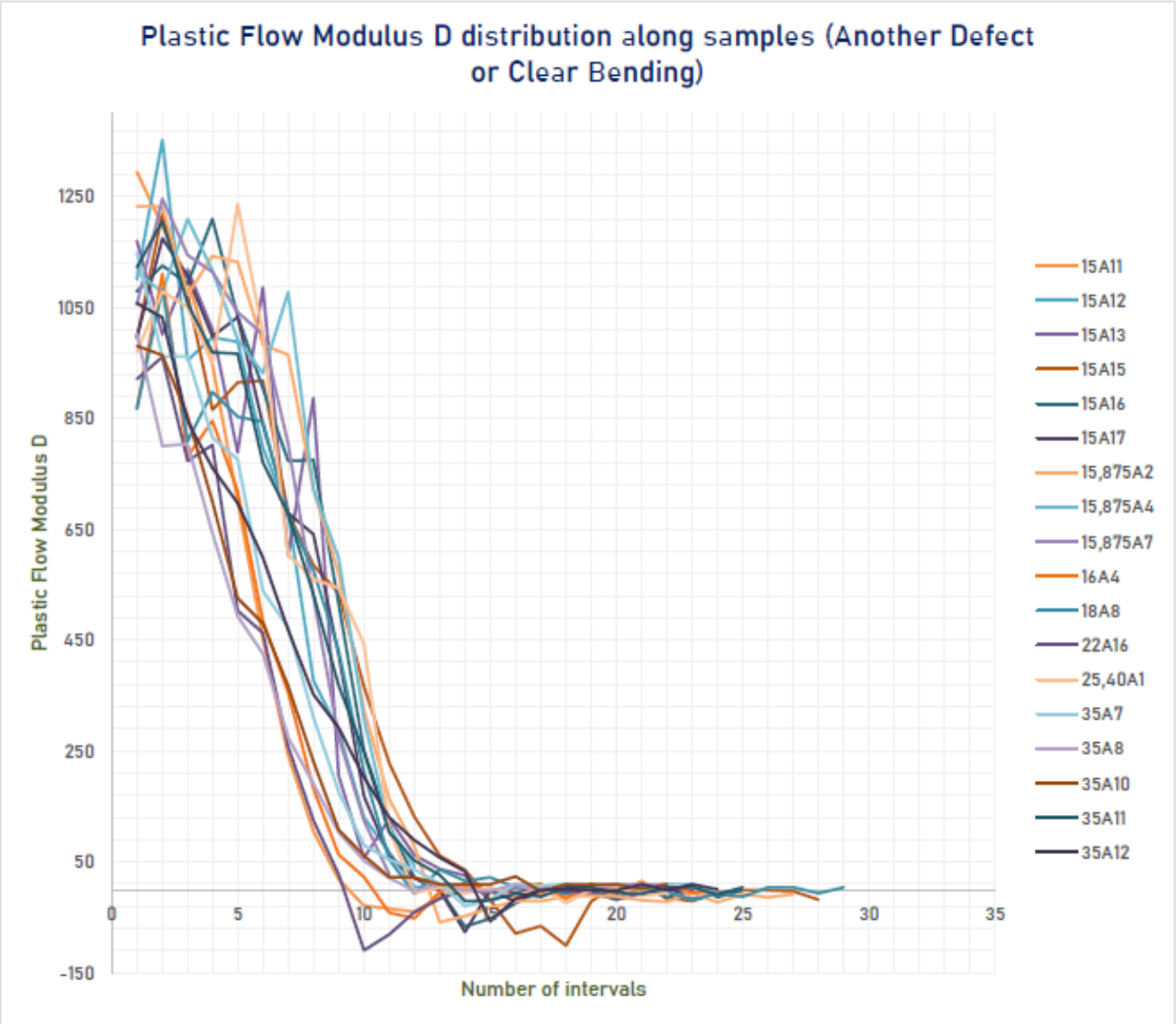

Figure 44: Plastic flow modulus' visualization for the remaining samples

An important difference compared to the other graph is that plastic flow modulus seems to take higher values near the elastic region. In addition, a more gradual (linear) decrease is observed. Finally, a more asymptotic behaviour is noted, as plastic flow modulus gets almost zero value if the plastic deformation is relatively high.

5.4 On the longitudinal deformation $\delta_x\ (a = 0\ rad)$

Based on these qualitative observations given by these 2 above graphs, we can identify the proper value of plastic flow modulus. We have to decide on a constant value of this material parameter, as tangent modulus of elasticity is a function which fluctuates with the strain ε.

We try out some promising plastic flow modulus' parameters such as the value computed in the first 5 data points or the absolute value of the minimum value of the plastic flow modulus. We deem that the most representative material parameter is D_{start}.

where: D_{start} is the plastic flow modulus computed in the 1st interval
$D_{start} = Slope\ of\ the\ first\ 5\ data\ points\ (\varepsilon_p,\sigma(\varepsilon_p))$

An example of the computation of this parameter is attached so as to have the best possible definition without any confusion:

=(AH61-AH57)/(AG61-AG57)

AD	AE	AF	AG	AH	AI
		0,205189	0,203147	214,5289	AG57)
		0,212374	0,210262	221,9422	1079,79
		0,219559	0,217389	228,0114	1051,256
		0,228539	0,226298	235,4309	949,1077
		0,233926	0,231622	242,1703	1236,939
		0,241109	0,238728	250,2604	1003,278
		0,246496	0,244064	255,656	603,6592
		0,251982	0,249492	261,7252	560,7025
		0,259164	0,256604	269,1453	544,0549
		0,266345	0,26374	273,8748	443,6677
		0,269935	0,267266	280,6138	109,0399

Table 59: Example of the plastic flow modulus' computation

So, the 1st metric linked to the plastic flow theory equals to:

$$\delta_x\ (a = 0\ rad) = \frac{\sigma_{start}}{D}$$

Implementing this formula, we create a table including all the essential information (sample's code, material parameters, index, bender type and bending outcome) that includes all the available 35 physical samples. This table is shown to the next page of this chapter.

We will ground the plastic flow analysis by taking the worst - case scenario as for the bending result, meaning Luder Lines. We will sort the results of the table according to the longitudinal deformation $\delta_x\ (a = 0\ rad)$ in an ascending order, so as to determine experimentally the critical strain ε_{cr}.

Sample ID	σ_{start}	D_{start}	$\delta_x\ (a = 0\ rad)$	Bender Type	Defect
15,875A2	172,2582	1233,4311	0,1397	REMS OR VIRAX	OK
15,875A4	165,0730	1114,4968	0,1481	REMS OR VIRAX	OK
15,875A7	176,6241	1055,3493	0,1674	REMS OR VIRAX	Kinking
15A11	229,1427	1295,0649	0,1769	REMS OR VIRAX	Light Wrinkling OR Buckling
15A12	174,9932	1101,4217	0,1589	REMS OR VIRAX	OK OR Buckling
15A13	204,2755	1170,8276	0,1745	REMS OR VIRAX	Buckling
15A15	148,1988	995,0243	0,1489	REMS OR VIRAX	Buckling OR Crack
15A16	171,4708	1079,8608	0,1588	REMS OR VIRAX	OK OR Buckling + Cracking
15A17	166,7800	996,0768	0,1674	REMS OR VIRAX	OK OR Buckling
16A4	234,5569	868,4494	0,2701	REMS OR VIRAX	Buckling
18A10	196,8128	1146,3755	0,1717	REMS OR VIRAX	OK OR Kinking + Luders
18A11	200,3140	997,3471	0,2008	REMS OR VIRAX	OK OR (Kinking + Slight Luder Lines)
18A2	252,5291	1080,0590	0,2338	Virax	Luder Lines (with some crack)
18A5	295,7627	1121,9220	0,2636	REMS OR VIRAX	OK OR Luder Lines + LL Fracture
18A6	265,8177	892,3254	0,2979	REMS OR VIRAX	OK OR Slight Luders, Light Wrinkling, Kinking
18A8	253,0539	867,3486	0,2918	REMS OR VIRAX	OK OR Buckling
18A9	214,0612	1161,8695	0,1842	REMS OR VIRAX	OK OR Kinking + Slight Luder Lines
22A14	263,7908	847,0655	0,3114	REMS OR VIRAX	One Wrinkle at the beginning or Luders
22A16	270,6705	921,3996	0,2938	REMS OR VIRAX	Buckling
25,40A1	214,5289	970,7454	0,2210	REMS	OK
25,40A2	293,4254	908,7663	0,3229	REMS	Slight Luders
28,575A5	176,8695	1081,7596	0,1635	REMS	Luder Lines
28,575A6	229,4602	941,0039	0,2438	REMS	Luder Lines
28,575A8	224,9090	831,0913	0,2706	REMS	Luder Lines
28A2	284,5001	927,6673	0,3067	REMS OR VIRAX	Light Wrinkling OR Luder Lines + LL Fracture
28A22	244,0725	1038,9070	0,2349	REMS OR VIRAX	One Wrinkle at the beginning or Luder Lines
28A23	159,4438	926,1493	0,1722	REMS OR VIRAX	Light Wrinkling Tendency or Luder Lines
28A24	242,6229	932,4150	0,2602	REMS OR VIRAX	OK OR Luder Lines
28A25	239,7965	892,9436	0,2685	REMS OR VIRAX	OK OR Kinking + Luder Lines
28A27	239,4282	994,8699	0,2407	REMS OR VIRAX	Light Kinking + Luder Lines OR Kinking + Luders
35A10	166,2143	981,3423	0,1694	REMS	OK
35A11	125,9071	1122,9622	0,1121	REMS	Flattening
35A12	173,9318	1058,3464	0,1643	REMS	OK
35A7	188,7393	1149,4415	0,1642	REMS	OK
35A8	209,9019	1002,6691	0,2093	REMS	OK

Table 60: Informative table regarding the 1st metric δ_x

5.4.1 1st Metric $\delta_x\ (a = 0\ rad)$ influence on the Luder Lines' appearance

As we dispose the final results coming from this formula, we can assess the effect that this parameter disposes to the bending result and more specifically to Luder Lines' formation. We present distinctive images from the respective Excel file.

$0{,}1121 \leq \delta_x\ (a = 0\ rad) \leq 0{,}2210\ [\%]$

Sample's Code	σ_start	ε_start	|D|min	Dstart	δ_x (a=0 rad)
35A11	125,9071	0,1065	20,8526	1122,9622	0,1121
15,875A2	172,2582	0,1251	58,8290	1233,4311	0,1397
15,875A4	165,0730	0,1088	41,6733	1114,4968	0,1481
15A15	148,1988	0,1180	100,9396	995,0243	0,1489
15A16	171,4708	0,1113	66,6315	1079,8608	0,1588
15A12	174,9932	0,1467	4,4316	1101,4217	0,1589
28,575A5	176,8695	0,2036	18,1482	1081,7596	0,1635
35A7	188,7393	0,1433	29,8630	1149,4415	0,1642
35A12	173,9318	0,1219	57,2565	1058,3464	0,1643
15,875A7	176,6241	0,1245	27,1571	1055,3493	0,1674
15A17	166,7800	0,1167	76,5458	996,0768	0,1674
35A10	166,2143	0,1351	3,1416	981,3423	0,1694
18A10	196,8128	0,1403	101,1274	1146,3755	0,1717
28A23	159,4438	0,1268	32,9718	926,1493	0,1722
15A13	204,2755	0,1545	21,5001	1170,8276	0,1745
15A11	229,1427	0,1833	40,0441	1295,0649	0,1769
18A9	214,0612	0,1571	56,0121	1161,8695	0,1842
18A11	200,3140	0,1570	71,1143	997,3471	0,2008
35A8	209,9019	0,1892	3,0582	1002,6691	0,2093
25,40A1	214,5289	0,2031	24,2416	970,7454	0,2210

Table 61: 1st Metric δ_x - Table 1

It seems to be valid that lower values of longitudinal deformation $\delta_x\ (a{=}0\ rad)$ do not favour the Luder Lines' appearance, as most rows are red coloured. Red colour stands for Another Defect or Clear Bending. Light green colour denotes Luder Lines' formation. Caution should be given to the close region $0{,}1717 \leq \delta_x\ (a = 0\ rad) \leq 0{,}2008\ [\%]$, in which it is difficult to estimate the probability of Luder Lines' occurrence.

Luder Lines' appearance: **5/20-> 25 %**
NO Luder Lines: 15/20-> 75 %

$0{,}2338 \leq \delta_x\ (a = 0\ rad) \leq 0{,}3229\ [\%]$

In this interval most rows are green indicating that most samples have suffered from Luder Lines on their surface during bending test. So, there is more likely to observe Luder Lines in cases of higher longitudinal deformation values.

18A2	252,5291	0,1935	18,0401	1080,0590	0,2338
28A22	244,0725	0,1969	23,2945	1038,9070	0,2349
28A27	239,4282	0,2484	66,1410	994,8699	0,2407
28,575A6	229,4602	0,1834	14,3473	941,0039	0,2438
28A24	242,6229	0,1952	18,3478	932,4150	0,2602
18A5	295,7627	0,2370	94,7516	1121,9220	0,2636
28A25	239,7965	0,1967	10,4552	892,9436	0,2685
16A4	234,5569	0,2032	51,8804	868,4494	0,2701
28,575A8	224,9090	0,1868	68,6467	831,0913	0,2706
18A8	253,0539	0,2122	18,9538	867,3486	0,2918
22A16	270,6705	0,2483	109,7321	921,3996	0,2938
18A6	265,8177	0,2153	9,1459	892,3254	0,2979
28A2	284,5001	0,1955	41,9995	927,6673	0,3067
22A14	263,7908	0,2110	46,6900	847,0655	0,3114
25,40A2	293,4254	0,2450	17,4165	908,7663	0,3229

Table 62: 1st Metric δ_x - Table 2

Luder Lines' appearance: **12/15-> 80** %
NO Luder Lines: 3/15-> 20 %

Consequently, this plastic deformation region is really hazardous, as there is a great risk of Luder Lines' formation.

Therefore, the 1st metric of longitudinal deformation $\delta_x\,(a{=}0\,rad)$ is proportional to the probability of Luder Lines' appearance Adopting a mathematical representation, the following relation can be written down:
$\delta_x\,(a = 0\,rad)$ ↑ => Chance of **Luder Lines'** appearance ↑

The same conclusion has been reached in case of the material property ε_{start}, which is a deformation indicator. So, these results come to an agreement that seems to be quite expected.

5.4.2 1st Metric $\delta_x\,(a = 0\,rad)$ plot along samples

This metric could be a predictive index for the critical strain ε_{crit} so as to avoid Luder Lines defect due to bending test of the hard copper tubes. To get an idea about the effectiveness of this metric, the following scatter graph is shown:

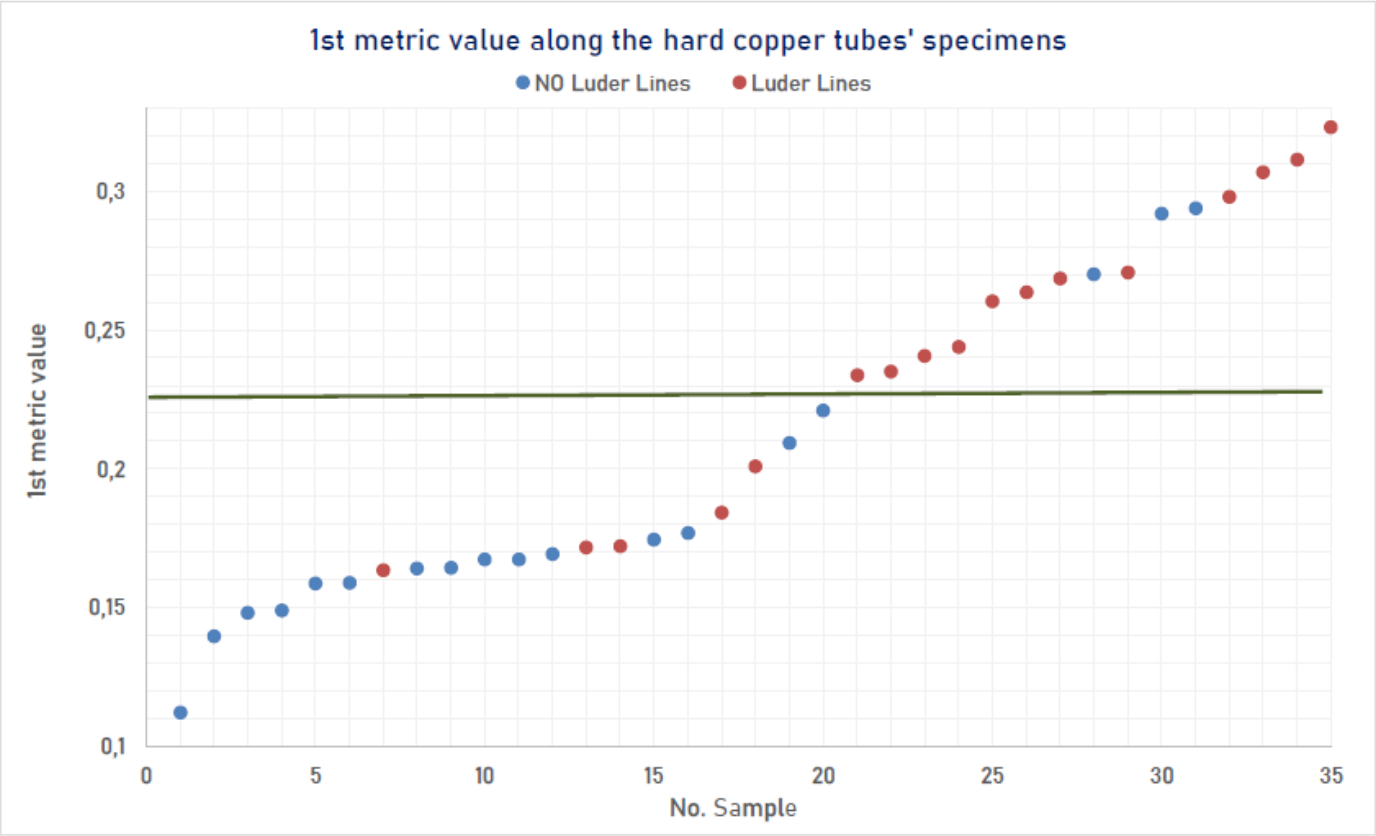

Figure 45: 1st Metric δ_x versus number of samples

There is a certain threshold, which seems to determine the hard copper tubes' behaviour during bending test. Therefore, we can estimate a critical strain ε_{crit} above which there is a really high chance of Luder Lines' appearance.

This value is indicated through a thick dark green horizontal line on the scatter graph, and it is supposed to be $\boldsymbol{\varepsilon_{crit} = 0,221}$ %.

5.5 On the longitudinal deformation $\delta_x \left(a = \frac{\pi}{2}\, rad\right)$

This deformation formula implies the combination of both geometrical and material parameters, as it requires the stress at the starting point of the plastic region σ_{start}, the plastic flow modulus D, the average wall thickness WT_{av} and the bending radius CLR. The geometrical properties are incorporated in the $k-factor$.

As plastic flow modulus D we decide to use as previously D_{start}, which is the plastic flow modulus computed in the 1st interval. Given that, the formula that gives the longitudinal deformation at $a = \frac{\pi}{2}\, rad$ point is given by:

$$\delta_x \left(a = \frac{\pi}{2}\, rad\right) = \frac{\sigma_{start}\,(2k + 1{,}5)}{D\,(2k + 2)}$$

Doing all the computational work for 60 distinct samples (35 physical), we have identified the value of this 2nd metric for all these specimens. The quantitative data are presented on the following extended table.

We do not follow the idea of worst – case scenario, because a hard copper tube may have been bent twice (both with REMS CURVO and Virax bender type). The only problem is that using a different bender type constitutes a different process affecting the bending outcome, as the material comes under bigger strains in case of lower bending radius CLR.

Sample ID	σ_{start}	k	D_{start}	$\delta_x\,(a = \frac{\pi}{2}\, rad)$	Bender Type	Bending Result
15,875A2	172,2582	3,0265	1233,4311	0,1310	Virax	OK
15,875A2	172,2582	3,9723	1233,4311	0,1326	REMS-CURVO	OK
15,875A4	165,0730	3,0255	1114,4968	0,1389	Virax	OK
15,875A4	165,0730	3,9710	1114,4968	0,1407	REMS-CURVO	OK
15,875A7	176,6241	3,9735	1055,3493	0,1589	REMS-CURVO	Kinking
15,875A7	176,6241	3,0274	1055,3493	0,1570	Virax	Kinking
15A11	229,1427	3,6667	1295,0649	0,1675	REMS-CURVO	Light Wrinkling
15A11	229,1427	3	1295,0649	0,1659	Virax	Buckling
15A12	174,9932	3	1101,4217	0,1489	Virax	Wrinkling
15A12	174,9932	3,6667	1101,4217	0,1504	REMS-CURVO	OK
15A13	204,2755	3,6642	1170,8276	0,1651	REMS-CURVO	Buckling
15A13	204,2755	2,9980	1170,8276	0,1636	Virax	Buckling
15A15	148,1988	2,9930	995,0243	0,1396	Virax	Crack
15A15	148,1988	3,6581	995,0243	0,1409	REMS-CURVO	Buckling
15A16	171,4708	3,0020	1079,8608	0,1489	Virax	Buckling + Cracking
15A16	171,4708	3,6691	1079,8608	0,1503	REMS-CURVO	OK
15A17	166,7800	3,0020	996,0768	0,1570	Virax	Buckling
15A17	166,7800	3,6691	996,0768	0,1585	REMS-CURVO	OK
16A4	234,5569	3,7500	868,4494	0,2559	REMS-CURVO	Buckling
16A4	234,5569	3,0000	868,4494	0,2532	Virax	Buckling
18A10	196,8128	3,0000	1146,3755	0,1610	Virax	Kinking + Luder Lines
18A10	196,8128	3,8889	1146,3755	0,1629	REMS-CURVO	OK
18A11	200,3140	3,8911	997,3471	0,1906	REMS-CURVO	OK
18A11	200,3140	3,0017	997,3471	0,1883	Virax	Kinking + Slight Luder Lines
18A8	253,0539	3,8878	867,3486	0,2768	REMS-CURVO	OK
18A8	253,0539	2,9992	867,3486	0,2735	Virax	Buckling

18A9	214,0612	3,0017	1161,8695	0,1727	Virax	Kinking + Slight Luder Lines
18A9	214,0612	3,8911	1161,8695	0,1748	REMS-CURVO	OK
18A2	252,5291	2,9983	1080,0590	0,2192	Virax	Luder Lines (with some crack)
18A2	252,5291	3,8867	1080,0590	0,2218	REMS-CURVO	No Wrinkling
18A5	295,7627	3,8878	1121,9220	0,2501	REMS-CURVO	OK
18A5	295,7627	2,9992	1121,9220	0,2471	Virax	Slight Luders
18A6	265,8177	3,8889	892,3254	0,2827	REMS-CURVO	OK
18A6	265,8177	3,0000	892,3254	0,2793	Virax	Slight Luders, Light Wrinkling, Kinki
22A14	263,7908	3,4960	847,0655	0,2941	REMS-CURVO	One Wrinkle at the beginning
22A14	263,7908	2,9966	847,0655	0,2919	Virax	Luders
22A16	270,6705	3,5032	921,3996	0,2775	REMS-CURVO	Buckling
22A16	270,6705	3,0027	921,3996	0,2754	Virax	Buckling
25,40A1	214,5289	3,9787	970,7454	0,2099	REMS-CURVO	OK
25,40A2	293,4254	3,9803	908,7663	0,3067	REMS-CURVO	Slight Luders
28,575A5	176,8695	4,0294	1081,7596	0,1554	REMS-CURVO	Luder Lines
28,575A6	229,4602	4,0287	941,0039	0,2317	REMS-CURVO	Luder Lines
28,575A8	224,9090	4,0245	831,0913	0,2572	REMS-CURVO	Luder Lines
28A22	244,0725	3,0000	1038,9070	0,2202	Virax	Luders
28A22	244,0725	3,6429	1038,9070	0,2223	REMS-CURVO	One Wrinkle at the beginning
28A23	159,4438	3,0000	926,1493	0,1614	Virax	Luders
28A23	159,4438	3,6429	926,1493	0,1629	REMS-CURVO	No Wrinkling (Tendency Light Wrinkling)
28A24	242,6229	2,9989	932,4150	0,2439	Virax	Luders
28A24	242,6229	3,6416	932,4150	0,2462	REMS-CURVO	OK
28A25	239,7965	3,0005	892,9436	0,2518	Virax	Luders and Kinking
28A25	239,7965	3,6435	892,9436	0,2541	REMS-CURVO	OK
28A27	239,4282	3,0000	994,8699	0,2256	Virax	Kinking + Luder Lines
28A27	239,4282	3,6429	994,8699	0,2277	REMS-CURVO	Light Kinking + Luder Lines
28A2	284,5001	3,0005	927,6673	0,2875	Virax	Luder Lines & LL Fracture
28A2	284,5001	3,6435	927,6673	0,2902	REMS-CURVO	Light Wrinkling
35A10	166,2143	3,9977	981,3423	0,1609	REMS-CURVO	OK
35A11	125,9071	3,9994	1122,9622	0,1065	REMS-CURVO	Flattening
35A12	173,9318	3,9943	1058,3464	0,1561	REMS-CURVO	OK
35A7	188,7393	3,9977	1149,4415	0,1560	REMS-CURVO	OK
35A8	209,9019	3,9954	1002,6691	0,1989	REMS-CURVO	OK

Table 63: Informative table regarding the 2nd metric δ_x

5.5.1 2nd Metric $\delta_x \left(a = \frac{\pi}{2}\, rad\right)$ influence on the Luder Lines' appearance [REMS – CURVO specimens]

As noted earlier, bending a tube with the aid of a different bender type means a different manufacturing process. For this reason, we divide the whole dataset into 2 sub-datasets with respect to the bender type.

$$0{,}1065 \leq \delta_x \left(a = \frac{\pi}{2}\, rad\right) \leq 0{,}2223\ [\%]$$

In general, very few specimens appear Luder Lines on their surface, when they are bent with REMS – CURVO machine. So, it is expected that this metric has not so much to predict regarding Luder Lines defect. However, we know that larger strains enhance the danger of the formation of this local failure.

Sample's Code	σ_start	k [GF]	εstart	D_start	D_min	δ_x (α = π/2 rad)
35A11	125,9071	3,9994	0,1065	1122,9622	20,8526	0,1065
15,875A2	172,2582	3,9723	0,1251	1233,4311	58,8290	0,1326
15,875A4	165,0730	3,9710	0,1088	1114,4968	41,6733	0,1407
15A15	148,1988	3,6581	0,1180	995,0243	100,9396	0,1409
15A16	171,4708	3,6691	0,1113	1079,8608	66,6315	0,1503
15A12	174,9932	3,6667	0,1467	1101,4217	4,4316	0,1504
28,575A5	176,8695	4,0294	0,2036	1081,7596	18,1482	0,1554
35A7	188,7393	3,9977	0,1433	1149,4415	29,8630	0,1560
35A12	173,9318	3,9943	0,1219	1058,3464	57,2565	0,1561
15A17	166,7800	3,6691	0,1167	996,0768	76,5458	0,1585
15,875A7	176,6241	3,9735	0,1245	1055,3493	27,1571	0,1589
35A10	166,2143	3,9977	0,1351	981,3423	3,1416	0,1609
28A23	159,4438	3,6429	0,1268	926,1493	32,9718	0,1629
18A10	196,8128	3,8889	0,1403	1146,3755	101,1274	0,1629
15A13	204,2755	3,6642	0,1545	1170,8276	21,5001	0,1651
15A11	229,1427	3,6667	0,1833	1295,0649	40,0441	0,1675
18A9	214,0612	3,8911	0,1571	1161,8695	56,0121	0,1748
18A11	200,3140	3,8911	0,1570	997,3471	71,1143	0,1906
35A8	209,9019	3,9954	0,1892	1002,6691	3,0582	0,1989
25,40A1	214,5289	3,9787	0,2031	970,7454	24,2416	0,2099
18A2	252,5291	3,8867	0,1935	1080,0590	18,0401	0,2218
28A22	244,0725	3,6429	0,1969	1038,9070	23,2945	0,2223

Table 64: 2nd Metric δ_x - Table 1 [REMS]

Luder Lines' appearance: **1/22 -> 4,55** %
NO Luder Lines: 21/22-> 95,45 %

$$0{,}2277 \leq \delta_x \left(a = \frac{\pi}{2}\, rad\right) \leq 0{,}3067\ [\%]$$

The number of the green rows is increasing, whilst the value of the 2nd metric is rising accordingly. However, most samples avoid the Luder Lines' occurrence thanks to this bender type.

28A27	239,4282	3,6429	0,2484	994,8699	66,1410	0,2277
28,575A6	229,4602	4,0287	0,1834	941,0039	14,3473	0,2317
28A24	242,6229	3,6416	0,1952	932,4150	18,3478	0,2462
18A5	295,7627	3,8878	0,2370	1121,9220	94,7516	0,2501
28A25	239,7965	3,6435	0,1967	892,9436	10,4552	0,2541
16A4	234,5569	3,7500	0,2032	868,4494	51,8804	0,2559
28,575A8	224,9090	4,0245	0,1868	831,0913	68,6467	0,2572
18A8	253,0539	3,8878	0,2122	867,3486	18,9538	0,2768
22A16	270,6705	3,5032	0,2483	921,3996	109,7321	0,2775
18A6	265,8177	3,8889	0,2153	892,3254	9,1459	0,2827
28A2	284,5001	3,6435	0,1955	927,6673	41,9995	0,2902
22A14	263,7908	3,4960	0,2110	847,0655	46,6900	0,2941
25,40A2	293,4254	3,9803	0,2450	908,7663	17,4165	0,3067

Table 65: 2nd Metric δ_x - Table 2 [REMS]

Luder Lines' appearance: **4/13 -> 30,77** %
NO Luder Lines: 9/13 -> 69,23 %

So, it can be stated that the critical strain for REMS – CURVO specimens is estimated at $\boldsymbol{\varepsilon_{crit}\ (REMS - CURVO) = 0,222}$ %

5.5.2 2nd Metric $\delta_x \left(a = \frac{\pi}{2}\, rad\right)$ influence on the Luder Lines' appearance [Virax specimens]

The exact opposite situation happens in case of Virax bender type's usage. Most samples appear Luder Lines than any other defect. Almost none had clear bending.

$$0{,}1310 \leq \delta_x \left(a = \frac{\pi}{2}\, rad\right) \leq 0{,}1659\ [\%]$$

The expected outcome is observed, which is that small strains do not enable Luder Lines to be formed easily on the hard copper tubes' surface. More specifically, only 2 specimens in this plastic deformation interval appear this failure.

Sample's Code	σ_start	k [GF]	εstart	D_start	D_min	δ_x (α = π/2 rad)
15,875A2	172,2582	3,0265	0,1251	1233,4311	58,8290	0,1310
15,875A4	165,0730	3,0255	0,1088	1114,4968	41,6733	0,1389
15A15	148,1988	2,9930	0,1180	995,0243	100,9396	0,1396
15A16	171,4708	3,0020	0,1113	1079,8608	66,6315	0,1489
15A12	174,9932	3	0,1467	1101,4217	4,4316	0,1489
15,875A7	176,6241	3,0274	0,1245	1055,3493	27,1571	0,1570
15A17	166,7800	3,0020	0,1167	996,0768	76,5458	0,1570
18A10	196,8128	3,0000	0,1403	1146,3755	101,1274	0,1610
28A23	159,4438	3,0000	0,1268	926,1493	32,9718	0,1614
15A13	204,2755	2,9980	0,1545	1170,8276	21,5001	0,1636
15A11	229,1427	3	0,1833	1295,0649	40,0441	0,1659

Table 66: 2nd Metric δ_x - Table 1 [Virax]

Luder Lines' appearance: **2/11 -> 18,18** %
NO Luder Lines: 9/11-> 81,82 %

$$0{,}1727 \leq \delta_x \left(a = \frac{\pi}{2}\, rad\right) \leq 0{,}2919\ [\%]$$

Most samples suffer from this non – linear phenomenon, whilst 3 samples had buckling defect, which means that the total deformation energy is released in another way.

18A9	214,0612	3,0017	0,1571	1161,8695	56,0121	0,1727
18A11	200,3140	3,0017	0,1570	997,3471	71,1143	0,1883
18A2	252,5291	2,9983	0,1935	1080,0590	18,0401	0,2192
28A22	244,0725	3,0000	0,1969	1038,9070	23,2945	0,2202
28A27	239,4282	3,0000	0,2484	994,8699	66,1410	0,2256
28A24	242,6229	2,9989	0,1952	932,4150	18,3478	0,2439
18A5	295,7627	2,9992	0,2370	1121,9220	94,7516	0,2471
28A25	239,7965	3,0005	0,1967	892,9436	10,4552	0,2518
16A4	234,5569	3,0000	0,2032	868,4494	51,8804	0,2532
18A8	253,0539	2,9992	0,2122	867,3486	18,9538	0,2735
22A16	270,6705	3,0027	0,2483	921,3996	109,7321	0,2754
18A6	265,8177	3,0000	0,2153	892,3254	9,1459	0,2793
28A2	284,5001	3,0005	0,1955	927,6673	41,9995	0,2875
22A14	263,7908	2,9966	0,2110	847,0655	46,6900	0,2919

Table 67: 2nd Metric δ_x - Table 2 [Virax]

Luder Lines' appearance: **8/11 -> 72,73** %
NO Luder Lines: 3/11-> 27,27 %

So, it can be stated that the critical strain for Virax bent specimens is estimated at $\boldsymbol{\varepsilon_{crit}\ (Virax) = 0{,}1727}$ %.

5.6 Discussion on the computation of the critical strain

The aim of this chapter is to find a deformation metric, which identifies a threshold so as to pinpoint the danger of Luder Lines' appearance on the upper surface of the hard copper tubes. We have 2 ways at our disposal so as to specify the critical strain:

- Experimental way (from the stress – strain curve)
- Computational way (from the plastic – deformation theory) using experimental data at the same time

Experimental procedure

The experimental way gives us the quantity named ε_{start}. Utilizing this material parameter, we have computed previously that the limit is equal to $\boldsymbol{\varepsilon_{crit} = 0,1545}$ %.

Moreover, it is reminded that the true strain ε_{start} is proportional to the probability of Luder Lines' formation. Adopting a mathematical representation, the following relation is valid:
$\boldsymbol{\varepsilon_{start}}$ ↑ => Probability of **Luder Lines'** appearance ↑

The following schematic visualizes the point in which ε_{start} is defined from the experimental stress – strain curves.

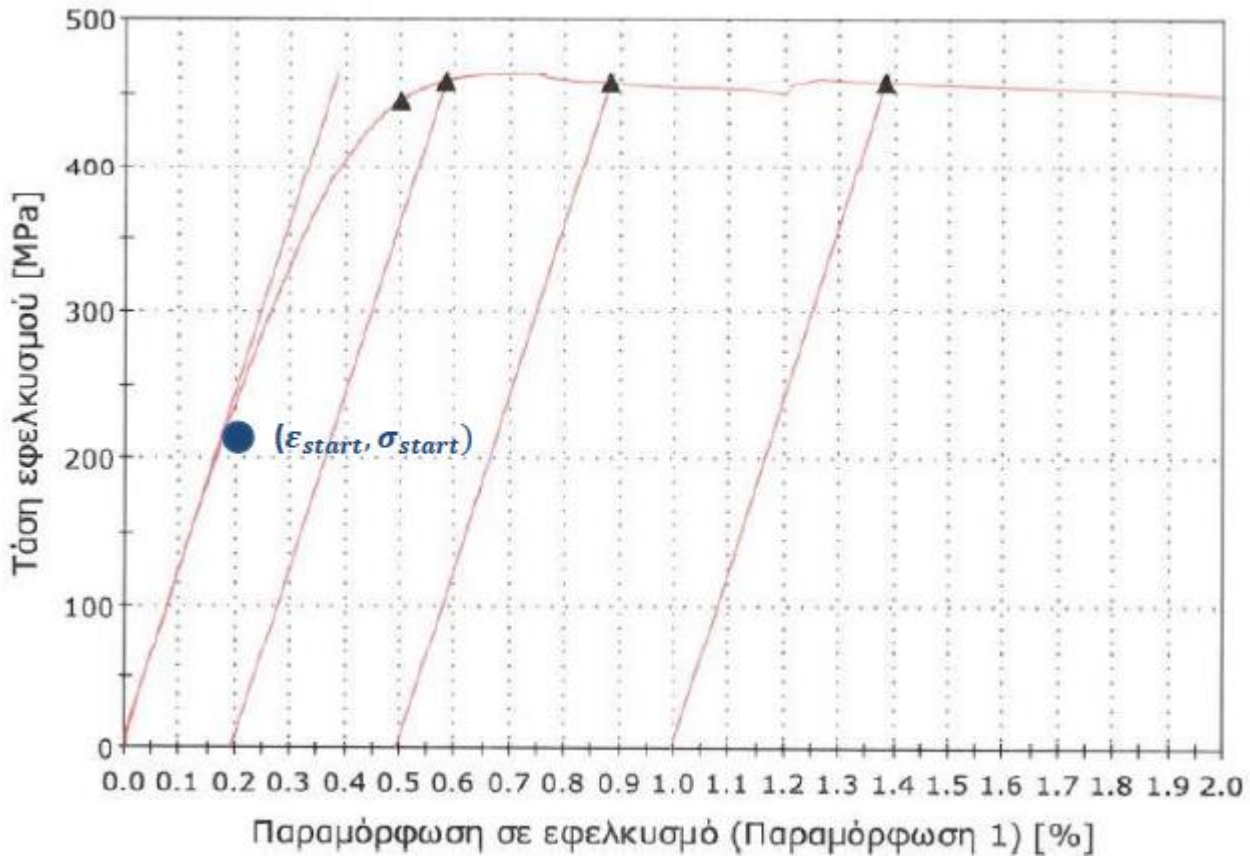

Figure 46: Reminder of definition of ε_{start}

Computational process

We have algebraically manipulated the following mathematical equation, so as to create two different formulas that give strains with respect to the angle a.

$$\delta_x = \frac{1}{D}\left(\sigma_x - \mu(\sigma_c + \sigma_r)\right)$$

In this way, we present two metrics $\delta_x\ (a = 0\ rad)$ & $\delta_x\ (\alpha = \frac{\pi}{2}\ rad)$. The former involves the worst case – scenario as for Luder Lines eliminating the parameter of bender type. The latter separates the whole dataset into 2 sub – datasets with respect to bending machine.

$$\begin{cases} \delta_x\ (a = 0\ rad) = \dfrac{\sigma_{start}}{D} \\ \delta_x\ \left(\alpha = \dfrac{\pi}{2}\ rad\right) = \dfrac{\sigma_{start}\ (2k + 1{,}5)}{2k + 2} \end{cases}$$

According to the results of the previous pages, it is estimated that there are 3 critical strains given in the list:

$$\begin{cases} \varepsilon_{crit}(\delta_x\ (a = 0\ rad)) = 0{,}221\ \% \\ \varepsilon_{crit}(\delta_x\ \left(a = \dfrac{\pi}{2}\ rad\right)) = 0{,}222\ \%\ [REMS - CURVO] \\ \varepsilon_{crit}(\delta_x\ \left(a = \dfrac{\pi}{2}\ rad\right)) = 0{,}1727\ \%\ [Virax] \end{cases}$$

It seems quite reasonable that the critical strain for Virax bent specimens takes lower value than the one referring to the REMS – CURVO samples. And that is why more specimens have suffered from Luder Lines defect in terms of percentage when bent with the aid of Virax bender.

Finally, we can give the following informative table, containing the quantitative data relating to the critical strain's estimation, which indicates a danger of Luder Lines' formation.

Critical strain ε_{crit} computation				
Metric acronym	ε_{start}	ε_{crit} $(\delta_x\,(a = 0\ rad))$	$\varepsilon_{crit}\ (\delta_x\,(a = \frac{\pi}{2}\ rad))\ [REMS]$	$\varepsilon_{crit}\ (\delta_x\,(a = \frac{\pi}{2}\ rad))\ [Virax]$
Value	0,1545%	0,2210%	0,2220%	0,1727%

Table 68: Critical strain ε computation for all possible cases

6. Design of the optimum predictive model

6.1 Design of the suitable formula

In this chapter, we will focus on the design of the proper tool so as to predict Luder Lines' occurrence. For this reason, we wish to create a specialized function which will engage the most influencing parameters and will be easily comprehended and utilized. In this way, we will create a useful and powerful criterion that will be able to predict this non – linear phenomenon.

Relied on our previous analysis, the properties that affect most this bending defect have to do with geometrical and material factors. In the following list, we gather these important characteristics:

No. (#)	Characteristic	Type
1	ε_{start}	Material
2	σ_{start}	Material
3	σ_Y	Material
4	ε_{UTS}	Material
5	OD_{av}	Geometry
6	WT_{av}	Geometry
7	CLR	Geometry
8	HV	Material
9	R_m	Material

Table 69: Parameters that affect most Luder Lines' appearance

Our formula (objective function) will incorporate these 9 factors (geometry+ material) introducing their overall significance. This predictive formula can be expressed by the general form, that is noted right down:

$$ObjFun = \varepsilon_{start}^{n_1}\ \sigma_{start}^{n_2}\ \sigma_Y^{n_3}\ \varepsilon_{UTS}^{n_4}\ OD_{av}^{n_5}\ WT_{av}^{n_6}\ CLR^{n_7}\ HV^{n_8}\ R_m^{n_9}$$

The aim of this analysis it to find out the optimum exponents n_i in order to separate the two bending results (Luder Lines or Another Defect / Clear Bending) the best way possible. So, we need a repetitive process which will achieve countless iterations to give us the optimum superscripts $n_1 - n_9$. Therefore, the idea of genetic algorithm (ga) should be introduced and implemented in MATLAB programming environment.

This method will enable us to solve this highly non – linear problem while considering all the properties that affect it in a different degree itself.

6.2 The idea of Genetic Algorithm

A genetic algorithm (GA) is a method for solving both constrained and unconstrained optimization problems based on a natural selection process that mimics biological evolution. The algorithm repeatedly modifies a population of individual solutions. At each step, the genetic algorithm randomly selects individuals from the current population and uses them as parents to produce the children for the next generation. Over successive generations, the population "evolves" toward an optimal solution.

The genetic algorithm can be applied to solve problems that are not well suited for standard optimization algorithms, including problems in which the objective function is discontinuous, nondifferentiable, stochastic, or highly nonlinear.

The genetic algorithm differs from a classical, derivative-based, optimization algorithm in two main ways, as summarized in the following table.

Classical Algorithm	Genetic Algorithm
Generates a single point at each iteration. The sequence of points approaches an optimal solution.	Generates a population of points at each iteration. The best point in the population approaches an optimal solution.
Selects the next point in the sequence by a deterministic computation.	Selects the next population by computation which uses random number generators.

Table 70: Differences between a classical algorithm and a genetic one

Let us realize how the genetic algorithm actually works based on the following outline which summarizes the information hidden behind this computing method [20, 21].

1. The algorithm begins by creating a random initial population.
2. The algorithm then creates a sequence of new populations. At each step, the algorithm uses the individuals in the current generation to create the next population. To create the new population, the algorithm performs the following steps:

    a. Scores each member of the current population by computing its fitness value. These values are called the raw fitness scores.
    b. Scales the raw fitness scores to convert them into a more usable range of values. These scaled values are called expectation values.
    c. Selects members, called parents, based on their expectation.
    d. Some of the individuals in the current population that have lower fitness are chosen as *elite*. These elite individuals are passed to the next population.
    e. Produces children from the parents. Children are produced either by making random changes to a single parent—*mutation*—or by combining the vector entries of a pair of parents—*crossover*.
    f. Replaces the current population with the children to form the next generation.

3. The algorithm stops when one of the stopping criteria is met.
4. The algorithm takes modified steps for linear and integer constraints.
5. The algorithm is further modified for nonlinear constraints.

6.3 Implementation of the genetic algorithm in our problem

We have adopted a specific objective function, that is designed according to the previous quantitative and qualitative analysis of the problem's parameters. The goal is to find the suitable exponents $n_1 - n_9$ so as to separate the two bending results (Luder Lines or Another Defect / Clear Bending) effectively. To avoid the categorical variables ("characters") we denote 1 in case of Luder Lines' occurrence otherwise we note 0 in the column named Result in the dataset. For sake of completeness, the dataset, which includes 60 distinct samples, is given below. This dataset will be used as input data to our genetic algorithm. We create the table that retains the raw data.

We possess 35 physical samples, but we would like to incorporate the different bending result in case of a different bender type usage. That is why there are 60 distinct samples. CLR quantity describes the bending radius that is determined by the bending machine. Another approach to create our dataset would be to take the worst-case scenario for every physical sample and not insert the CLR values. In this way, we hide from the genetic algorithm this information and make the problem more limited and ambiguous.

The following table includes the raw data regarding our 60 samples.

Sample ID	ε_{start}	σ_{start}	σ_Y	ε_{UTS}	OD_{av}	WT_{av}	CLR	HV	R_m	Result
15,875A2	0,1251	172,2582	367,7683	0,6129	15,86	0,74	63	137	460	0
15,875A2	0,1251	172,2582	367,7683	0,6129	15,86	0,74	48	137	460	0
15,875A4	0,1088	165,0730	367,0485	0,6840	15,865	0,71	63	137,6	461	0
15,875A4	0,1088	165,0730	367,0485	0,6840	15,865	0,71	48	137,6	461	0
15,875A7	0,1245	176,6241	371,9012	0,7059	15,855	0,56	63	139,1	480	0
15,875A7	0,1245	176,6241	371,9012	0,7059	15,855	0,56	48	139,1	480	0
15A11	0,1833	229,1427	365,9946	0,6818	15	0,65	55	128	465	0
15A11	0,1833	229,1427	365,9946	0,6818	15	0,65	45	128	465	0
15A12	0,1467	174,9932	341,0256	0,8079	15	0,75	55	129	445	0
15A12	0,1467	174,9932	341,0256	0,8079	15	0,75	45	129	445	0
15A13	0,1545	204,2755	349,5525	0,9505	15,01	0,535	55	139	476	0
15A13	0,1545	204,2755	349,5525	0,9505	15,01	0,535	45	139	476	0
15A15	0,1180	148,1988	330,4146	0,8616	15,035	0,455	55	139	465	0
15A15	0,1180	148,1988	330,4146	0,8616	15,035	0,455	45	139	465	0
15A16	0,1113	171,4708	372,3482	0,7590	14,99	0,695	55	140	473	0
15A16	0,1113	171,4708	372,3482	0,7590	14,99	0,695	45	140	473	0
15A17	0,1167	166,7800	350,5183	0,7237	14,99	0,69	55	132	456	0
15A17	0,1167	166,7800	350,5183	0,7237	14,99	0,69	45	132	456	0
16A4	0,2032	234,5569	317,9579	0,7568	16	0,47	55	117,2	463	0
16A4	0,2032	234,5569	317,9579	0,7568	16	0,47	45	117,2	463	0
18A10	0,1403	196,8128	359,4972	0,7038	18,000	0,605	70	143	477	0
18A10	0,1403	196,8128	359,4972	0,7038	18,000	0,605	54	143	477	1
18A11	0,1570	200,3140	337,7381	0,6678	17,990	0,700	70	126	453	0
18A11	0,1570	200,3140	337,7381	0,6678	17,990	0,700	54	126	453	1
18A2	0,1935	252,5291	358,0081	0,8972	18,010	0,735	70	120	459	0
18A2	0,1935	252,5291	358,0081	0,8972	18,010	0,735	54	120	459	1
18A5	0,2370	295,7627	358,6906	0,6305	18,005	0,735	70	120	473	0
18A5	0,2370	295,7627	358,6906	0,6305	18,005	0,735	54	120	473	1
18A6	0,2153	265,8177	345,4550	0,9081	18,000	0,700	70	119	463	0
18A6	0,2153	265,8177	345,4550	0,9081	18,000	0,700	54	119	463	1
18A8	0,2122	253,0539	335,5439	0,8253	18,005	0,61	70	126	464	0
18A8	0,2122	253,0539	335,5439	0,8253	18,005	0,61	54	126	464	0
18A9	0,1571	214,0612	357,9361	0,6844	17,99	0,65	70	136	454	0
18A9	0,1571	214,0612	357,9361	0,6844	17,99	0,65	54	136	454	1
22A14	0,2110	263,7908	342,1936	0,6862	22,025	0,7	77	128	457	0
22A14	0,2110	263,7908	342,1936	0,6862	22,025	0,7	66	128	457	1
22A16	0,2483	270,6705	316,9394	0,7298	21,98	0,56	77	137	456	0
22A16	0,2483	270,6705	316,9394	0,7298	21,98	0,56	66	137	456	0
25,40A1	0,2031	214,5289	312,3414	0,5833	25,385	0,875	101	134	444	0
25,40A2	0,2450	293,4254	343,7388	0,6809	25,375	0,79	101	136	456	1
28,575A5	0,2036	176,8695	269,2586	0,9658	28,54	0,875	115	129	437	1
28,575A6	0,1834	229,4602	340,5911	0,5338	28,545	0,88	115	138,1	445	1
28,575A8	0,1868	224,9090	331,6060	0,7357	28,575	0,94	115	130,9	464	1
28A2	0,1955	284,5001	379,2652	0,6297	27,995	0,89	102	130,2	476	0
28A2	0,1955	284,5001	379,2652	0,6297	27,995	0,89	84	130,2	476	1
28A22	0,1969	244,0725	337,8830	0,6807	28	0,89	102	131,3	454	0
28A22	0,1969	244,0725	337,8830	0,6807	28	0,89	84	131,3	454	1
28A23	0,1268	159,4438	315,6628	0,8629	28	0,9	102	134,5	453	0
28A23	0,1268	159,4438	315,6628	0,8629	28	0,9	84	134,5	453	1
28A24	0,1952	242,6229	342,1382	0,6115	28,01	0,97	102	128,9	452	0
28A24	0,1952	242,6229	342,1382	0,6115	28,01	0,97	84	128,9	452	1
28A25	0,1967	239,7965	330,2097	0,6562	27,995	0,895	102	120,7	436	0
28A25	0,1967	239,7965	330,2097	0,6562	27,995	0,895	84	120,7	436	1
28A27	0,2484	239,4282	292,1406	0,8452	28	0,78	102	138,1	467	1
28A27	0,2484	239,4282	292,1406	0,8452	28	0,78	84	138,1	467	1
35A10	0,1351	166,2143	302,4728	1,7021	35,02	1,01	140	136,4	404	0
35A11	0,1065	125,9071	312,2545	0,8939	35,005	0,9	140	139,4	441	0
35A12	0,1219	173,9318	318,9995	0,9649	35,05	1,035	140	136,2	455	0
35A7	0,1433	188,7393	331,9144	0,9056	35,02	1,085	140	140,4	439	0
35A8	0,1892	209,9019	301,5775	0,9065	35,04	1,09	140	135,3	436	0

Table 71: Raw dataset for the genetic algorithm

It can be easily observed that all these 9 characteristics do not have the same size class. This means automatically that every variable has a different weight value in the objective function, which cannot be allowed. So, we realize that the raw information needs some pre – processing before the implementation of the algorithm.

What we wish to is that all variables have the same size class. In other words, we desire that all values satisfy the following inequation:

$0 \leq x_i{}' \leq 1$
where: $x_i{}'$ stands for the new random variable of the 9 available ones.

To manage the upper situation, we have to implement the following formula 9 times for every single characteristic:

$$x_i{}' = \frac{x_i - x_{max}}{x_{max} - x_{min}}$$

where: x_i a random characteristic of the 9 available ones
x_{max} the maximum value of each column / characteristic
x_{min} the minimum value of each column / characteristic

After the computing work, we have algebraically manipulated the raw dataset and we have created a similar one that includes the information in a standardized and dimensionless form. In this way, all parameters are equally important.

In the next page of this chapter, we provide this new processed dataset, which will be inserted as input in our MATLAB program.

Sample ID	$\varepsilon_{start}{}'$	$\sigma_{start}{}'$	$\sigma_Y{}'$	$\varepsilon_{UTS}{}'$	$OD_{av}{}'$	$WT_{av}{}'$	CLR'	HV'	$R_m{}'$	Result
15,875A2	0,1310	0,2729	0,8955	0,0677	0,0434	0,4488	0,1895	0,7674	0,7368	0
15,875A2	0,1310	0,2729	0,8955	0,0677	0,0434	0,4488	0,0316	0,7674	0,7368	0
15,875A4	0,0163	0,2306	0,8889	0,1286	0,0436	0,4016	0,1895	0,7907	0,7500	0
15,875A4	0,0163	0,2306	0,8889	0,1286	0,0436	0,4016	0,0316	0,7907	0,7500	0
15,875A7	0,1270	0,2986	0,9331	0,1473	0,0431	0,1654	0,1895	0,8488	1,0000	0
15,875A7	0,1270	0,2986	0,9331	0,1473	0,0431	0,1654	0,0316	0,8488	1,0000	0
15A11	0,5417	0,6078	0,8794	0,1267	0,0005	0,3071	0,1053	0,4186	0,8026	0
15A11	0,5417	0,6078	0,8794	0,1267	0,0005	0,3071	0,0000	0,4186	0,8026	0
15A12	0,2836	0,2890	0,6524	0,2346	0,0005	0,4646	0,1053	0,4574	0,5395	0
15A12	0,2836	0,2890	0,6524	0,2346	0,0005	0,4646	0,0000	0,4574	0,5395	0
15A13	0,3384	0,4614	0,7299	0,3567	0,0010	0,1260	0,1053	0,8450	0,9474	0
15A13	0,3384	0,4614	0,7299	0,3567	0,0010	0,1260	0,0000	0,8450	0,9474	0
15A15	0,0814	0,1312	0,5559	0,2806	0,0022	0,0000	0,1053	0,8450	0,8026	0
15A15	0,0814	0,1312	0,5559	0,2806	0,0022	0,0000	0,0000	0,8450	0,8026	0
15A16	0,0339	0,2682	0,9371	0,1928	0,0000	0,3780	0,1053	0,8837	0,9079	0
15A16	0,0339	0,2682	0,9371	0,1928	0,0000	0,3780	0,0000	0,8837	0,9079	0
15A17	0,0723	0,2406	0,7387	0,1625	0,0000	0,3701	0,1053	0,5736	0,6842	0
15A17	0,0723	0,2406	0,7387	0,1625	0,0000	0,3701	0,0000	0,5736	0,6842	0
16A4	0,6817	0,6397	0,4427	0,1909	0,0503	0,0236	0,1053	0,0000	0,7763	0
16A4	0,6817	0,6397	0,4427	0,1909	0,0503	0,0236	0,0000	0,0000	0,7763	0
18A10	0,2387	0,4174	0,8203	0,1456	0,1500	0,2362	0,2632	1,0000	0,9605	0
18A10	0,2387	0,4174	0,8203	0,1456	0,1500	0,2362	0,0947	1,0000	0,9605	1
18A11	0,3561	0,4381	0,6225	0,1147	0,1496	0,3858	0,2632	0,3411	0,6447	0
18A11	0,3561	0,4381	0,6225	0,1147	0,1496	0,3858	0,0947	0,3411	0,6447	1
18A2	0,6130	0,7455	0,8068	0,3111	0,1505	0,4409	0,2632	0,1085	0,7237	0
18A2	0,6130	0,7455	0,8068	0,3111	0,1505	0,4409	0,0947	0,1085	0,7237	1
18A5	0,9199	1,0000	0,8130	0,0828	0,1503	0,4409	0,2632	0,1085	0,9079	0
18A5	0,9199	1,0000	0,8130	0,0828	0,1503	0,4409	0,0947	0,1085	0,9079	1
18A6	0,7672	0,8237	0,6927	0,3204	0,1500	0,3858	0,2632	0,0698	0,7763	0
18A6	0,7672	0,8237	0,6927	0,3204	0,1500	0,3858	0,0947	0,0698	0,7763	1
18A8	0,7451	0,7486	0,6026	0,2495	0,1503	0,2441	0,2632	0,3411	0,7895	0
18A8	0,7451	0,7486	0,6026	0,2495	0,1503	0,2441	0,0947	0,3411	0,7895	0
18A9	0,3565	0,5190	0,8061	0,1289	0,1496	0,3071	0,2632	0,7287	0,6579	0
18A9	0,3565	0,5190	0,8061	0,1289	0,1496	0,3071	0,0947	0,7287	0,6579	1
22A14	0,7369	0,8118	0,6630	0,1305	0,3507	0,3858	0,3368	0,4186	0,6974	0
22A14	0,7369	0,8118	0,6630	0,1305	0,3507	0,3858	0,2211	0,4186	0,6974	1
22A16	0,9998	0,8523	0,4334	0,1678	0,3485	0,1654	0,3368	0,7674	0,6842	0
22A16	0,9998	0,8523	0,4334	0,1678	0,3485	0,1654	0,2211	0,7674	0,6842	0
25,40A1	0,6813	0,5217	0,3916	0,0424	0,5182	0,6614	0,5895	0,6512	0,5263	0
25,40A2	0,9761	0,9862	0,6771	0,1259	0,5177	0,5276	0,5895	0,7287	0,6842	1
28,575A5	0,6847	0,3000	0,0000	0,3698	0,6755	0,6614	0,7368	0,4574	0,4342	1
28,575A6	0,5420	0,6097	0,6484	0,0000	0,6757	0,6693	0,7368	0,8101	0,5395	1
28,575A8	0,5658	0,5829	0,5668	0,1728	0,6772	0,7638	0,7368	0,5310	0,7895	1
28A2	0,6271	0,9337	1,0000	0,0821	0,6483	0,6850	0,6000	0,5039	0,9474	0
28A2	0,6271	0,9337	1,0000	0,0821	0,6483	0,6850	0,4105	0,5039	0,9474	1
28A22	0,6370	0,6957	0,6238	0,1257	0,6486	0,6850	0,6000	0,5465	0,6579	0
28A22	0,6370	0,6957	0,6238	0,1257	0,6486	0,6850	0,4105	0,5465	0,6579	1
28A23	0,1430	0,1974	0,4218	0,2817	0,6486	0,7008	0,6000	0,6705	0,6447	0
28A23	0,1430	0,1974	0,4218	0,2817	0,6486	0,7008	0,4105	0,6705	0,6447	1
28A24	0,6253	0,6871	0,6625	0,0665	0,6491	0,8110	0,6000	0,4535	0,6316	0
28A24	0,6253	0,6871	0,6625	0,0665	0,6491	0,8110	0,4105	0,4535	0,6316	1
28A25	0,6356	0,6705	0,5541	0,1048	0,6483	0,6929	0,6000	0,1357	0,4211	0
28A25	0,6356	0,6705	0,5541	0,1048	0,6483	0,6929	0,4105	0,1357	0,4211	1
28A27	1,0000	0,6683	0,2080	0,2665	0,6486	0,5118	0,6000	0,8101	0,8289	1
28A27	1,0000	0,6683	0,2080	0,2665	0,6486	0,5118	0,4105	0,8101	0,8289	1
35A10	0,2015	0,2373	0,3019	1,0000	0,9985	0,8740	1,0000	0,7442	0,0000	0
35A11	0,0000	0,0000	0,3908	0,3083	0,9978	0,7008	1,0000	0,8605	0,4868	0
35A12	0,1088	0,2827	0,4522	0,3690	1,0000	0,9134	1,0000	0,7364	0,6711	0
35A7	0,2594	0,3699	0,5696	0,3183	0,9985	0,9921	1,0000	0,8992	0,4605	0
35A8	0,5829	0,4945	0,2938	0,3190	0,9995	1,0000	1,0000	0,7016	0,4211	0

Table 72: Processed dataset for the genetic algorithm – Input

6.4 Discussion on the program results

For sake of completeness, we will provide the program results for both the raw dataset and the transformed one. Running many iterations of the genetic algorithm, we can take quite different values as for the exponents $n_1 - n_9$ and the separation process regarding the bending result. (1 = Luder Lines | 0 = Another Defect or Clear Bending)

Besides that, we will give the respective quantitative information for both the "worst - case scenario" dataset and the whole dataset. Therefore, we compute different superscripts' values for these cases.

So, we have 4 different cases, which are listed right down:

- 1st Case: Worst – Case Scenario | Raw Dataset
- 2nd Case: Worst – Case Scenario | Transformed Dataset
- 3rd Case: Whole Raw Dataset
- 4th Case: Whole Transformed Dataset

6.4.1 1st Case: Worst – case Scenario | Raw Dataset

Thanks to the genetic algorithm, we can get the exponents that we are interested in, and we gather them to the following table:

Exponent	n_1	n_2	n_3	n_4	n_5	n_6	n_8	n_9
Value	-0,9605	1,5511	-0,6958	1,0496	1,848	0,5921	-1,1349	0,4766

Table 73: Exponents of the objective function - 1st case

For size class reasons we adopt a coefficient to our objective function. Based on these exponents, we give the specific objective function that matches to this case:

$$ObjFun_1 = 0{,}001\varepsilon_{start}^{-0,9605}\ \sigma_{start}^{1,5511}\ \sigma_Y^{-0,6958}\ \varepsilon_{UTS}^{1,0496}\ OD_{av}^{1,848}\ WT_{av}^{0,5921}\ HV^{-1,1349}\ R_m^{0,4766}$$

Relied on this objective function, we can sort the objective function's values for each sample and in this way, we can find a major trend for Luder Lines' formation. In the next page, we present the output table of the main program in MATLAB environment, which summarizes the information.

Sample ID	Bending Result	$ObjFun_1$ Value
15A15	0	1,7778
15,875A2	0	2,0526
15,875A7	0	2,0965
15A11	0	2,2524
15A17	0	2,3058
15,875A4	0	2,4008
15A16	0	2,4284
15A12	0	2,4353
16A4	0	2,6700
15A13	0	2,6712
18A10	1	2,8846
18A9	1	3,0961
18A11	1	3,2271
18A5	1	3,9938
18A8	0	4,0675
22A16	0	4,4006
25,40A1	0	5,1140
18A6	1	5,4207
18A2	1	5,4326
22A14	1	5,4428
28,575A6	1	6,4776
25,40A2	1	7,1585
28A24	1	8,5226
28A27	1	8,5676
28A22	1	8,9762
28,575A5	1	9,1604
28A25	1	9,2536
28A23	1	9,3142
28,575A8	1	9,9416
28A2	1	10,0627
35A11	0	11,4346
35A7	0	17,3163
35A8	0	17,4583
35A12	0	20,0754
35A10	0	29,6370

Table 74: Output of the genetic algorithm - 1st case

It seems that the data can be separated in a satisfying way along the 35 samples. We can visualize this table trough a scatter plot, which is given right down:

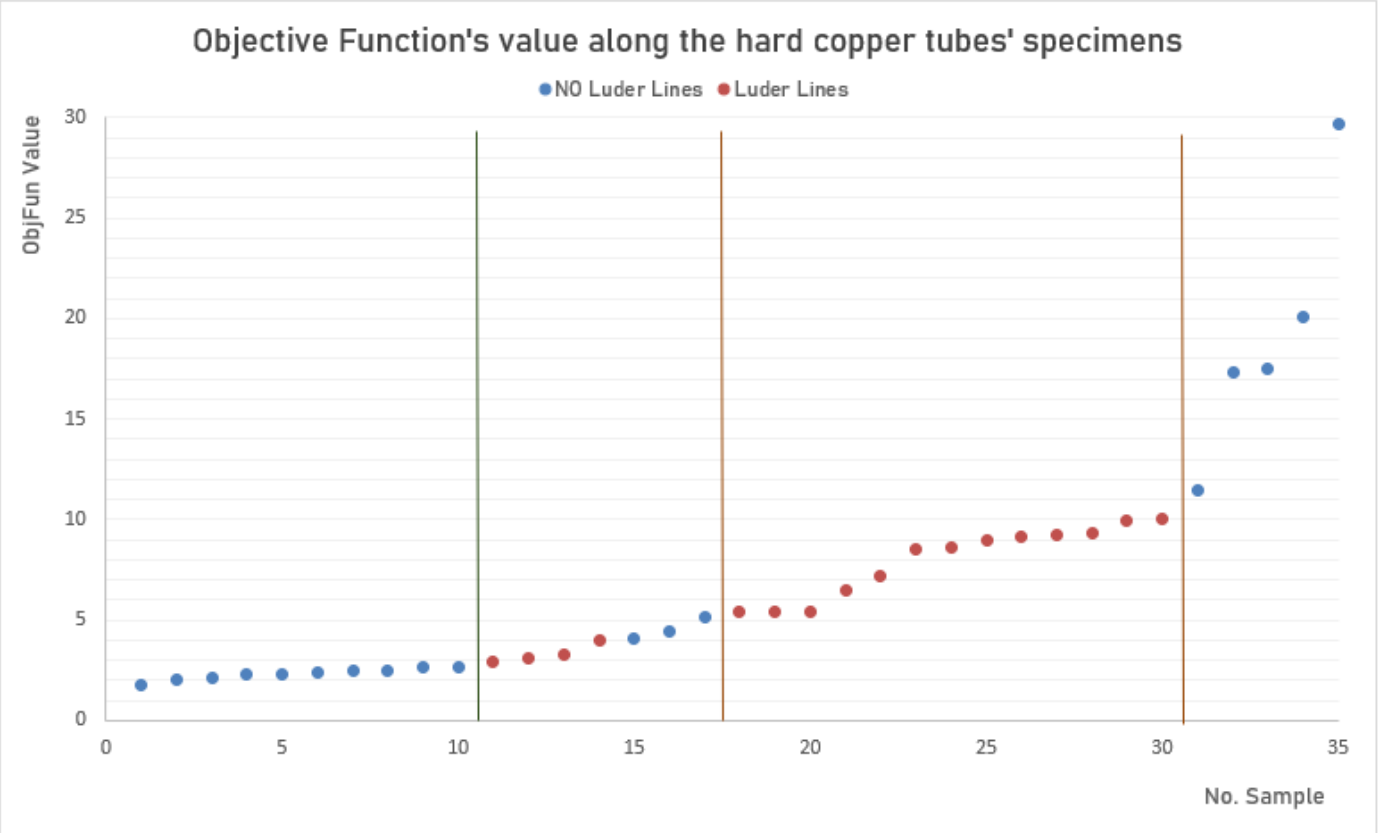

Figure 47: Visualization of the algorithm's output - 1st case

Consequently, we realize that this objective function named $ObjFun_1$ could be used as a predictive tool for Luder Lines' appearance with high accuracy.

There are some certain thresholds, which seem to determine the hard copper tubes' behaviour during bending. Therefore, we write down a semi – empirical rule to predict the Luder Lines' occurrence for hard copper tubes:

- $1{,}7778 \leq ObjFun_1 \leq 2{,}6712$: **NO** Luder Lines (10/10 -> **100 %)**
- $2{,}6712 < ObjFun_1 \leq 5{,}114$: **Ambiguous situation** (Almost equal probability of Luder Lines' manifestation according to the 7 samples of the dataset.)
- $5{,}114 < ObjFun_1 \leq 10{,}0627$: **Luder Lines** appearance (13/13-> **100%**)
- $ObjFun_1 > 10{,}0627$: **NO** Luder Lines (5/5 -> **100 %)**

In this way, there are 3 clear regions as for the bending result and a vague one which seems to confuse the objective function $ObjFun_1$.
We will go on with the 2nd case to give the proper data analysis.

6.4.2 2nd Case: Worst – case Scenario | Transformed Dataset

In this case, we do not compute the transformation explained in a previous page, as it seems to give somewhat not so adequate results when it comes to genetic algorithm implementation for this specific dataset.

$$x_i{}' = \frac{x_i - x_{max}}{x_{max} - x_{min}}$$

For this reason, we adopt a rather similar transformation from which we get a dimensionless form of our values in the same size class.

$$x_{adj} = \frac{x_i - x_{max}}{x_{max} - x_{min}} + 1 = x_i' + 1$$

As previously, we can create a table which contains the exponents of this current objective function.

Exponent	n_1	n_2	n_3	n_4	n_5	n_6	n_8	n_9
Value	1,6727	1,8716	1,1497	-0,9759	1,6203	1,6539	-1,9249	1,6672

Table 75: Exponents of the objective function - 2nd case

Because we do not wish to have relatively high objective function's values, we introduce a coefficient to this predictive function. So, we can write down this objective function and we can use it for our dataset.

$$ObjFun_2 = 0{,}2\ \varepsilon_{start}^{1,6727}\ \sigma_{start}^{1,8716}\ \sigma_Y^{1,1497}\ \varepsilon_{UTS}^{-0,9759}\ OD_{av}^{1,6203}\ WT_{av}^{1,6539}\ HV^{-1,9249}\ R_m^{1,6672}$$

Sorting the arising function values, we can get an idea of the effectiveness of the objective function as for the separation possibility. We would like to have 2 distinct regions as the outcome of the genetic algorithm.

The following table contains the computed quantities for every single sample in a listed form. In this way, we can optically observe the effectiveness of this method.

Sample ID	Bending Result	$ObjFun_2$ Value
15A15	0	0,3094
35A10	0	0,8297
15,875A4	0	0,8681
15A16	0	0,8764
15A17	0	0,9206
35A11	0	0,9743
15,875A7	0	0,9978
15A13	0	1,0524
15,875A2	0	1,2534
15A12	0	1,3251
18A10	1	1,3820
28A23	1	1,9047
18A9	1	2,0192
28,575A5	1	2,7166
18A11	1	2,8889
35A12	0	3,1335
35A7	0	3,5721
15A11	0	3,9181
22A16	0	4,3791
16A4	0	4,5380
25,40A1	0	5,1608
18A8	0	5,3989
35A8	0	5,8640
28,575A6	1	6,3093
28A27	1	6,3786
22A14	1	8,3935
18A2	1	8,9301
28,575A8	1	9,8534
28A22	1	10,1957
18A6	1	10,9765
25,40A2	1	12,0074
28A24	1	13,3667
28A25	1	13,5313
18A5	1	22,0904
28A2	1	23,5157

Table 76: Output of the genetic algorithm - 2nd case

The objective function $ObjFun_2$ values could be plotted with respect to the number of hard copper tube's sample.

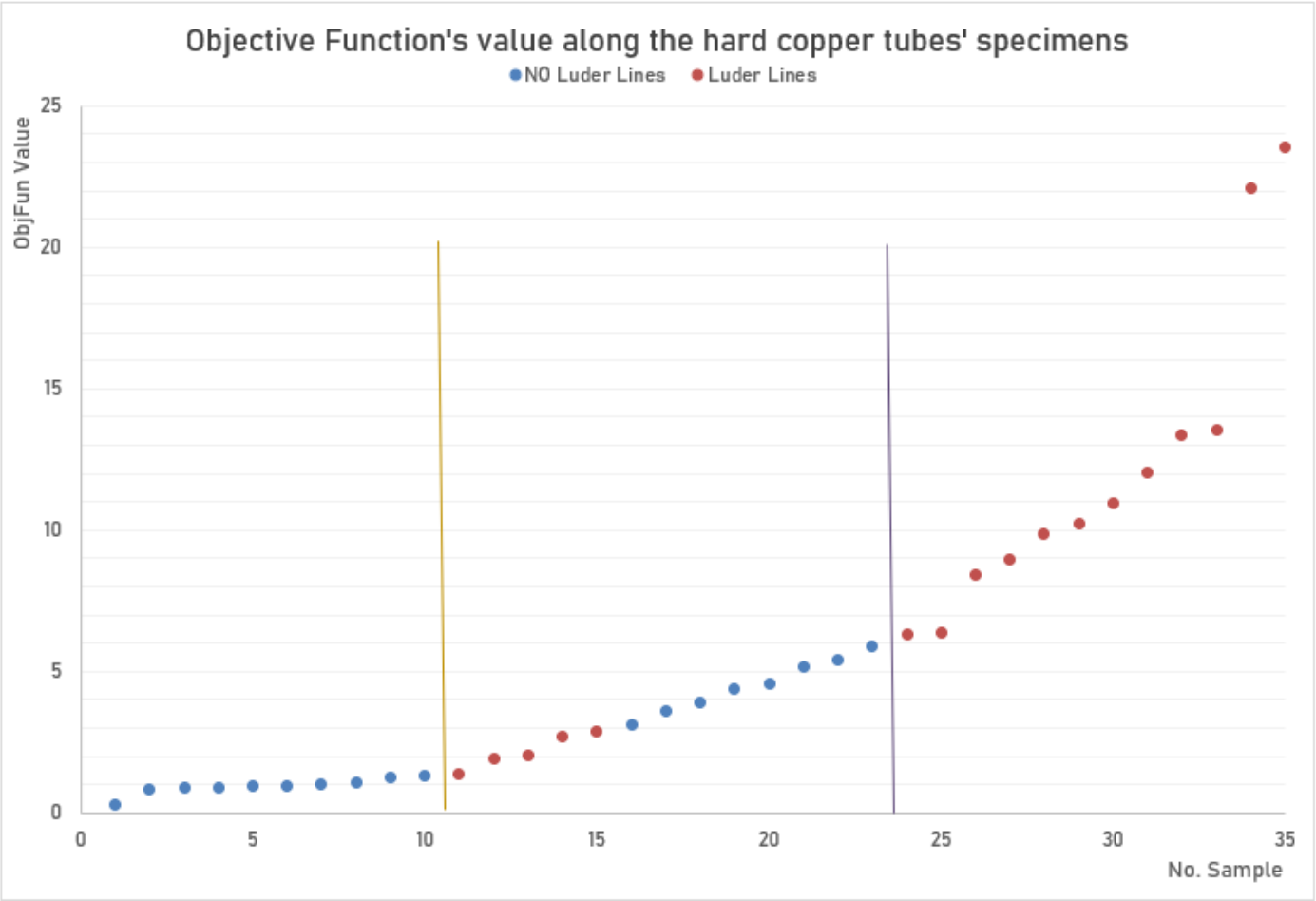

Figure 48: Visualization of the algorithm's output - 2nd case

In this figure, three distinct regions are depicted: a safe one, a vague one and a hazardous one for Luder Lines' occurrence.

- $0{,}3094 \leq ObjFun_2 \leq 1{,}3251$: **NO** Luder Lines (10/10 -> **100 %)**
- $1{,}3251 < ObjFun_2 \leq 5{,}8640$: **Ambiguous situation** (Almost equal probability of Luder Lines' manifestation according to the 15 samples of the dataset.)
- $ObjFun_2 > 5{,}8640$: **Luder Lines** appearance (10/10-> **100%**)

6.4.3 3rd Case: Whole Raw Dataset

In this case, we take into account the CLR parameter, which means that we consider the different bending result in relation to the bender type (REMS or Virax). In this way, we have at our disposal an enriched dataset that includes 60 specimens.

Unfortunately, as it will be shown in advance, the separation process involves many different zones and there is not one or two thresholds that can determine the copper tubes' bending outcome. So, it is difficult to predict the Luder Lines' appearance if this is the case.

Enabling the CLR parameter (exponent n_7) there are 9 exponents in contrary to the previous cases (1st and 2nd case <--- Worst – Case Scenario).

Exponent	n_1	n_2	n_3	n_4	n_5	n_6	n_7	n_8	n_9
Value	-0,4739	0,5125	-0,6941	-0,0658	1,4624	1,3139	1,3595	1,1873	-1,0845

Table 77: Exponents of the objective function - 3rd case

Relied on these superscripts, an analytical form of the objective function can be given for the whole dataset, if raw values are used. As previously, we can introduce a coefficient for size class reasons.

$$ObjFun_3 = 0{,}001\varepsilon_{start}^{-0,4739}\ \sigma_{start}^{0,5125}\ \sigma_Y^{-0,6941}\ \varepsilon_{UTS}^{-0,0658}\ OD_{av}^{1,4624}\ WT_{av}^{1,3139} CLR^{1,3595} HV^{1,1873} R_m^{-1,0845}$$

The table containing the sample ID, the objective function's $ObjFun_3$ value and the bending result is provided.

Sample ID	Bending Result	$ObjFun_3$ Value
16A4	0	0,9136
15A15	0	0,9645
15A13	0	1,1488
16A4	0	1,2002
15A15	0	1,2670
15A11	0	1,3335
15,875A7	0	1,4388
15A13	0	1,5092
15A17	0	1,6532
15A16	0	1,7064
15A12	0	1,7148
15A11	0	1,7518
18A8	0	2,0780
15,875A7	0	2,0824
15,875A4	0	2,1143
15,875A2	0	2,1397
15A17	0	2,1717
15A16	0	2,2416
15A12	0	2,2526
18A6	1	2,3117
18A10	1	2,3928
18A5	1	2,4496

18A2	1	2,5178
18A9	1	2,5958
18A11	1	2,6408
18A8	0	2,9571
15,875A4	0	3,0600
15,875A2	0	3,0967
18A6	0	3,2897
18A10	0	3,4051
18A5	0	3,4859
18A2	0	3,5829
18A9	0	3,6940
22A16	0	3,7011
18A11	0	3,7580
22A16	0	4,5640
22A14	1	4,6525
22A14	0	5,7372
28A27	1	10,9516
28A2	1	12,3959
28A25	1	12,5891
25,40A2	1	12,6369
28A22	1	13,0924
28A23	1	14,0419
28A27	1	14,2598
28A24	1	14,4097
25,40A1	0	14,7127
28A2	0	16,1404
28A25	0	16,3918
28A22	0	17,0472
28A23	0	18,2836
28A24	0	18,7625
28,575A5	1	19,6560
28,575A8	1	21,4259
28,575A6	1	22,3511
35A11	0	40,5470
35A12	0	49,7669
35A10	0	51,0012
35A8	0	51,5292
35A7	0	53,7326

Table 78: Output of the genetic algorithm - 3rd case

The following schematic is illustrated for visualizing purposes so as to find a semi – empirical rule to predict this phenomenon.

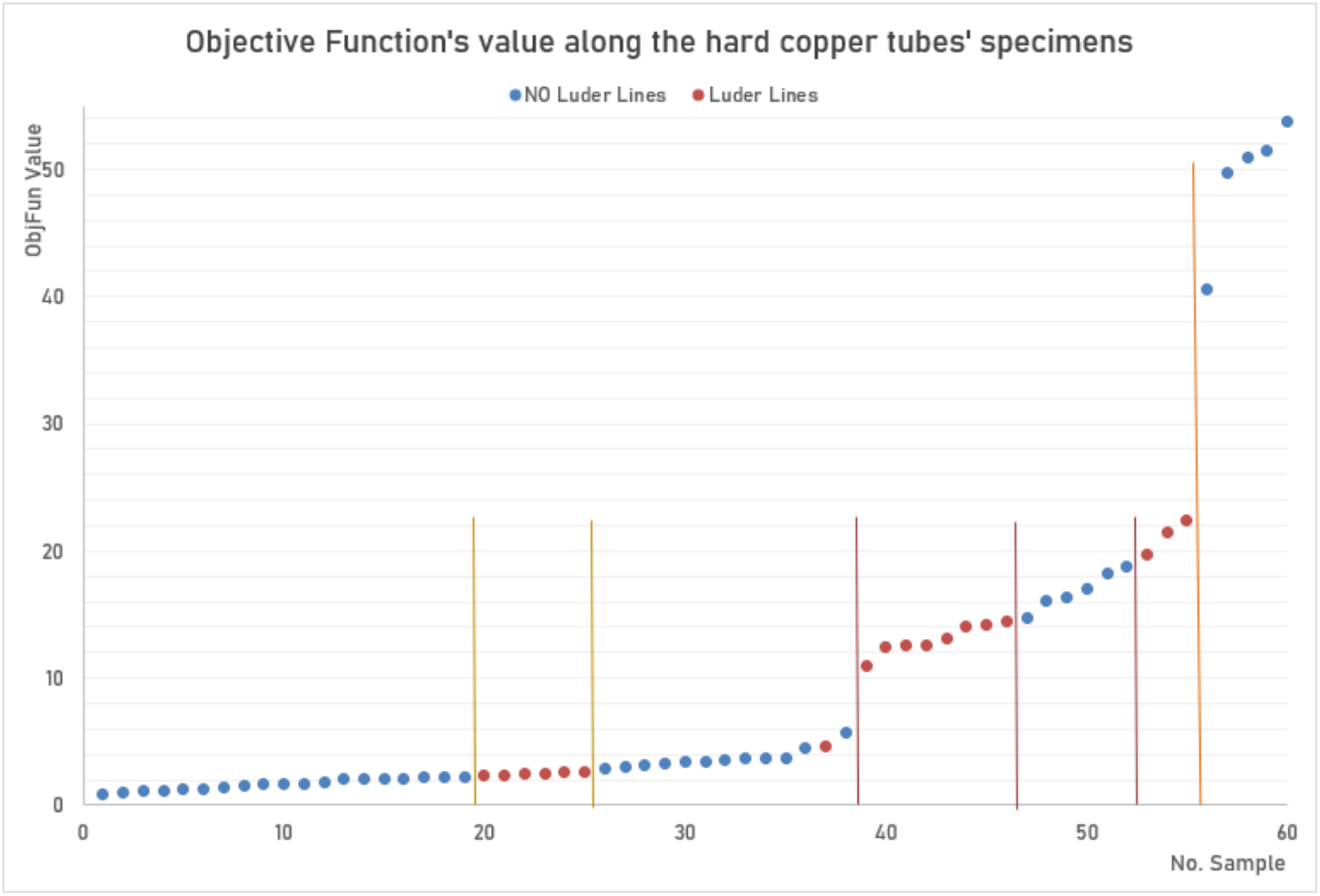

Figure 49: Visualization of the algorithm's output - 3rd case

There are many different regions in which copper tubes suffer from Luder Lines or another bending result occurs. So, we give a pseudo – code that will give a predictive norm:

No Luder Lines' case
IF $0{,}9136 \leq ObjFun_3 \leq 2{,}2526$ **OR** $2{,}9571 \leq ObjFun_3 \leq 5{,}7372$ **OR** $14{,}7127 \leq ObjFun_3 \leq 18{,}7625$ **OR** $40{,}5470 \leq ObjFun_3 \leq 53{,}7326$ => **NO** Luder Lines

Luder Lines' appearance case
IF $2{,}3117 \leq ObjFun_3 \leq 2{,}6408$ **OR** $10{,}9516 \leq ObjFun_3 \leq 14{,}4097$ **OR** $19{,}6560 \leq ObjFun_3 \leq 22{,}3511$ => **Luder Lines'** appearance

6.4.4 4th Case: Whole Transformed Dataset

Surprisingly, this case was the most difficult for the genetic algorithm to produce an efficient separation along the 60 specimens. Therefore, we need to perform many iterations / trials of the program in order to give us a precise and satisfying result.

First of all, we do not adopt the standardization explained in the previous pages:

$$x_i' = \frac{x_i - x_{max}}{x_{max} - x_{min}}$$

What we actually do is to introduce a quite adjusted Z – Score function, which links to the uniform distribution of a random dataset. However, although the values of this dataset do not obey to a specific statistical distribution, this approach seems to give interesting results.

$$Z_{adj} = \frac{x_i - \bar{x}}{s} + C$$

where: x_i: a random characteristic of the 9 available ones
$\bar{x}$: the mean value of each characteristic / column
s: the standard deviation of each characteristic / column
$C = 5$: a constant value so as to all values are positive (> 0)

As previous, the 9 superscripts are listed in the following vector:

Exponent	n_1	n_2	n_3	n_4	n_5	n_6	n_7	n_8	n_9
Value	1,0558	-1,2747	-0,2555	-0,0666	0,8085	1,6210	-1,4379	-0,6882	0,8450

Table 79: Exponents of the objective function - 4th case

The resultant objective function is given in its analytical form right down. We utilize it so as to have the best possible separation.

$$ObjFun_4 = \varepsilon_{start}^{1,0558}\ \sigma_{start}^{-1,2747}\ \sigma_Y^{-0,2555}\ \varepsilon_{UTS}^{-0,0666}\ OD_{av}^{0,8085} WT_{av}^{1,6210} CLR^{-1,4379} HV^{-0,6882} R_m^{0,845}$$

The respective table is received, as follows, including the sample code (ID) of each distinct sample, the bending outcome and the objective function's $ObjFun_4$ values. In addition, the whole information is summarized to a scatter plot.

In this way, it is easier to obtain the quantitative impact of this design analysis and to find an easily perceivable predictive tool.

Sample ID	Bending Result	$ObjFun_4$ Value
35A10	0	0,9180
15A15	0	1,5366
18A9	0	1,6769
22A16	0	1,6786
15A13	0	1,7292
15A15	0	1,7423
18A10	0	1,7681
15,875A7	0	1,7772
22A16	0	1,8858
15A13	0	1,9608
18A9	1	2,0120
25,40A2	1	2,0980
28,575A6	1	2,1140
18A10	1	2,1214
15,875A4	0	2,1215
15,875A7	0	2,1277
18A8	0	2,2722
15A16	0	2,3021
15,875A2	0	2,3926
16A4	0	2,3945
22A14	0	2,3951
15A17	0	2,4103
35A7	0	2,4716
15A11	0	2,5002
15,875A4	0	2,5400
18A11	0	2,5648
15A16	0	2,6104
22A14	1	2,6907
35A11	0	2,7132
16A4	0	2,7152
18A8	0	2,7262
15A17	0	2,7331
15A11	0	2,8351
15A12	0	2,8441
15,875A2	0	2,8645
18A2	0	2,9159
25,40A1	0	2,9530
28A2	0	2,9618
28A22	0	2,9660
28A25	0	3,0010
35A8	0	3,0733
18A11	1	3,0772
18A6	0	3,0794
35A12	0	3,1456

15A12	0	3,2250
18A5	0	3,4069
28A24	0	3,4557
28A23	0	3,4887
28A2	1	3,4916
28A22	1	3,4965
18A2	1	3,4984
28A25	1	3,5378
28A27	1	3,5516
28,575A8	1	3,5840
18A6	1	3,6947
28,575A5	1	4,0442
28A24	1	4,0738
18A5	1	4,0876
28A23	1	4,1127
28A27	1	4,1868

Table 80: Output of the genetic algorithm - 4th case

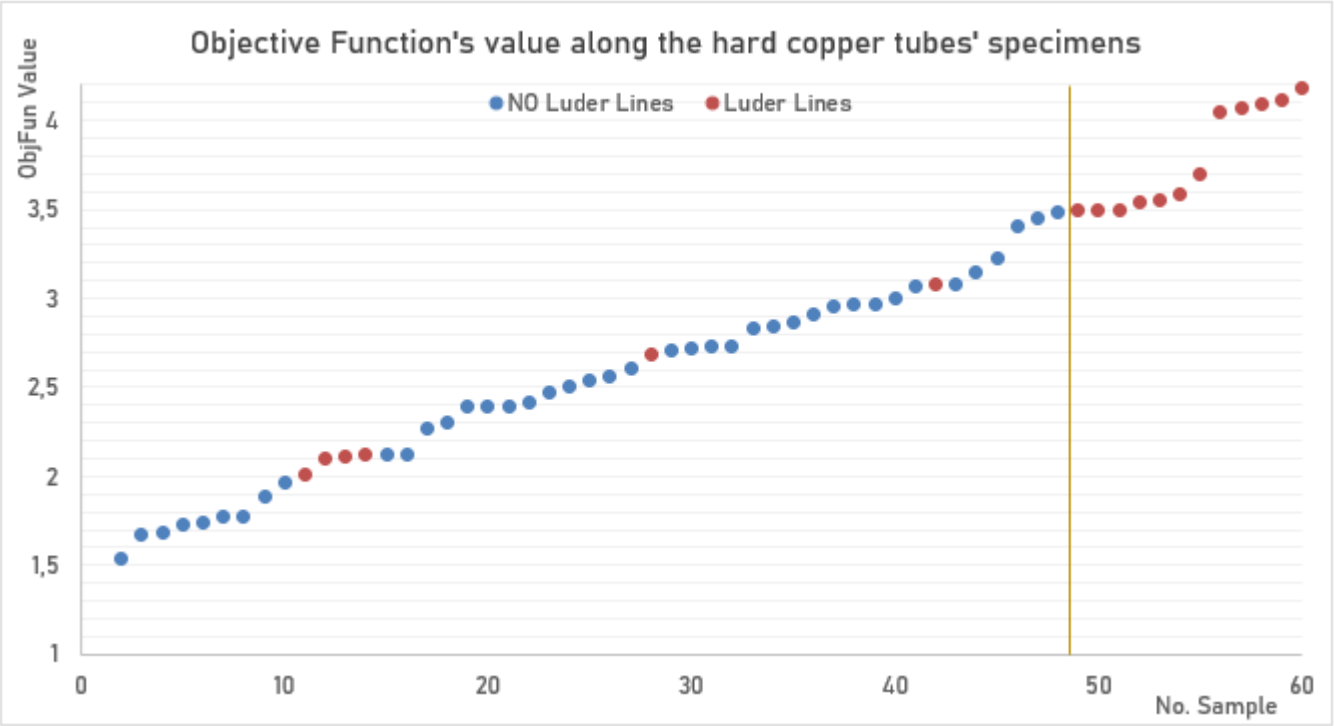

Figure 50: Visualization of the algorithm's output - 4th case

In terms of accuracy (%), this is the best separation of the 4 cases.

- $0{,}918 \leq ObjFun_4 \leq 3{,}4887$: **NO** Luder Lines (42/48 -> **87,5 %)**
- $3{,}4887 < ObjFun_4 \leq 4{,}1868$: **Luder Lines** appearance (12/12-> **100%**)

6.5 Short review regarding the design of the optimum predictive model

We have categorized our specimens to 4 distinct datasets, so as to determine Luder Lines defect the detailed way possible! These 4 cases are given to the following list:

- 1st Case: Worst – Case Scenario | Raw Dataset
- 2nd Case: Worst – Case Scenario | Transformed Dataset
- 3rd Case: Whole Raw Dataset
- 4th Case: Whole Transformed Dataset

Based on these cases, we wanted to apply this input data to an exponential objective function in order to separate the 2 conditions.

$$ObjFun = \varepsilon_{start}^{n_1}\ \sigma_{start}^{n_2}\ \sigma_Y^{n_3}\ \varepsilon_{UTS}^{n_4}\ OD_{av}^{n_5}\ WT_{av}^{n_6}\ CLR^{n_7}\ HV^{n_8}\ R_m^{n_9}$$

We will create a characteristic table which includes the useful quantitative results, after the end of the genetic algorithm's analysis, so as to summarize the whole information extracted from the initial MATLAB program.

Case	1st	2nd	3rd	4th
n_1	-0,9605	1,6727	-0,4793	1,0558
n_2	1,5511	1,8716	0,5125	-1,2747
n_3	-0,6958	1,1497	-0,6941	-0,2555
n_4	1,0496	-0,9759	-0,0658	-0,0666
n_5	1,8480	1,6203	1,4624	0,8085
n_6	0,5921	1,6539	1,3139	1,6210
n_7	0	0	1,3595	-1,4379
n_8	-1,1349	-1,9242	1,1873	-0,6822
n_9	0,4766	1,6672	-1,0845	0,8450
Luder Lines' prediction accuracy	100%	100%	100%	87,5%
NO Luder Lines' prediction accuracy	100%	100%	100%	100%
Middle vague situation (uncertainty region)	YES	YES	Many distinct regions	NO

Table 81: Detailed table as for the results of the genetic algorithm for all cases

As it can be easily observed and mentioned previously, the 4th case constitutes the best predictive model for Luder Lines' phenomenon. It requires all the specimens taking into account the bender type and it needs an algebraic manipulation to the raw data. In this way, they have the same size class and possess the same gravity to the genetic algorithm selection process.

$$Z_{adj} = \frac{x_i - \bar{x}}{s} + 5$$

So, considering all 9 most influencing variables, the most suitable and precise model is given down below:

Most Proper Predictive Model

$$ObjFun_4 = \varepsilon_{start}^{1,0558}\ \sigma_{start}^{-1,2747}\ \sigma_Y^{-0,2555}\ \varepsilon_{UTS}^{-0,0666}\ OD_{av}^{0,8085} WT_{av}^{1,6210} CLR^{-1,4379} HV^{-0,6882} R_m^{0,845}$$

$0{,}918 \le ObjFun_4 \le 3{,}4887$: **NO** Luder Lines (42/48 -> **87,5 %)**
$3{,}4887 < ObjFun_4 \le 4{,}1868$: **Luder Lines** appearance (12/12-> **100%**)

** No existence of uncertain region, but adjusted z – score transformation needed!

Table 82: The most efficient predictive tool

6.6 Utilizing Genetic Algorithm with less parameters

6.6.1 Scope of this analysis

The aim of this chapter is to implement the MATLAB program (with some modifications), so as not to need 9 variables for every single sample. These variables are difficult to obtain and gathering these numbers is a time – consuming procedure. Except for these, 3 technological tests are needed: Copper tubes' measuring, Hardness Test & Uniaxial Tensile Test.

For these reasons, we introduce a simplified from of the former objective function, so as to acquire a more easily perceivable model:

$$ObjFun = \varepsilon_{start}^{w_1} OD_{av}^{w_2} WT_{av}^{w_3} CLR^{w_4}$$

As we are interested in the 4th case of whole transformed dataset, we use only these quantitative content as input data. Consequently, we focus on 3 geometrical characteristics (OD_{av}, WT_{av}, CLR) and 1 material property ε_{start}.

6.6.2 Discussion on the adjusted program results

After many iterations (runs), the program can separate the values only through 4 distinct regions as for Luder Lines defect. The ideal scenario is to have 2 regions. The 4 exponents $w_1 - w_4$ are calculated though the adjusted MATLAB program using genetic algorithm technique:

Exponent	w_1	w_2	w_3	w_4
Value	0,5505	7,1963	-0,7225	-5,0449

Table 83: Exponents of the objective function of the adjusted genetic algorithm

For size class reasons we adopt a coefficient to our objective function. Based on these exponents, we give the specific objective function that matches to this case:

$$ObjFun = 0{,}1\ \varepsilon_{start}^{0,5505} OD_{av}^{7,1963} WT_{av}^{-0,7225} CLR^{-5,0499}$$

Relied on this objective function, we can sort the objective function's values for each sample and in this way, we can find a major trend for Luder Lines' formation. In the next page, we present the output table of the main program in MATLAB environment, which summarizes the information.

As for the column named Bending Result:

- 0 means Clear Bending or Another Defect
- 1 stands for Luder Lines' formation

Sample ID	Bending Result	$ObjFun$ Value
15,875A4	0	0,8290
15,875A2	0	0,8512
15A16	0	0,9267
15A17	0	0,9492
15A12	0	0,9883
15,875A7	0	1,0260
15A11	0	1,2014
15A13	0	1,2754
15A15	0	1,2794
18A11	0	1,2897
18A9	0	1,3569
18A10	0	1,3614
18A2	0	1,3746
15A16	0	1,4403
15A17	0	1,4753
18A6	0	1,4886
18A5	0	1,5068
15A12	0	1,5361
15,875A4	0	1,5590
15,875A2	0	1,6007
18A8	0	1,6263
15A11	0	1,8673
15,875A7	0	1,9295
15A13	0	1,9823
15A15	0	1,9884
16A4	0	2,0576
25,40A1	0	2,2453
18A11	1	2,4436
28,575A8	1	2,5042
18A9	1	2,5710
18A10	1	2,5794
28,575A6	1	2,5859
18A2	1	2,6044
25,40A2	1	2,6219
28,575A5	1	2,7190
18A6	1	2,8206
18A5	1	2,8550
28A23	0	2,8724
22A14	0	2,9185

35A12	0	3,0148
18A8	0	3,0814
35A7	0	3,1053
35A11	0	3,1251
35A10	0	3,1840
16A4	0	3,1980
28A24	0	3,2923
28A25	0	3,4835
28A2	0	3,4873
28A22	0	3,5018
35A8	0	3,5055
22A16	0	3,6277
28A27	1	4,2698
22A14	1	4,3904
28A23	1	5,1164
22A16	0	5,4572
28A24	1	5,8642
28A25	1	6,2047
28A2	1	6,2116
28A22	1	6,2374
28A27	1	7,6053

Table 84: Output of the adjusted genetic algorithm

We visualize the output data through a scatter graph, indicating with the aid of horizontal lines the 4 distinct regions with respect to bending outcome:

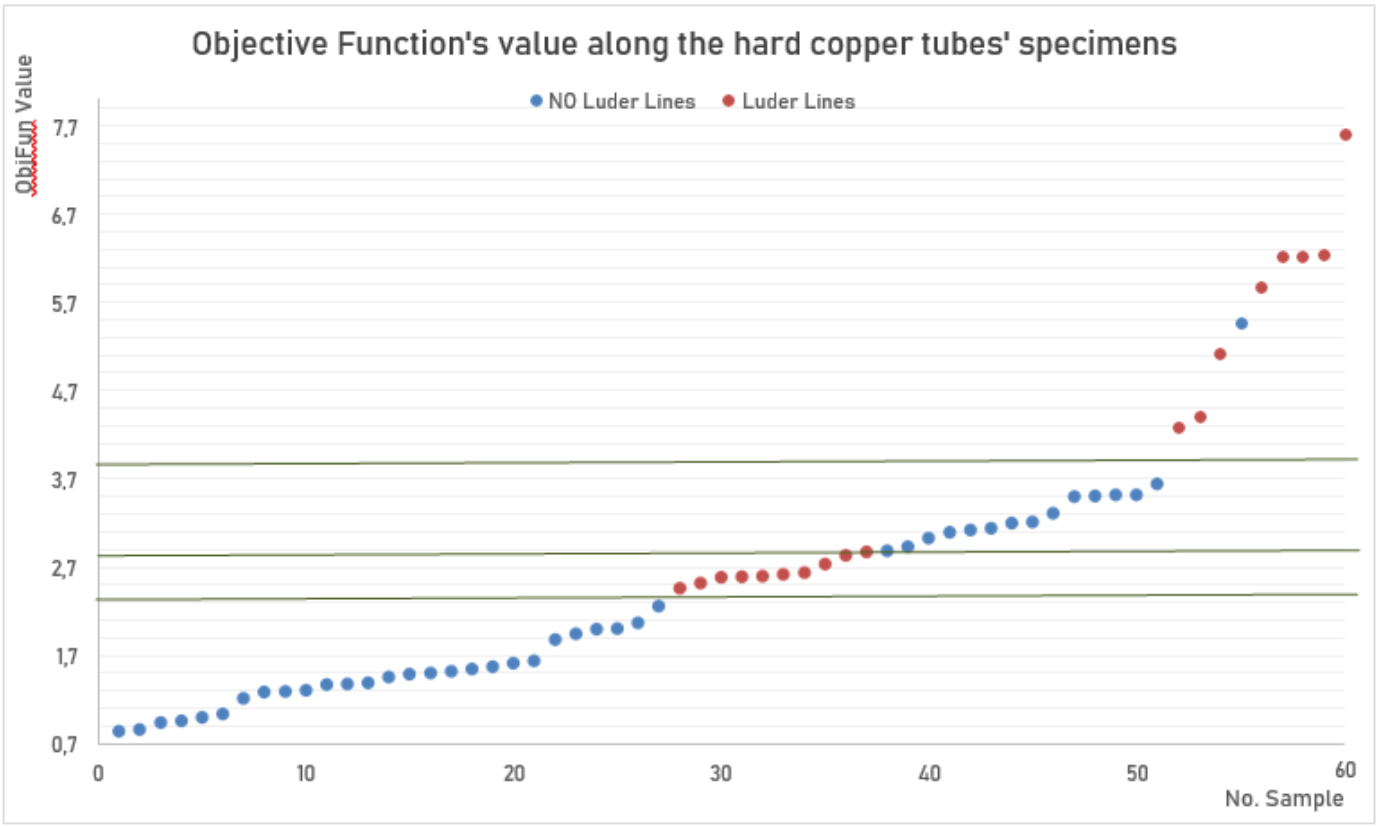

Figure 51: Visualization of the adjusted algorithm's output

In this figure, four (4) distinct intervals are depicted: Two safe ones (marked with blue circles) and two dangerous one (marked with dark red circles) for Luder Lines' occurrence.

- $0{,}829 \leq ObjFun \leq 2{,}2453$: **NO** Luder Lines (27/27 -> **100 %)**
- $2{,}2453 < ObjFun \leq 2{,}855$: **Luder Lines** appearance (**10/10** -> **100 %**)
- $2{,}855 < ObjFun \leq 3{,}6277$: **NO** Luder Lines (14/14 -> 100 %)
- $2{,}855 < ObjFun \leq 7{,}6533$: **Luder Lines** appearance (**8/9 -> 88,89 %**)

7. Images from Microscope

7.1 Design of Experiments (DOE)

In order to investigate the micro-structure of the copper material of the hard tubes, we will examine specific specimens with respect to their bending result. More specifically, we take 3 distinct tubes that correspond to 3 different bending outcomes:

- Extreme / Acute Luder Lines (28A27 | Virax)
- Slight Luder Lines (28A27 | REMS CURVO)
- Clear Bending (18A5 | REMS CURVO)

We can take 3 samples from each category by cutting them with the aid of a cutting wheel. In this way, we have at our disposal 9 samples overall. We provide the respective photos right down:

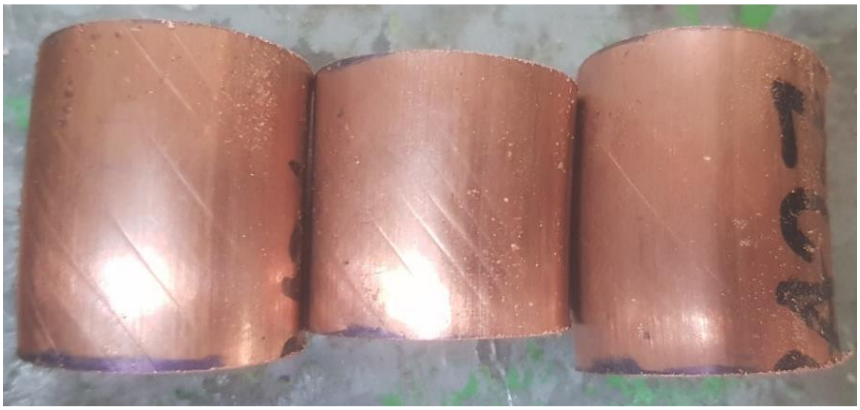

Image 15: Hard copper tubes' rings that have formatted severe Luder Lines

Image 16: Hard copper tubes' rings that have formatted slight Luder Lines

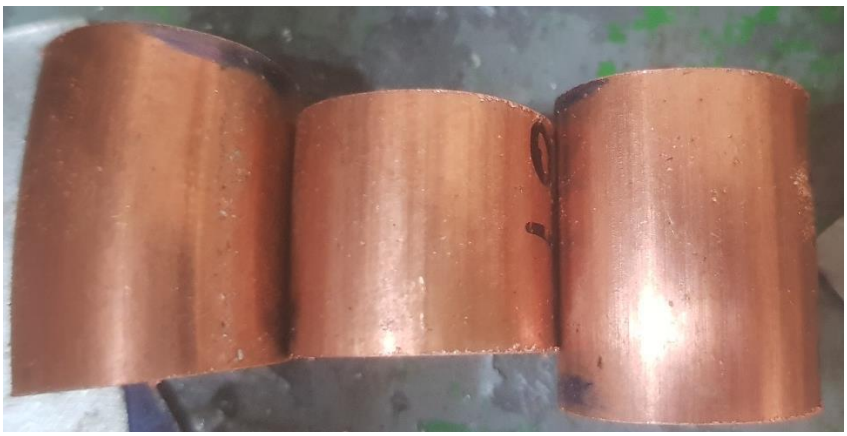

Image 17: Hard copper tubes' rings that had Clear Bending

We would like to research the outer surfaces of the hard copper tubes from a microscopic point of view, adopting a forensic analysis. The main scope of this procedure is to observe these surfaces and may find a convincing cause of Luder Lines defect. Therefore, we propose two approaches in this topic:

I. Observation of the top view of the tubes along the length L
II. Observation of the right view of the tubes along the wall thickness WT

To implement the first approach all these surfaces should be cleaned properly through chemical substances such as acetone $(CH_3)_2CO$, which serves as a solvent. In addition, toothpaste including fluorine F can be utilized so as to clean the tubes' surfaces easily.

Image 18: Chemical substances to use them as cleaning means [22], [23]

After the cleaning of the surfaces, we wipe and dry them with absorbent cotton. So, we are ready to observe them with the aid of the microscope which is placed in the Manufacturing Technology Lab (MTL) at NTUA.

Image 19: Microscope of the Manufacturing Technology Lab

7.2 Photos taken under the microscope [Longitudinal Direction]

We choose the microscope's lens, which has $\times 50$ magnification always and we adjust the focal length $[mm]$ each time. To be more precise, we use the following experiment conditions:

- 1st image: Magnification $\times 8$
- 2nd image: Magnification $\times 6{,}3$
- 3rd image: Magnification $\times 40$
- 4th – 10th images: Magnification $\times 6{,}3$

The 1st and 2nd images are referred to the same region of sample, that has suffered from acute Luder Lines. 3rd and 4th images are linked to severe Luder Lines defect. 5th to 7th images have to do with Slight Luder Lines and finally 8th to 10th images are correlated with Clear Bending.

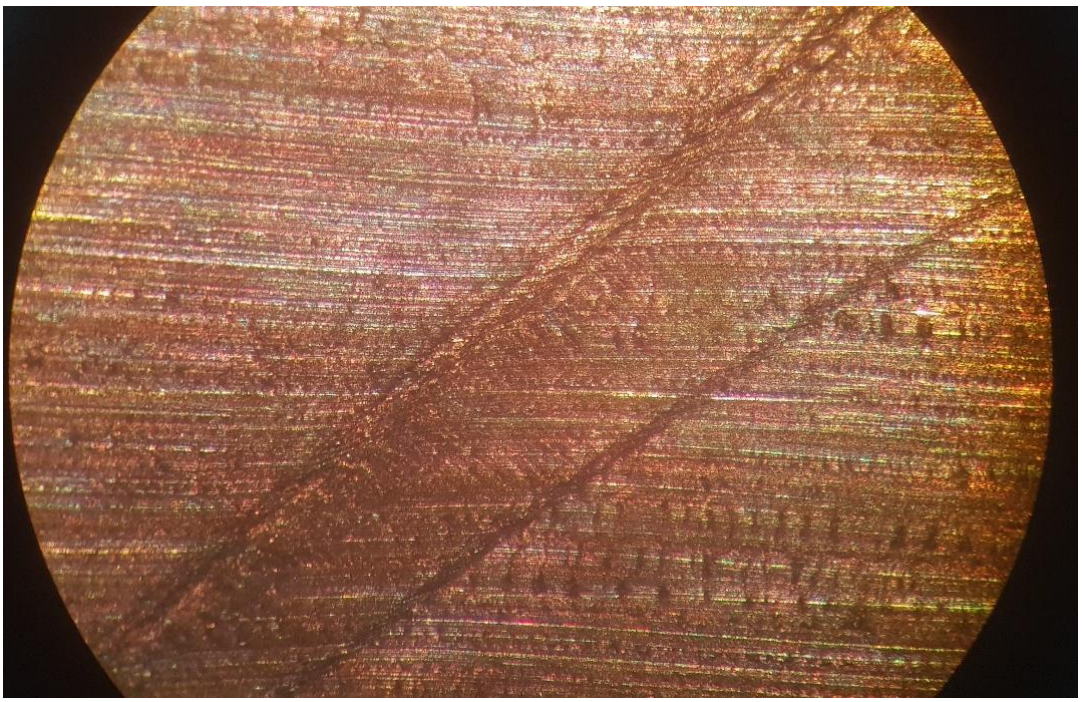

Image 20: Outer surface of a copper tube that manifested extreme Luder Lines (×8)

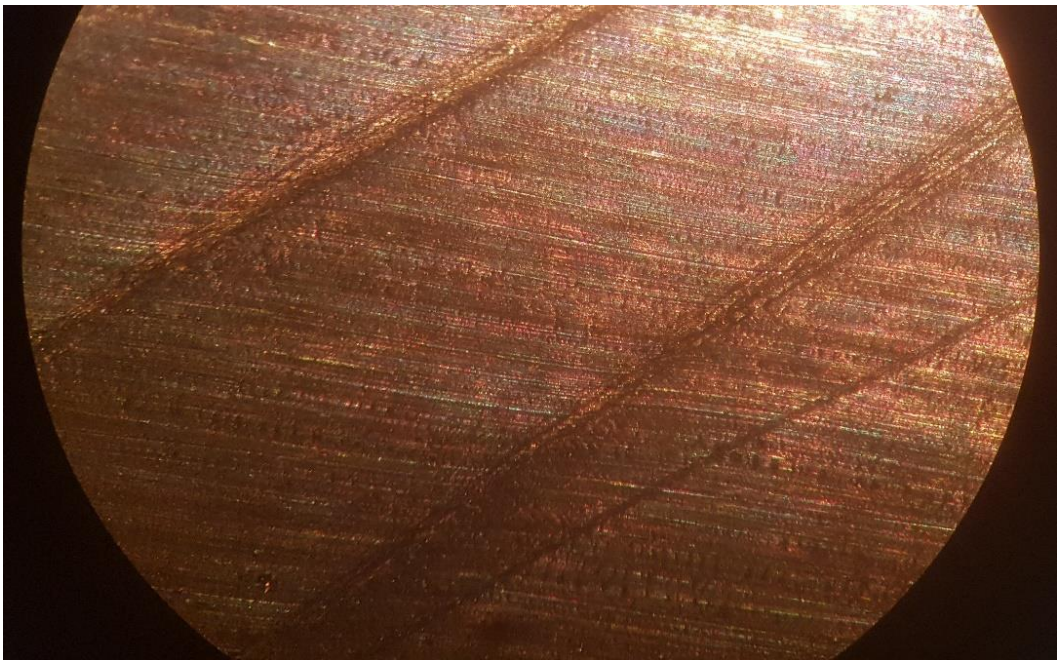

Image 21: Outer surface of a copper tube that manifested extreme Luder Lines (×6,3)

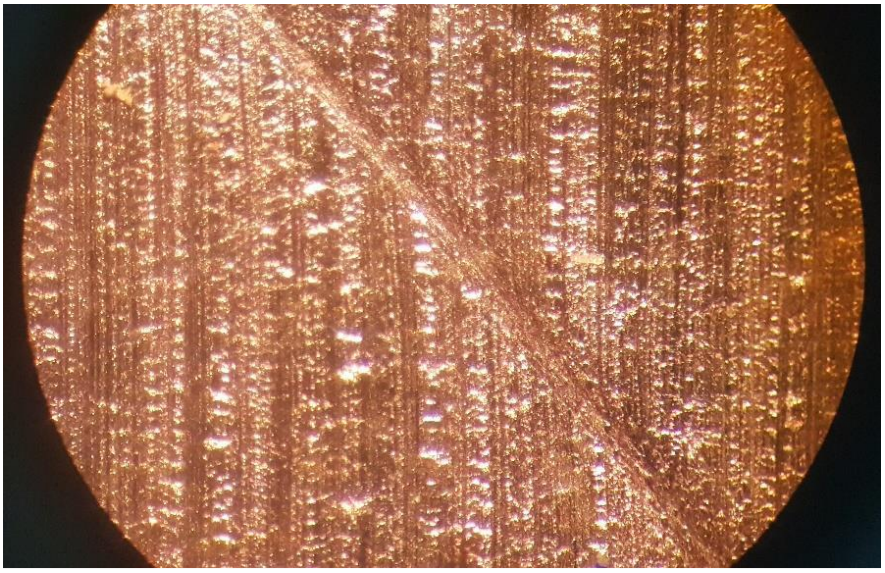

Image 22: Figure: Outer surface of a copper tube that had extreme Luder Lines as result (×40)

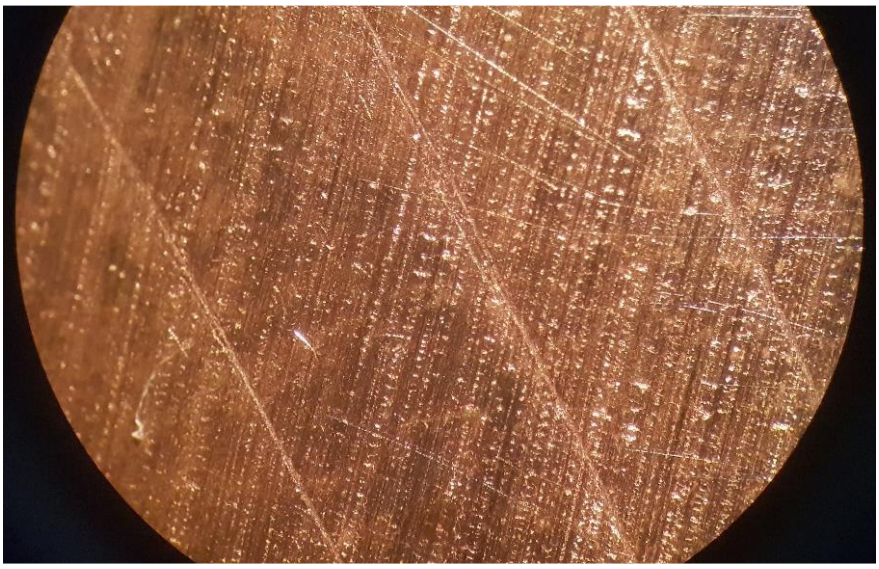

Image 23: Figure: Outer surface of a copper tube that experienced extreme Luder Lines (×6,3)

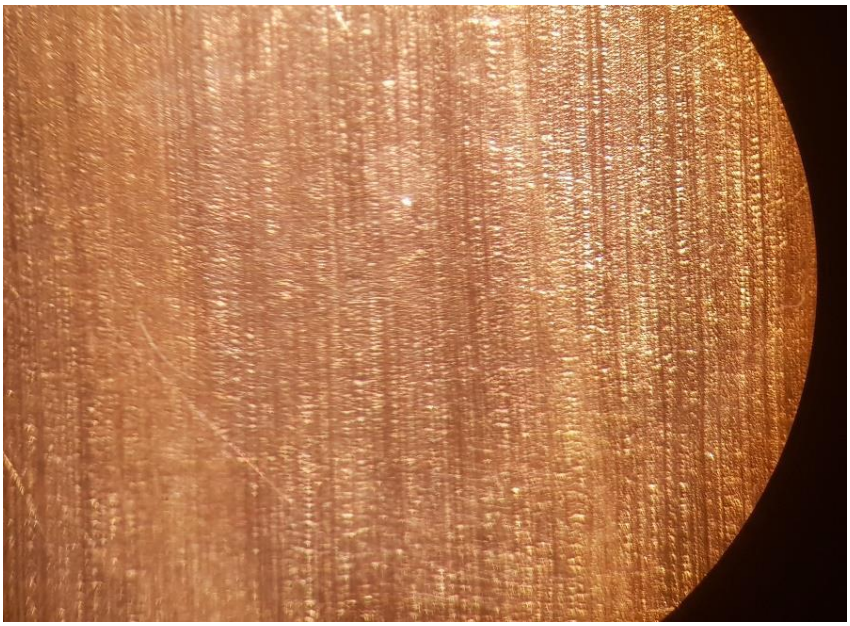

Image 24: Figure: Outer surface of a copper tube that had slight Luder Lines as bending outcome (×6,3)

Image 25: Outer surface of a copper tube that has formatted slight Luder Lines (×6,3)

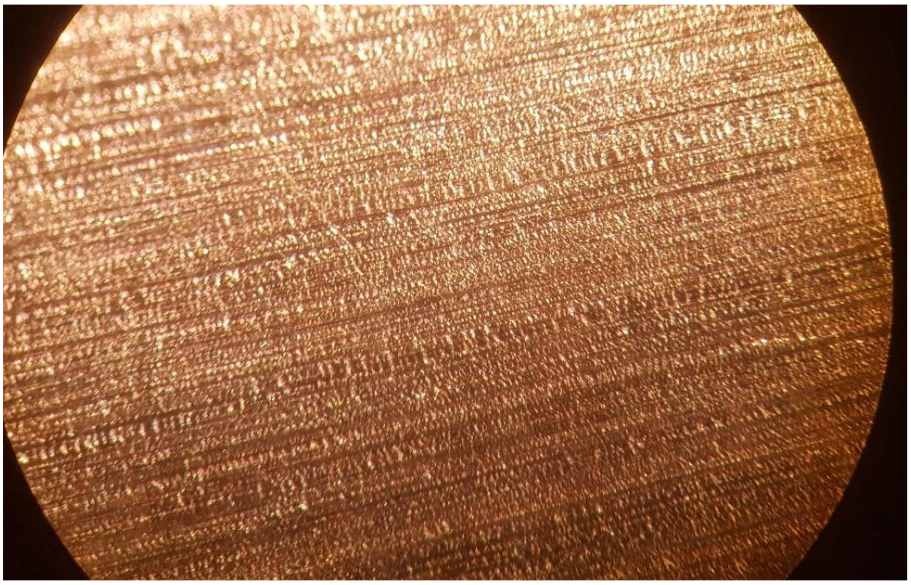

Image 26: Outer surface of a copper tube that has manifested slight Luder Lines (×6,3)

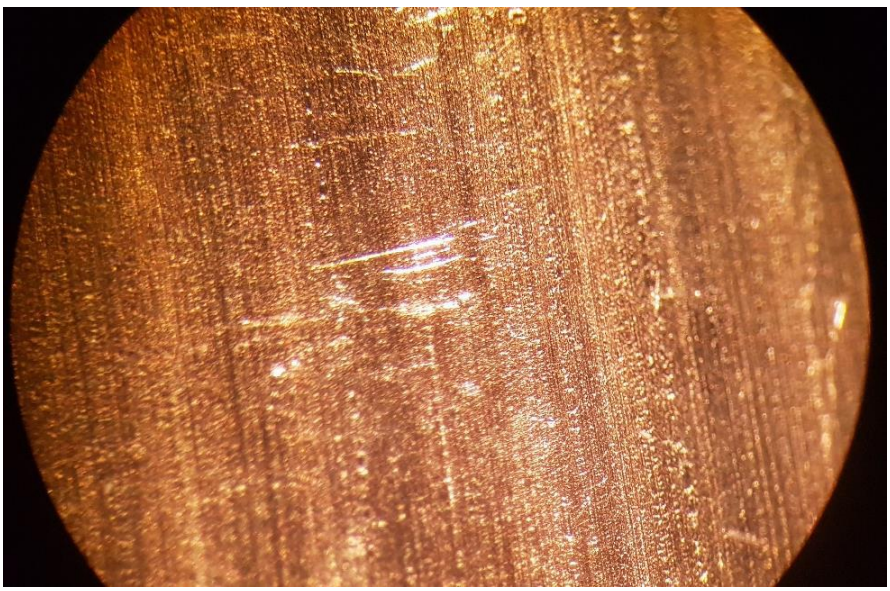

Image 27: Outer surface of a copper tube that did not have any defect (×6,3)

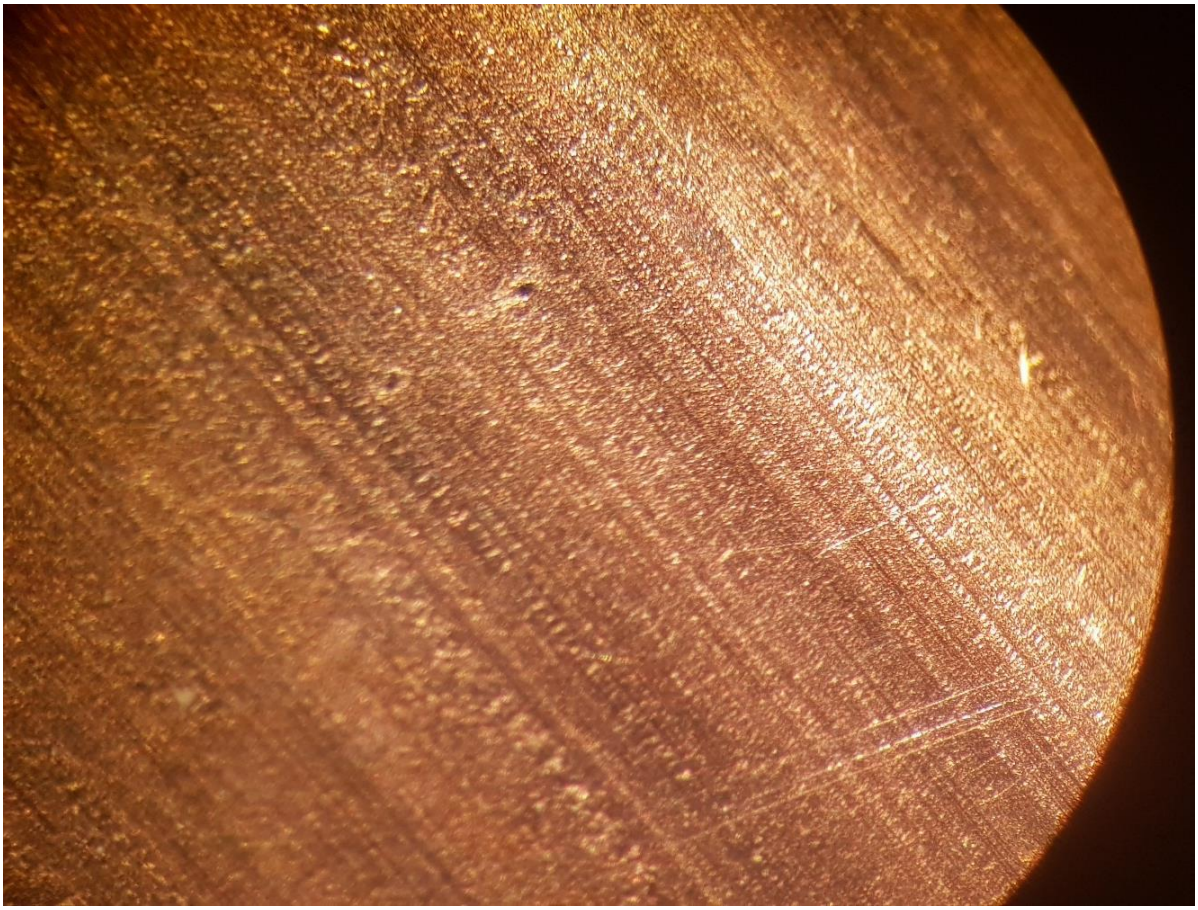

Image 28: Outer surface of a copper tube that had clear bending (×6,3)

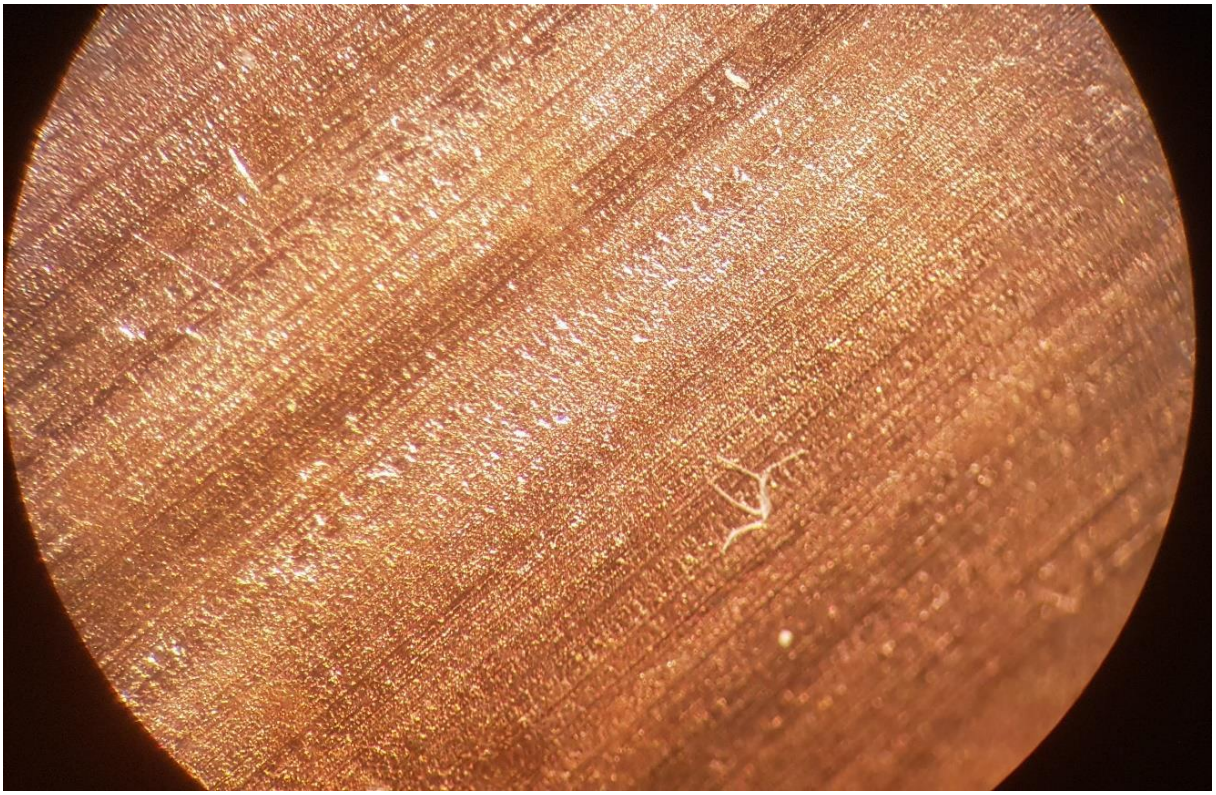

Image 29: Outer surface of a copper tube that had clear bending (×6,3)

7.3 Discussion on the form of microscope images [Top View]

It can be easily seen that all 10 pictures have almost the same morphology as the color (orange) and the direction of the lines. Countless lines with negligible thickness are captured that have the same direction, as they are diagonal (about 45 °). The grain size is not always identical for all specimens, but it quite reasonable. However, the form of these images seem to be metallographically typical of the material Cu – DHP (99,9% Cu), as it is presented in the following schematic:

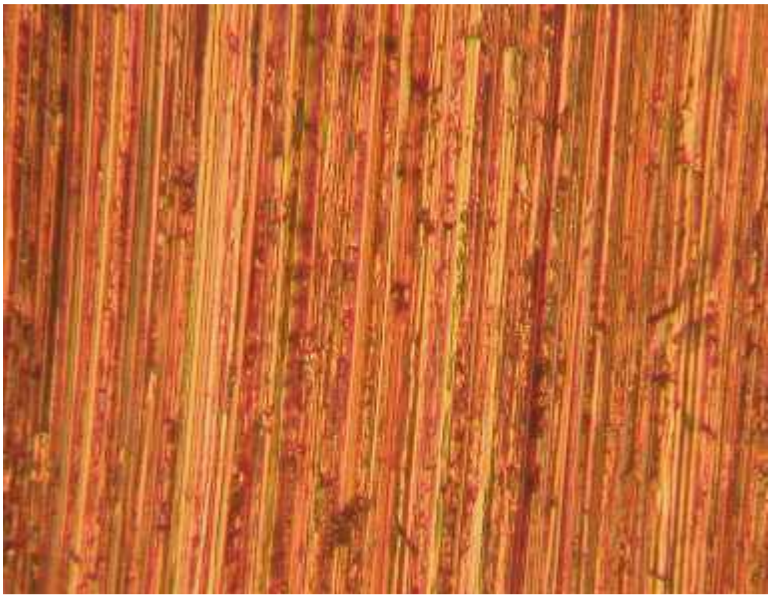

Image 30: Typical copper specimen that has been tested under microscope [24]

Apart from these, it can be observed in the above pictures (1st to 4th) that Luder Lines are formed and seem to be like longitudinal cavities that undermine the uniformity of the wall thickness. So, it may degrade the mechanical properties of the material. At the same time, these Luder Lines do not equally refrain one another and do not "dig" the upper surface in the same degree, although the macroscopic view gives a different aspect. In addition, Luder Lines seem to be parallel but this is not the case. They have also absolutely different direction compared to the inherent lines due to the microstructure of the pure copper.

The remaining images do not present any obvious differences. This means that stereoscope cannot separate microscopically Slight Luder Lines and Clear Bending results. The only problem is that many hard copper tubes present some micro – scratches and abrasions, which aesthetically affect the copper tube. These negligible defects are randomly oriented and cannot be easily attributed to a specific reason.

7.4. Preparation of the specimens – Microscope ---> Mounting

To extract information regarding the microstructure of the material along the wall thickness direction, a specific experimental procedure is followed so as to prepare properly the specimens. The metallographic specimen preparation requires both mounting and grinding.

Mounting of these hard copper tubes' rings is necessary to allow them to be handled easily. It also minimizes the amount of damage likely to be caused to the specimen itself. General guidance prescribes that the mounting material used should not influence the specimen as a result of chemical reaction or mechanical stresses. It should adhere well to the specimen [25]. As mounting mean we use some thermoplastic caps, that are presented in the following picture:

Image 31: Plastic cup used to prepare the specimens

We use 5 plastic cups (equal to number of available specimens) of the presented ones so as to proceed to the mounting experiment. These cups will include the tube ring and the proper mixture. More specifically, a cold-setting resin is used (epoxy resin) ensuring 25/3 ratio between the EpoFix Hardener and the EpoFix Resin. Porous materials must be impregnated by resin before mounting to prevent grit, polishing media or etchant being trapped in the pores, and to preserve the open structure of the material.

Image 32: The components of the liquid mixture

A mounted specimen usually has a thickness of about half its diameter, to prevent rocking during grinding. The edges of the mounted specimen should also be rounded to minimize the damage to grinding discs / sheets.

We prepare the mixture and put it in a common plastic mug so as to inject it to the plastic cup. By doing so, we can capture the following snapshot which shows that these samples will be cured.

Image 33: Mounting specimens be prepared to metallographic examination

We let the mixture to be concreted so as this liquid will be transformed to solid physical condition. In other words, the curing lasts 1 day (24 hours). The next day we can receive our 5 specimens which are presented in the following schematic:

Image 34: Cured samples after the mounting procedure

7.5 Preparation of the specimens – Microscope ---> Grinding

Some surface layers are damaged due to cutting and must be removed by grinding process. Mounted specimens are ground with rotating discs of abrasive paper such as wet silicon carbide paper. The coarseness of the paper is indicated by a number: the number of grains of silicon carbide per square inch. The grinding method involves several stages, using a finer paper (higher number) each time. Each grinding stage removes the scratches from the previous coarser paper [25].

In our case, we follow the further steps for each specimen in order to grind it properly. We use the grinding machine, that includes a rotating disc, on which our specimen is placed. Then, we utilize the grinding papers that can be categorized according to the number of grains of silicon carbide per square inch. The experimental conditions are the same for every single sample and they are given in the following table:

Grinding procedure conditions		
Grinding paper's coarseness	Rotational speed of Rotating disc [RPM]	Duration [min]
P#320	250	5
P#500	300	5
P#1200	300	5
P#2000	300	5

Table 85: Indicative grinding conditions for the 5 cured samples

Distinctive photographs of the grinding machine at Manufacturing Technology Lab (NTUA) and the grinding papers are attached:

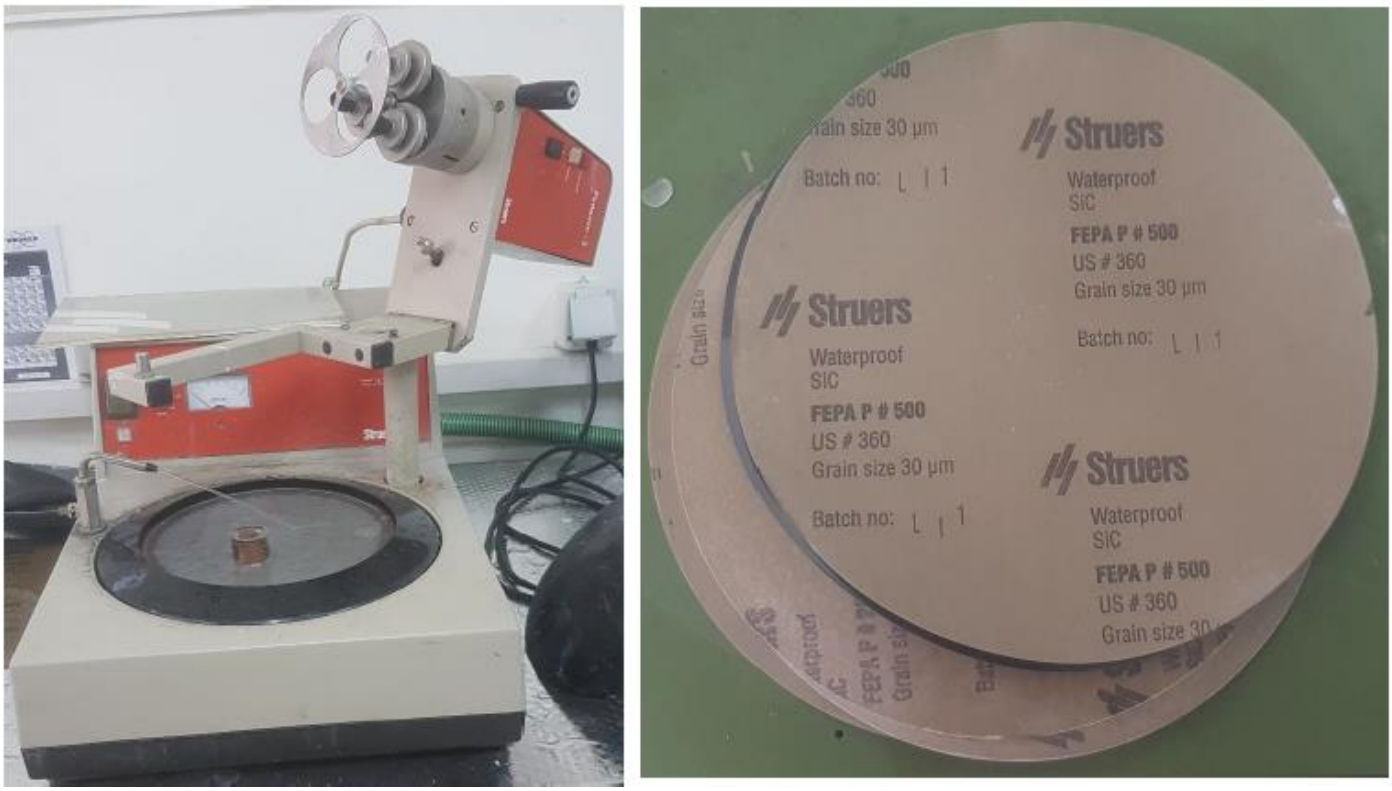

Image 35: The grinding machine of the lab during the experimental procedure and the grinding papers

7.6 Preparation of the specimens – Microscope ---> Levelling

Finally, a terminal process is needed so as to achieve the best possible microscopic examination of the copper tubes' rings. The requirement is the perfect flatness of the surface so as not to face technical problems. For instance, as the viewing area is moved across the surface it will pass in and out of focus, if the above prerequisite is not met.

For all these reasons, we make use of a specimen levelling press (which is shown below) to avoid this problem, as it presses the mounted specimen into plasticene on a microscope slide, making it level. The role of the small piece of paper is relied on covering the sample's surface to avoid scratching [25].

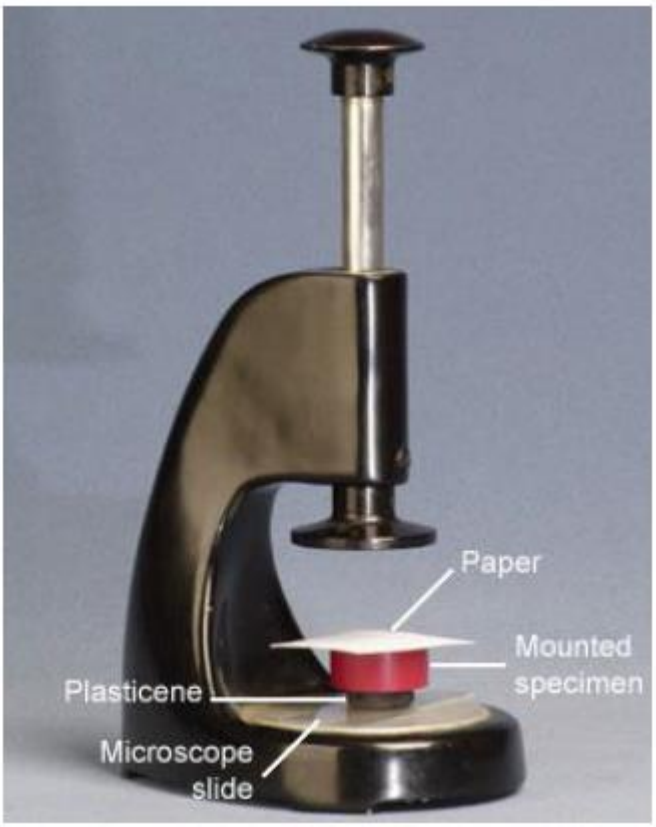

Image 36: The specimen levelling press placed at the University of Cambridge [26]

7.7 Photos taken under the microscope [Wall Thickness Direction] 200× magnification

After all these preliminary procedures (mounting, grinding and levelling) are done, we are able to examine the specimens with the aid of the microscope placed at the Manufacturing Technology Lab (shown right down). This microscope enables us to observe the specimens in the circumferential (wall thickness) direction and realize the microscopic impact of Luder Lines defect.

Image 37: The optical microscope used for the examination of the specimens

In order to acquire easily the images, which reveal the microscopic structure of the samples' material, we utilize the program "IC Capture 2.5". This application can be connected to the high – resolution camera that is installed on the microscope. In this way, we can achieve pretty reliable optical results thanks to this interconnection.

This program can capture and display single images, image sequences and image data streams from all cameras, manufactured by the company named "The Imaging Source". We can give an example of this software application's window, while examining a random defected sample:

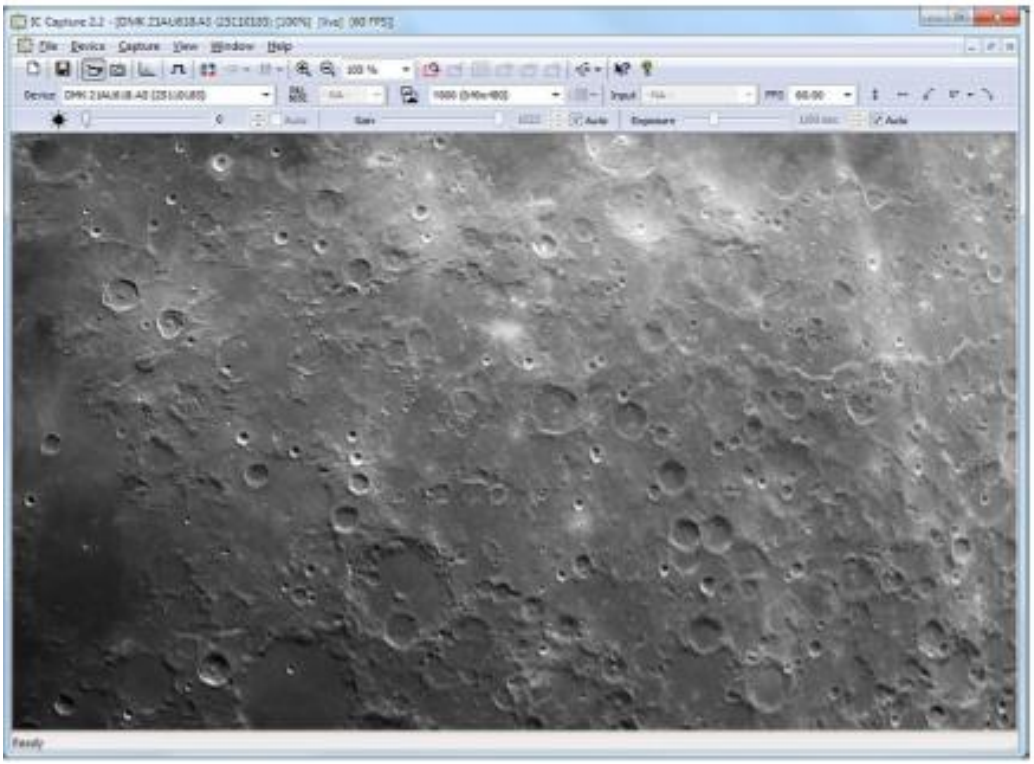

Image 38: An examined surface through the microscope and IC Capture software

Five (5) different lenses are installed on the microscope, that offer the following orders of magnification: $50\times$, $100\times$, $200\times$, $500\times$ and $1000\times$. After careful examination, we decide to use $200\times$ magnification for all mounted samples magnification so as to observe the wall thickness' surface the best way possible.

In the following pages, we will provide the respective images captured by the specialized software application. We will give 5 distinct photos categorized according to the samples' bending result:

- 2 samples that have formatted Extreme Luder Lines defect
- 2 samples that have manifested Slight Luder Lines defect
- 1 sample which did not have any defect --> Clear Bending

7.8 Defected samples due to Acute Luder Lines under the microscope [Right View] 200× magnification

Image 39: Wall thickness' surface at the point in which Extreme Luder Lines end (1st sample)

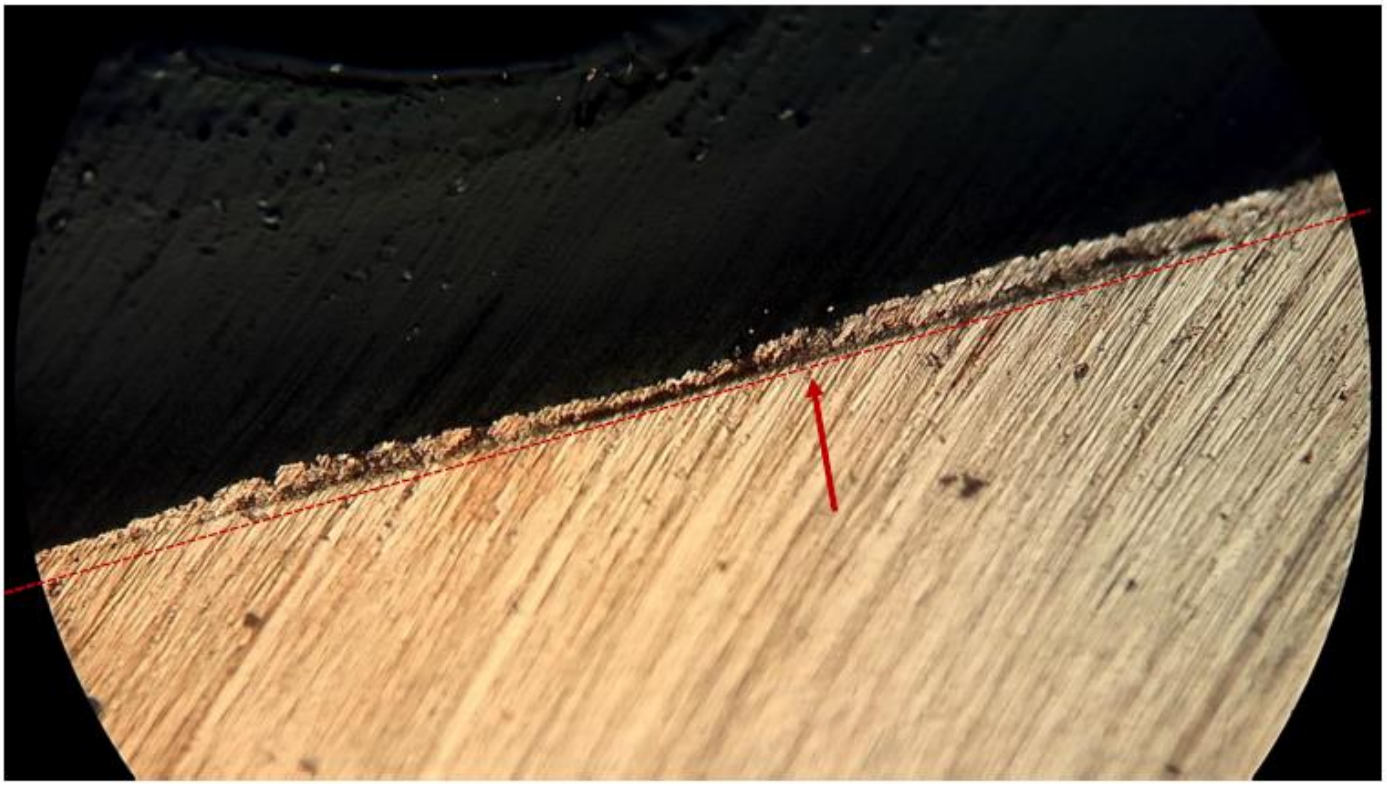

Image 40: Wall thickness' surface at the point in which Extreme Luder Lines end (2nd sample)

7.9 Defected samples due to Slight Luder Lines under the microscope [Right View] 200× magnification

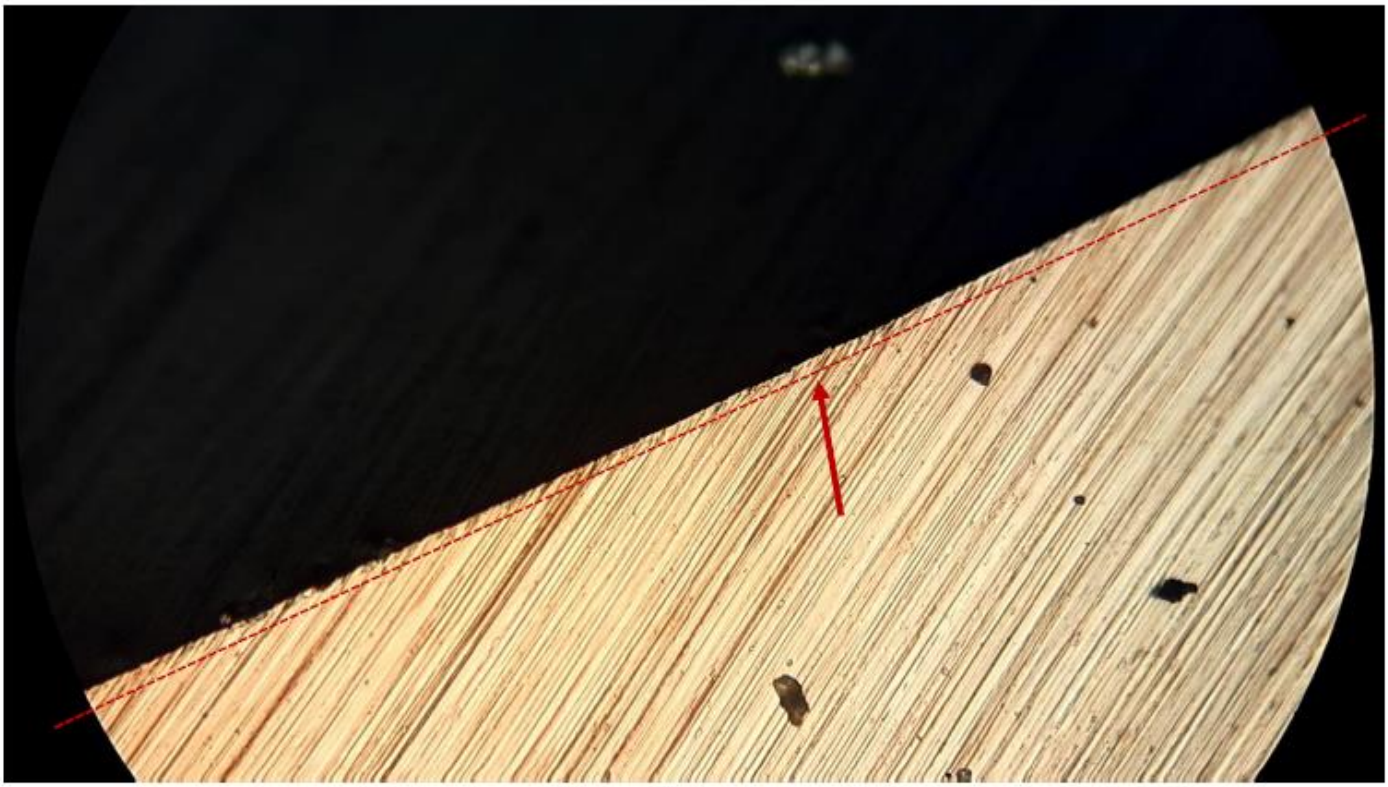

Image 41: Wall thickness' surface at the region in which Slight Luder Lines end (3rd sample)

Image 42:Wall thickness' surface at the region in which Slight Luder Lines end (4th sample)

7.10 Non - Defected sample (Clear Bending) under the microscope [Right View] 200× magnification

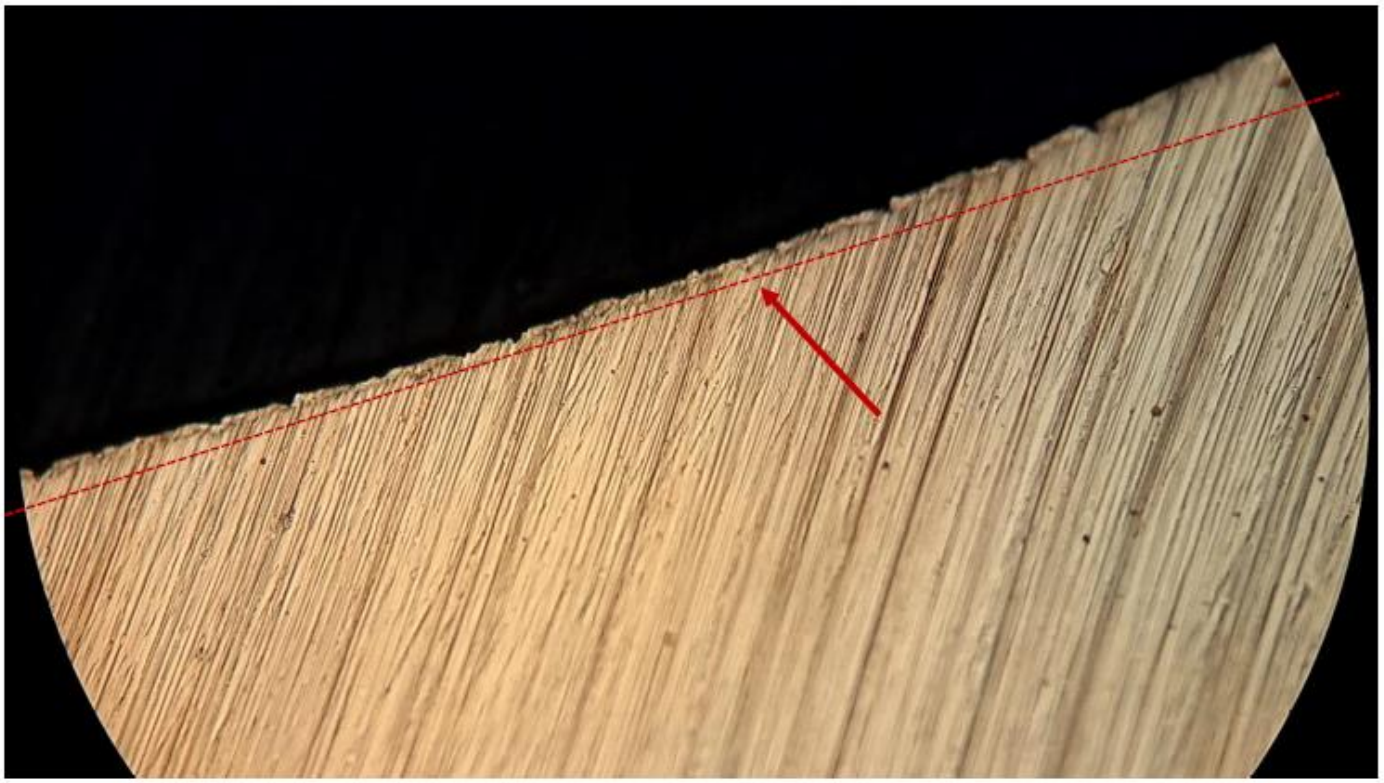

Image 43: Wall thickness' surface at a random point of the non – defected sample (5th sample)

7.11 Discussion on optical microscope images [Right View] - 200× magnification

As in the 1st case (microscope), there are distinctive diagonal lines in the circumferential direction of the sample. Rather small black pits can be observed on the surface in random positions indicating potential scratches, dents or a lack of uniformity in the crystal lattice of the copper material.

The region of our interest is always the same and it is limited with the aid of a dotted dark red line and it is indicated with the red thick arrow. The black color means the resin material due to mounting of the tubes' rings.

The most "convincing" picture is the second one that fits to the case of Extreme Luder Lines' appearance, which proves that Luder Lines cause severe damage to these respective regions. As for the 1st sample, the corresponding points do not indicate acute surface's degradation. However, the 5th schematic seems to have a thin film maybe because of inadequate grinding. In addition, 3rd and 4th figure seem to be very alike. They resemble one another as they have suffered from Slight Luder Lines defect.

Concluding, we cannot extract any direct correlation regarding the microscope images and Luder Lines phenomenon. The only thing we know for certain is that only really severe Luder Lines can be observed in the circumferential direction through an optical microscope.

7.12 Photos taken under the microscope [Top View – Longitudinal Direction] - Comparative Analysis

We wish to investigate further the images coming from the microscope. For this reason, we could cut 2 tube's rings from 28,575A8 – 2 REMS hard copper tube with the aid of a cutting wheel to observe their microstructure. What we actually do is to compare the surfaces of a non -defected sample to a Luder Lines suffered one. A photograph of the specimens is shown down below:

Image 44: 28,575A8 – 2 REMS hard copper tube's upper surface indicating Luder Lines

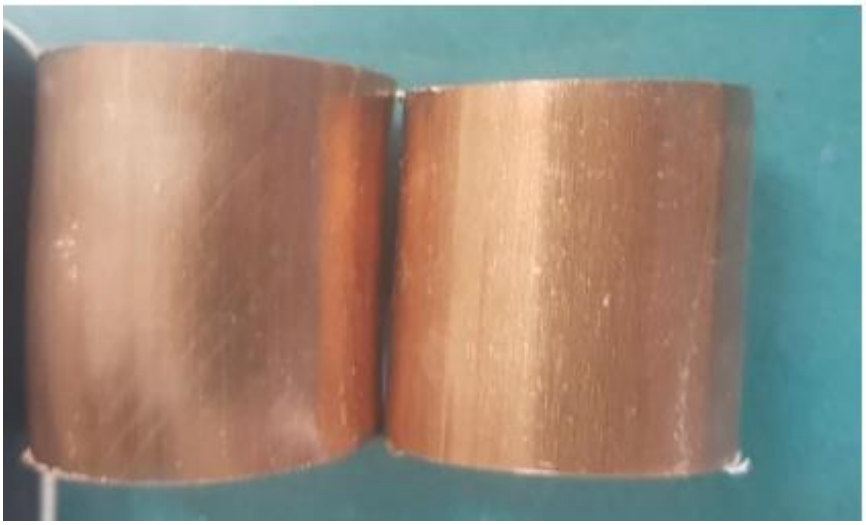

Image 45: 2 tube's rings cut from 28,575A8 – 2 REMS tube

We use the lens that magnifies the interested region 50 times (50×), so as to have the best possible optical appearance of the samples. These two images have a lot in common, but they should show many discrepancies. We take a random region of two specimens for comparing reasons only. Before doing so, we clean these surfaces by utilizing the methods that we have been referred to previously.

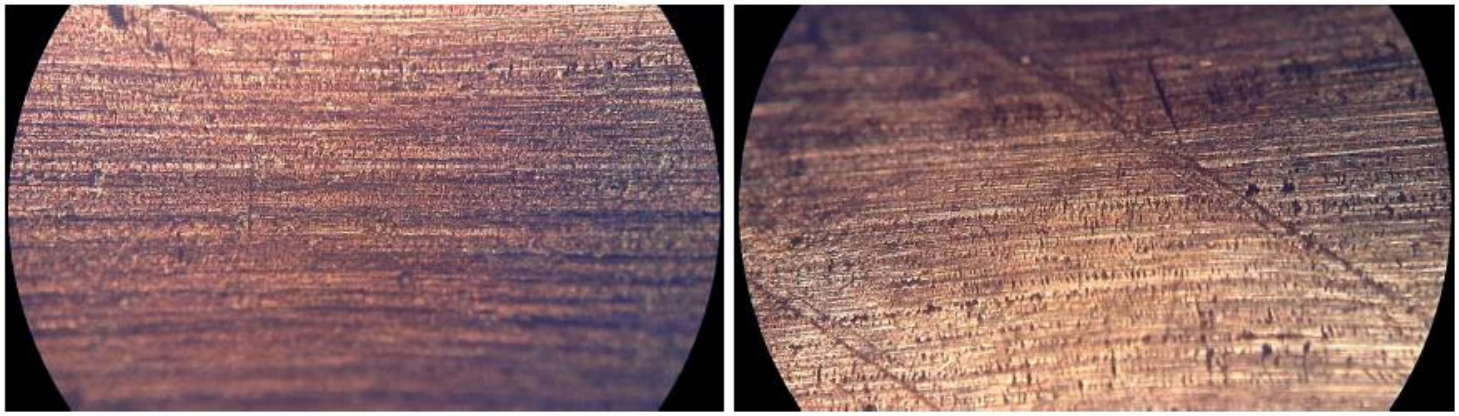

Image 46: Upper surfaces of 2 tube's rings that either had Clear bending result or had formatted Luder Lines defect (×50)

We can easily observe that these 2 images possess the distinctive appearance of the copper material. Both pictures display some formations like dents and scratches which may imply that the wall thickness is not uniform along the longitudinal direction of the outer surface. The aforementioned heterogeneity is not sure that enhances the chance of Luder Lines' formation. However, part of Luder Lines is captured to the right image indicating both the aesthetic and the crystal lattice deterioration. The diagonal lines are pretty apparent and can be hazardous as they reduce the nominal wall thickness and cause geometrical imperfections to the outer surface. This means that this non – linear phenomenon might affect the mechanical behavior of the hard copper tube and should be researched further adopting experimental methods (e.g. tensile test and 3 – point bending test). The radial loss of the material cannot be estimated easily as Luder Lines are not identical although it seems that they are almost the same from a macroscopic point of view.

In the 2nd figure, we can observe 4 lines in total, of which two are more apparent and major. The remaining 2 lines are adjacent to the major ones and "dig" the material not so deep as the 2 main lines do.

** The microscope images are not the optimum ones, as the observed surfaces are curved and have a limited flat region. That is why the lens cannot focus properly and causes some blurs or clouds on the photos despite the existence of a high - resolution camera (1920 ×1080 pixels). This applies to all other photos that will be attached in this chapter because of the geometrical shape.

On this page, 2 images of the same region of the non – defected sample are given using a different magnification order, i.e a different lens. The aim is to observe with extra caution the structure of the material.

Image 47: Outer surface of a non – defected tube (×50)

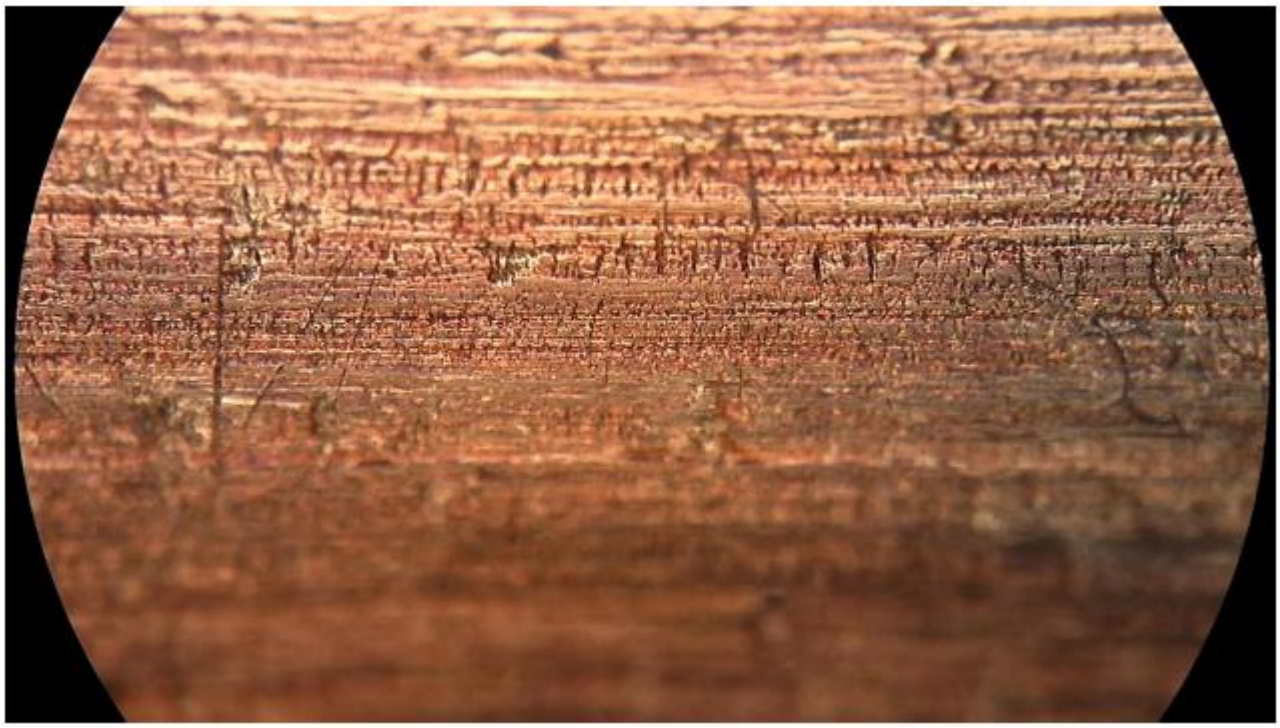

Image 48: Outer surface of a non – defected tube at the same point (×100)

It should be noted that the copper surface is not characterized of a sufficient degree of flatness. Instead of this, there are many serrations, striations, dents and randomly oriented imperfections to the outer region of the hard copper tube. Even craters are shown on the enlarged image. All these notes highlight the fact that these characteristics are typical of a hard copper's upper surface along the longitudinal direction.

7.13 Photos taken under the microscope – Progressive Failure Front [Top View – Longitudinal Direction]

In order to monitor the Luder Lines' appearance in a systematic way, we use the magnification lens ×50 and we take 5 successive photos along the length of the upper surface of the tube's ring. During this procedure, the lateral position remains the same, while the longitudinal one is moving.

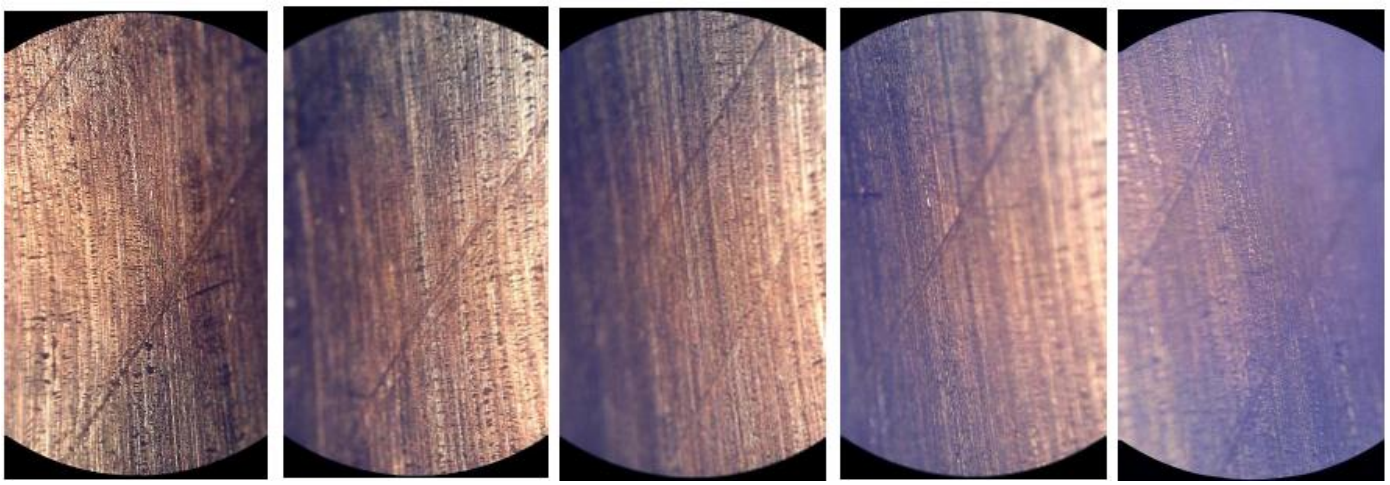

Image 49: The five successive photos of Luder Lines defected sample (×50)

At first glance, all Luder Lines (diagonal lines) are parallel one another. The microscopic examination seems to verify the macroscopic observation of this defect. What can be also seen is that they do not equally abstain each other. Moreover, some Luder Lines are likely to be more acute than others verifying the high non – linear character of this phenomenon. Another interesting thing that should be mentioned is that a sharp diagonal line may be really adjacent to a slight one. This fact is obvious in 1st, 4th and 5th photo. In addition, a Luder Line does not affect the wall thickness' tube the same amount. This means automatically that there is a profile probability function to describe mathematically the wall thickness' reduction because of Luder Lines appearance. On the next page, we will discuss on the negative effects of a distinct Luder Line.

7.14 Photo taken under the microscope – Focus on a Luder Line [Top View – Longitudinal Direction]

In order to investigate the microscopic morphology of the outer surface of the hard copper tube, we focus on a specific Luder Line, which will be focused through the magnification lens ×200. This will enable us to observe this defect the best way possible.

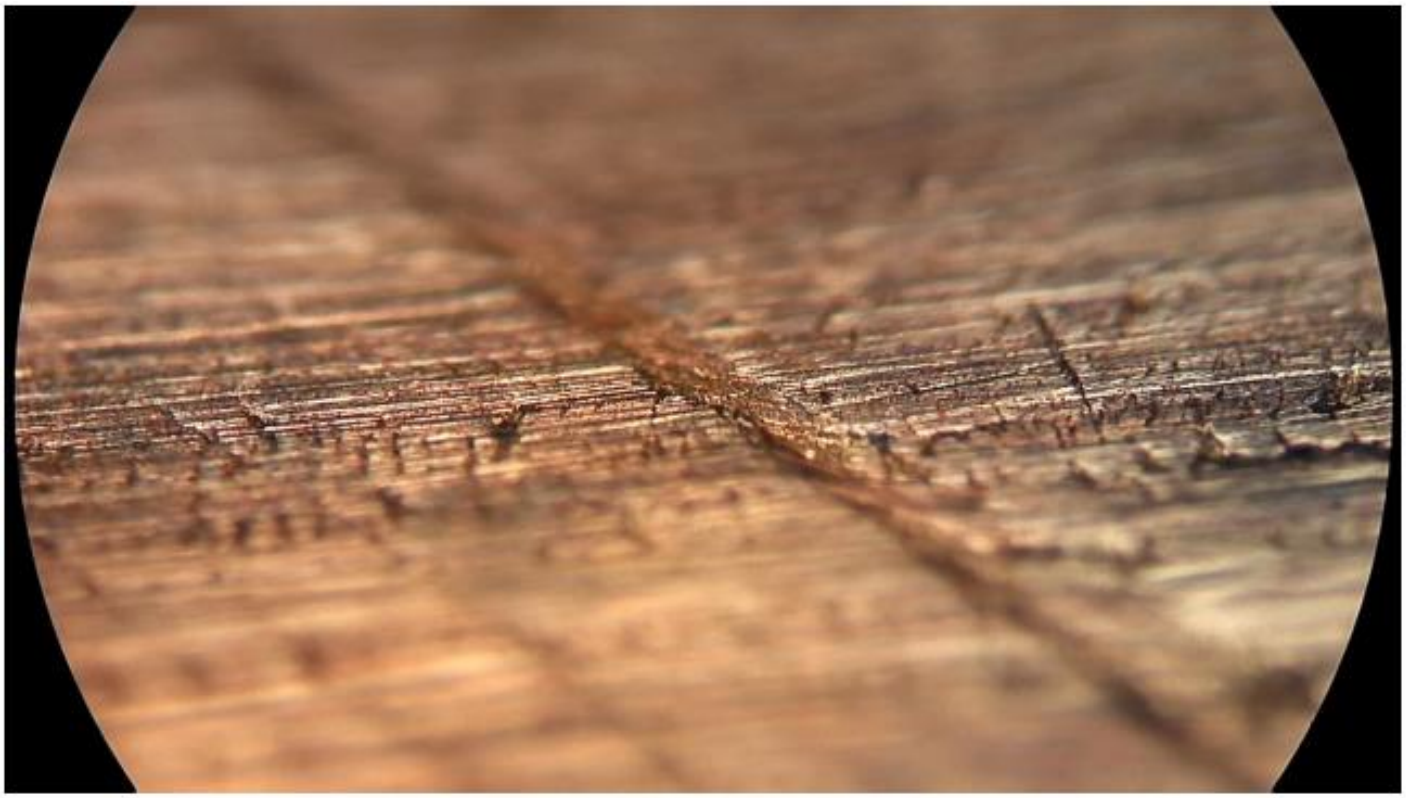

Image 50: Focus on a specific Luder Line (×200)

There can be seen some plasticized regions, that have been subjected to permanent deformation. Also, many scattered scratches and striations are shown as well. All these imperfections should not be neglected, as they may enhance the chance of Luder Lines' appearance. ×200 magnification allow us to note that Luder Lines must be faced as a local failure, creating a diagonal crack. This crack creates a material gap in the circumferential direction, which might be a starting point of stresses' concentration. If this hypothesis is true, the hard copper tube cannot be used safely in many industrial applications.

8. Conclusion & Further Steps

8.1 Conclusion

In this chapter, we make an effort to accumulate all the useful qualitative and quantitative data as for the experimental investigation and the development of the predictive tool for Lüders Lines' appearance in hard copper tubes' bending tests. Consequently, there we can find the whole useful and usable information for anyone that wishes to go deeply and realize this non – linear phenomenon. Except for these, this content is the one in which we reach a conclusion that it may be utilized by Halcor's Technology, R&D Department and another engineers.

By creatively combining the geometrical and the material properties of the experimental investigation's samples, we managed to produce some interesting trends that enhance Lüders Lines formation. According to this analysis, we can present the most important findings:

Usable and key conclusions for Lüders Lines manifestation

1. **No** sufficient correlation among the values of the **Nominal Outer Diameter** ($\boldsymbol{OD}$) and the probability of **Luder Lines'** appearance.

Result	$OD = 15\ mm$ $OD = 15{,}875\ mm$ $OD = 16\ mm$ $OD = 25{,}4\ mm$	$\boldsymbol{OD = 18\ mm}$	$OD = 22\ mm$	$\boldsymbol{OD = 28\ mm}$	$\boldsymbol{OD = 28{,}575\ mm}$
Lüders Lines' Chance	0%	**43,75%**	28,57%	**62,50%**	**100%**

Risky Nominal Outer Diameters: $\boldsymbol{OD = 18\ mm\ or\ OD = 28\ mm\ or\ OD = 28{,}575\ mm}$

2. **Considerable** influence of the **Average Wall Thickness** ($\boldsymbol{WT_{av}}$) on the chance of **Luder Lines'** occurrence!

Semi – empirical rule extracted:
($0{,}455 \leq WT_{av} \leq 0{,}56$ **OR** $0{,}605 \leq WT_{av} < 0{,}75$ **OR** $0{,}89 \leq WT_{av} \leq 1{,}09$) **AND** (REMS – CURVO Bender) => **NO Luder Lines**
($0{,}78 \leq WT_{av} \leq 0{,}885$) **AND** (REMS – CURVO **OR** Virax) => **Luder Lines**

3. $\boldsymbol{R_m}$ ↑=> Probability of **Luder Lines'** appearance ↓

4. $\boldsymbol{HV}$ ↑=> Probability of **Luder Lines'** appearance ↓

5. Significant effect of Bending Radius on **Luder Lines'** formation.

IF ($\boldsymbol{CLR = 54\ OR\ CLR = 66\ OR\ CLR = 88\ OR\ CLR = 102\ OR\ CLR = 115}$) => Great probability of **Luder Lines'** occurrence
ELSEIF => **NO** Luder Lines

6. **Bender Type** (REMS – CURVO or Virax) plays a major role in the upcoming **bending outcome**. In addition, the strain rate $\dot{\varepsilon}$, which is controlled through the **bending speed** $\boldsymbol{v}$, affects the **severity of Lüders Lines**, that is to say how **acute** they are (Ultra Slight, Slight, Medium, Extreme) and the **length** that they possess on the copper tubes' surface.

   The **faster** the **bending speed** is, the **slighter Lüders Lines** appear! =>
   $\boldsymbol{v}$ ↓=> **Lüders Lines'** Intensity ↑

7. Introducing the pure geometrical metric BF_{adj} we can predict reliably the probability of **Luder Lines'** appearance with high accuracy.

$$BF_{adj} = \frac{OD^{2,2}}{CLR^{1,3}\ WT_{av}{}^{-0,7}}$$

Bender type	BF_{adj} interval	Probability of Luder Lines' occurrence
Virax	$0 \leq BF_{adj} \leq 2{,}25$	0%
	$\boldsymbol{BF_{adj} > 2{,}25}$	**83,33%**
REMS - CURVO	$0 \leq BF_{adj} \leq 3$	0%
	$\boldsymbol{3 < BF_{adj} \leq 3{,}45}$	**58,33%**
	$BF_{adj} > 3{,}45$	0%

8. Clear correlation between the true strain ε_{start} and the probability of the Luder Lines' appearance.

True strain ε_{start} interval [MPa]	Luder Lines' appearance (probability)
$0{,}1065\ \% \leq \varepsilon_{start} \leq 0{,}1545\ \%$	14,29 %
$0{,}1570\ \% \leq \varepsilon_{start} \leq 0{,}2484\ \%$	**71,43 %**

$\boldsymbol{\varepsilon_{start}}$ ↑ => Probability of **Luder Lines'** appearance ↑

9. The true strain ε_{UTS} is inversely related to the chance of Luder Lines' appearance.

$\boldsymbol{\varepsilon_{UTS}}$ ↓ => Probability of **Luder Lines'** appearance ↑

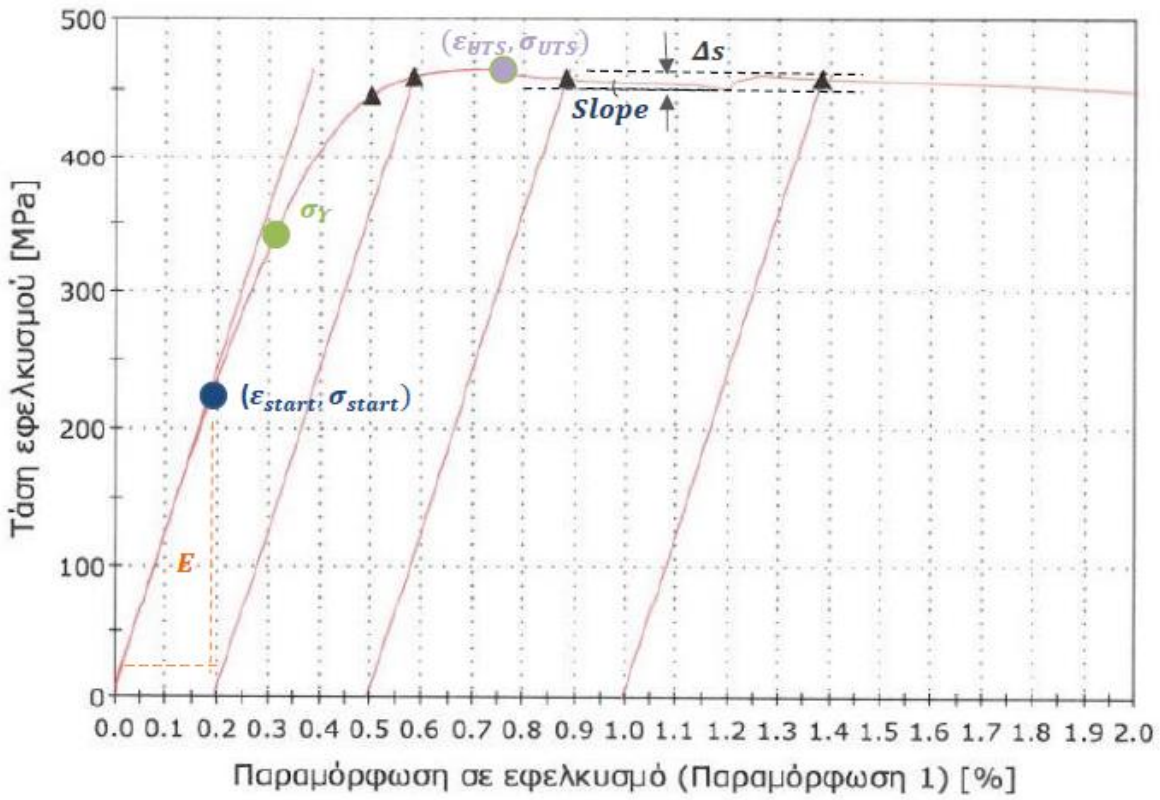

10. The semi – empirical rule (including material properties) can predict accurately the Luder Lines' appearance and it can be easily obtained through the tensile test curve in the plastic region.

$$f_3 = 100\frac{\varepsilon_{start}^{1,5}}{\varepsilon_{UTS}}$$

$0 \le f_3 < 7{,}47$: **NO** Luder Lines (12/13 -> **92,31 %)**
$f_3 \ge 7{,}47$: **Luder Lines** appearance (16/22 -> **72,73%**)

11. Another separating formula includes all 6 material characteristics and requires both uniaxial tensile test ($\sigma - \varepsilon$) graph and hardness test (***HV*** parameter). However, it gives satisfying results regardless of these requirements.

$$f_{10} = \frac{100\ \varepsilon_{start}^{\left(\frac{\sigma_{start}}{100}\right)}\varepsilon_{UTS}\ \sigma_Y}{0{,}7\ R_m\ \cdot\ 0{,}01\ HV}$$

$0 \le f_{10} \le 1{,}38$: **Luder Lines** appearance (14/17 -> **82,35 %**)
$f_{10} > 1{,}38$: **NO** Luder Lines (15/18 -> **83,33 %**)

12. By implementing a genetic algorithm on MATLAB environment, we managed to create a multi – parameter predictive criterion for the Luder Lines' formation.
But we have to introduce an adjusted Z – score function for every single characteristic so as $Objfun_4$ gives the right prediction.

$$ObjFun_4 = \varepsilon_{start}^{1,0558}\ \sigma_{start}^{-1,2747}\ \sigma_Y^{-0,2555}\ \varepsilon_{UTS}^{-0,0666}\ OD_{av}^{0,8085} WT_{av}^{1,6210} CLR^{-1,4379} HV^{-0,6882} R_m^{0,845}$$

$Z_{adj} = \frac{x_i - \bar{x}}{s} + 5$ which applies to every parameter!

$0{,}918 \le ObjFun_4 \le 3{,}4887$: **NO** Luder Lines (42/48 -> **87,5 %)**
$3{,}4887 < ObjFun_4 \le 4{,}1868$: **Luder Lines** appearance (12/12-> **100%**)

13. Utilizing the genetic algorithm using less parameters, we can get another predictive tool that may give us more limited results, as there are more sub – intervals for this approach.

$$ObjFun = 0{,}1\ \varepsilon_{start}^{0,5505} OD_{av}^{7,1963} WT_{av}^{-0,7225} CLR^{-5,0499}$$

$0{,}829 \le ObjFun \le 2{,}2453$: **NO** Luder Lines (27/27 -> **100 %)**
$2{,}2453 < ObjFun \le 2{,}855$: **Luder Lines** appearance (10/10 -> 100%)
$2{,}855 < ObjFun \le 3{,}6277$: **NO** Luder Lines (14/14 -> 100 %)
$2{,}855 < ObjFun \le 7{,}6533$: **Luder Lines** appearance (8/9 -> 88,9 %)

14. Overview of **Critical** Strain ε_{cr}

Critical strain ε_{crit} computation				
Metric acronym	ε_{start}	ε_{crit} $(\delta_x(a = 0\ rad))$	ε_{crit} $(\delta_x(a = \frac{\pi}{2}\ rad))$ $[REMS]$	ε_{crit} $(\delta_x(a = \frac{\pi}{2}\ rad))$ $[Virax]$
Value	0,1545%	0,2210%	0,2220%	0,1727%

The critical strain for **Virax** bent specimens takes **lower** value than the one referring to the **REMS** – CURVO samples. And that is why **more** specimens have suffered from **Luder Lines** defect in terms of percentage when bent with the aid of Virax bender, as we have more adverse bending test.

Table 86: Usable and key conclusions for Luder Lines' appearance

8.2 Recommendations for further research

To reach more reliable and remarkable results in Lüders Lines Project [LLP], the following further steps are proposed:

- More focused bending tests of hard copper tubes' samples so as to validate the extracted trends for Lüders Lines' appearance and even observe more interesting findings. Therefore, we introduce this Design of Experiments (DOE):

Nominal Outer Diameter (OD)	Nominal Wall Thickness (WT)	Temper	Mean Lightweight	Number of physical tubes
15	$> 0{,}53$	Hard (H)	0%	4
16	$> 0{,}53$	Hard (H)	0%	8
25,40	$\geq 0{,}79$	Hard (H)	0%	12
28	$\geq 0{,}78$	Hard (H)	0%	4
28,575	$\geq 0{,}835$	Hard (H)	0%	8
35	$\geq 0{,}9$	Hard (H)	0%	8

Table 87: Detailed information regarding the proposed DOE

This table contains the needed samples for Luder Lines Project (LLP). We would like to have 4 physical tubes for each sample for the following reasons:

- Tensile test (Engineering stress – strain graph) + Hardness test (Mechanical and material measurements) → Measurements' report
- Bending tests [Various Bending Speeds]
- Bending tests [High Temperature]
- Back - up tube

** With the term "physical tube" we mean a hard copper tube about one (1) meter long like the previous ones that have been bent in the past. Consequently, we can enrich our new dataset.

- As Lüders Lines are affected by lubrication, we shall confirm the main finding that the presence of lubrication enhances the chance of the appearance of this defect.

- Similarly, we have to examine the influence of high temperature, as Lüders Lines may not form on hard copper tubes' surface in this case according to some preliminary bending tests.

- Systematic categorization of the types of Lüders Lines with respect to their severity as follows:
  1. Ultra-Slight
  2. Slight
  3. Medium
  4. Extreme – Acute Lüders

  This classification helps us to realize which types of Lüders Lines cause only cosmetic or functional problems or both of them. Some Lüders Lines are only superficial, and others seem to be like longitudinal notches (slotted lines). We have to examine this issue further to understand the prerequisites for every kind of Lüders Lines.

- Measurement of the distances of Lüders Lines in order to see any significant statistical difference and extract some useful quantitative measurements for the available samples. The same applies to the angle of these lines. In the case of severe Lüders Lines it also possible to measure (with the aid of a micrometre) the depth of these Lines, that affect the real wall thickness of the hard copper tube.

- Simulation of the bending test through LS – DYNA or ABAQUS and focus on the boundary conditions during the development of this model (Available 3D Parts .sldprt)
  - Better understanding of the critical plastic strain ε upon which the danger of any defect is real
  - Visualization of the process
  - Estimation of the stresses σ applied on the hard copper tube during a bending test for each sample for every angle.
  - Capability of using different strain rates $\dot{\varepsilon}$, friction's models (lubrication's modelling), tooling (through CLR), outer diameter OD, wall thickness WT, bending angle and even more!
  - Comparative evaluation with respect to the material's stress – strain curve.

- Grain Size measurements for some specimens with the aid of specialized equipment.

- Composition of a comprehensive, detailed publication / paper that will zero in on Lüders Lines' appearance on the hard copper tubes' surface during bending tests.
  - Literature Review (Potential Cause of this non – linear phenomenon)
  - Experimental Investigation (Old + New one)
  - Lüders Lines Photos (All Types)
  - Development of the parametric predictive tools
  - Photos taken under the microscope (Progressive Failure Front + Focus on a Luder Line $\times 200$)
  - Useful SEM images (if it is possible)
  - Conclusion

Table of Figures

List of Tables

List of Images

Bibliography – List of references

[1] Technology & Research – Halcor (last accessed on 10/10/2022)
https://halcor.com/technology-research/technology-research/

[2] Plastic strain localization in metals: origins and consequences, Stephen D. Antolovich, Ronald W. Armstrong, *Progress in Materials Science* (2013)

[3] A Note on the Portevin-Le Chatelier Effect, A. H. COTTRELL, *Metallurgy Department, University of Birmingham* (1953)

[4] THE PORTEVIN-LE CHATELIER EFFECTS IN Cu-Ti, Cu-P AND Cu-Si ALLOYS, R. ONODERA,' T. ISHIBASHI, H. ERA' and M. SHIMIZU, *Kyushu University Higashiku Hakozaki* (1984)

[5] The Portevin–Le Chatelier effect: A review of experimental findings, Ahmet Yilmaz, *Science and Technology of Advanced Materials* (2011)

[6] Ait-Amokhtar H and Fressengeas C 2010 Acta Mater

[7] On the effect of Lüders bands on the bending of steel tubes. Part I: Experiments, Julian F. Hallai, Stelios Kyriakides, International Journal of Solids and Structures (2011)

[8] Kinetics and morphology of Lüders deformation in specimens with homogeneous structure and with a weld joint, V.I. Danilov, V.V. Gorbatenko, L.B. Zuev, D.V. Orlova, Materials Science & Engineering A (2018)

[9] Effect of Lüders Plateau on Fracture Response and Toughness of Pipelines Subject to Extreme Plastic Bending, Nikzad Nourpanah, Farid Taheri, *Department of Civil and Resource Engineering Dalhousie University* (2011)

[10] On the effect of Lüders bands on the bending of steel tubes. Part II: Analysis, Julian F. Hallai, Stelios Kyriakides, *International Journal of Solids and Structures* (2011)

[11] The influence of rate of deformation on the tensile test with special reference to the yield point in iron and steel, C. F. Elam (1938)

[12] A Highly Formable Aluminium Alloy 5182-SSF, David S. Thompson, *Reynolds Metals Co.* (1978)

[13] The Influence of Specimen Thickness on the Lüders Effect of a 5456 Al-Based Alloy: Experimental Observations, Yu-Long Cai, Su-Li Yang, Shi-Hua Fu and Qing-Chuan Zhang, *Metals | An Open Access Journal form MDPI* (2016)

[14] The Portevin–Le Chatelier (PLC) effect and shear band formation in an AA5754 alloy, Herdawandi Halim, David S. Wilkinson, Marek Niewczas, *Acta Materialia 55* (2007)

[15] Naphon, P. Study on the heat transfer and flow characteristics in a spiral-coil tube. Int. Commun. Heat Mass Transfer, 2011, 38(1), 69–74.

[16] A. Mentella and M. Strano., Rotary draw bending of small diameter copper tubes: Predicting the quality of the cross-section, 2011, Proc. IMechE Vol. 226 Part B: J. Engineering Manufacture.

[17] Greg G. Miller, Tube Forming Processes, A comprehensive guide, Society of Manufacturing Engineers, 2003

[18] Handbook - Basics of Tube Bending, Tube Form Solutions (TFS)

[19] Plastic - deformation analysis in tube bending, N.C. Tang, *International Journal of Pressure Vessels and Piping 77* (2000)

[20] MathWorks - Genetic Algorithm - Find global minima for highly nonlinear problems
https://www.mathworks.com/discovery/genetic-algorithm.html (last accessed on 10/10/2022)

[21] MathWorks – How the genetic algorithm works?
https://www.mathworks.com/help/gads/how-the-genetic-algorithm-works.html (last accessed on 10/10/2022)

[22] https://www.labsupply.co.nz/images/thumbs/0007561_wash-bottle-250ml-acetone-wn-ldpe-pk-5_550.jpeg
(last accessed on 24/05/2022)

[23] https://www.midtownrichmonddentist.com/storage/app/media/toothpaste.jpg
(last accessed on 24/05/2022)

[24] http://www.icbl.hw.ac.uk/learnem/doitpoms/OpticalMicroscopy/images/1200x200.jpg
(last accessed on 24/05/2022)

[25] http://www.icbl.hw.ac.uk/learnem/doitpoms/OpticalMicroscopy/metallography.htm
(last accessed on 24/05/2022)

[26] https://dl-gui.theimagingsource.com/en_US/0fdc634b-cd08-5089-92ed-1d86ea5bc4a5/
(last accessed on 25/05/2022)

Main_opt.m

```
[num2,txt,raw] = xlsread('DatasetDesignFormulav2.xlsx');
clearvars -except num2

global num

num = num2(1:60,25:34);

fun = @objfun;
nvars = 9;
A = []; b = [];
Aeq = []; beq = [];
lbl = -1.7; ubl = 1.7;
lb = [lbl lbl lbl lbl lbl lbl lbl lbl lbl];
ub = [ubl ubl ubl ubl ubl ubl ubl ubl ubl];
nonlcon = [];
options = optimoptions('ga','PopulationSize',1000,'MutationFcn','mutationadaptfeasible');

x = ga(fun,nvars,A,b,Aeq,beq,lb,ub,nonlcon,options)

fun_sort = objfun_2(x);
```

Objfun.m

```
function [obj] = objfun(x)

global num

fun_tot=zeros(size(num,1),2);
for i=1:size(num,1)
    fun = 1;
    for j=1:size(num,2)-1
        fun = fun*num(i,j)^x(j);
    end
    fun_tot(i,1) = fun;
    fun_tot(i,2) = num(i,10);
end

fun_sort = sortrows(fun_tot,1);

k=fun_sort(1,2);
flag = 0;
for i=2:size(num,1)
    if fun_sort(i,2)~=k
        flag = flag + 1;
        k = fun_sort(i,2);
    end
end
obj = flag;


end
```

Objfun_v2.m

```
function [obj] = objfun_v2(x)
```

```
global num

fun_tot=zeros(size(num,1),2);
for i=1:size(num,1)
    fun = 1;
    for j=1:size(num,2)-1
        fun = fun*num(i,j)^x(j);
    end
    fun_tot(i,1) = fun;
    fun_tot(i,2) = num(i,10);
end

% fun_sort = sortrows(fun_tot,1);

sum0=0; sum1=0;
for i=1:size(num,1)
    if num(i,9) == 1
        sum0 = sum0 + fun_tot(i,1);
    else
        sum1 = sum1 + fun_tot(i,1);
    end
end
% if sum1/sum0 < 1
    obj = sum1/sum0;
% else
%     obj = sum0/sum1;
% end

end
```

Objfun_2.m

```
function [fun_sort] = objfun_2(x)

global num

fun_tot=zeros(size(num,1),2);
for i=1:size(num,1)
    fun = 1;
    for j=1:size(num,2)-1
        fun = fun*num(i,j)^x(j);
    end
    fun_tot(i,1) = fun;
    fun_tot(i,2) = num(i,10);
end

fun_sort = sortrows(fun_tot,1);
```